MATHEMATICAL MODELLING OF THE BIOMECHANICAL PROPERTIES OF ARTICULAR CARTILAGE

Submitted by

THANH CONG NGUYEN
Bachelor of Science (Honours),
University of Queensland

A final thesis submitted in total fulfillment of the requirements for the degree of Doctor of Philosophy

School of Mechanical, Manufacturing and Medical Engineering
Centre for Rehabilitation Science and Engineering
Queensland University of Technology,
Brisbane, Australia

August, 2005

KEY WORDS

Anisotropy, Articular Cartilage, Continuity, Consolidation, Damage, Heterogeneity, Hyperelasticity, Laceration, Mathematical Model, Permeability, Rheological Analogue.

ABSTRACT

Articular cartilage is the translucent, heterogeneous three-component biological load processing gel that overlays the end of the articulating bones of mammalian joints. Normally, healthy intact articular cartilage performs two biomechanical functions very effectively. These are (i) redistribution of stresses due to loads acting on the joint; (ii) act as a near-frictionless interface between contacting bone ends. These principal functions are enabled by its highly elastic properties. Under normal physiological conditions, these essential biomechanical functions are provided over the lifetime of a mammalian joint with little or no degenerative changes. However, certain levels of physiological and traumatic loads and degenerative processes induced by activities such as running, walking, extreme sport, and aging can alter the composition and structure of the tissue, leading to changes in its biomechanical properties. This, inturn, influences its functional characteristics. The most common degenerative change in articular cartilage is osteoarthritis and the management and treatment of this disease is pivotal to all research targeted toward articular cartilage.

Several scientific groups around the world have developed models of articular cartilage to predict its fundamental and functional responses to load and altered biochemical conditions through both in vivo and in vitro studies. The most predominant of these models are the biphasic and triphasic models, which are based on the conceptualisation of articular cartilage as a dispersed mixture of its three main components namely collagen fibrils proteoglycan aggregates and water. The triphasic model is an extension of the biphasic model and incorporates swelling as a separate identifiable component of the tissue's biomechanical response. While these models are capable of predicting the elastic and viscoelastic behaviour and certain aspects of the swelling characteristics of articular cartilage, they are incapable of accounting for its short-term responses where the fluid component is the main carrier of the applied pressure.

The hydrostatic and swelling components of the fluid content determine the manner of stress-sharing and hence transient load processing within the matrix as stress is transmitted to the underlying structure. Furthermore, the understanding of the nature of this stress-sharing between fluid and solid components of the tissue is fundamental to

the comprehension of the nature of degeneration and its biomechanical consequence in the function of the articulating joint. The inability of the biphasic and triphasic theories to predict, in accordance with experimental results, the transient behaviour of the loaded matrix fluid requires a more representative model. This imperative therefore forms the basis for the research work presented in this thesis.

In this thesis, a new mathematical model of articular cartilage load carriage is presented which can predict the transient load-induced responses. The model is based on a continuum framework invoking the principle of mechanical consolidation of fluid-saturated, swollen porous elastic materials. The cartilage matrix is conceptualised as a heterogeneous anisotropic fluid-saturated porous material in which its solid component responds to load as a hyperelastic material and whose interaction with the swelling component produces a partially distributed time-varying permeability.

In accordance with the principle of consolidation, a phenomenological approach is adopted for developing both analogue/engineering models and mathematical models for the tissue. The models are then used to predict both bulk matrix responses and the properties of the hypothetical layers of the tissue when subjected to physiological loading conditions. Ultimately, the generalized mathematical model is used to analyse the effect of superficial layer laceration on the stress-processing or stress-sharing characteristic of normal healthy articular cartilage. Finally, predicted results are shown to compare with experimental data demonstrating that the new models for swelling deformation, the hyperelastic law for solid skeletal structure and the distributed, time-dependent permeability are representative of the articular cartilage.

Publication Arising from the Thesis

[Nguyen and Oloyede, 1998] Nguyen, T. and Oloyede A., 1998. One-dimensional porohyperelastic model of articular cartilage, 1998. The 4th Pan Pacific Conference, Tissue Societies of Symposium.

[Nguyen and Oloyede, 2000] Nguyen, T. and Oloyede A., 2000. Finite element analysis of articular cartilage using Rheological models with addition of physio-chemical effect, 10th International Conference Biomedical Engineering.

[Nguyen and Oloyede, 2001] Nguyen, T. and Oloyede A., 2001. Phenomenological model of articular cartilage structure and consolidation. BIOROM (Bioengineering Conference)

[Nguyen and Oloyede, 2001] Nguyen, T. and Oloyede, A., 2001. Predictive rheological models for the consolidation behaviour of articular cartilage under static loading. Proc Instn Mechanical Engineering, vol. 215 Part H, pp 565-577.

[Nguyen and Oloyede, 2002] Nguyen, T. and Oloyede, A., 2002. Continuum modelling of the large strain behaviour of the constrained articular cartilage. Proceedings of 5th Biennial Engineering Mathematics and Applications Conference, pp 151-156.

CONTENTS

1. Introduction ……

1.1 Background ……. 1

1.2 Problem definition …… 4

1.3 Principal parameters of articular cartilage structure and function 7

1.4 Objective of research ……... 8

1.5 Layout of thesis ……. 9

2. Articular cartilage matrix and the existing models …….

2.1 Introduction ……. 11

2.2 Function of articular cartilage …….. 12

2.3 Architecture of articular cartilage …… 12

2.4 The composition of the articular cartilage matrix …… 14

2.4.1 Type II Collagen …… 14

2.4.2 Proteoglycans …….…... 16

2.4.3 Chondrocytes …….….. 17

2.5 Existing models …….…... 18

2.5.1 Biochemical models ….……..... 19

2.5.2 Viscoelastic models …….. 21

2.5.3 Mixture theory – based models …… 23

2.5.4 Consolidation model ……. 27

2.5.4.1 Continuum of cartilage …… 28

2.5.4.2 Hydrostatic excess pore pressure in cartilage ……..… 30

2.5.4.3 Solid-fluid interactions in cartilage …… 31

2.5.5 Cartilage hyperelasticity and poro-hyperelastic model …… 33

2.6 Requirements for the development of cartilage consolidation models …. 34

2.6.1 The biosynthesis of the load-bearing structure of articular cartilage …..…… 34

2.6.2 A perspective on cartilage load-carriage biomechanics …… 35

2.7 Conclusion …… 38

3. Predictive rheological models for articular cartilage consolidation

3.1 Introduction …….. 40

3.2 Mathematical description of the Oloyede-Broom model ……. 42

3.2.1 General relationship for volume change …… 42

3.2.2 An approximate relationship for dependence of permeability on compressive strain ……. 43

3.2.3 General continuity equation of fluid flow…….. 44

3.2.4 Stress-strain relationship for solid skeleton …….. 44

3.2.5 Approximate expression for matrix osmotic potential ……. 47

3.2.6 The effective stress relationship for the articular cartilage matrix 48

3.2.7 Results …….. 49

3.3 Modified rheological analogues of articular cartilage…… 50

3.3.1 The “series-element” analogue …….. 50

3.3.2 The "parallel-element” analogue …… 56

3.4 Conclusion ……. 59

4. Experimental investigation of the biomechanical responses of normal and damaged cartilage

4.1 Introduction …… 61

4.2 Experiment ……. 63

4.2.1 Equipment ……. 63

4.2.2 Sample preparation and repeatability tests …… 65

4.2.3 Consolidation tests …… 66

4.3 Results and discussions ……. 67

4.4 Conclusion ……. 72

5. Theoretical prediction of normal and surface damaged cartilage-using the rheological analogue model for numerical analysis

5.1 Introduction …… 73

5.2 Rheological analogues of articular cartilage …….. 73

5.3 Development of constitutive relationships for the layer analogue ……. 76

5.3.1 Stress-strain relationship ……... 76

5.3.2 Continuity equation …… 78

5.3.3 Physico-chemical effect ……. 79
5.3.4 Effective stress relationship for matrix equilibrium …….. 80
5.3.5 Model of permeability ……... 81
5.3.6 Idealization of articular cartilage with the superficial layer impaired ……. 82
5.4 Discretized equations …… 82
5.5 Result and discussions …….. 84
5.6 Conclusion ……. 94

6. Generalized continuum theory for articular cartilage consolidation
6.1 Introduction …….. 95
6.2 Simplifying assumptions …….. 96
6.3 Mathematical description …….. 97
6.3.1 Volumetric deformation ……. 97
6.3.2 Hyperelastic formulation of collagen fibril meshwork deformation 97
6.3.3 Determination of the material parameters ……..….. 101
6.3.4 Large strain poroelasticity theory for articular cartilage consolidation …… 104
6.3.5 Continuity equation …….. 105
6.3.6 Model for permeability variation …….. 107
6.4 Mathematical description in cylindrical coordinates ……. 110
6.4.1 Description of large strain ……. 110
6.4.2 Constitutive equation for a cylindrical matrix ……... 111
6.4.3 Continuity equation …… 111
6.5 Conclusion …… 112

7. Prediction of the consolidation responses of normal intact and lacerated articular cartilage matrix
7.1 Introduction ……. 113
7.2 Assumption of the model for case study ……. 113
7.3 Analysis of the intact cartilage model …… 114
7.3.1 Theoretical formulation ……. 115
7.3.2 Discretized equations for numerical analysis …… 116

7.3.3 Results and discussions ……. 118
7.4 Modelling and analysis of the effects of lacerations in articular cartilage 125
7.4.1 Mathematical description …….. 125
7.4.2 Idealization of surface laceration in articular cartilage ……..……. 125
7.4.3 Results and discussions …… 126
7.5 Static axial loading of unconfined cartilage matrix …….. 129
7.5.1 Relationship between parameters …… 129
7.5.2 Permeability distribution …… 131
7.5.3 Results and discussion …….. 133
7.6 Conclusion ……. 137

8. Conclusion and Future research
8.1 Conclusion …… 139
8.2 Future research ……. 140

9. References ……. 141

10. Appendices
Appendix A1 …….. 161
Appendix A2 ……. 163
Appendix A3 ……. 167
Appendix A4 ……. 169
Appendix A5 ……. 172

LIST OF FIGURES

Figure 1	Comparison chart of existing models and appropriate one	6
Figure 2.1	The mammalian joint showing the location of articular cartilage and the meniscus cartilage ……..	11
Figure 2.2	The microstructure of articular cartilage ……..……	13
Figure 2.3	Schematic illustration of type II collagen meshwork and the cell distribution and orientations in the articular cartilage …….	13
Figure 2.4	Idealized schematic illustration of the cartilage architecture ….……	14
Figure 2.5	Micrographs of the collagen fibrils architecture in articular cartilage.	15
Figure 2.6	Schematic illustration of the proteoglycan macromolecule ..…….	16
Figure 2.7	The histomorphometric analysis of localized cells…….	17
Figure 2.8	Mechanical analogue illustrating the principle of one-dimensional classical consolidation	27
Figure 2.9	Comparison of the prediction of the patterns of the hydrostatic excess pore pressure …… ……. ……	36
Figure 3.1	The original rheological analogue proposed for the articular cartilage matrix by Oloyede and Broom …….	41
Figure 3.2	Comparison of the experimental hydrostatic excess pore pressure and creep strain published by Oloyede and Broom to the predicted results of the original analogue …….. ..…….	50
Figure 3.3	The modified ‘series’ rheological analogue for the cartilage matrix ..	51
Figure 3.4	Comparison of the experimental hydrostatic excess pore pressure and creep strain published by Oloyede and Broom to the predicted results of the new serial analogue. ……..	53
Figure 3.5	The influence of the level of initial osmotic pressure on the predicted values of the hydrostatic excess pore pressure and strain…	54
Figure 3.6	The influence of the level of initial permeability and transient permeability variation on the responses. ……..…	55
Figure 3.7	The influence of increasing or decreasing the permeability relative to that used for predicting the responses. ……...……	56

Figure 3.8 The modified 'parallel' rheological analogue for the articular cartilage matrix. ……..…… 57
Figure 3.9 Predicted values of the applied stress (I), hydrostatic excess pore pressure (II), creep strain of the matrix. …..…….. 58
Figure 4.1 Schematic structure of fibrils in normal and softened cartilage matrices…… 61
Figure 4.2A The static loading rig showing the consodometer and linear variable displacement transducer (LVDT) in situ. …….. 64
Figure 4.2B The one-dimensional consolidometer. …….……... 65
Figure 4.3 The thin-walled cylindrical punch for cutting the cartilage specimens used in experiments and cartilage specimen. ……. 66
Figure 4.4 The responses of normal and artificially lacerated cartilage (medial bovine cartilage, thickness 1.71mm) ……. 68
Figure 4.5 The responses of normal and artificially lacerated cartilage (lateral bovine cartilage, thickness 1.55mm) ……. 68
Figure 4.6 The responses of normal and artificially lacerated cartilage (lateral bovine cartilage, thickness 1.57mm) ……. 69
Figure 4.7 The responses of normal and artificially lacerated cartilage (medial bovine cartilage, thickness 1.59mm) ……. 69
Figure 4.8 The responses of normal and artificially lacerated cartilage (medial bovine cartilage, thickness 1.53mm) ……. 70
Figure 4.9 The responses of normal and artificially lacerated cartilage (lateral bovine cartilage, thickness 1.92mm) ……. 70
Figure 4.10 The responses of normal and artificially lacerated cartilage (lateral bovine cartilage, thickness 1.70mm) ……. 71
Figure 5.1 The 'parallel' rheological analogue for the articular cartilage layer .. 74
Figure 5.2 The modified 'parallel' rheological analogue for a articular cartilage layer. …… 75
Figure 5.3 Experimental values of the total matrix strain and hydrostatic excess pore pressure for normal intact and lacerated cartilage matrix. …..... 85
Figure 5.4 Patterns of the variation of permeability with strain and position within the matrix of articular cartilage ……. ……. 86
Figure 5.5 Predicted depth-dependent compression coefficients. …. ……. 87

Figure 5.6 Predicted depth-dependent initial Donnan osmotic pressure for the normal intact cartilage matrix……. 87
Figure 5.7 Predicted values of the effective solid stress. ……. 88
Figure 5.8 Comparison of the experimental total matrix strain with the predicted values of the time-dependent strain. ..…….. 89
Figure 5.9 Predicted distribution of the hydrostatic excess pore pressure in the normal matrix at the time 0, 0.5 min., 1 min,…, 90 min. …….. 90
Figure 5.10 Predicted values of the permeability versus the normalized stiffness at the different depths…….. 90
Figure 5.11 Comparison of the predicted depth-dependent compression coefficients of the presented model …… 91
Figure 5.12 Comparison of the predicted values of the responses of the normal lacerated cartilage matrix to experimental data. …….. 92
Figure 5.13 Comparison of the predicted stress-strain responses of the hypothetical layers of articular cartilage …….. 93
Figure 6.1 Schematic diagram of the idealized porous structure used for developing the new permeability function. …… 96
Figure 6.2 Mesh for the 3-dimensional axi-symmetric disc representing an articular cartilage sample and a selected element …….. 110
Figure 7.1 Schematic mesh of the articular cartilage matrix under one-dimensional constraints and axial static loading …….. 114
Figure 7.2 Comparison of the total matrix strain from the experimental data and the computed value of strain ……... 119
Figure 7.3 Predicted values of the hydrostatic excess pore pressure at the different depths. …….……. 119
Figure 7.4 Predicted values of the effective solid stress at the different depths. 120
Figure 7.5 Predicted variation of the strain and depth-dependent permeability at the different depths. ……..…… 120
Figure 7.6 The influence of permeability on the total matrix strain and the hydrostatic excess pore pressure. …….……... 122
Figure 7.7 The influence of the axial compressive stiffness on the total matrix strain and the hydrostatic excess pore pressure. …… 122
Figure 7.8 Predicted distribution of stiffness. ……. 123

Figure 7.9 The influence of changing the drag coefficient on the load carriage parameters of articular cartilage. ……..…… 124

Figure 7.10 Experimental values of the total matrix strain and hydrostatic excess pore pressure for normal lacerated cartilage matrix. ……. 126

Figure 7.11 Comparison of the experimental and predicted values of the responses of the normal lacerated cartilage matrix. …… 128

Figure 7.12 Comparison of the experimental and predicted values of the responses of the normal cartilage matrix with a laceration of 780μm. 129

Figure 7.13 Element mesh of a three-dimensional axi-symmetric disc. The fluid flows out at the top and in the radial direction ……. 130

Figure 7.14 Mesh for the finite elements of an axi-symmetric disc. The central axis is at the left hand side. The right side is unconstrained ……..… 133

Figure 7.15 Predicted transient patterns of the hydrostatic excess pore pressure at the centre of the layers. ……..……. 134

Figure 7.16 Predicted strains in each layer and total matrix strain of the unconfined cartilage matrix. ……..…….. 135

Figure 7.17 The contour plots of the predicted hydrostatic excess pore pressures at an instant time. …… 136

LIST OF TABLES

Table 3.1	Parameters for analysis resulting in Figure 3.2 ……..	49
Table 3.2	Parameters for analysis resulting in Figure 3.4 ……..	53
Table 3.3	Parameters for analysis resulting in Figure 3.5 …….	54
Table 3.4	Parameters for analysis resulting in figures 3.6 and 3.7 ……	56
Table 3.5	Parameters for analysis resulting in Figure 3.9 ……..	59
Table 7.1	Parameters for analysis resulting in figures 7.2 and 7.3 ……..	118
Table 7.2	Parameters for analysing the results depicted in figures 7.7 and 7.8…	123
Table 7.3	Parameters for analysis resulting in Figure 7..9 ……..	125
Table 7.4	Parameters used for the analysis of results in Figure 7.11 ……..	128
Table 7.5	Parameters used for analysing the results depicted in Figure 7.12 …..	129
Table 7.6	Parameters used for the analysis presented in figures 7.15 to 7.17 ….	134
Table A1	Experimental data presented in Figure 4.4 ……	179
Table A2	Experimental data presented in Figure 4.5 ……	180
Table A3	Experimental data presented in Figure 4.6 ……	181
Table A4	Experimental data presented in Figure 4.7 ……	182
Table A5	Experimental data presented in Figure 4.8 ……	183
Table A6	Experimental data presented in Figure 4.9 ……	184
Table A7	Experimental data presented in Figure 4.10 …….	185

NOMENCLATURE

A	area of cross sectional area of the layer/ the matrix	[m^2]
A_i	cross area of i^{th} spring element	[m^2]
A_i	area of the spring element I (ref. ch. 5)	[m^2]
C	instantaneous mass concentration of all molecules	[kgm^{-3}]
C_0	initial mass concentration of all molecules	[kgm^{-3}]
C_2	instantaneous concentration of proteoglycan component	[kgm^{-3}]
C_{20}	initial weight concentration of proteoglycan component	[kgm^{-3}]
$\underline{\underline{C}} = \lfloor c_{ij} \rfloor$	constant coefficient matrix of stiffness	
D	drag coefficient	[Pa.s]
D, D_1, D_2	characteristic constants of the represented daspots (ref. Ch. 3)	[Pa.s]
d_i	distance between the two ends or gap of the i^{th} dent	[m]
D_v	constant coefficients of the drag in the x, y and z-directions	[Pa.s]
D_i	drag coefficient in the i^{th} direction	[Pa.s]
E	elastic modulus in the z-direction	[Pa]
E_i (i=1,2,3)	elastic modulus in the i^{th} direction	[Pa]
F	total force generated by all active springs	[N]
F_i	resulting tensile force of an active spring	[N]
$f(z)$	distribution function of permeability at the initial	[$m^4N^{-1}s^{-1}$]
H	thickness of the cartilage matrix	[m]
h	instantaneous thickness of a given layer	[m]
h	instantaneous thickness of the matrix (ref ch. 3)	[m]
h_0	initial thickness of a given layer	[m]
h_0	initial thickness of the matrix (ref ch. 3)	[m]
h_n	limit thickness of compressing (dry) matrix (ref. ch. 3)	[m]
i	index	
j	index	
K	Strain and depth-dependent permeability in the z-direction	[$m^4N^{-1}s^{-1}$]
K_0	permeability at the surface	[$m^4N^{-1}s^{-1}$]
K_i $(i=1,2,3)$	principal permeability in the *x, y and z*-directions	[$m^4N^{-1}s^{-1}$]
K_1, K_2, K_3	principal permeability coefficients in the *x, y and z*-directions	[$m^4N^{-1}s^{-1}$]
$\underline{\underline{K}} = \lfloor K_{ij} \rfloor$	symmetrical tensor of six different components of permeability	[$m^4N^{-1}s^{-1}$]
k_i	stiffness of the i^{th} spring	[Nm^{-1}]
k_v	stiffness of the instantaneous spring	[Nm^{-1}]
L	cutting depth from the surface of the lacerated matrix	[m]
l_i	length of the undeformed molecular chain in i^{th} direction	[m]
M	number of layers used for numerical analysis	
m	iteration of steps	
m	total mass of all molecules (ref. Ch. 6)	[kg]
M_2	molar mass of the proteoglycan component	[$kgmol^{-1}$]
m_s	mass of the solid skeleton in the matrix	[kg]

n	iteration of steps	
n_i	constant for a simple distribution in ith direction	
$\hat{n}$	Normal unit vector of small area	
N	number of molecular chains in the network (ref. Ch. 6)	
N	radial intervals (ref. Ch. 7)	
q	instantaneous permeability coefficient of the matrix (ref. Ch. 3)	[ms^{-1}]
Q	instantaneous permeability coefficient of the matrix (ref. Ch. 3)	[$m^4N^{-1}s^{-1}$]
Q_0	initial permeability of the matrix (ref. Ch. 3)	[$m^4N^{-1}s^{-1}$]
r	instantaneous radial displacement	[m]
r_o	instantaneous radial displacement	[m]
s	small surface area	[m^2]
S	stiffness of the matrix (ref. Ch. 3)	[Pa]
$\underline{\underline{S}} = \lfloor S_{ij} \rfloor$	stiffness matrix of element	[Pa]
t	time	[s]
T	temperature of the matrix	[^oK]
u	hydrostatic excess pore pressure	[Pa]
u_e	effective porous pressure	[Nm^{-2}]
u_o	total osmotic pressure	[Nm^{-2}]
u_{o1}	initial osmotic pressure due to proteoglycan swelling	[Nm^{-2}]
u_{o2}	depth-dependent initial osmotic pressure of element (matrix)	[Pa]
$\bar{u}_h$	instantaneous average hydrostatic excess pore pressure	[Nm^{-2}]
V	instantaneous volumes of the element/ matrix (ref. ch. 3)	[m^3]
V_0	initial volume of the element	[m^3]
v_d	Darcy's velocity of fluid outflow	[m/s]
v_f	velocity of fluid outflow	[ms^{-1}]
$\bar{v}_h$	average velocity of fluid outflow	[ms^{-1}]
V_b	volume of the bound fluid in a layer	[m^3]
V_f	volume of fluid content	[m^3]
V_f	volume of fluid in the matrix (ref. ch. 3)	[m^3]
V_s	volume of solid skeleton in the matrix	[m^3]
V_u	volume of the unbound fluid in a layer	[m^3]
w	length of a layer	[m]
w_i	instantaneous lengths of the element in the i^{th} direction	[m]
w_{i0}	initial lengths of the element in the i^{th} direction	[m]
x	change in displacement of the surface (ref. Ch. 3 &5)	[m]
x_{si}	change in the length of the i^{th} active spring	[m]

GREEK

ΔA_{fi}	total cross-section area of pores in the ith direction	[m^2]
$\Delta\pi$	change in osmotic pressure due to Donnan effect	[Pa]
ΔV_b	change in the volumes of the bound fluid (ref. ch. 5)	[m^3]
ΔV_f	change in fluid content	[m^3]
ΔV_{fi}	volumes of pores, which fluid flows through it in ith direction	[m^3]
ΔV_u	changes in the volumes of the unbound fluid (ref. ch. 5)	[m^3]
Δx	change in displacement at the matrix surface	[m]
γ	gravitational density of the fluid	[Nm^{-3}]
ε	instantaneous volumetric strain of the matrix	
ε_{ii}	normal strain of element in ith direction	
ε_{sw}	limit of strain where the solid skeleton being active	
θ	angular displacement in cylindrical coordinate	[rad]
λ	volumetric stretch ratio of the deformation of the element	
λ_i	principal stretch ratio of the deformation of the element in ith direction	
μ	constant coefficient	[m^2]
μ	constant coefficient (ref. Ch. 3 and 5)	[s]
μ_i	constant coefficient in ith direction	[m^2]
ν_{ij}	Poison's ratios of the anisotropic material	
σ_a	applied stress	[Pa]
ρ	matrix overall density	[kgm^{-3}]
ρ_f	fluid content density	[kgm^{-3}]
Φ	depth-dependent stiffness coefficient	[Pa]
Φ_0	stiffness coefficient at the surface of the matrix	[Pa]
$\underline{\underline{\Phi}} = [\Phi_{ij}]$	depth-dependent stiffness coefficient matrix	[Pa]
ϕ	porosity	
σ_i	total stresses in the ith directions in a given element	[Pa]
ω	constant coefficient	
σ_s	stress generated by the solid component	[Pa]
σ_{s0}	initial solid stress balanced to the initial osmotic pressure	[Pa]

STATEMENT OF ORIGINAL AUTHORSHIP

The work contained in this thesis has not been previously submitted for a degree or diploma at any other higher education institution. To the best of my knowledge and belief, the thesis contains no material previously published or written by another person except where due reference is made.

Signed: _____

Date: _____

ACKNOWLEDGMENTS

The preparation of a substantial work such as this is impossible without the assistance and advice from a number of people. I would like to take this opportunity to acknowledge all those people who have in some way contributed to this work. A person I owe a great debt is my Principal Supervisor, Dr. Adekunle Oloyede, whose character will always remember in my mind. I would not have been able to remain sufficiently motivated to complete this complicated research without his support, encouragement, good humour and gentle advice on the fundamental knowledge as well as documentary support to the financial sources for my living conditions. The director of the Centre for Rehabilitation Science and Engineering at Queensland University of Technology, Professor John Evans, deserves my sincere thanks for his constant commitment to this research. I also thank to my Associate Supervisor, Dr Ian Turner for the advice on mathematical modeling at the beginning of the research and help to proof read the thesis.

The great deal of the experimental work contained herein was conducted by or with the assistance of many people. I would like to thank Dr. Adekunle Oloyede for advising me in developing the equipment designs for the experiments and the technician in setting up the experiment.

Finally, I would thank all my friends and colleagues with their encouragement and support to complete this thesis.

Chapter 1: Introduction

1.1 Background

The fundamental reasons for interest in articular cartilage research are the tissue's importance to joint function, and its susceptibility to osteoarthritis and related diseases. The Center for Disease Control and Prevention in Atlanta, GA statistical data (October 2002) revealed that nearly 70 million adults in the United States suffer from arthritis and chronic joint symptoms [1]. Arthritis and other rheumatic diseases are the number one cause of disability in the United States. According to the National Arthritis Action Plan [2], the costs of treatment and rehabilitation to the U.S. economy is close to 2% of the Gross National Product which is equivalent to $65 billion per year in medical care and lost wages. With obesity on the rise and more than half of American adults currently overweight or obese, there is likely to be an increase in this painful joint condition and it is projected that over 40 percent of the population will become affected by 2020 at an estimated cost of $95 billion over next few years [2].

According to the document released by The Canadian Orthopaedic Association (COA) and The Arthritis Society (TAS) in Toronto, Ontario (April 2001) [3], 42% of Canadians were affected by joint and bone problems including arthritis in 1997 [3] with a total cost of $17.9 billion spent on the treatment and rehabilitation of patients.

McCormick et al. (1995) [4] found that 45% of adults in the United Kingdom (UK) have experienced pain caused by arthritis and related conditions for at least one week in 1991-1992; and 7.1 million UK adults report long-standing ill-health due to this disease in 2000. The estimated total real cost to the UK's national health services in 1998/1999 for arthritis and related conditions was £1.11 billion including £675 million for arthritis and an equivalent loss of production of £18.114 billion in 2000 [5].

In Australia, Arthritis is a major cause of disability and chronic pain affecting an estimated 3.1 million people [6]. The overall financial cost of arthritis and associated diseases in Australia is enormous, approaching $9 billion per annum, which was equivalent to 1.4% of gross domestic product in 2000.

The overwork and low living standard in poorer countries may also cause excessive loading of the joint, which may result from repeated untreated injuries or deformity affecting people at an earlier age, with associated progressive cartilage wear and tear. The number of people affected by one form of arthritis or another in the developing countries may be much higher than that in the developed countries, but this has not been documented yet. Some Asian governments and organizations consider this disease a serious matter and have spent billions of dollars in their campaigns to seek a lasting solution.

Most of these diseases pose significant clinical and socio-economic problems, and often necessitate surgery or cartilage transplantation. For cartilage transplantation especially the donor or patient's own articular cartilage is used with associated problems such as the impairment of the area of the patient's joint in which tissue is harvested, rejection of donor cartilage and transmission of disease between donor and recipient. Even more important is the increasing shortage of donor material with an increasing number of joint injuries and age-related osteoarthritis as humans become more active in sports and fitness activities, and with more and more people living longer. This situation necessitates alternatives, such as the creation of replacement artificial biomaterials and tissue-cultured materials for articular cartilage. In order to do this successfully the fundamental and functional properties of articular cartilage need further resolution and mathematical models are very important in obtaining such insight.

Osteoarthritis

Arthritis is a painful condition that affects the articulating joints of humans and mammalian animals. There are more than 100 different types of this disease and it is usually accompanied by swelling, heat, aches, pains and redness of the joint. Some forms of arthritis can result in substantial or complete disability if left untreated. Others may cause only a mild discomfort that may be controlled with medication and other types of treatment.

The most common forms of arthritis are osteoarthritis, rheumatoid arthritis, gout, pseudogout and ankylosing spondylitis [5]. These five account for more than half of all

types of arthritis diagnosed in the world today. Osteoarthritis is the most common kind of arthritis, and is a degenerative joint disease, which is a consequence of the wearing out of the cartilage that covers the ends of articulating joint bones. Rheumatoid arthritis is one in which the body attacks itself and is commonly painful and can sometimes result in substantial or complete disability (Silman and Hochberg, 2001). It causes joint stiffening, swelling, and renders full joint movement difficult and painful, and for unknown reasons, it attacks women more than men. Gout and pseudogout are types of arthritis, resulting from uric acid crystals deposited in the joint. They are among the most painful diseases known to mankind and are far more common than most people believe (Silman and Hochberg, 2001). Another type is ankylosing spondylitis that affects almost exclusively men in the lower back and also spreads between the spine's vertebrae, causing permanent stiffening and severely affecting bending, twisting and stretching causing intense pain. The most common age for the onset of this disease is between 18 and 28 years.

Mathematical Models of Articular Cartilage

Due to the large occurrences of this serious disease, there is a need to know more about articular cartilage and its load-induced properties, with a potential outcome of cost reduction in treatment and the tissue engineering of replacement cartilage for cartilage transplant surgery. Because of the functional requirements, such materials must possess both adequate strength (load-carriage stiffness) and toughness (resistance against fracture propagation). Consequently, it is necessary to develop realistic models of articular cartilage to predict and benchmark its strength, stiffness and swelling properties so that the biomechanical efficacy of replacement cartilage biomaterial can be assured.

Over the years many models have been introduced to represent articular cartilage, ranging from elastic, viscoelastic, electro-mechanic, bi-component, biphasic, to the triphasic, but there has not been a “perfect” model that can reconcile fully the experimental data obtained from loaded samples of this important tissue (Chen et al., 2001; Oloyede and Broom, 1993 (b), 1994 (a), 1996). The models based on mixture theory predict certain aspects of the stages of cartilage transient deformation (Lai et al.,

1991; Mow et al., 1989) but exhibit gross inadequacy in their agreement with the tissue's response in the early stages of loading (Brown and Singermann, 1986; Chen et al., 2001; Oloyede and Broom, 1993 (b), 1994 (a), 1994 (b), 1996). Several experimental methods yielding insight into the behaviour of loaded articular cartilage have been published in the literature to study the intact material (Bentley and Minas, 2000; Burton-Wurster et al., 1993), and models of degenerate matrices of the tissue (Atkinson and Haut, 1995; Buckwalter and Mankin, 1997; Mizrahi et al., 1986; Myers et al., 1995). Exceptionally, the consolidation experiments have presented the most promising methodology for studying experimental models of the tissue, such as the intact, proteoglycan-depleted (Oloyede and Broom, 1994 (a), 1994 (b), 1996), lipid-depleted (Oloyede et al., 2003).

Consequently, the basis for this thesis is the application of the principle of mechanical consolidation to the prediction of the behaviour of the loaded cartilage matrix. To this end, previously published models are reviewed and a continuum hybrid model incorporating both phenomenological and fundamental principles is developed based on poroelasticity and mechanical consolidation theory. The mathematical model results in a system of equations that is solved using MATLAB software for numerical analysis. The results are then compared to experimental data to establish parameters of the model and used thereafter to predict the behaviour of the normal, damaged and degenerative cartilage matrices. This work establishes a basis for future research on cartilage or its disease, and the evaluation of artificial replacement materials for the tissue.

1.2 Problem Definition

Articular cartilage is a load-bearing gel that consists of three major components, namely a 3D collagen fibrillar meshwork, negatively charged proteoglycan aggregates and water. Any applied load would act to generate three types of stresses and pressures within the matrix, namely, solid skeleton stress, fluid hydrostatic excess pore pressure and the Donnan osmotic pressure which is due to the fixed charged ions. Most published models account for the fact that cartilage contains fluid and solid constituents (Lai et al., 1991; Lanir, 1987 (a), (b); Mow et al., 1980, 1989, 1990; Simon, 1990; Spilker et al., 1992). The triphasic model (Lai et al., 1991) includes an extra component

to represent the effect of swelling and osmosis in the loaded and unloaded cartilage matrix.

It has been argued that the structure and interconnectivity of the components of the matrix right up to the ultramicroscopic level is that of a continuum of functionally indistinguishable elements. Harrigan and Mann (1987) argued that if the cartilage matrix is considered with respect to its function, only models relying on several defined state variables are most likely to accurately describe its structure and predict its load-induced behaviours. This is in contrast to the philosophy embraced by most of the other models (Lai et al., 1991; Lanir, 1987 (a), (b); Mow et al., 1980, 1989, 1990; Spilker et al., 1992; Suh, and Bai, 1997) which have described the tissue, but suits the phenomenological approach of the concept of poroelasticity. This continuum approach is well accounted for in the theory of mechanical consolidation (Biot, 1941; Biot and Willis, 1957; Terzaghi, 1947). Specifically the biphasic, triphasic (Lai et al., 1991; Mow et al., 1980; 1989; 1990; Spilker et al., 1992) and biocomponent (Lanir, 1987 (a); (b)) models consider an isotropic mixture of components and adopt a control volume approach to the mathematical description of the tissue. Because articular cartilage is a heterogeneous material with dissimilar layer properties from its top to bottom, and since its components act in unison during function, their models could not represent its functional response to load, with the consequence that a new more representative model such as that developed in this thesis is required.

It is proposed in this research that any model for describing the function of the cartilage gel structure is best developed using a continuum approach such as found in the theory of consolidation of fluid saturated poroelastic materials.

Various gaps can be identified in the existing models of articular cartilage, with the leading models accounting for certain characteristics of the cartilage material and physiological function. The chart shown in Figure 1 summarizes the various components of the existing models (marked with ×) while also highlighting the important characteristics of articular cartilage that are omitted. It can be seen that even the leading models of articular cartilage, such as the triphasic model, contain very important omissions. It is the inclusion of these omitted properties that is the main focus of this thesis.

Articular cartilage architecture	**Solid** (collagen and proteoglycans) Anisotropy, depth dependence, nonlinearity and large deformation								**Fluid** Anisotropy, depth and strain dependence						FCD Depth & strain dependence		Interaction between components
	Stress-strain relationship								**Continuity equation**						**Osmotic effects**		**Drag effect**
Models	Isotropy	Anisotropy	Homogeneity	Heterogeneity	Linearity	Nonlinearity	Small strain	Large strain	**Darcy's law**	**Permeability** Constant	Strain dependence	Position dependence	Isotropy	Anistotopy	Strain dependence	Depth dependence	Strain-rate dependence
Biochemical model															×	×	
Viscoelastic model	×		×		×		×			×			×				
Biphasic model	×		×		×		×		×		×		×				
Triphasic model	×		×		×		×		×		×		×		×		
Mixture-based extended models	×	×	×	×	×	×	×		×		×		×		×		
Poroelastic model	×		×		×		×		×		×		×				
Hyperelastic model	×			×		×		×	×	×							
Appropriate model		×		×		×		×	×		×	×		×	×	×	×

Figure 1: Comparison chart of existing models and appropriate one. (FCD = Fixed charged density)

1.3 Principal Parameters of Articular Cartilage Structure and Function

Permeability

The response of articular cartilage during its load-bearing function is closely related to its permeability which in turn relates to the state of its solid skeleton of swollen proteoglycans entrapped in a three-dimensional collagen meshwork. This parameter varies significantly between healthy and degenerate matrices (Mansour and Mow, 1976; Maroudas and Bullough, 1968). In an experiment where degeneration of articular cartilage was modelled by proteoglycan digestion it was shown that the hydrostatic excess pore pressure, which is an expression of the behaviour of the fluid within the loaded tissue, exhibited dissimilar patterns with time for normal and proteoglycan-depleted matrices (Oloyede and Broom, 1994 (a), 1996). This work demonstrated conclusively that altering the characteristics of the internal structure of the tissue modifies its permeability with significant consequences for its function. Permeability has been proposed to vary with time or strain and the level of applied loading, or a combination of all of these parameters (Higginson et al., 1976; Lai and Mow, 1980; Lai et al., 1981; Mow et al., 1987).

In this thesis the permeability coefficient of articular cartilage is related to the distributed and variable nature of its structure which varies from its superficial layer to the tidemark at the bone end. Therefore, a key addition in this research is the creation of a "submodel" of the permeability's dependence on position within the matrix. This is super-imposed on the variation with deformation parameters so that the influence of structure on this parameter is uniquely accounted for.

Articular Cartilage Stiffness

The variation in layer structure (Glenister, 1976) and the deformation mapping of Schinagl et al. (1996, 1997) suggest a high probability of a position-dependent stiffness as a fundamental characteristic of articular cartilage. Furthermore, the stiffness of the matrix has been previously argued to be hyperelastic and anisotropic in nature (Barocas and Tranquillo, 1997; Chen et al., 2001; Singhnal et al., 1996, 1997; Woo et al., 1979).

While such experimental observations have been modelled with finite element analysis (Ateshian et al., 1997; Mukherjee and Wayne, 1998; Oloyede and Broom, 1993 (b), 1994 (a), 1994 (b), 1996; Torzilli, 1990; Li et al., 1999; Woo et al., 1976), there has been no inclusion of a hyperelastic anisotropic stiffness in any existing mathematical models which can adequately represent the heterogeneous nature of this specialized biological gel. This imperative will be addressed in the new model presented in this thesis.

Continuity of fluid flow

The relatively large volume of fluid content and its transient percolation through the ultra-low permeable matrix of articular cartilage under load is best described by Darcy's law, and its relationship to the solid skeleton's deformation has been shown to be similar in pattern to those observed in swelling clays and soils whose responses can be predicted by the principle of mechanical consolidation (Jacob, 1967; Kezdi, 1979; Klausner, 1991; Malvern, 1969; Terzaghi, 1943). To date there is no rigorous model of cartilage, which mathematically and explicitly describes the relationships between cartilage fluid responses, osmotic swelling potential and its hyperelastic stiffness. This will be addressed in this thesis where fluid flow, large skeleton deformation, variable and distributed permeability and osmotic swelling will be accounted for within the framework of the principle of mechanical consolidation.

1.4 Objectives of Research

The research objectives in this thesis include, but are not limited to the following:

(i) Appraisal of existing theoretical models of articular cartilage, with specific reference to the fundamental properties of this specialized gel.

(ii) Development of viable rheological models of articular cartilage which can be used to predict and study the effect of various parameters on the tissue's load-induced responses. The results of this study will then contribute insight into the key parameters to be considered for the generalized mathematical model. For example a submodel of

permeability variation will be carried out.

(iii) Development of a phenomenological model which combines the capabilities for predicting the large strain deformation and other characteristics of articular cartilage within the framework of mechanical consolidation and poroelastic deformation theory.

(iv) Experimentally investigate the responses of normal intact and lacerated matrices under load and one-dimensional constraints, and use the result to validate the ability of the model to predict observable phenomena of articular cartilage normal physiological characteristic, wear and tear as a result of age, function, trauma, and disease. These analyses will include predictions of the consolidation hydrostatic excess pore pressure, swelling pressures and solid skeleton responses in loaded articular cartilage.

1.5 Layout of Thesis

* Chapter 1 provides a brief insight into the arthritis disease and outlines the main motives for modelling the biomechanical properties of articular cartilage. The capabilities and short coming of previous models are summarised and the objectives, method of modelling and structure of the thesis are stated.

* Chapter 2 presents the structure and architecture of articular cartilage in accordance with the literature.

* Chapter 3 details the mathematical description of the previous rheological analogue. The model is analysed numerically to determine the important parameters for viable analogues of the matrix. The new ‘series’ and ‘parallel’ analogues and their mathematical descriptions with their numerical predictions are discussed.

* Chapter 4 presents the consolidation experiments on normal intact and lacerated matrices of articular cartilage using the consolidometer and one-dimensional constraints.

* Chapter 5 gives a detailed analysis of the numerical solutions for the mathematical

equations for the rheological analogues including the comparison between the normal intact matrix, and those containing shallow lacerations.

* Chapter 6 presents the theoretical formulation underling the generalised model including the new permeability submodel in Cartesian and cylindrical coordinates.

* Chapter 7 provides an application of the generalised model to one-dimensional confined normal matrix of intact and lacerated, and the unconfined normal matrix.

* Chapter 8 presents the conclusions on the representative capacities of the models developed in this thesis.

Chapter 2: Articular cartilage matrix and the existing models.

2. 1 Introduction

Cartilage is a relatively soft tissue found in many parts of the body, such as the nose, ear, and joints. Articular cartilage is the hyaline type that covers the ends of the long bones in the knee, shoulder and hip joint to facilitate load-carriage and lubrication within the synovial environment, for example, as shown in Figure 2.1. It is not enervated, has no lymphatic drainage and is avascular. Nutrition is provided by diffusion from the surrounding synovial fluid (Elmore et al., 1963; Kempson, 1979).

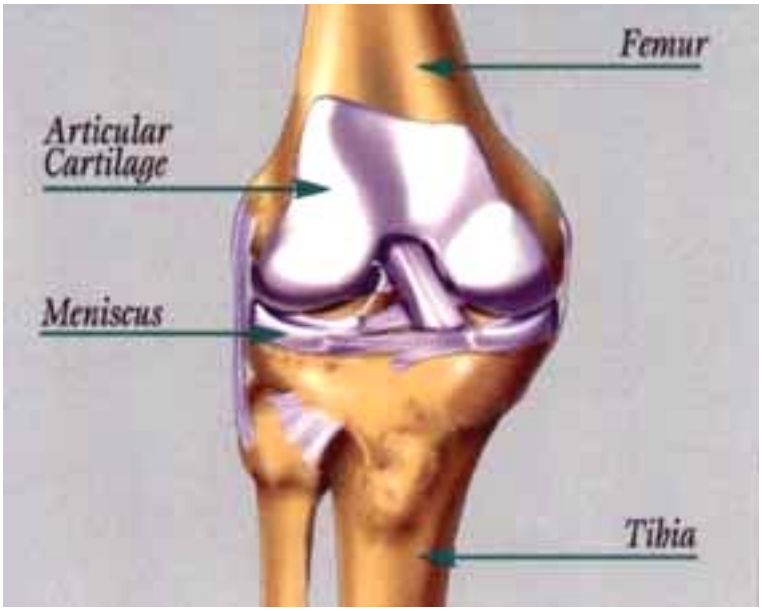

Figure 2.1: The mammalian joint showing the location of articular cartilage and the meniscus cartilage

The thickness of articular cartilage ranges from 2 to 4mm, comprising a complex structure that is made up of chondrocytes, proteins and sugars that are interwoven in a deliberate architecture (Kempson, 1979). Its complex structure can withstand enormous compressive forces and is capable of creating a low friction surface for the joint to glide on.

The architecture of articular cartilage and its function, as well as the mathematical and rheological models developed to predict its response to load are reviewed in this chapter.

2.2 Function of articular cartilage

Articular cartilage is a fibrillar, hydrated connective tissue. There is wide agreement in the literature that cartilage functions as a highly optimised articulation tissue which is able to redistribute, and slowly transmit applied stresses to the subchondral bone (Grodzinsky, 1983; Maroudas, 1979; 1985; Mow and Ratcliffe, 1997; Weightman and Kempson, 1979), whilst also providing joint lubrication by virtue of the characteristics of its superficial layer. Several authors have proposed different lubrication mechanisms such as weeping (McCutchen, 1975), boundary effect (Afoke et al., 1987; Ateshian, 1997; Lipshitz et al., 1975; Mow and Ateshian, 1997), hydrodynamic (Anderson et al., 1990; 1993; MacConnail, 1951; McCutchen, 1980), for the joint where articular cartilage facilitates lubrication. This thesis does not consider cartilage/joint lubrication but contemplates the biomechanical properties of the matrix under a static load that is important in biomechanical engineering in the study of the normal and degenerate articular cartilage.

2.3 Architecture of articular cartilage

Articular cartilage has a very specific zonal structure that is thought to determine its unique mechanical properties. It is believed to consist of four hypothetical layers, namely the superficial or articular surface, two midzone layers and a calcified region (Broom, 1982, 1984, 1986; Broom and Silyn-Roberts, 1989; Myers and Mow, 1983). The superficial or tangential layer consists of bundles of collagen fibrils which are aligned parallel to the articular surface, and occupies about 5-10% of the matrix volume with a low proteoglycan content (Glenister, 1976; Maroudas, 1985). The transitional or midzone layer, which is 40-45% of the matrix volume, contains a significant increase in the proteoglycan content, together with a complex, three-dimensional network of collagen fibrils which exhibits an overall radial arrangement of elements that repeatedly interact along their length through the cartilage depth. The fibrils in this pseudo-random meshwork interact to form a cross-link that determines the three-dimensional cohesivity of the matrix (Broom and Silyn - Roberts, 1989; 1990). The deep or radial layer also occupies 40-45% of the matrix volume with a high proteoglycan concentration (Maroudas 1979; Maroudas et al., 1969; 1987; Preston et al., 1972). The fibrillar

meshwork in this region is similar to that in the transitional layer. The calcified cartilage layer, which occupies the region from the tidemark to the cement line (bony end), is heavily impregnated with crystals of calcium salt and is devoid of proteoglycans but contains more smaller chondrocytes in comparison to those in the deep layer.

In consequence, articular cartilage is a highly heterogeneous, anisotropic and multiphase biomaterial consisting mainly of collagen fibrils, proteoglycans and water. The collagen fibrils in the deep zone (near the bone) are perpendicular to the cartilage-bone interface; they are somewhat randomly oriented in the middle zone, and there is a very thin layer of a maximum depth of 200μm at the surface where fibrils run parallel to the surface of the cartilage. The proteoglycan concentration also varies with depth within the cartilage. It is maximum in the middle zone and is significantly reduced near the surface (Urban et al, 1979). In the deep zone, the cells are round and oriented perpendicular to the cartilage-bone interface, while they are flattened and oriented parallel in the superficial layer.

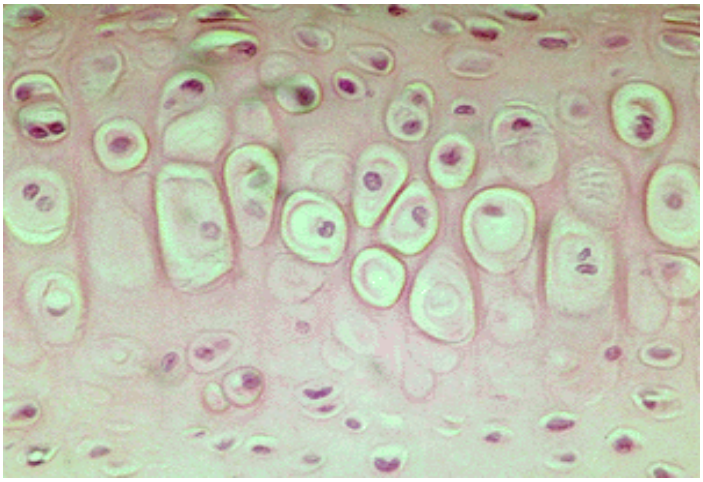

Figure 2.2: The microstructure of articular cartilage showing the chondrocyte cells [7].

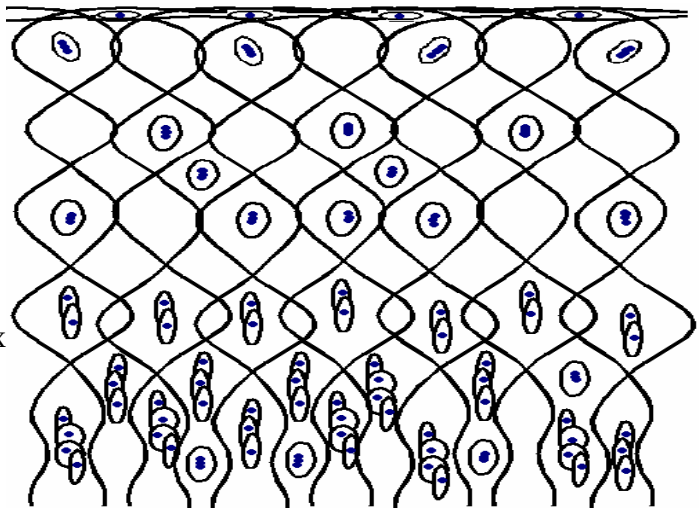

Figure 2.3: Schematic illustration of type II collagen meshwork and the cell distribution and orientations in the articular cartilage matrix

Figure 2.2 shows the microscopic structure of the articular cartilage, with the cells surrounded by the extracellular matrix, the major components of which are collagen and proteoglycans. Figure 2.3 is a schematic representation of the arrangement of collagen fibrils and the distribution of proteoglycan concentration in the matrix.

2.4 The composition of the articular cartilage matrix

The matrix of articular cartilage mainly consists of a 3-D network of type II collagen fibrils that entrap an aggregation of water-swollen proteoglycan macromolecules (Bentley and Minas, 2000; Broom and Marra, 1985; Broom and Silyn-Roberts, 1989; 1990; Quinn et al., 1998). The schematic picture of the cartilage is shown below in Figure 2.4.

This figure is not available online.
Please consult the hardcopy thesis
available from the QUT Library

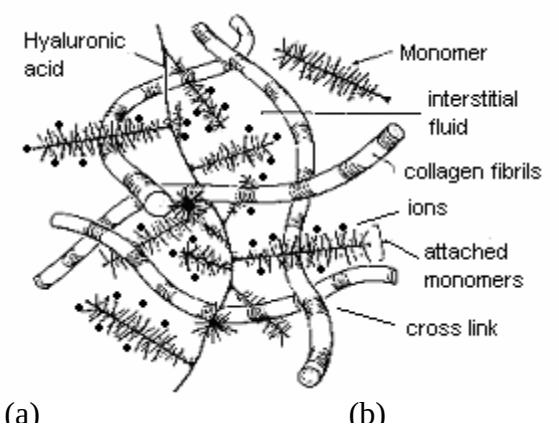

Figure 2.4: Idealized schematic illustration of the cartilage architecture.
(a) Spatial relations of collagen, proteoglycans, and cells in articular cartilage. In this diagram, 1 represents type II collagen; 2- chondrocyte; 3-proteogycan (Bentley and Minas, 2000). (b) Collagen meshwork entraps swollen proteoglycans.

2.4.1 Type II Collagen

Collagen fibrils account for about half the dry weight or about 20- 30% of the wet weight of articular cartilage (Broom and Marra, 1986; Broom and Silyn - Roberts, 1989; Maroudas, 1985). They are composed of aggregates of molecules known as tropocollagen which consists of three polypeptide chains wound around one another in a superhelix, which is formed by the combination of three identical amino acid chains (alpha 1(II)), approximately 1000 amino acids long (Bentley and Minas, 2000).

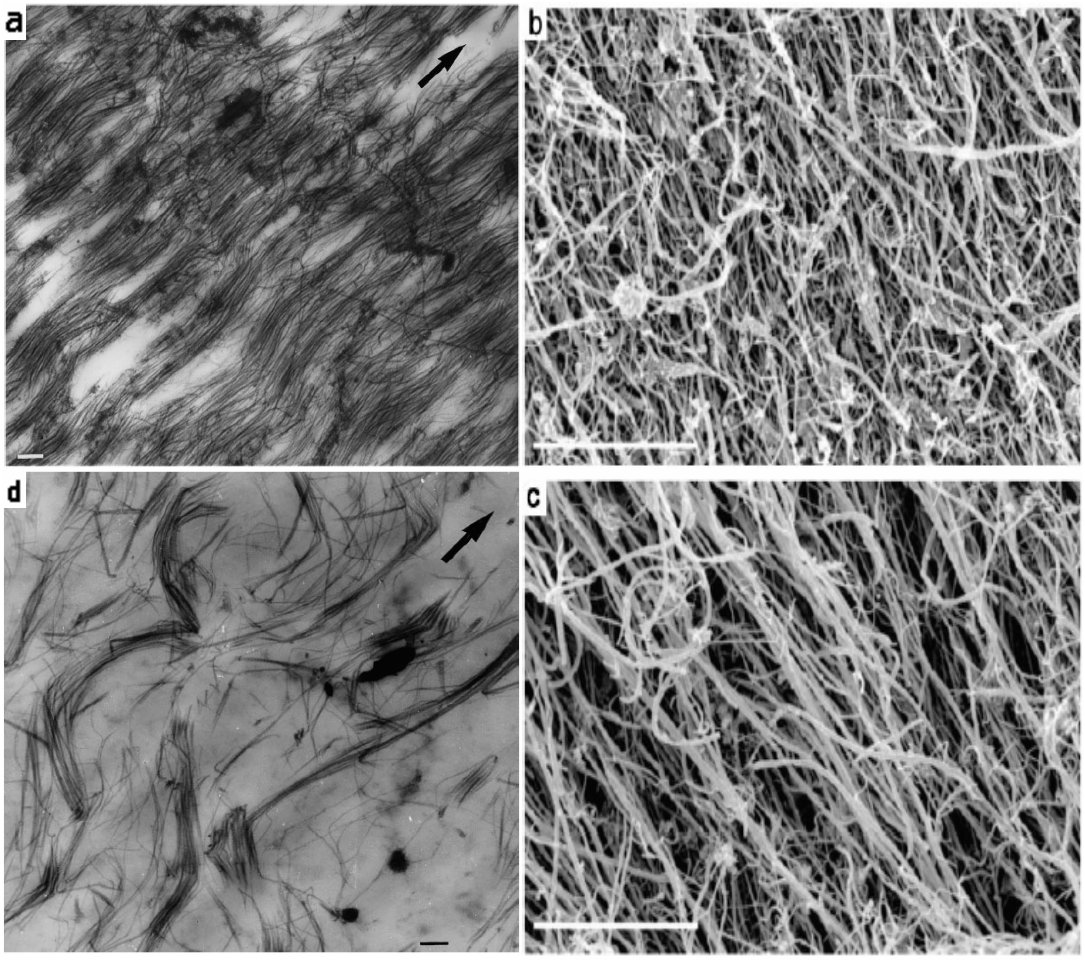

Figure 2.5: TEM of the softened general matrix structure (a), the transition from clearly fibrous to the normal matrix in the osteoarthritic cartilage (b, c) and the softened general matrix with some fibril aggregation (d). The arrows indicate radial directions. Bar of 0.5 μm (a, c) and 5μm (b,c). (Broom et al, 2001; Chen and Broom, 1999)

The general pattern of its microscopic appearance is uniform in the fibril concentration but exhibits a different arrangement among the adult population (Eggli et al., 1988; Oloyede and Broom 1996; Schenk et al., 1986). The thickness, density and alignment of collagen fibrils vary from the superficial zone, where fibrils are oriented parallel to the articular surface, to the mid- and calcified zones, where fibrils are orientated perpendicularly to the boundary between bone and cartilage. Most collagen fibrils of the normal cartilage are arranged radially as shown in Figure 2.5a and form cross-links between molecules and between the three chains of polypeptide. These collagen fibrils, like tropocollagen, are stabilised by the covalent cross-links between adjacent fibril monomers. This arrangement of collagen fibrils changes under loading and is affected by degenerative processes (figures 2.5b-2.5c).

2.4.2 Proteoglycans

Proteoglycans (Figure 2.6) constitute approximately 30% of the dry weight of the cartilage, and consist of a protein core to which is attached side chains of glycosaminoglycan (GAG) with different disaccharide repeating formation (Broom and Silyn - Roberts, 1990; Buschmann and Grodzinsky, 1995; Fosang et al., 1996; Kempson et al., 1976; Maroudas, 1979; Maroudas et al., 1969; Ogston, 1970; Oloyede and Broom, 1994). Keratan sulphate and chondroitin sulphate of GAG are bound to the central region of the protein chain. Many thousands of chondroitin sulphate molecules and many hundreds of keratan sulphate molecules are present in one aggrecan molecule. The amino terminal end of the protein chain of aggrecan is non-covalently bound to hyaluronic acid (HA), which is also a GAG chain composed of disaccharide repeats and has many aggrecan molecules attached along its length to form a branched structure of the proteoglycan.

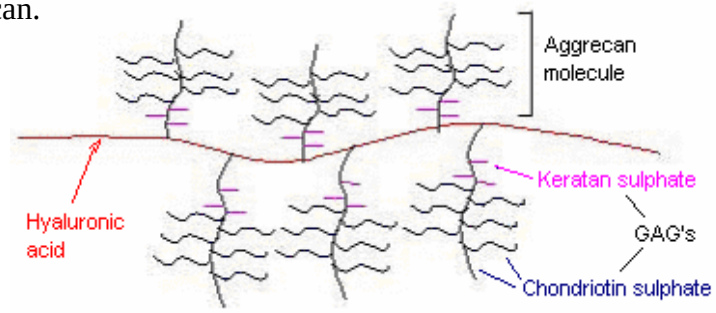

Figure 2.6: Schematic illustration of the proteoglycan macromolecule, which is based on the published works (Kempson et al., 1976; Maroudas, 1979;Maroudas et al., 1969; Ogston, 1970).

The GAG chains of the aggrecan molecule have a negative charge resulting in numerous counter ions that are associated with the chains (Broom and Oloyede, 1998; Kempson et al., 1976; Khalsa and Eisenberg, 1997; Myers and Mow, 1983; Pickard et al, 1998; Valhmu et al, 1998). The associated ions drawing water to the proteoglycan content of the cartilage roughly vary inversely with the collagen content, being lowest in the superficial layer and increasing with the depth from the articular surface (Hunziker, 1992). They combine with the collagen fibrils and fluid to create the three-component biological gel that makes up the matrix. Under applied load, the cartilage fluid is pushed out, resulting in an increase in its osmotic pressure, thereby ensuring the equilibrium of the system. The osmotic pressure is much greater than the applied force

when the load is removed, and the cartilage is rehydrated. Hence, proteoglycans in the cartilage act like a sponge that cushions the underlying bone responding to any applied forces. The expansion and contraction of the proteoglycan matrix and the network of interwoven collagen fibrils creates a material that combines structural integrity with a degree of flexibility, ideally suited to the function of the cartilage.

2.4.3 Chondrocytes

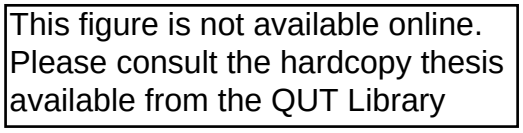

Figure 2.7: The 3-D view of human articular cartilage (**A**), the 2-D virtual sections from Fig. **A** (**B, C, D**), the processed image of **C** leaving only cell nuclei (**E**) and the cellularity as a function of depth (**F**). (Sah et al., 2002)

Chondrocytes are cells that consist mainly of water and are located within the matrix of interwoven collagen and proteoglycans (Guilak et al., 1995). The density of chondrocytes within cartilage varies (Wong et al, 1995; 1997). They are most abundant adjacent to the underlying bone, and more diffuse towards the surface of the cartilage. Chondrocytes are responsible for secreting the components of the cartilage matrix. The protein core of the proteoglycans passes through the rough endoplasmic reticulum of the chondrocytes, where the GAG chains are added. Hyaluronic acid is synthesised in the plasma membrane of the chondrocytes.

A histomorphometric analysis of localized cells indicated the distribution of the cells within the matrix as shown in Figure 2.7 (Sah et al., 2002). The figure shows that the number of cells increases downwards from the surface and then steadily through the middle and deep zones. The corresponding cell density, which decreases with depth from the articular surface, results in the non-uniform characteristic of the cartilage. Collagen is also synthesised by the chondrocytes that regulate cartilage turnover through the synthesis and release of degradative enzymes. The net activity of chondrocytes is regulated by growth factors (Wong et al, 1997).

Under compressive axial loading, the stiffness of cartilage is provided by its solid skeleton entrapment system (Basser et al, 1998; Oloyede and Broom, 1993), with significant contribution from the changing osmotic and chemical swelling of the confined proteoglycan macromolecules (Khalsa et al, 1997; Valhmu et al, 1998). During deformation, the matrix deforms due to fluid (water and ions) outflow from its different layers (Broom and Oloyede, 1998; Oloyede and Broom, 1996; Valhmu et al, 1998; Wong et al, 1995). The changes in solvent and ion concentration may also result in changes in electrical potential (Boustany et al, 1995; Eisenberg and Grodzinsky, 1985; Maroudas, 1968).

In summary, the articular cartilage is a biological gel that consists of type II collagen entrapping the fluid-swollen proteoglycans (fixed charges), ions, and chondrocyte cells. The structural arrangement produces the heterogeneity and anisotropy of this complex hydrated matrix. Under compression, the matrix environment changes to respond to the external load and all components act in unison in reaction to the applied pressure, thereby leading to the hypothesis that the only realistic model for articular cartilage is one based on continuum mechanics of heterogeneous and plane-isotropic media. This type of modelling is the objective of this thesis.

2.5 Existing models

As far as is known from present research, a realistic comprehensive model for the cartilage is still not available, although there have been many models developed for this tissue in the last 30 years. A soft tissue, especially articular cartilage, is a material that

displays mechanical responses through the complicated characteristics of layer heterogeneity, anisotropy and non-linearity. To date, several models of articular cartilage have been proposed to describe its mechanical behaviour; however, none of these has addressed the full spectrum of the tissue's complex responses. In this thesis, a phenomenological approach is adopted for developing a more representative model that captures these characteristics within the framework of the principle of mechanical consolidation and poro-hyperelasticity material laws. The existing model types are reviewed in this section.

2.5.1 Biochemical models

In the earliest work by Johnson and Wilson (1967), a differential equation was developed to describe volume changes as a function of time for a cell system that is undergoing osmotically induced volume changes due to a solute that penetrates the cell membrane or boundary of the system. This study emphasized the osmotic reflection coefficient and the solute permeability coefficient as significant in determining small changes in cell volume.

Maroudas (1968, 1975, 1979) proposed relationships between permeability, diffusivity, electrical conductivity and streaming potential derived using ion exchange theory. She concluded that the concentration of fixed negatively charged groups in the cartilage was the most important parameter governing cartilage deformation. Fixed charged density was found to increase with depth into the matrix from the articular surface and this variation was found to influence other load-carriage properties (Maroudas and Bannon, 1981; Maroudas et al, 1969, 1987; Schmidt et al, 1990; Schneiderman et al, 1986; Urban et al, 1979). An estimated permeability was obtained from the study for full-thickness cartilage (Mow et al., 1980), and it was determined that there is a marked decrease in matrix permeability with increasing depth and that an inverse relationship can be established between permeability and fixed charge density of the tissue, where the fixed charge density increased with increasing depth (Maroudas and Bullough, 1968).

Furthermore, Garcia et al (1996) used neutral and charged solute to confirm the intrinsic

transport properties of the solutes (e.g. diffusivity, electrical mobility, hydrodynamic hindrance factors) and its contributions through diffusion, fluid flow and electrical migration to molecular transport through articular cartilage explants. It was demonstrated (Broom and Oloyede, 1998; Chen et al., 2001; Maroudas, 1968; 1975; Maroudas and Bannon, 1981; Pickard et al., 1998) that the proteoglycan distribution contributed to the heterogeneity and anisotropy of the cartilage matrix. Quantification of swelling effects of proteoglycans in articular cartilage has been used for its ability to detect material heterogeneity and anisotropy, as well as degenerative changes associated with osteoarthritis. Myers et al. (1995) used this technique to measure dimensional swelling changes in thin samples of bovine articular cartilage and demonstrated that cartilage swelling was heterogeneous and anisotropic. In fact, negative charges associated with the glycosaminoglycans (GAGs) give rise to an interstitial swelling pressure, which must be balanced by tensile forces in the cartilage solid network and the tractions generated when loaded (Lai et al., 1991; Maroudas et al., 1986). As a result, there exists a non-zero strain in the cartilage solid matrix in the unloaded state under physiological condition, which is practically mechanically equivalent to a residual strain. A significant swelling-induced strain was observed in the deep zone of cartilage with no evidence of a swelling effect in the superficial layer. Evidence of these swelling-induced strains include the tendency for cartilage to wrap around itself, curling upwards away from the bottom layer upon removal from the subchondral bone (Setton et al., 1997), as well as a tendency to swell, or imbibe fluid, in test baths at hypotonic concentrations (Eisenberg and Grodzinsky, 1985; Maroudas, 1976; Myers and Mow, 1983). In addition, Pickard and his co-workers (Pickard et al., 1998) investigated the role of the hydrophilic properties of the proteoglycan molecules within the cartilage. Their compression tests showed the cartilage and meniscus deform at the same rate, but the degraded cartilage deformed more quickly to reach its equilibrium. Their friction tests demonstrated that the degraded cartilage has less friction. Although the reduced proteoglycan content of the degraded cartilage substantially altered the biphasic compression response, it did not have an effect on the frictional properties of the tissue.

Consequently, the more recent attempts at modelling have been used to explain the fundamental mechanisms of load-carriage in articular cartilage relative to the intrinsic properties using various models that particularly account for the interactions between

the externally applied compressive forces and its unique physico-chemical characteristics. These studies have demonstrated the effects of swelling on the tissue's behaviour and showed the evidence for heterogeneity and anisotropy in the cartilage matrix as well as establishing that its permeability is strain-dependent. However, there is ample room for further improvement in established models in order to further understand the biomechanical responses of articular cartilage and thereby provide insight into the property requirements for replacement materials for this important tissue.

2.5.2 Viscoelastic models

Viscoelasticity, as its name implies, is a combination of elastic and viscous responses in a material and can be modeled using the spring and dashpot to idealize the linear elastic and viscous element behaviours respectively.

The earliest models of the biomechanical response of cartilage represented its matrix as either perfectly elastic or a fluid-saturated composite material with an elastic solid phase (Elmore et al, 1963; Weightman and Kempson, 1979). These models were based on the assumption that the matrix contains an elastic solid coexisting with a viscous fluid (Hayes and Bodine, 1978; Mak, 1986; Mow et al., 1990).

To study the mechanical properties of cartilage and analyze the indentation of the tissue's matrix, Hayes et al (1972) developed a linear elastic mathematical model in which the cartilage was modeled as an infinite elastic layer bonded to a rigid half space, and indented with a rigid axi-symmetric punch. This model only provided a theoretical basis for quantifying the elastic shear modulus of cartilage in situ under low loads. Based on viscoelastic theory McCutchen, (1975) proposed that a simple model for the cartilage layer was essentially a two-dimensionally distributed series of springs and dashpots and included a representation of the flow of fluid between the cartilage layers to account for heterogeneity. Experimental results obtained by Macirowski et al. (1994) in studying the response of the loaded human hip joint have shown that cartilage in the normal synovial joint is saturated with fluid, loading pressurizes the fluid and compresses the cartilage matrix, and where the saturated sponge (the cartilage matrix) is

squeezed, incompressible fluid is expressed and flows out of the matrix. Other authors (Akizuki et al., 1986; Broom and Marra, 1985; Jurvelin et al., 1995; 1997; Mow et al., 1980; Oloyede et al, 1992) have also indicated that cartilage exhibits flow-dependent viscoelasticity, anisotropy, and tension-compression nonlinearity.

While investigating the permeability of bovine articular cartilage under variable strain across fluid pressure gradients through the depth of the matrix, Mansour and Mow concluded that the permeability of the cartilage decreased as the compressive strain increased (Mansour and Mow, 1976)· They stated that the increasing compressive strain of the tissue would cause an increase in the compaction of the collagen network, generating increased frictional resistance to the flow of interstitial fluid as the fixed charge density-water ratio increased. These authors further developed a theoretical model for studying the movement of interstitial fluid through articular cartilage and the influence of this on the creep behaviour of the tissue due to a unit step load function. They concluded that there is a nonlinear interaction between the hydraulic permeability of the tissue and its compressive strain, which retards the progress of the consolidation of its skeletal structure during uniaxial compression. In this model, the equilibrium displacement of the matrix depended only on the elastic constant of the parallel spring and viscoelastic dashpot, which represented the behaviour of the solid component.

Hayes and Bodine (1978) developed a sinusoidal shear generator to measure the viscoelastic complex shear moduli for bovine articular cartilage, with inferences on the effects of its solid meshwork on this parameter. The increased cross-linking was considered to cause significant increase in the shear modulus, while proteoglycan depletion and collagen digestion caused significant decrease in this parameter. Also a viscoelastic computational model based on the finite element method was proposed (Rybicki et al, 1977) to study the role of compliant surfaces in the mechanism of operation of a squeeze film compliant bearing. They found that changes in viscosity of the lubricant had a greater influence on deformation than changes in cartilage modulus, and that the lubrication qualities of the compliant system were superior to those of rigid surfaces when the same lubricants were used.

In summary, most theoretical results of the viscoelastic models are very different from

the experimental results at high loads or large strains. It is now well known (McCutchen, 1982; Mow et al., 1987; Oloyede and Broom, 1991) that for low velocity percolation of fluid through the tissue, there is negligible viscosity thereby excluding drag in the traditional sense of this property (McCutchen, 1982; Oloyede and Broom, 1991; Oloyede et al., 1992). However, changes in permeability with deformation may lead to drag-like effects and attempts have been made to include this phenomenon in existing models (Lai and Mow, 1980; Lai et al., 1981). In this thesis, an extended model of permeability decrease with deformation will be presented. Also, matrix heterogeneity is an important factor in the structural aspects of cartilage modelling, which has not been adequately modelled in the literature. This will be accounted for in this research.

2.5.3 Mixture theory – based models

Using mixture theory, Mow et al. (1980; 1989) modelled articular cartilage as a biphasic material composed of both solid and interstitial fluid phases. The solid matrix was assumed to be linearly elastic and nondissipative and the interstitial fluid intrinsically incompressible and nondissipative. The constitutive equations that describe the homogeneous and isotropic media included viscoelastic and viscous dissipation parameters (Mow et al., 1980), i.e

$$\sigma = -PI + \lambda_s tr(E)I + 2\mu_s E \qquad (2.1)$$

where, σ is the stress of the tissue mixture (solid and fluid phases); P is the fluid pressure in the tissue; I is the unit matrix; λ_s and μ_s are Lame constants of solid matrix; E is the deformation tensor of solid matrix; and $tr(E)$ is the trace of matrix E.

Assuming constant deformation-independent permeability with a linear non-homogenous material model (Mow et al., 1990), they obtained different responses that were compared to experimental biphasic creep and biphasic stress relaxation data. They also observed a large spread in the permeability coefficients and developed an exponential function for the permeability variation with deformation (Lai et al., 1981). These authors concluded that the frictional drag from the relative motion between the fluid and solid components is the most important factor governing the apparent viscoelastic properties of the tissue in compression (Lai et al., 1981). These results agree more closely with those obtained at sites of *in vitro* cartilage failure than previous

models (Mow et al., 1980; 1987) and formed the basis for including viscoelasticity in the mixture theory for articular cartilage deformation.

The complexity of cartilage mechanical response cannot be explained by an isotropic biphasic model whether describing an impact load with high stress or load carriage with small deformation conditions. Curve fitting in situ indentation response of humeral head cartilage (Cohen et al., 1993) using the linear, transversely isotropic, biphasic model was found to predict the tension–compression nonlinear properties in good agreement with published experimental data. The linear, isotropic, biphasic models of cartilage predicted that peak stresses in the tissue occur at the cartilage–bone interface, away from the area of contact, which is at the articular surface (Ateshian et al., 1994; 1997; Ateshian and Wang, 1995; Donzelli and Spilker, 1998). This finding is in good agreement with the site of tissue failure in the impact studies of diarthrodial joints that demonstrate separation of the cartilage layer from the underlying subchondral bone (Armstrong et al., 1985; Atkinson and Haut, 1995; Thompson et al., 1991; Vener et al., 1992). Other studies focusing on the surface of cartilage immediately after loading (Bachrach et al., 1998; Haut et al., 1995; Newberry et al., 1997; Thompson et al., 1991) concluded that the failure at these sites could not be predicted by the isotropic biphasic model. It is plausible to argue that the agreement with the impact and small strain conditions is due to the fact that only very small fluid shifts, if any, are involved in deformation under such conditions, so that matrix response is essentially elastic and isotropic in nature.

Furthermore, Eisenberg and Grodzinsky (1985) studied the relationship between tissue swelling stress and the solid component for bovine articular cartilage and corneal stroma in uniaxial confined compression as a function of the ionic strength of the bathing medium. Their results showed that two concentration-dependent material properties are required to describe the chemical dependence of tissue swelling stress in uniaxial compression over the range of deformations and concentrations explored. In acknowledgement of this observation, the triphasic mathematical model incorporating three components, namely fluid, solid and ion phases, was published as a further development of Mow et al's biphasic mixture theory (Lai et al., 1991), i.e

$$\sigma = -PI - T_c I + \lambda_s tr(E) I + 2\mu_s E \qquad (2.2)$$

where, σ is the stress of the tissue mixture (solid, fluid phases and ions); $-T_c I$ is the chemical-expansion stress in the solid phase; and the other parameters were defined as in the above in this section under equation (2.1).

The model assumed the fixed charge groups remain unchanged and that the counter-ions are the cations of a single salt of the bathing solution. The authors derived a more complicated formula for Donnan pressure, T_c, which accounted for osmotic effect, and was added to the constitutive equation of the biphasic model. The result indicated that all three mechanisms are important in determining the overall compressive stiffness of cartilage.

In a further study directed at extending the biphasic theory, Mak proposed a rheological model of articular cartilage, namely a biphasic poroviscoelastic material (Mak, 1986). The creep and the rate controlled stress-relaxation experiments on articular cartilage under confined compression were analysed using this model. He concluded that both the interstitial fluid flow and intrinsic matrix viscoelasticity contribute significantly to the apparent viscoelastic behaviour of the tissue under confined compression. Some others have attempted its extended model with the depth dependence by modelling the distributions of the elastic modulus and Poison's ratio (Li et al, 1999 (a); 2000), ie

$$E_m = \hat{E}_m\left(1+\alpha_E z/H\right) \text{ and } \nu_m = \hat{\nu}_m\left(1+\alpha_\nu z/H\right) \qquad (2.3)$$

where, E_m is the depth-dependent elastic modulus; $\hat{E}_m$ is the elastic modulus at the matrix surface; ν_m is the depth-dependent Poison's ratio; $\hat{\nu}_m$ is the Poison's ratio at the matrix surface; H is the matrix thickness; α_E and α_ν are the constants; and z is the displacement from the surface.

Recent contact studies of articular cartilage have provided valuable insight into the state of stress in tissue models based on that of cartilage as solid–fluid mixtures or poroelastic materials (Ateshian et al., 1994; 1997; Ateshian and Wang, 1995; Donzelli and Spilker, 1998; Macirowski et al., 1994; Wu et al., 1998). These studies have demonstrated some agreement between predicted regions of high stress and experimental evidence of tissue damage (Ateshian et al., 1994; Buckwater and Mankin, 1997). Some observed failure modes have also been predicted with this tissue model

(Atkinson and Haut, 1995; Haut et al., 1995; Newberry et al., 1997; Thompson et al., 1991; Vener et al., 1992).

Consequently, the biphasic or triphasic models and their development address the issues of solid phase non-linearity and the matrix as non-linear, permeable, isotropic (or anisotropic), homogeneous (or heterogeneous), viscoelastic and completely filled with a dissipative fluid phase. However, these models developed from the linear viscoelasticity theory are inadequate when compared to the initial stage and longer term deformation data, or only partly adequate under conditions of very high applied stress (impact) or under experimentally small strain deformation. This contrasts with the fact that the deformation of cartilage is in general very considerable. Moreover, it is worth noting that the equations for these models have been reviewed by Simon (1990) who concluded that they are practically similar to the classical consolidation models of Terzaghi (1943) and more specifically that the generalized form of the biphasic model is the same as Biot's poroelastic theory (Biot, 1941) for soil behaviour. Furthermore, when the biphasic theory is applied to the creep behaviour of an isotropic, homogeneous, linearly elastic material, the governing equations predict a strain-time response under confined loading that is similar to Biot's results (Biot, 1941; Biot and Willis, 1957)

The concept of a consolidated solid phase may need qualification when applied to the articular cartilage matrix. The solid phase in the articular cartilage at all stages of the deformation includes the entrapped proteoglycan aggregates, so that water, necessary for gel formation, must remain intimately associated with the solid and this must be considered separate from that water which will be freely exuded during the process of consolidation. In accordance with the principle of consolidation, any interstitial fluid remaining in the consolidated matrix does not play a separate role in carrying the applied stress. Instead, a new equilibrium balance exists between this applied stress and the internal resistance to deformation offered by the proteoglycan/remaining water gel and fibrils comprising the consolidated matrix. Due to the fact that the matrix contains a quantity of this residual water during the deformation, it must be considered as in intimate association with the solid constituents of the porous material, which has been similarly modeled with poroelastic or poro-hyperelastic large strain deformation theory

(Harrigan, 1987, Oloyede and Broom, 1991). Their explanation of the existing co-relationships between the complicated structure and biomechanical properties of articular cartilage (Oloyede and Broom, 1991) provides an experimental foundation for a realistic model. However, this work currently lacks a mathematical theory to predict those properties of soft tissue.

2.5.4 Consolidation model

In engineering analysis, the classical theory of consolidation (Taylor, 1948; Terzaghi, 1943) is used to determine the pattern of behaviour of water-filled porous materials. The mechanism of this theory is shown in idealized form in Figure 2.8 (Oloyede and Broom, 1991). With this scheme, a hydrostatic excess pressure is maximized as the fluid phase initially carries the total applied stress without a solid stress. The consolidation commences with transmission of stress to the solid components and the limiting deformation is reached when the hydrostatic excess pore pressure finally decays to zero.

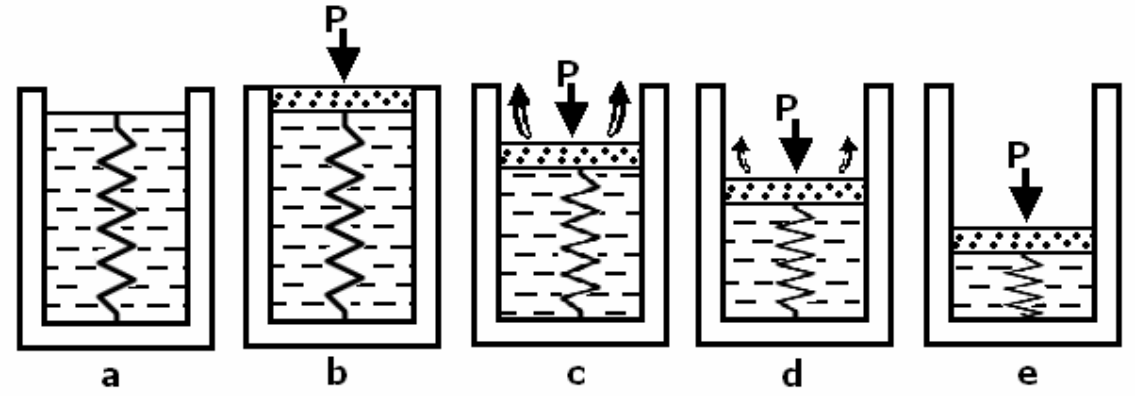

	a	b	c	d	e
% Stress carried by fluid	0	100	75	50	0
% Stress carried by spring (solid)	0	0	25	50	100

Figure 2.8: Mechanical analogue illustrating the principle of one-dimensional classical consolidation (Oloyede and Broom, 1991).

However, several factors such as the low matrix permeability (Maroudas, 1979), physicochemical properties, and non-uniform architectural rearrangements within the cartilage matrix contribute to a hydrodynamic lag in the incipient stages of its loading behaviour (Oloyede and Broom, 1991, 1993 (b), 1994 (a), 1994 (b)). This lag time is considerably longer than the delay time observed in soils. Therefore, a new

consolidation model for the articular cartilage, which accounts for its architecture and characteristics is needed to predict this consolidation response of the loaded articular cartilage matrix.

According to Harrigan and Mann (1987), an appropriate consolidation model of cartilage has to satisfy the principle of conservation of energy that consists of changes in mechanical and other potentials such as mass, physico-chemical and electrical ones, ie

$$dU = \sigma_{ij} d\varepsilon_{ij} + \varphi dm + \mu^c dc + \phi_e d\rho_e \qquad (2.4)$$

where dU is the change in the internal energy; σ_{ij} denotes total stress; ε_{ij} denotes strain; dm, dc, and $d\rho_e$ are the increments in fluid mass content, concentration, and charge density respectively; and φ, ϕ_e, and μ^c are respectively the mass potential, electric potential, and chemical potential of a known reference medium such as the saline bath in which cartilage is usually tested. These parameters of energy for a realistic model for cartilage matrix have to include all the internal factors (Oloyede and Broom, 1993 (b)) such as the physico-chemical and structural effects of the matrix, the elastic properties of the solid, the osmotic pressure, the direction effect on the diffusion and the drag when fluid diffuses through the solid for the consolidation process. These are presented in the following sections.

2.5.4.1 Continuum of cartilage

The classical theory of consolidation (Terzaghi, 1943; Taylor, 1948) is commonly used to determine the pattern of behaviour of water-filled porous materials such as soils and clays. A gradual settlement depending on the rate at which the water is being squeezed out of the voids in the porous material under load is known as soil consolidation and was first proposed by Terzaghi. He applied these concepts to the analysis of the behaviour of soil under a one-dimensional static load and successfully predicted the settlement for many types of soils. Based on these concepts, Rendulic (1936) and Biot (1941) developed the general theory of the three-dimensional consolidation where Rendulic's theory uses the bulk modulus and the Biot's involves the confined compression modulus in the similar way to that in which soil or clay loses much water

under loading. These theories work for isotropic soils, which have linear stress-strain relationships and exhibit small strain deformation under equilibrium conditions. During deformation, the water contained in the pores is incompressible and may contain air bubbles, and the outflow water is very slow through the porous skeleton and can be described using Darcy's law of percolation.

The response of the articular cartilage matrix to compressive stress involves the exudation of fluid through the articular surface (Weightman and Kempson, 1979), thereby suggesting that articular cartilage might exhibit similar consolidation behaviour to that of other porous materials. However, articular cartilage in its unloaded equilibrium state contains about 70-80% water, which is much higher than that contained by soil. This relatively higher water content proportion might require modifications to the classical theory of consolidation when applied to the deformation of this tissue. For example, the application of the consolidation principle, albeit indirectly, to articular cartilage was carried out by Higgingson et al. (1976). They investigated the behaviour and mechanical stiffness of bovine and human articular cartilage using a compression test that allows strain and slow fluid flow in the direction of loading ie. through the superficial layer. The pattern of fluid exudation observed in their work has formed the basis of many theoretical and experimental investigations into the mechanical behaviour of articular cartilage (Biot, 1941; Edwards, 1976; Higginson et al, 1976; McCutchen, 1980; 1982; Mow et al, 1980; Torzilli, et al, 1983; 1990). Some of these studies, for example in Higginson et al (1976) and in the biphasic theory of Mow et al (1980), also suggest the applicability of Darcy's law relating the rate of outflow of water to the permeability of the porous solid. The flow law is one of the key assumptions of the theory of consolidation.

Moreover, cartilage consolidation experiments have indicated that permeability decreases more rapidly with applied uniaxial strain in the direction perpendicular to loading than in the direction parallel to it (Oloyede and Broom, 1994 (a); (b)). Direct measurement of this phenomenon in a fibrous filter material with uncompressed solid volume fraction (Higginson et al., 1976) has also revealed that permeability is independent of direction at low strain and had a similar behaviour to cartilage (Oloyede and Broom, 1994 (a); (b)). A permeability-strain relationship for the articular cartilage

was developed by Lai et al (1981) and Mow et al (1987) and was often used in cartilage studies over the years, but it is not adequate for heterogeneous materials, and hence requires further development for it to be representative of cartilage whose characteristics are different from layer to layer (Schinagl et al, 1996). Consequently, a new more generalized permeability function will be developed in this thesis to represent both strain and position dependence of this parameter in the heterogeneous and anisotropic cartilage matrix.

2.5.4.2 Hydrostatic excess pore pressure in cartilage

The hydrostatic excess pore pressure generated within the porous cartilage matrix was measured and shown to exhibit a similar pattern of development and decay to that predicted by the consolidation theory, since the development and dissipation of the hydrostatic excess pore pressure of the fluid phase is of fundamental importance in the deformation of a consolidable porous medium (Taylor, 1948). Some of the past studies citing the consolidation theory have depended on the measurement of the equilibrium strain under different static loads to quantify the behaviour of articular cartilage. For example, Higginson et al (1976) used this method to establish empirically what they considered to be the relationship between solid component stress and strain in articular cartilage. The equilibrium strain parameter will be of secondary importance, especially in theoretical modeling, where the internal hydrostatic excess pore pressure can be measured directly. The fluid phase initially carries the total applied stress and a hydrostatic excess pore pressure is then developed within it (Mukherjee and Wayne, 1998; Oloyede and Broom, 1991,1993 (b)). As this pressure builds up, the fluid retains its presence within the matrix for a period and then reaches a maximum level. This pressure then immediately transmits to the solid stress until the matrix deformation reaches equilibrium when the hydrostatic excess pore pressure finally decays to zero. Oloyoede and Broom (1991) developed the experimental methodology for articular cartilage consolidation that is used in today's cartilage load-bearing analysis (Broom and Oloyede, 1992; Mukherjee and Wayne, 1998; Nguyen and Oloyede, 2001; 2002; Oloyede and Broom, 1996; Soltza and Ateshian, 1998). They showed that the time-dependent response of articular cartilage to static loading is different from that proposed for soils in the classical consolidation theory. Their results indicated that under a

compressive static load, the internal stress state that is generated over and above the intrinsic osmotic pressure involves a controlled stress-sharing mechanism between its fluid and solid constituents. They determined experimentally the influence of physico-chemical swelling on the consolidation of cartilage (Oloyede and Broom, 1994 (a)). The results indicated that the influence of glycosaminoglycan reduction was to decrease the time to reach maximum excess pore pressure, increase the magnitude of maximum excess pore pressure towards that of the applied stress, increase the level of strain induced in the matrix in order to support the same load as normal tissue and decrease the rate of decay of the excess pore pressure in the immediate post maximum excess pore pressure phase. Their results also showed that cartilage can only redistribute locally high contact stresses if the solid skeleton's effective stress is developed at levels of deformation that are sufficient to allow load-spreading, but not so high as to represent structural collapse.

In other research Oloyede and Broom (1993 (b)) studied the response of articular cartilage to compression whilst measuring simultaneously its strain and fluid excess pore pressure using a newly developed experimental apparatus for testing the tissue in its unconfined state. The results demonstrated that the patterns of the hydrostatic excess pore pressure for axial and three-dimensional consolidation were similar, but differ significantly from that obtained under the more physiologically relevant condition in which the matrix exhibits radial fluid loss when loaded either through a non-porous polished stainless steel indenter or an opposing cartilage disc. They finally concluded that consolidation is indeed the controlling mechanism of cartilage biomechanical function.

2.5.4.3 Solid-fluid interactions in cartilage

The concept of a consolidated solid phase may need to include the effect of the interaction between the components when load is applied to the articular cartilage matrix. If it is assumed that the solid phase in the articular cartilage at all stages of the deformation includes the entrapped fluid-swollen proteoglycan aggregates, so that (as mentioned in section 2.5.3) water, necessary for gel formation, must remain intimately associated with the solid and will be freely exuded during the process of consolidation.

Oloyede and his co-workers (Broom and Oloyede, 1998; Oloyede and Broom, 1996) experimentally studied the factors affecting the biomechanical properties of articular cartilage. Their results indicated that the average ratios of the maximum excess pore pressure to the normal applied stress for unconstrained and constrained loading were different and physio-chemically generated swelling played an important part in determining the internal mechanical response of the disc to an externally applied load. With special emphasis on the effect of compressive strain-rate on the short and long-term responses of the fluid and the solid components (Oloyede and Broom, 1993 (b)), the general theory of one-dimensional consolidation was used to account for strain-rate, and simultaneously obtain the stiffness due to the fluid and solid components. It was concluded that a parameter representing the degree of drag could be calculated explicitly.

Using a model of a hydrogel system (Broom and Oloyede, 1998), the experimental result showed that the pattern of stress-sharing in turn influences the manner in which cartilage consolidates or deforms in compression via the outflow of fluid. Synthetic hydrogels exposed to a variety of cationic blocking solutions provide simplified model systems for exploring quantitatively the influence of the intrinsic swelling parameter on consolidation behaviour, yielding the fundamental parameters controlling the biomechanical properties of articular cartilage. On the other hand, Khalsa and Eisenberg (1997) observed the changes in the radial and axial stress in confined compression. The results indicated that the observed change in axial stress was always substantially greater than the change in radial stress over the range of strain (5-26%) and saline concentration (0.05-0.15 mol/l) tested. The observation was described using an elastic isotropic model. The result also indicated that the shear modulus is independent of saline concentration and so is the flow-independent shear modulus. They therefore concluded that the mechanical behaviours of cartilage in confined compression could not solely be explained by changes in proteoglycan osmotic pressure only. Basser et al. (1998) used an isotropic osmotic stress technique to assess the swelling pressures of human articular cartilage and found that for normal cartilage the collagen network did not change in stiffness until the volume of cartilage had decreased by 20-25% of its initial value and that this stiffness contributed to the balance of forces in cartilage.

Consequently, it seems plausible to hypothesize that the consolidation of articular cartilage might exhibit behaviour similar in principle to that of other porous materials where the Darcy's law should be applied to model for continuity of fluid outflow. Furthermore, the hydrostatic excess pore pressure generated within the porous cartilage matrix must be measured and be shown to exhibit a pattern of development and decay as predicted by a development of the classical consolidation theory. According to the new theory, several factors such as the low matrix permeability, physicochemical properties and architectural rearrangements within the matrix would probably contribute to a hydrodynamic lag considerably longer than that observed in, for example, soil, and which will introduce a delay in the time required in the incipient stages of loading for the internal pressure of the matrix.

2.5.5 Cartilage hyperelasticity and poro-hyperelastic model

The constitutive behaviour of a hyperelastic material is defined as a total stress-strain relationship which is normally non-linear and which is derived from the strain energy developed in the material under load.

Higgingson and Snaith, (1979) determined a limited range of response to oscillating loads of physiological magnitudes and frequencies where cartilage was approximated to a simple linear/elastic solid, hereby discussed earliest statement about a need for its general mechanical description as a non-linear, time-dependent, visco-elastic solid.

The localized stiffness of the solid component would not accurately represent the true material properties of the cartilage matrix (Kelly and O'Conner, 1996; Schinagl et al., 1996). An elastostatic model of rapidly loaded articular cartilage was presented by Kelly and O'Connor (1996), where they considered the case of a small change of volume due to the interstitial fluid outflow while loaded instantaneously. They found that the localized tensile stresses occur in regions close to the cartilage-bone interface as well as at the articular surface. However, Schinagl and his coworkers (1996) used the video epifluorescent microscopic method to determine the equilibrium confined compression modulus of articular cartilage as it varies through the depth of the tissue. Their results indicated the non-linear relationships between displacement, composition

and structure, thereby illlustrating the heterogeneous property of normal articular cartilage. The variations are reflected in depth-dependent cartilage mechanical properties. Therefore, the classical mechanical testing methods to obtain measurements on the surface may not accurately describe the true material properties.

Simon (1990) surveyed recent applications of poroelastic and mixture-based theories and the associated FEMs for the study of the biomechanics of soft tissues. Equivalent finite-strain poroelastic and mixture continuum biomechanical models were presented and special attention was given to the identification of material properties using a porohyperelastic constitutive law and a total Lagrangian strain formulation. He indicated future directions for research in this area and suggested that a realistic model of cartilage matrix should include viscoelasticity, transport phenomena and a swelling component. In consequence, the classical consolidation relationship can be extended for a heterogeneous porous hyperelastic material and this will be done in this thesis. The required consolidation model would consist of the characteristics which will be discussed in the following sections.

2.6 Requirements for the development of cartilage consolidation models

2.6.1 The biosynthesis of the load-bearing structure of articular cartilage

There is wide agreement in the published literature that cartilage functions as a highly successful mechanical tissue which is able to redistribute and transmit applied stresses to the subchondral bone, whilst also providing joint lubrication by virtue of the mechanical manifestation of the physico-chemical characteristics of its fluid-swollen solid skeleton (Grodzinsky, 1983; Maroudas, 1979; Mow et al, 1993; Mow and Ratcliffe, 1997; Oloyede and Broom, 1994; Weightman and Kempson, 1979). This specialised load-bearing union of components, which when separated would be unable to carry compressive loads on their own, is analogised in the balloon-string model (Broom and Marra, 1985). Specifically, the three-dimensional array of strings in this physical model would be unable to support a significant compressive load without collapsing in the absence of the swollen balloons that it entraps.

In principle, this analogue represents a stiff, highly structured ‘gel’ system to which

articular cartilage can be compared. The swelling of articular cartilage and its associated stress is partly derived from the repulsive interactions between the negatively charged groups of proteoglycan aggregates confined within an ultra-low permeability collagenous membrane and its related osmotic swelling component generated by the increased concentration of counter ions which provide for electro-neutrality. Therefore, matrix function can be considered as analogous to the response of an osmotically active, fluid-swollen, cross-linked "polymeric" gel that can expand (or contract) to a limiting volume according to the balance of the prevailing forces acting on it. It is therefore of optimum importance for any investigative method to retain the complicated structure of the tissue. This requirement especially emphasizes the attractiveness of a new continuum theory for the consolidation principle-based investigative method that will be discussed in this thesis.

2.6.2 A perspective on cartilage load-carriage biomechanics

A functional unit of load-bearing in the normal cartilage matrix can be idealised as shown in Figures 2.3 and 2.4, where the distribution of the interconnecting nodal points of the rope-like structures in the picture idealizes the connection points of the radial fibrils which serve to hold together the semipermeable membrane which contains the swelling component. This structural attribute strongly supports the representation of the solid skeleton of the matrix as a hyperelastic structure. The reduction in the frequency of these nodal or 'knitting' points producing the unit's intrinsic shear stiffness and general resistance to compression will be greatly reduced (assuming the hypothetical case of no reduction in the amount nor swelling potential of the proteoglycans). This idealization of structural degeneration is consistent with the findings of an earlier study by Broom (1982), in which the micro-compressive stress/strain responses obtained for cartilage samples containing a much reduced fibrillar knit exhibited a much lower stiffness than that of the normal matrix. In order to capture this influence of structural change in the tissue, non-invasive methods of quantifying its internal load-carriage mechanism are required, without introducing any artificial damage in the process of testing.

Fortunately, the consolidation method (Biot, 1941; Klausner, 1991; Terzaghi, 1943) is

capable of measuring the hydrostatic excess pore pressure which governs the internal processes of load bearing (Oloyede and Broom, 1991), and can reveal the extent of any reduction in physiological viability without the additional complications that could be introduced from probing the tissue to obtain internal measurements. The consolidation approach yields two parameters directly, i.e. fluid pressure and the deformation characteristics of the solid, which when combined for the purpose of load-bearing analysis can provide a more complete insight into the functional characteristics of both intact healthy and degenerate cartilage samples. Furthermore, the swelling characteristics of the tissue can be inferred from these data.

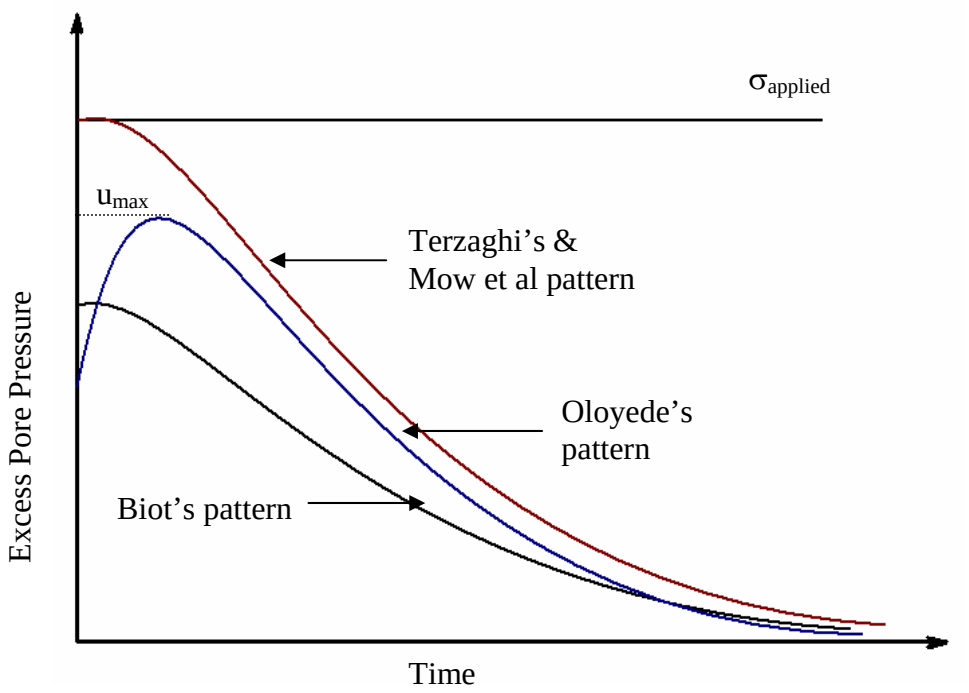

Figure 2.9: Comparison of the prediction of the patterns of the hydrostatic excess pore pressure by the mixture theory, classical consolidation, and the experimental data of Oloyede and Broom (1991).

Experiments which were based on this principle of mechanical consolidation using the unique tissue consolidometers introduced to the literature by Oloyede and Broom, (1991, 1992, 1993, 1994 (a), 1994 (b)) and one of which was recently replicated by Soltza and Ateshian (1998); and Fortin et al (2000) have demonstrated that this method produces highly representative data which could be used to predict the behaviour of articular cartilage with a high level of confidence. In fact, one indirect, but very much related, outcome from the unconstrained consolidation of cartilage (Oloyede and

Broom, 1994 (b)) is the light it indirectly shed on the probable mechanism underlying weeping lubrication by articular cartilage in the joints as was originally proposed by McCutchen (1980). The result revealed that a certain pattern of pressure distribution on the surface of the tissue under physiological boundary conditions is responsible for this mechanism.

Furthermore, the published consolidation experimental data (Oloyede and Broom, 1993) showed that the applied stress was initially carried by the matrix fluid and subsequently shared by its solid content (Figure 2.9). In response to load, the experimental curve obtained from consolidation experiments demonstrate that the pressure of the fluid increases over and above its intrinsic osmotic value to a level that is proportional to the applied stress. This additional pressure carried by the fluid is referred to as the hydrostatic excess pore pressure (u) of the fluid. The pressure u attains its maximum level (u_{max}) soon after loading and is responsible for fluid outflow from the matrix. In comparison with classical consolidatable materials in which the hydrostatic pressure initially carries to the level of the applied stress in full (Biot, 1941; Terzaghi, 1943), experiments have shown that the pattern for the development of u_{max} is modified in articular cartilage (Oloyede and Broom, 1991, 1993 (b)). Therefore any model of the tissue must be able to account for this tissue's specific behaviour. Attempts have been made more recently to reconcile experimental consolidation results with predictions of the biphasic theory (Ateshian et al 1994, 1997). However, the inability of the model to capture this important initial stage of loading constitutes a major inadequacy as this stage is, without doubt, significant in the responses of articular cartilage, as demonstrated in the comparison between the normal intact and proteoglycan digested samples (Oloyede and Broom, 1994 (a), (b)).

Their experiments also revealed that fluid loss and the related decay in the hydrostatic excess pore pressure towards zero leads to the transient transmission of stress into the solid skeleton, in a similar manner to that obtained in the classical consolidation or mixture theories (Biot, 1941; Lai et al, 1991; Mow et al, 1980, 1987; Terzaghi, 1943). It must be emphasized here that it is only in the stages beyond the maximum hydrostatic excess pore pressure that the consolidation/ poroelastic and mixture theories are comparable. The stress transferred to the solid consolidates (or compresses) it, and it is

known as the “effective stress”. It should be noted that this process is more complex in articular cartilage because of its swelling component that is related in load sharing between the solid and fluid components. In fact it has been noted that this influence of swelling accounts for the maximum excess pore pressure being lower than the applied pressure in contrast to the classical consolidation theory.

However, despite the success of the consolidation experiments in providing insights into the exact nature of the cartilage material, it carries a severe limitation in that only the data from the bottom layer closest to the pressure transducer can be obtained in these experiments. This situation is inadequate for making informed predictions of the responses of any of the layers above this region, especially as the properties of the matrix layers vary from one another (Maroudas, 1968, McCutchen, 1975). As mentioned above, it is also unacceptable to use probing devices which could damage or modify the tissue for the purpose of measuring the variation of this fundamental pressure parameter of load carriage. Hence the necessity for a mathematical model can be implemented computationally and used to determine the behaviours of all layers of the tissue under a given load and matrix conditions.

2.7 Conclusion

Various attempts have been made to model the mechanical and physico-chemical responses of articular cartilage in the past as shown on the summary diagram (Figure 1). These include both linear and finite strain isotropic elastic representations of the matrix in which bulk elastic properties such as Young’s and bulk moduli and various types of Poisson’s ratio were used to characterize the tissue (Kempson, 1979; Mizrahi et al, 1986; Woo et al, 1976, 1979), viscoelastic formulations (Elmore et al, 1963; Hayes and Bodine, 1978), and adaptations of mixture theory (Lai et al, 1991; Lanir, 1987 (a), (b); Mow et al, 1980, 1987). However, because of its physico-chemistry, structure, and fluid exudation-dependent deformation, most of these models have proved to be inadequate for predicting physiologically plausible or realistic load-bearing data. The biphasic model of cartilage, which is based on mixture theory, is unable to predict cartilage response in the important incipient stages of load-carriage under slow loading (Brown and Singermann, 1986). Unmodified conventional parameters such as the elastic moduli

and the Poisson's ratio have no practical use in the position- dependent deformation of a tissue such as articular cartilage.

However, it is argued presently that, in order to make conventional mechanics relevant, pseudo-elastic parameters that have been corrected for their fluid exudation or strain-dependence should be used. In relation to tissue structure, it is well acknowledged in the literature that articular cartilage is neither a mixture (Harrigan, 1987) nor a viscoelastic material (McCutchen, 1982). Rather this tissue responds to load as a poroelastic/ porohyperelastic material (Harrigan, 1987; Simon, 1990), with marked similarities to the behaviours observed in high swelling clays (Oloyede and Broom, 1994 (a)). Both the triphasic model of Lai et al (1991) and the models of Lanir (1987 (a); (b)) have incorporated the concepts of poroelasticity, but there has been no model that accounts for the structure relating to the heterogeneous and anisotropic characteristics of the solid and fluid of the matrix, and no rigorous experimental evidence to support their accuracy or representative capacity in predicting articular cartilage load-carriage bio-mechanical behaviour.

In fact, analysis and modelling of articular cartilage has been carried out in a manner that introduced extreme mathematical difficulties, especially in relation to its fundamental function and structural coupling (Mizrahi et al., 1986; Mow et al, 1980, 1987; Oloyede and Broom, 1994). Experimental evidence reveals that the existing theories and their parameters are mostly unable to replicate experimental results or have little agreement between theoretical prediction and experimental data.

It is believed that the consolidation models should be developed as heterogeneous, anisotropic and poro-hyperelastic non-viscous systems. The resulting relations should be evaluated against experimental data. The purpose of this thesis is to develop an improved model of articular cartilage (Figure 1) based on the principle of the consolidation of fluid- saturated swollen gel-like material exhibiting large strain deformation. The cylindrical samples of patellar grooves, which are likely flat, were selected for the experiments under the static loading and modelled regarding with the experimental conditions, thereby restricting the complication of the cartilage properties in this depth of study of the cartilage behaviours.

Chapter 3: Predictive rheological models for articular cartilage consolidation.

3.1 Introduction

Rheological analogues of articular cartilage load-carriage responses exist in published literature representing a phenomenological view of articular cartilage behaviour. McCutchen (1975) proposed the layer model, while Higginson et al. (1976) suggested a serial arrangement of a non-linear elastic spring and dashpot to account for the influence of fluid exudation and drag on the load-carriage properties of articular cartilage. Radin et al. (1970) suggested a rheological body that captures the observed increase in cartilage stiffness with increasing strain-rate. Whilst these models address aspects of cartilage load-induced behaviour, the rheological analogue proposed by Oloyede et al. (1992) is arguably the most sophisticated and with a significant potential for capturing more rigorously the important features of the behaviour of articular cartilage under both static and quasi-static loading. But it lacked a mathematical description for evaluating its degree of accuracy in predicting the response of the cartilage matrix to mechanical loading.

In this chapter the analogue of Oloyede et al. or 'OB body' will be described mathematically and evaluated against published experimental data within the framework of mechanical consolidation. It will be extended to account for physico-chemical swelling and the rate-dependence of cartilage deformation. The rheological analogue in its original form is presented in Figure 3.1 and it consists of the individual elements. The almost instantaneous elastic reaction of the matrix is represented by the elastic spring k_v. The hyperelastic behaviour of the solid skeleton is represented by the spring-dent elements. The dents model time lag and act as switches to include springs cumulatively into the deformation process so that the matrix is progressively stiffened as successive dents close. As the population of these spring-dent elements tends to infinity, the characteristic J-curve of soft tissues describing the relationship between stress and strain results. This system has the dents' jaws carefully spaced to represent the increasing stiffness due to the combined effects of the loaded network of fibrils and entrapped swollen proteoglycan macromolecules. The specialized dashpot models the role of water in the deformation process and is set in motion immediately a pressure

gradient is established between the matrix and its surrounding on the application of load.

It should be noted that the rheological models considered here can only model the tissue under one-dimensional constraints, consequently the analysis presented in subsequent sections has been restricted to axial deformation in the thickness direction only. This analogue is developed mathematically to evaluate its degree of accuracy in predicting the response of cartilage load carriage.

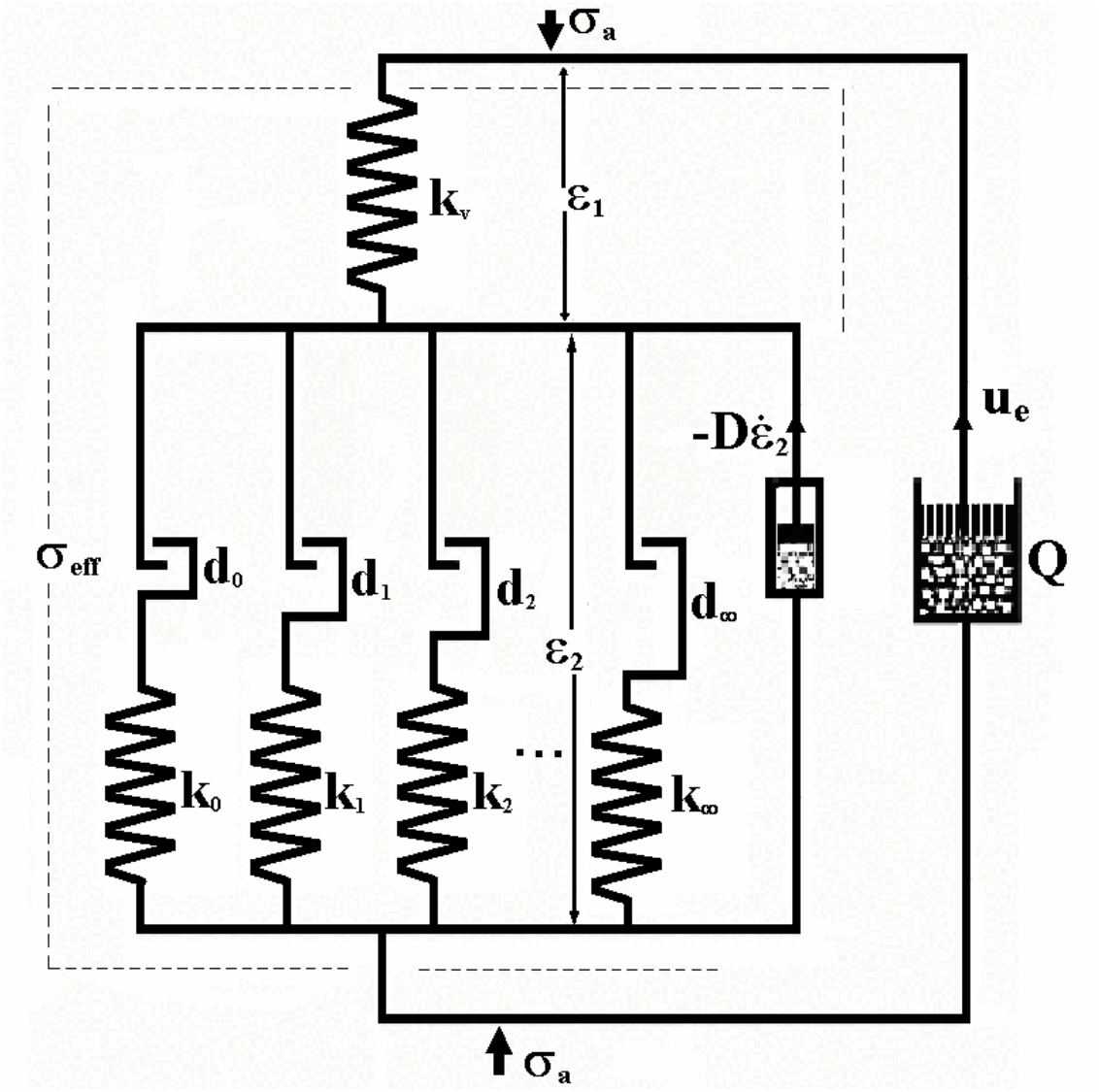

Figure 3.1: The original rheological analogue proposed for the articular cartilage matrix by Oloyede et al. ("OB" body) (1992)

σ_a is the applied stress, k_v is the instantaneous reaction element acting immediately upon loading, d_i (i=0, 1, 2,…) is the length of the i^{th} dent, k_i (i=0,1,2,…) is the stiffness of the i^{th} spring, D is the damping coefficient of the dashpot, σ_{eff} is the solid's effective stress, Q is permeability coefficient of the matrix.

3.2 Mathematical description of the Oloyede-Broom model

3.2.1 General relationship for volume change

The cartilage matrix is conceptualized as a consolidatable poro-hyperelastic material that consists of 60-80% fluid (Weightman and Kepson, 1979) and is osmotically active. Under load it exudes its fluid and reswells when unloaded. Its solid component comprises swollen proteoglycan aggregates entrapped within a three-dimensional meshwork of collagen fibrils. Since the cartilage matrix is known to be able to deform in excess of 60% of its unloaded thickness under compression, a true strain formulation is carried out here. Therefore, a cylindrical block of cartilage matrix of instantaneous volume *V*, in which the volumes occupied by both mobile and trapped fluid and the solid skeleton are V_f and V_s respectively ($V = V_f + V_s$), would exhibit volumetric deformation that can be quantified as,

$$\frac{dV}{V} = d\varepsilon \Rightarrow V = V_o \exp(\varepsilon), \tag{3.1}$$

where ε is the instantaneous volumetric strain of the matrix and V_o is the initial volume of the matrix. Using equation (3.1), and the above definition of the matrix total volume, we can write for the fully saturated matrix the following relationship,

$$\frac{V_f}{V} = 1 - \frac{V_s}{V} = 1 - \frac{V_s}{V_o}\frac{1}{\exp(\varepsilon)} \tag{3.2}$$

For a one-dimensional deformation of an element at position z into the depth *h* of the cylindrical matrix, the bulk deformation can be written as,

$$\frac{dV}{V} = \frac{dz}{z} = d\varepsilon, \quad \text{or} \quad z = z_o \exp(\varepsilon)$$

This can be rewritten for the whole matrix as,

$$\frac{V}{V_0} = \frac{h}{h_0} = \exp(\varepsilon) \tag{3.3}$$

where *h* and h_o are the instantaneous and initial thicknesses of the matrix, respectively. Equations (3.1), (3.2) and (3.3) represent the changes in (i) overall matrix volume, (ii) specific fluid content with respect to incremental volumetric deformation and (iii) change in thickness or compressive deformation of the matrix over a given period of sustained loading respectively.

3.2.2 An approximate relationship for dependence of permeability on compressive strain

The matrix exudes water and exchanges ionic solutes during deformation (Oloyede and Broom, 1993 (a); 1994 (a); Weightman and Kempson, 1979) leading to an increase in the proteoglycan-water ratio (i.e. fixed charge density) and a concomitant reduction in the matrix permeability (Weightman and Kempson, 1979). In this present formulation, we observe that the rate of fluid exudation decreases significantly towards the end of consolidation and therefore note that the effect of matrix permeability can be represented by a fluid dashpot (see Figure 3.1). Therefore, the matrix's response to loading is characterized by a non-constant coefficient of permeability, whose magnitude is assumed to vary according to an inverse power relationship, i.e.

$$Q = \frac{a}{\left(\frac{\rho}{\rho_f} - 1\right)^{\alpha}} \tag{3.4}$$

where, ρ (kg/m^3) and ρ_f (kg/m^3) are the matrix overall density and fluid content density, respectively, both a (m^4/Ns) and α are characterizing constants, and Q (m^4/Ns) is the coefficient of permeability.

Since both the fluid and solid components of the tissue are incompressible (Myers and Mow, 1983; Oloyede and Broom, 1996), ie. $dV_f \approx dV$, and the change in solid mass with time is assumed to be negligible, then for a given matrix containing solid mass m_s, we have

$$m_s = \rho V - \rho_f V_f \Rightarrow dm_s \approx V d\rho + \rho dV - \rho_f dV_f = 0$$

or

$$\frac{d\rho}{\rho - \rho_f} \approx -\frac{dV}{V} = -d\varepsilon \Rightarrow \rho - \rho_f = b\exp(-\varepsilon) \tag{3.5}$$

where b (kg/m^3) is a constant. Substituting equation (3.5) into (3.4), we obtain

$$Q = Q_o \exp(\alpha\varepsilon) \tag{3.6}$$

where, $Q_o = \frac{a}{(b\rho_f)^{\alpha}}$ is defined as the initial permeability.

Equation (3.6) is similar to that proposed earlier by Mow et al. (1980).

3.2.3 General continuity equation of fluid flow

Because the velocity of fluid exudation, v_f, is very low, Darcy's law can be applied, i.e.

$$v_f = -\frac{q}{\gamma}\frac{\partial u_h}{\partial z} \tag{3.7}$$

where, q (m/s) is the instantaneous permeability of the matrix due to fluid outflow at time t, γ (N/m^3) is the gravitational density of fluid, u_h is the hydrostatic excess pore pressure of the fluid in an element at the depth z from the surface and z is the displacement from the surface as the previous defining in equation (3.2).

Equation (3.7) can be rewritten for the whole matrix in terms of the fluid's average hydrostatic excess pore pressure, $\bar{u}_h$, as,

$$\bar{v}_f = -Q\frac{\bar{u}_h}{h} \tag{3.8}$$

where, $\bar{v}_f$ is the average velocity of the outflow and $Q = q/\gamma$ (m^4/Ns) is the permeability coefficient.

Since both the fluid and solid components of the tissue are incompressible, the deformation of an element due to fluid outflow can therefore be described by,

$$div(\underline{v}_f) = \sum_{i=1}^{i=3}\frac{\partial v_i}{\partial x_i} = \frac{1}{V}\frac{\partial V}{\partial t} = \frac{\partial \varepsilon}{\partial t}$$

Therefore the flux of fluid out of the matrix can be expressed in one-dimensional form for the whole thickness of the matrix as,

$$div(\underline{v}_f) = \frac{\partial v_f}{\partial z} \approx \frac{\bar{v}_f}{h} = \frac{\partial \varepsilon}{\partial t} \tag{3.9}$$

We combine equations (3.3), (3.6), (3.8) and (3.9) to get

$$\bar{u}_h = -\frac{h_o^2}{Q_o}\exp\big((2-\alpha)\varepsilon\big)\frac{\partial \varepsilon}{\partial t} \tag{3.10}$$

3.2.4 Stress-strain relationship for solid skeleton

The solid skeleton of the cartilage matrix shares the applied load with the fluid, thereby developing a time or deformation-dependent stiffness (Oloyede et al., 1992; Oloyede

and Broom, 1994 (a); 1996). This stiffness is hyperelastic due to the non-linearity of the tissue's overall stress-strain response. In this section we propose rheological models from which the stress-strain laws for the matrix's solid component can be evaluated. We will also resolve the relationship between the fluid, solid and swelling components using the effective stress relationship (Oloyede et al., 1992).

Firstly, we consider the original rheological body of Oloyede and Broom (Oloyede et al., 1992), and assume that the proteoglycans and collagen entrapment system described in their paper as hyper-elastic and represented by a system of dent-carrying elastic springs, where the dents model time delay in the incremental stiffening process. The springs, whose stiffnesses are k_0 to k_∞, contribute cumulatively to the overall stiffness and are switched on into the deformation process when their respective dents close. The deformation of the matrix at time t as a result of fluid exudation of this hyperelastic system can be described mathematically as follows (see Figure 3.1).

First, we define h_n as the thickness of the given sample after maximum fluid exudation (thickness of the dry sample) and all springs become active, i.e.

$$h_n = h_0 - d_0 - n\Delta x = \frac{V_s}{V_0} h_0 \qquad (3.11a)$$

where, Δx is the incremental displacement of the matrix in the direction perpendicular to the articular surface at each time step, n is the number of displacement steps to achieve maximum deformation ($n \to \infty$ if Δx is very small), and d_i is the characteristic gap of the i^{th} dent. The incremental displacement Δx at an instant can be defined as $d_i - d_{i-1} = \Delta x_i$ for i = 1, 2, …. This relationship is assumed constant in this derivation to simplify the mathematical process involved (i.e. $\Delta x_i = \Delta x$). The total change in matrix thickness, $x = h_0 - h$ is reached at instant time $t = t_i$ in the following derivation.

If k_i (N/m) is the stiffness of the i^{th} spring (where i is the index), and F is the net force generated by all the active springs in the system at time, t_I;
Starting from time t =0 to t_0,

$$x \le d_0 \text{ and } F(t_0) = 0$$

At $t = t_1$,

$$d_0 < x = d_0 + \Delta x \le d_1$$
$$F(t_1) = k_0(x - d_0) = k_0 \Delta x$$

At $t = t_2$,

$$d_1 < x = d_0 + 2\Delta x \le d_2$$
$$F(t_2) = k_0(x - d_0) + k_1(x - d_1) = 2k_0 \Delta x + k_1 \Delta x$$

Similarly, at $t = t_i$,

$$d_{i-1} < x = d_0 + i\Delta x \le d_i$$
$$F(t_i) = ik_0 \Delta x + (i-1)k_1 \Delta x + ... + k_{i-1} \Delta x$$

For simplicity, we consider the ideal situation in which $k_0 = k_1 = k_2 = \ldots = k_n = k$, then

$$F(t_i) = (1 + 2 + ... + i)k\Delta x = \frac{1}{2} i(i+1)k\Delta x \qquad (3.11b)$$

Let S (N/m^2) be the stiffness of the whole matrix after all free fluid has been exuded (i.e maximum stiffness obtainable during effective load processing), then,

$$\frac{S.A}{h_n} = \left(k_0 + k_1 + ... + k_n\right) \Rightarrow \frac{S.A}{h_n} = (n+1)k \approx nk, \text{ (as n} \to \infty) \qquad (3.11c)$$

where A is the cross sectional area of the matrix and h_n is the thickness of the drained matrix.

Substituting equation (3.11c) into (3.11b) yields

$$F(t_i) = \frac{1}{2}\frac{S.A}{h_n}\frac{(i+1)}{n} i\Delta x = \frac{1}{2}\frac{S.A}{h_n}\frac{(i+1)}{n}(x - d_0) \approx \frac{1}{2}\frac{S.A}{h_n}\frac{i}{n}(x - d_0) \qquad (3.11d)$$

Furthermore, we have

$$d_0 + i\Delta x = x \qquad \text{or} \qquad i\Delta x = x - d_0 \qquad (3.11e)$$

Substitution of equations (3.11a) and (3.11e) into (3.11d) yields

$$\frac{F}{A} = \frac{S}{2h_n}\frac{(x - d_0)^2}{h_0 - d_0 - h_n} = \frac{Sh_0^2\left(\frac{x}{h_0} - \frac{d_0}{h_0}\right)^2}{2h_n(h_0 - d_0 - h_n)} = B\left(\frac{x}{h_0} - \frac{d_0}{h_0}\right)^2, \qquad (3.11f)$$

where $B = \dfrac{Sh_0^2}{2h_n(h_0 - d_0 - h_n)} = \dfrac{S}{2}\dfrac{h_0}{h_n}\left(1 - \dfrac{h_n}{h_0} - \dfrac{d_0}{h_0}\right)^{-1}$. (3.11g)

Letting $\varepsilon_{sw} = \ln\left(1 - \dfrac{d_0}{h_0}\right)$ is the limit strain, when the matrix deforms up to a level without any active springs. This formulae is rewritten as

$$\frac{d_0}{h_0} = 1 - \exp(\varepsilon_{sw}). \qquad (3.11h)$$

Substituting equations (3.11h) and (3.11a) into (3.11g) yields

$$B = \frac{S}{2}\frac{V_0}{V_s}\left(\exp(\varepsilon_{sw}) - \frac{V_s}{V_0}\right)^{-1}. \tag{3.11k}$$

Substituting equations (3.3) and (3.11h) into (3.11f), it can be formulated for the change in stress in terms of the stress-strain relationship including the initial stress (σ_{s0}), so that,

$$\begin{aligned} \sigma_s &= 0 \quad if \quad |\varepsilon| \le |\varepsilon_{sw}| \\ \sigma_s &= \frac{F}{A} = B(\exp(\varepsilon_{sw}) - \exp(\varepsilon))^2 \quad if \quad |\varepsilon| > |\varepsilon_{sw}| \end{aligned} \tag{3.11}$$

It is noted that the initial stress exists to balance the initial osmotic pressure in the matrix.

3.2.5 Approximate expression for matrix osmotic potential

It has been demonstrated that the articular cartilage matrix behaves as a 3-component biological gel in which physico-chemical swelling contributes to its overall stiffness (Broom and Oloyede, 1998). Assuming Donnan equilibrium swelling conditions, the osmotic pressure of the matrix, u_o, can be expressed approximately in accordance with the previous published (Broom and Oloyede, 1998; Tomb and Peacock ,1974),

$$u_o = RT\left(\frac{C_2}{M_2} + \beta C_2^2\right), \tag{3.12}$$

where C_2 is the instantaneous weight concentration of the proteoglycan component, M_2 is its molar mass, R is the universal gas constant, T is the temperature of the matrix and β is the second coefficient for a three-component biological gel under Donnan equilibrium. Since the change in fixed charge density to water ratio is due to the outflow of fluid from the matrix, then analysis based on conservation of mass yields,

$$C_2 V = C_{20} V_0 \quad or \quad C_2 = C_{20}\frac{V_o}{V} = \frac{C_{20}}{\exp(\varepsilon)} \tag{3.13}$$

where, C_{20} is the initial weight concentration of proteoglycans and the other terms are as defined previously. Substituting equation (3.13) into equation (3.12) yields,

$$u_o = RT\left(\frac{C_{20}}{M_2}\exp(-\varepsilon) + \beta C_{20}^2 \exp(-2\varepsilon)\right) = u_{o1}\exp(-\varepsilon) + u_{o2}\exp(-2\varepsilon) \tag{3.14}$$

where $u_{o1} = \dfrac{RTC_{20}}{M_2}$ and $u_{o2} = RT\beta C_{20}^2$

In addition, if we assume that the osmotic pressure also acts inside the pores of the matrix, then equation (3.14) can be rewritten to account for change in the volume occupied by pores, i.e

$$u_o = \frac{V_f}{V}\left(u_{o1}\exp(-\varepsilon) + u_{o2}\exp(-2\varepsilon)\right) \tag{3.15}$$

Furthermore, substitution of equation (3.2) into (3.15), yields the relationship for the osmotic pressure as,

$$u_o = \left(1 - \frac{V_s}{V_0}\exp(-\varepsilon)\right)\left(u_{o1}\exp(-\varepsilon) + u_{o2}\exp(-2\varepsilon)\right) \tag{3.16}$$

The initial osmotic pressure of the fluid without load is balanced by the initial stress in the solid skeletal structure of collagen fibril entrapped swollen proteoglycans expressed in equation (3.17).

3.2.6 The effective stress relationship for the articular cartilage matrix

Having obtained expressions for various components of the rheological analogue as shown in Figure 3.1, we can now consider the unloaded equilibrium condition at time $t = 0^-$ (just before loaded) for the matrix. In this respect, we can express the initial balance between the effective solid skeleton stress and the osmotic component as

$$\sigma_a = 0 = \sigma_{eff}(t = 0^-) + u_o(t = 0^-) \Rightarrow \sigma_{so} = -u_o = -\left(1 - \frac{V_s}{V_0}\right)\left(u_{o1} + u_{o2}\right), \tag{3.17}$$

where, σ_{s0} is the initial effective solid stress; and σ_{eff} denotes the instantaneous effective solid stress that is stress shared by the solid skeleton as fluid is exuded and consists of stress due to the solid and the resistant stress due to interaction between the solid and outflow.

Consequently, the stress-strain relationships for the original Oloyede-Broom (OB) model (Figure 3.1) are,

$$\sigma_a = \sigma_{eff} + u_e = \sigma_s - D\dot{\varepsilon}_2 + \sigma_{s0} + u_e$$
$$\sigma_a = \frac{k_v}{h_0}(1-\exp(\varepsilon_1)) + \sigma_{s0} + u_e \qquad (3.18)$$
$$\varepsilon = \varepsilon_1 + \varepsilon_2\,, \qquad u_e = \bar{u}_h + u_o$$

where σ_s is the solid stress that is similarly as the description in Equation 3.11 ie.

$$\sigma_s = 0 \quad if \quad |\varepsilon_2| \le |\varepsilon_{sw}|$$
$$\sigma_s = B\left(\exp(\varepsilon_{sw}) - \exp(\varepsilon_2)\right)^2 \quad if \quad |\varepsilon_2| > |\varepsilon_{sw}|$$

u_o, $\bar{u}_h$ and σ_{s0} are defined in equations (3.10), (3.15) and (3.16), respectively; ε_1, ε_2 and ε denote the partial strain of the instantaneous spring, the partial strain of the springs-dents system and the total matrix strain; and *B* is also as expressed previously. It is also noted that the first line of Equation 3.18 is resulted using the balance of the stresses at the bottom while the second line is applied at the top of the diagram.

3.2.7 Results

Figure 3.2 presents the solution of the system of equations (3.10), (3.16), (3.17) and (3.18) solved numerically using "MAPLE" code (Appendix A2.1) for the consolidation parameters σ_{eff}, $\bar{u}_h$, u_o, ε, where stress equilibrium for the matrix has been evaluated using the relationship,

$$\sigma_a = \sigma_{eff} + u_e = \sigma_s - D\dot{\varepsilon}_2 + \sigma_{s0} + u_e \text{ or } \sigma_{eff} = \sigma_a - u_e \qquad (3.19)$$

The pore pressure and compression strain curves in Figure 3.2 reveal that the "OB" body is capable of capturing accurately the behaviour of the tissue for the equilibrium stage ($t > 4000$ seconds), but is a poor predictor in the early stages of loading, thereby suggesting that a modification is required in order to predict this incipient and important stage of loading.

Table 3.1: Parameters for analysis resulting in Figure 3.2

h_0 mm	S MPa	k_v/h_0 MPa	D MPas	u_{o1} MPa	u_{o2} MPa	Q_0 (x 10^{-16}) m^4/Ns	α	$\frac{V_s}{V_0}$	ε_{sw}
1.5	3.8	300	500	0.02	0.2	7.5	2.95	0.28	–0.48

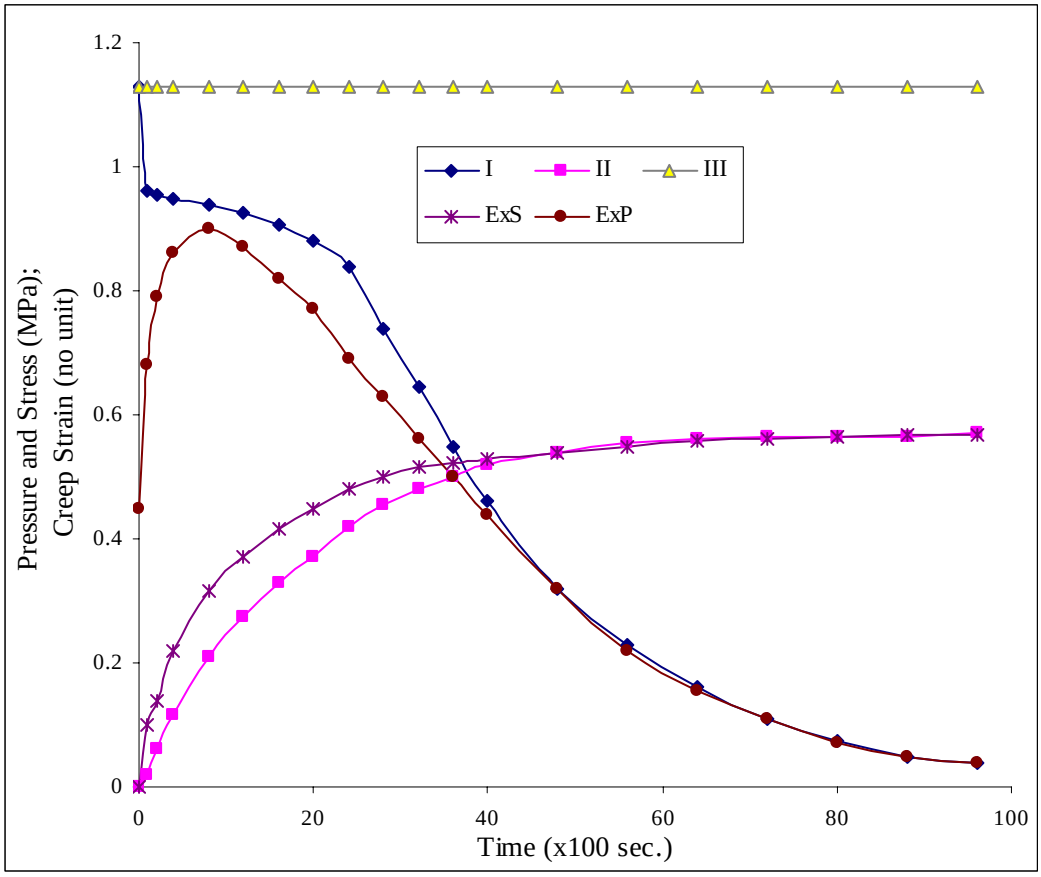

Figure 3.2: Comparison of the experimental hydrostatic excess pore pressure (ExP) and creep strain (ExS) published by Oloyede and Broom (1994 (a)) to the predicted results of the original Oloyede-Broom body for articular cartilage. The predicted values are: hydrostatic excess pore pressure (I) and creep strain of the matrix (II) under applied load (III). The parameters are given in Table 3.1

3.3 Modified rheological analogues of articular cartilage

3.3.1 The “series-element” analogue

In order to address the discrepancy between the prediction of the behaviour of the OB body and published consolidation experimental results (Oloyede and Broom, 1991, 1994a), the following analogues containing both mechanical and swelling elements incorporating the basic concept of the OB body, are proposed.

The "OB" body with swelling capability of this analogue is shown in Figure 3.3 and it incorporates

i. an additional dashpot, D_1 in parallel with the instantaneous reaction spring k_v of the OB body.

ii. a dashpot D_v that modifies the action of the original dashpot representing permeability Q across matrix layers in parallel.

iii. an osmotic component that introduces swelling into the matrix's overall response.

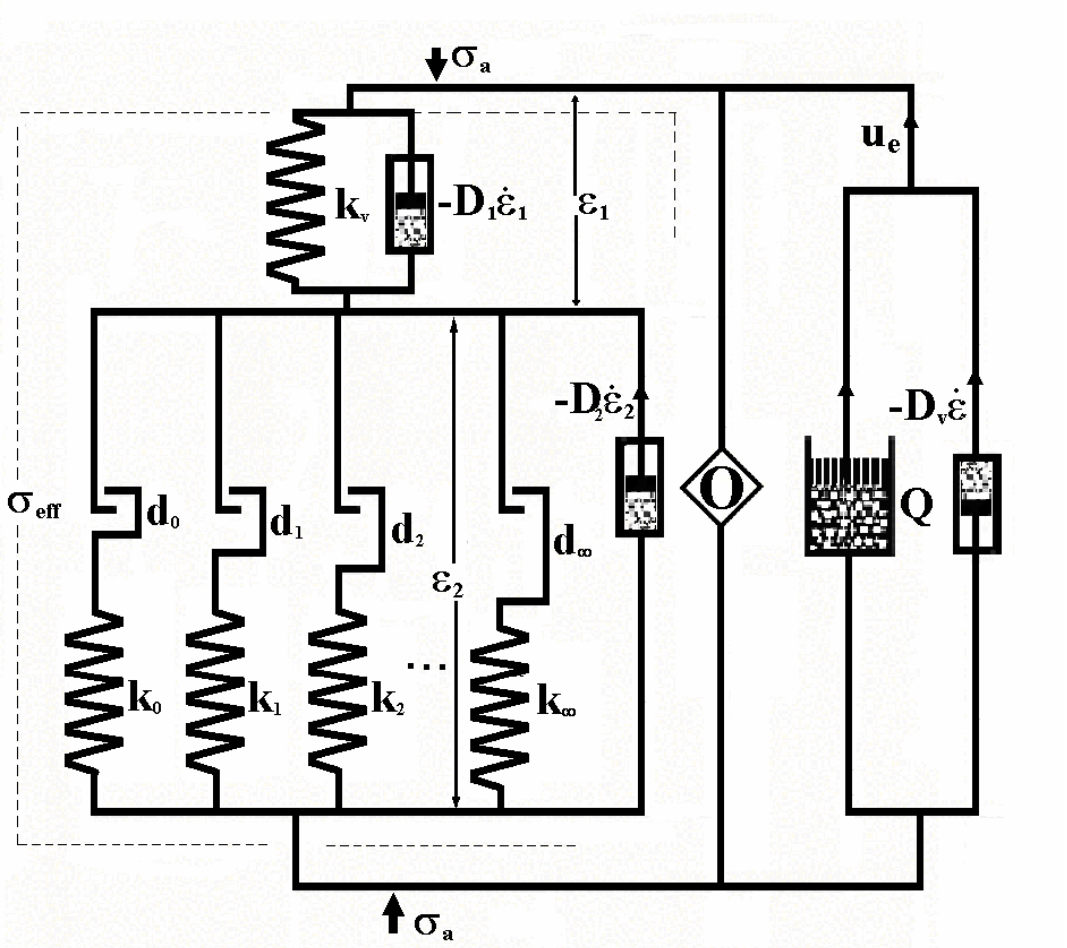

Figure 3.3: The modified 'series' rheological analogue for the cartilage matrix featuring an improved "instantaneous" reaction element (k_v+ D_1) and an additional swelling element.

σ_a is the applied stress, k_v is the stiffness of the instantaneous spring, d_i (i=0, 1, 2,…) is the length of the gap of the i^{th} dent, k_i (i=0,1,2,…) is the stiffness of the i^{th} spring, D_1 is instantaneous damping coefficient for unbounded fluid and D_2 is the damping coefficient relating to the bound fluid, D_v is the damping coefficient of the dashpot representing unbounded fluid, σ_{eff} is the solid's effective stress, Q is permeability coefficient of the matrix. "O" is the active osmotic component.

The dashpot D_1 combines with D_2 of the original analogue (see Figure 3.3) to represent the interaction between proteoglycans and the collagen meshwork, hence drag. The effects of D_1 and D_2 would be negligible if the proteoglycans possess a neutral charge.

As shown in Figure 3.3, the applied stress is balanced by the solid stress and effective pore pressure at the top and bottom of the matrix; therefore the mathematical equations for this new analogue can be shown to be

$$\sigma_a = \sigma_s - D_2\dot{\varepsilon}_2 + u_o + \bar{u}_h + \sigma_{s0}, \qquad \varepsilon = \varepsilon_1 + \varepsilon_2,$$
$$\sigma_a = \frac{k_v}{h_0}(1-\exp(\varepsilon_1)) + \sigma_{s0} - D_1\dot{\varepsilon}_1 + u_o + \bar{u}_h \tag{3.20}$$

where,

$$\sigma_s = 0 \quad if \quad |\varepsilon_2| \le |\varepsilon_{sw}|$$
$$\sigma_s = B(\exp(\varepsilon_{sw}) - \exp(\varepsilon_2))^2 \quad if \quad |\varepsilon_2| > |\varepsilon_{sw}|$$

and, $\bar{u}_h = -\frac{h_o^2}{Q_o}e^{(2-\alpha)\varepsilon}\frac{\partial\varepsilon}{\partial t} + D_v\frac{\partial\varepsilon}{\partial t}$ is a modification of equation (3.10); the other variables are as defined in equations (3.18).

In the present analysis, we have assumed that the response of the two new dashpots are linear functions of the initial osmotic pressure, and are represented by the functions,

$$D_1 = \mu_1(u_{o1} + u_{o2}) \quad and \quad D_2 = \mu_2(u_{o1} + u_{o2}) \tag{3.21}$$

where, μ_1 and μ_2 are coefficients associated with drag effects introduced by the resistance to fluid outflow with changes in matrix permeability and matrix swelling reaction, and u_o, σ_{s0} are previously defined in equations (3.15) and (3.16), respectively.

The system of equations (3.16), (3.17), and (3.20) can be solved numerically to obtain the parameters σ_{eff}, $\bar{u}_h$, u_o, ε and other unknowns using the same MAPLE code (Appendix A2.1) as in the previous set of equations (3.10), (3.16) and (3.17), but inputting a suitable parameter, D_1 for the different solution. In this model, the effective stress of the solid skeleton, in accordance with Oloyede and Broom (1994a), has been evaluated, using as in the previous model the relationship,

$$\sigma_{eff} = \sigma_a - \bar{u}_h - u_o$$

The solution of this modified model shown in Figure 3.4 shows that the hydrostatic excess pore pressure and creep strain values are close to the experimental results of Oloyede et al. (1994 a). In the first stage, the osmotic pressure influences significantly the behaviour of both the solid and fluid components of the matrix (Figure 3.5). It is noted that the osmotic pressure increases as the volume of the matrix decreases; with a concomitant increase in hydrostatic pressure which reaches a maximum at a time when

the solid's effective stress (i.e. the difference between the applied stress and the hydrostatic excess pore pressure) reaches its minimum value.

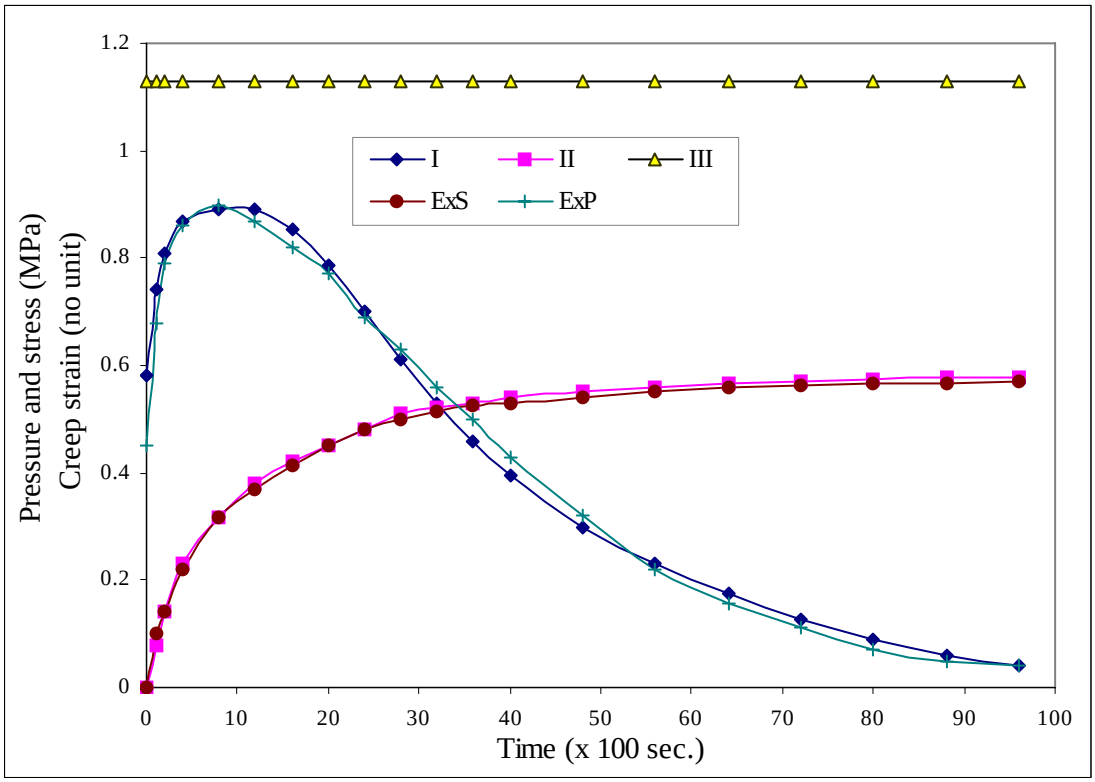

Figure 3.4: Comparison of the experimental hydrostatic excess pore pressure (ExP) and creep strain (ExS) published by Oloyede and Broom (1994 (a)) to the predicted results of the new serial analogue (figure 3.3) for articular cartilage. The predicted values are: hydrostatic excess pore pressure (I) and creep strain of the matrix (II) under applied load (III). The parameters of the analysis are given in Table 3.2

Table 3.2: Parameters for the analysis resulting in Figure 3.4

h_0 (mm)	S (MPa)	k_v/h_0 (MPa)	μ_1 (10^3s)	μ_2 (10^2s)	D_v (MPas)	u_{o1} (MPa)	u_{o2} (MPa)	Q_0 (x 10^{-16}) (m^4/Ns)	α	V_s/V_0	ε_{sw}
1.5	3.8	50	15	25	6100	0.2	0.18	3.44	2.95	0.28	–0.48

The results presented in Figure 3.5 also demonstrate the influence of the initial osmotic pressure on the pattern of the hydrostatic pressure, hence provide an understand of the effect of changes in the fixed charge density on the solid's effective stress in the incipient stages of loading and the effect of drag on the tissue's bulk response to load. By definition, this drag is a consequence of the interaction between bound and unbound fluids, proteoglycans and the collagen fibrils due to any movements within the loaded

matrix. The results obtained from changing the value of the initial osmotic pressure reveal that the development of the maximum hydrostatic excess pore pressure (or the effective stress of the solid) in the stage before the maximum value is reached is dependent on the initial osmotic pressure (u_{o1}, u_{o2}), thereby suggesting that this stage is characterized by structural rearrangement of the collagen-proteoglycan-water systems rather than mechanical deformation.

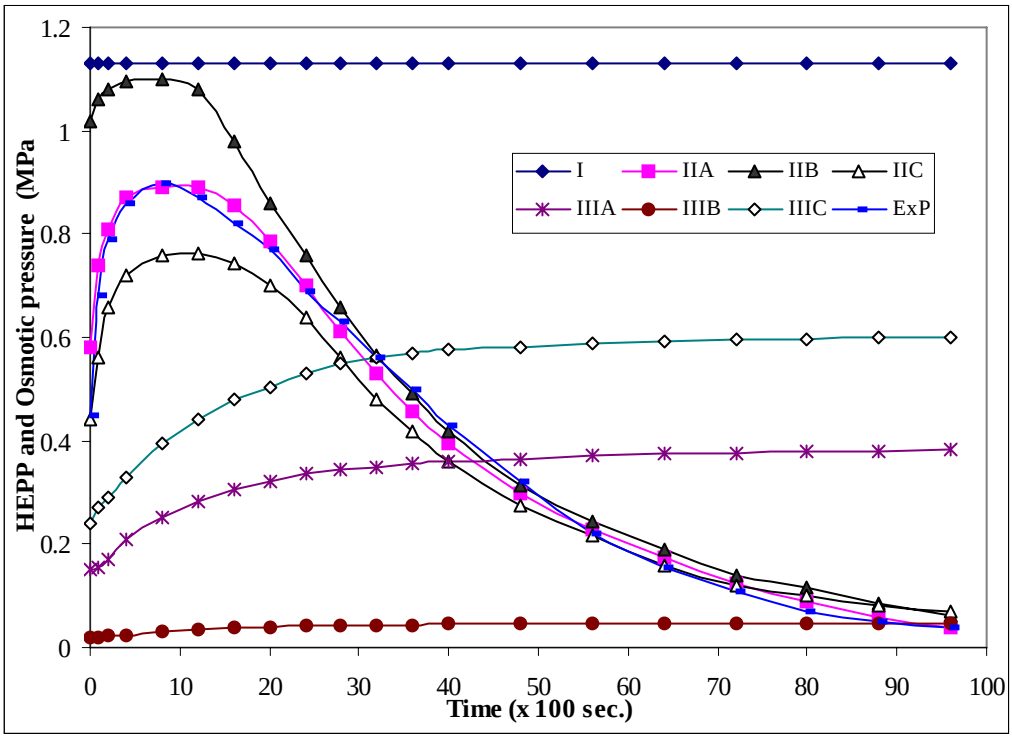

Figure 3.5: The influence of the level of initial osmotic pressure on the predicted values of the hydrostatic excess pore pressure (II), the osmotic pressure (III) under applied stress (I). These data are compared to the experimental hydrostatic excess pore pressure (ExP) of Oloyede and Broom (1994(a)). The parameters used in this analysis are given in Table 3.3.

Table 3.3: Parameters for the analysis resulting in Figure 3.5

h_0 mm	S MPa	k_v/h_0 MPa	μ_1 (10^3s)	μ_2 (10^2s)	D_v MPas	Q_0 (x 10^{-16}) m^4/Ns	α	$\frac{V_s}{V_0}$	$-\varepsilon_{sw}$
1.5	3.8	50	15	25	6100	3.44	2.95	0.28	0.48

Values Legend	A	B	C
u_{o1} (MPa)	0.2	0.003	0.04
u_{o2} (MPa)	0.18	0.02	0.3

Figure 3.6 reveals that the magnitude of the hydrostatic excess pore pressure of the loaded cartilage is significantly influenced by the parameters Q_0 and α that represent the non-linearity and variation of the coefficient of permeability, which is the exponential function of strain ($Q = Q_0 \exp(\alpha\varepsilon)$). This influence of permeability is also reflected in the patterns of the growth of the "creep" strain curves with a noticeable effect on when they achieve their asymptotic values. The importance of this lies in the fact that these predicted values of the hydrostatic excess pore pressure demonstrate that the incipient stages of the load-carriage process in cartilage are significantly determined by the type of permeability function applied in the analysis (Figure 3.7), rather than its initial constant value. It is therefore concluded that the phenomenological approach adopted in this present work is capable of predicting the response of both normal and degenerate matrices where the model can include either linear or non-linear permeability of varying degrees. For example, where degenerative processes have depleted the proteoglycan content and led to a relatively more linear permeability function.

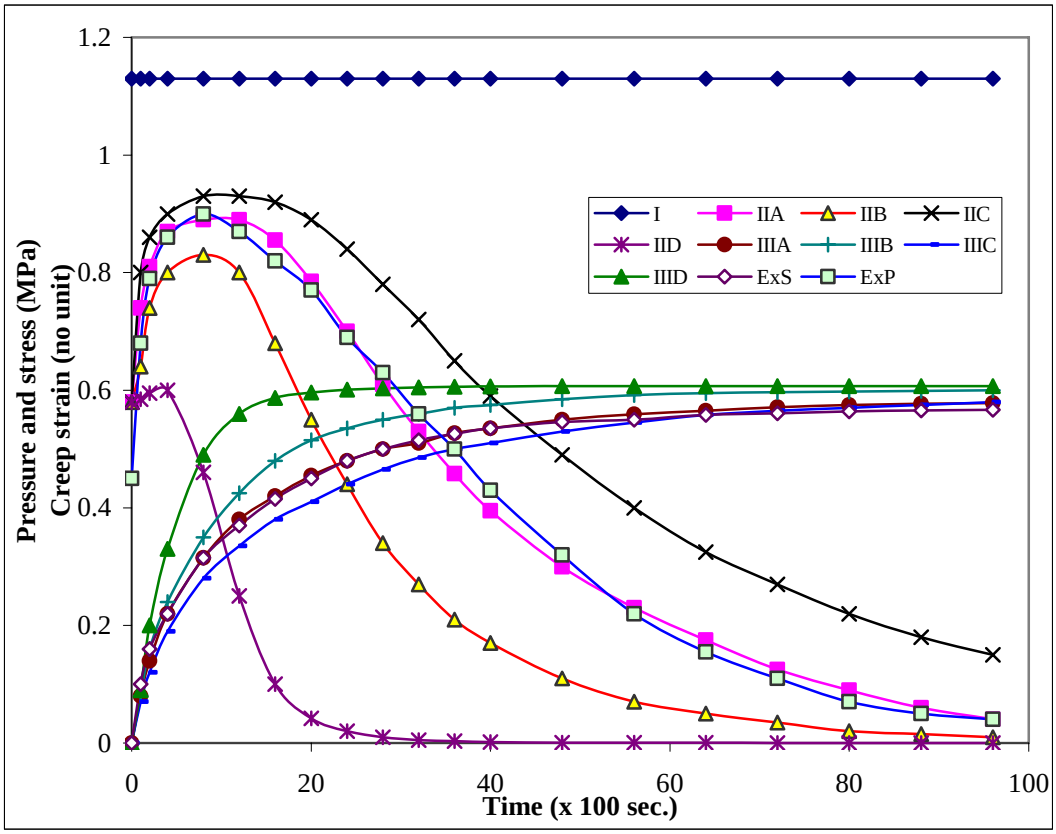

Figure 3.6: The influence of the level of initial permeability and transient permeability variation on the hydrostatic excess pore pressure (II) and the creep strain (III) under an applied stress (I) compared to the experimental results of Oloyede and Broom (1994 (a)). The parameters used in this analysis are given in Table 3.4.

Table 3.4: Parameters for analysis resulting in figures 3.6 and 3.7

h_0 mm	S MPa	k_v/h_0 MPa	μ_1 (10^3s)	μ_2 (10^2s)	D_v MPas	u_{o1} MPa	u_{o2} MPa	$\frac{V_s}{V_0}$	$-\varepsilon_{sw}$
1.5	3.8	50	15	25	6100	0.02	0.18	0.28	0.48

Values Legend	A	B	C	D
Q_0 ($x\ 10^{-16}$) m^4/Ns	3.44	6.25	2.34	3.44
α	2.95	2.95	2.95	2.1

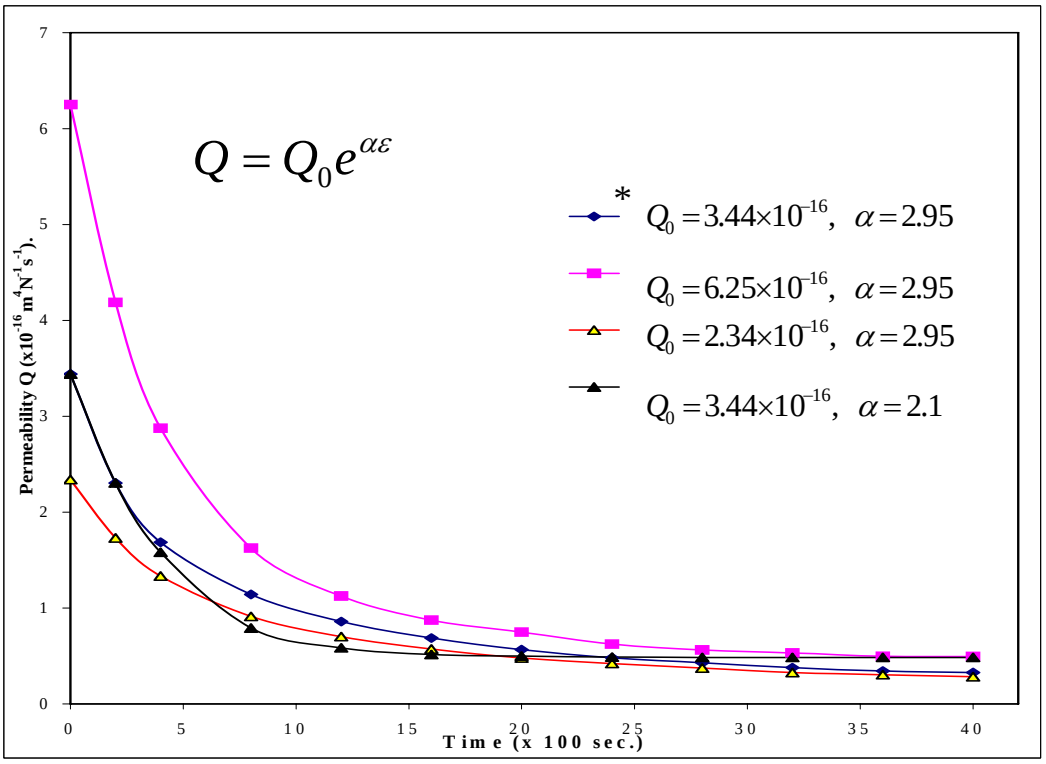

Figure 3.7: The influence of increasing or decreasing the permeability relative to that used for predicting the experimental hydrostatic excess pore pressure and matrix strain of Oloyede and Broom (1991). *Agreement with their experimental results of cartilage behaviour was obtained with the values of permeability coefficients ($Q_0 = 3.44\times10^{-16},\ \alpha = 2.95$).

3.3.2 The "parallel-element" analogue

The analogue presented in Figure 3.3 maintains the serial arrangement between the instantaneous reaction components and the subsequent transient deformation elements, namely the spring-dent and dashpot elements. However, close investigation reveals that

the mathematical modelling of this analogue (equation 3.20) is too cumbersome with the existence of two strains in the element; it is therefore proposed to use a "parallel-element" analogue such as shown in Figure 3.8 instead of the series model. This body can be shown to respond to loading in accordance with the following equations,

$$\sigma_a = (\sigma_s + \frac{k_v}{h_0}(1-\exp(\varepsilon)) - D\dot{\varepsilon} + \sigma_{s0}) + u_o + \bar{u}_h \qquad (3.22)$$

where, $\bar{u}_h = -\frac{h_o^2}{Q_o} e^{(2-\alpha)\varepsilon} \frac{\partial \varepsilon}{\partial t} + D_v \frac{\partial \varepsilon}{\partial t}$ is as in the previous modification

$\sigma_s = 0 \quad if \quad |\varepsilon| \le |\varepsilon_{sw}|$

$\sigma_s = B(\exp(\varepsilon_{sw}) - \exp(\varepsilon))^2 \quad if \quad |\varepsilon| > |\varepsilon_{sw}|$

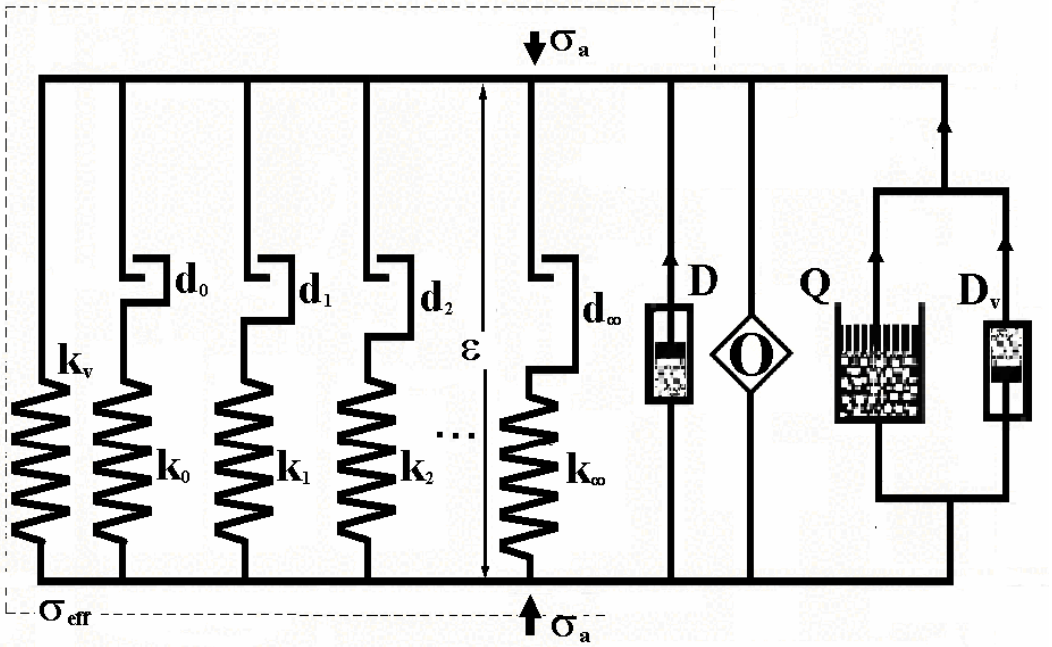

Figure 3.8: The modified 'parallel' rheological analogue for the articular cartilage matrix featuring an improved "instantaneous" reaction element and an additional swelling element. σ_a is the applied stress, k_v is the stiffness of the instantaneous spring, d_i (i=0, 1, 2,…) is the length of the i^{th} dent, k_i (i=0,1,2,…) is the stiffness of the i^{th} spring, D is the damping coefficient of the bounded fluid, D_v is the damping coefficient of unbounded fluid, σ_{eff} is the solid's effective stress, Q is the permeability coefficient of the matrix. "O" is the active osmotic component.

In this model, the stiffness of the instantaneous reaction spring, k_v is very small for this "parallel" model, so can be negligible; $D = \mu(u_{o1} + u_{o2})$, where μ is the coefficient representing drag effects caused by the resistance to fluid outflow with decrease in matrix permeability and increase in swelling; and u_o, $\bar{u}_h$ and σ_{s0} are as previously defined below equations (3.15) and (3.16), respectively.

The system of equations i.e. (3.16), (3.17) and (3.22) is numerically solved using the MAPLE code (Appendix A2.2) to obtain matrix load-cartilage parameters, σ_{eff}, $\bar{u}_h$, u_o, ε and other unknowns for this analogue. In a similar manner to the 'series' analogue, the effective stress of the solid skeleton has been evaluated using,

$$\sigma_{eff} = \sigma_a - \bar{u}_h - u_o + \sigma_{s0}$$

The predictions of this analogue are shown in Figure 3.9. It is reiterated that the advantage of this model is that of its mathematical simplicity with one matrix strain (equation 3.22), and its capability for predicting the position or layer-dependence of the response of the articular cartilage matrix to load. Its predictions accord well with published experimental results. Although mathematically much easier to establish, the results are practically the same as those obtained from the more mathematically complex series-element model.

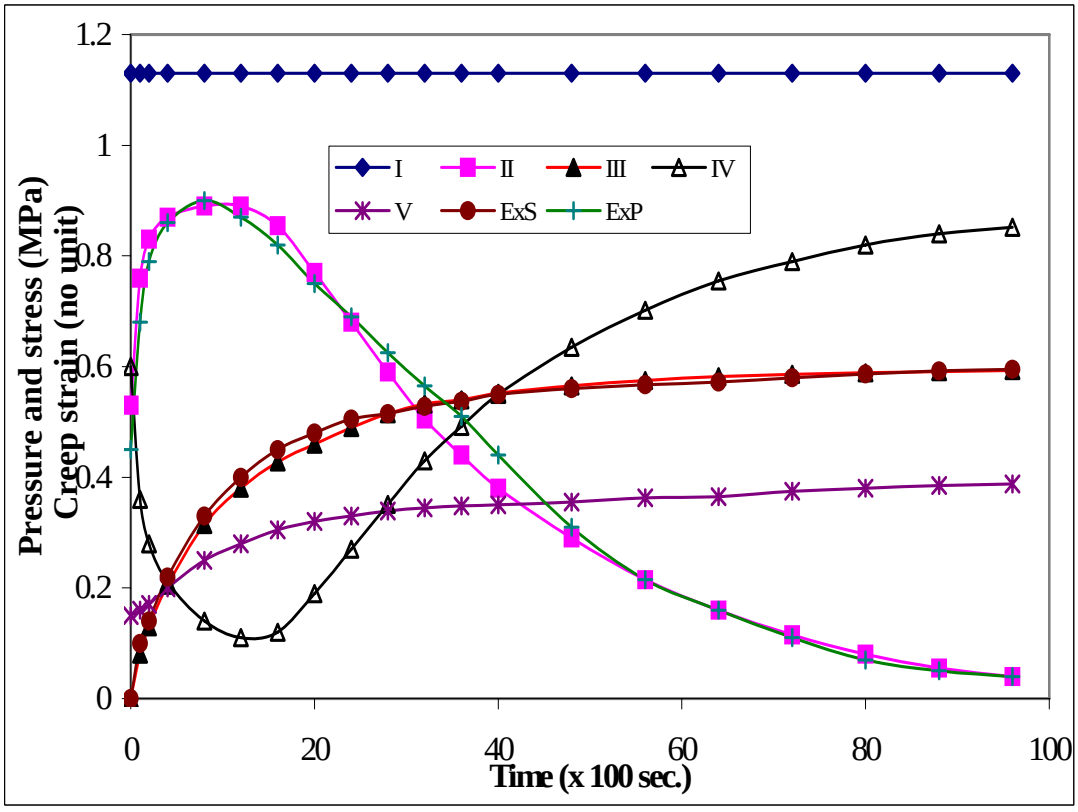

Figure 3.9: Predicted values of the hydrostatic excess pore pressure (II), creep strain of the matrix (III), effective stress of the solid's skeleton (IV), and osmotic pressure (V) under applied stress (I) using the "parallel" analogue of the articular cartilage matrix. The experimental hydrostatic excess pore pressure (ExP) and the creep strain (ExS) of Oloyede and Broom (1994 (a)) are compared to those of the prediction. The parameters used in this analysis are given in Table 3.5.

Table 3.5: Parameters for analysis resulting in Figure 3.9

h_0 mm	S MPa	k_v/h_0 MPa	μ (10^2)	D_v MPas	u_{o1} MPa	u_{o2} MPa	$Q_0 \times 10^{-16}$ (m^4/Ns)	α	$\frac{V_s}{V_0}$	$-\varepsilon_{sw}$
1.5	3.8	0.01	25	6100	0.02	0.18	3.44	2.92	0.28	0.48

3.4 Conclusion

The analyses carried out in this chapter demonstrate that the porohyperelastic analogue of Oloyede et al. (1992) was incapable of capturing the early stages of articular cartilage deformation and also proved inadequate for predicting the effect of physico-chemical swelling in the loaded tissue matrix. A revised model which incorporates a swelling element and which is capable of representing the various bulk responses of the matrix has been developed and published (Nguyen and Oloyede, 2001). Another finding relating to the rheological OB-body was that it was incapable of predicting the responses of the different layers of the tissue accurately. Consequently, new bodies that offer the capability for the analysis of the layers within a consolidating cartilage matrix was introduced to the literature (Nguyen and Oloyede, 2001). Two types of rheological configuration, namely serial and parallel, have been developed. It was demonstrated that the serial arrangement could only represent bulk properties. These analogues are the first to incorporate swelling elements with traditional mechanical elements for the analysis of soft tissue behaviour, thereby accounting for the contributions of both the mechanical, physico-chemical and unique architectural framework to cartilage load-bearing. The new "parallel-element" model was shown to be the most capable of the rheological bodies for capturing the experimentally observed consolidation behaviour of articular cartilage. This analogue is capable of predicting the hydrostatic excess pore pressure of matrix fluid, effective stress of the solid skeleton, "creep" strain and the influence of the degree of swelling on these parameters. Analysis using this model reveals the following combination of parameters necessary for evaluating and predicting the load-carriage responses of the cartilage matrix:

$$Q = 0.344 \times 10^{-15} e^{2.92\varepsilon} \qquad m^4 / Ns$$

$$\begin{cases} \sigma_s = -.144(MPa) \quad if \qquad |\varepsilon| \le 0.48 \\ \sigma_s = 20\left(0.62 - e^{\varepsilon}\right)^2 - 0.144(MPa) \quad if \qquad |\varepsilon| > 0.48 \end{cases}$$

$$\bar{u}_h = -\left(6540e^{-0.92\varepsilon} - 6100\right)\frac{\partial \varepsilon}{\partial t} \text{ (MPa)} ; \qquad u_o = \left(1 - 0.28e^{-\varepsilon}\right)\left(0.02e^{-\varepsilon} + 0.18e^{-2\varepsilon}\right) \text{ (MPa)}$$

The results of using these parameters in a single analysis is presented in Figure 3.9, where it can be seen that there is a close agreement with the experimental data between the predicted and the measured values of cartilage load-processing parameters.

Finally, both the series and parallel analogues presented in this work provide an additional dimension to cartilage analysis in that they offer the means for predicting the swelling characteristics (the swelling stress of the matrix) and therefore an avenue for future studies of degenerate tissue matrices.

Chapter 4: Experimental investigation of the biomechanical responses of normal and damaged cartilage.

4.1 Introduction

The specialized load-bearing structure of articular cartilage enables its physiological function, and any distortion to it would cause changes in the responses of the loaded matrix. For instance, its structural cohesivity would be deleteriously modified if the collagen architecture was damaged through laceration, with the concomitant effect of a reduction in its tensile strength and resistance to distension under compressive loading (Berkenblit et al., 1994; Broom and Oloyede, 1992; Newberry et al., 1997; Schmidt et al, 1990). Surface fibrillation was also examined in several other studies as an indicator of damage following repeated loading (Weightman, 1975; Weightman et al., 1973), but these studies could not identify any internal structural changes resulting in the observed biomechanical behaviour of damaged cartilage. Broom (1986) studied the structural changes induced in impacted cartilage matrix using microscopic methods. His results showed that the unimpacted or control cartilage was characterized by an arrangement of discrete fibril segments oriented about a radial mean. This was found to be transformed into a structure comprising fibrils which displayed a 'crimped' geometry in the radial direction as a consequence of the disruption of the interfibrillar linkage which is displayed by the normal untraumatised control samples as shown in Figure 4.1 below.

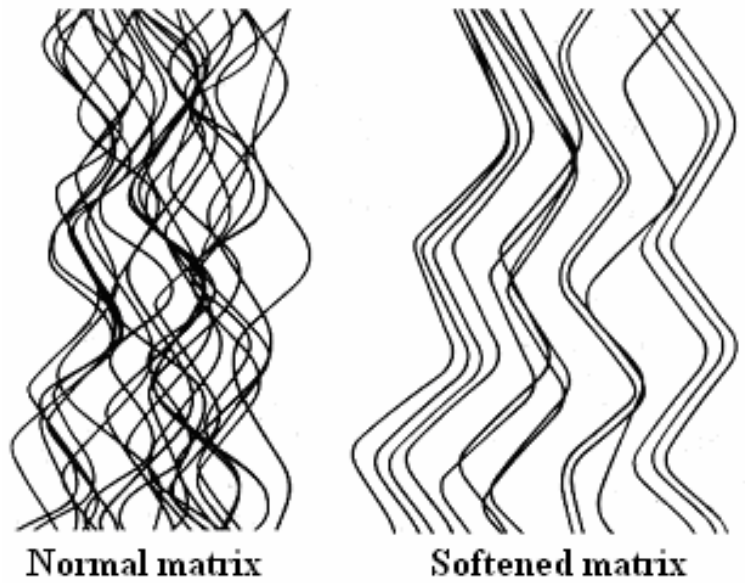

Figure 4.1: Schematic structure of fibrils in normal and softened cartilage matrices.

Weightman (1975) studied degenerated cartilage from osteoarthritic joints and inferred several characteristic features. Whilst this study provided the stiffness variation with the degree and location of degeneration, it did not establish the responses of its different layers, in processing load under conditions of localized damage (damage restricted to the superficial zone) or gross/ deep damage to the cartilage matrix. Such an insight would contribute to the understanding of how disease propagates through the layers of the matrix with direct consequences for clinical decisions in the treatment of joint diseases.

Cartilage Fibrillation degeneration is the second stage of osteoarthritis after the stage of osteoarthritic softening and is manifested as a series of lacerations and roughening of the superficial layer of the tissue. It is normally an indication of impairment due to excessive loading or disease. The physical properties of full-depth articular cartilage vary with degeneration and aging (Armstrong and Mow, 1982). The coexistent changes in the cartilage composition and function were analysed to test its mechanism. Such studies have typically been done on partial-thickness sections of cartilage (Bonassar et al., 1996; Frank et al., 1987; Sah et al., 1996; 1997), and the properties of the normal control partial-thickness samples often vary substantially from each other and also differ from those of full-thickness samples (Dumont et al., 1999).

On the other hand, a depletion of its proteoglycan content by ‘opening’ up the matrix through laceration would change the permeability characteristics and its compressive stiffness. All of these properties are significant in determining the deformation characteristics of the tissue and are important factors in the consolidation responses of cartilage under static to moderate velocity quasi-static loading.

Consequently, it was impossible to determine the severity, with respect to the proportion of the matrix that has been damaged, before a particular observed effect would occur. For example, the question of how cartilage would respond to load when it only carries lacerations confined to its superficial layer which is strain-limiting and with distinct properties from the underlying layers, and when the damage or degeneration is more general covering the surface and general matrix, needs to be answered. Such an insight would shed some light into the functional resilience of the normal and

degenerate cartilage matrix and answer the question of how severe mechanical impairments have to be before the tissue would become physiologically dysfunctional.

Moreover, the degree or depth of laceration is carefully controlled so that the excess pore pressure could be accurately related to the severity of mechanical impairment. A study of articular cartilage, which combines both mathematical and finite element modelling of the tissue, is presented to study the dependence of cartilage consolidation behaviour in its many layers and how such responses are influenced by artificial lacerations to known depths of its superficial layer. In this chapter, an experimental scheme for both the normal intact matrices and the artificially damaged ones with either shallow (i.e. less than 100 μm) or deep (more than 100 μm) lacerations will be set up to experimentally obtain the biomechanical properties of the normal intact and lacerated matrix of cartilage.

4.2 Experiment

The aim of the experiments reported is to investigate the deformation of a normal matrix with intact and lacerated cartilage with respect to the hydrostatic excess pore pressure measured at its bottom under a static axial load.

4.2.1 Equipment

The experimental rig used in the static loading experiments is shown in Figure 4.2A, with the main components being:

i- The frame with load
ii- Consolidometer cell
iii- Linear Variable Displacement Transducer
iv- Pressure transducer (Sensotec, model A-105/0278-11G (500 PSIG pressure))
v- Computer with Labview software
vi- A thin-walled cylindrical punch of 12 mm in diameter.
vii- A custom-built surface lacerator.

Articular cartilage matrices with both intact and lacerated superficial layers were

loaded statically in a consolidometer similar to that previously used by Oloyede et al. (1992) to measure the pattern of growth and decay of the hydrostatic excess pore pressure at the bottom of the cartilage matrix under one-dimensional deformation. The consolidometer used in this study is presented in Figure 4.2B. It consists of a thick-walled stainless steel cell, C, with an internal diameter of 12 mm. The internal base of the cell opens into a bore that communicates directly with a pressure transducer whose output is recorded through the LABVIEW software package. A LVDT is incorporated into the system to measure the total displacement of the matrix. The output of the LVDT is also logged via LABVIEW. A porous stainless steel disc, D1, is inserted into the base of the cell and the articular cartilage specimen (AC) is clamped firmly against it with the clamping ring S. Another porous stainless steel disc, D2, is placed above the specimen such that there is full drainage under the applied load P through the surface.

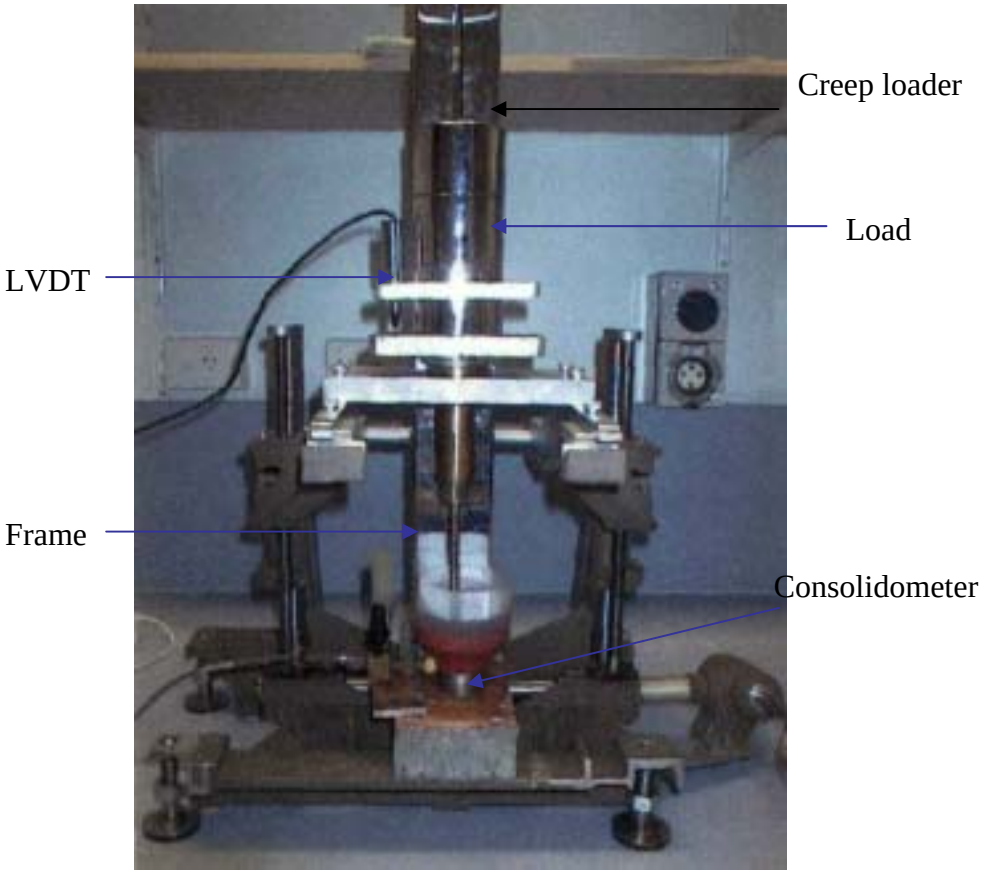

Figure 4.2A: The static loading rig showing the consolidometer and linear variable displacement transducer (LVDT) in situ to measure hydrostatic excess pore pressure and matrix strain respectively.

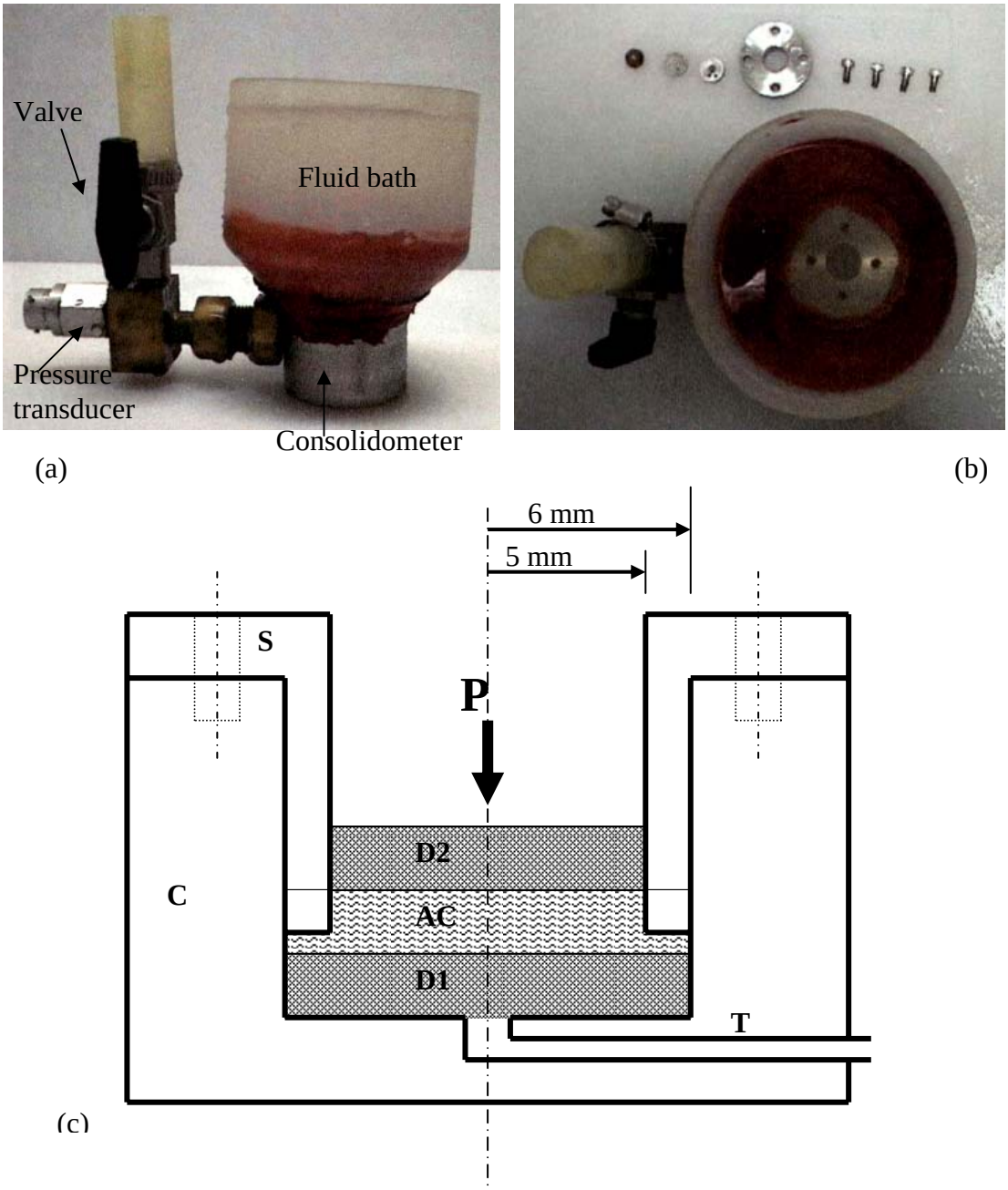

Figure 4.2B: The one-dimensional consolidometer (Oloyede et al., 1992).
(a) The assembled consolidometer with the pressure transducer in place.
(b) The view showing the consolidometer well.
(c) Schematic diagram of the consolidometer.

4.2.2 Sample preparation and repeatability tests

Full thickness (about 1.5-2 mm) medial and lateral scallops of AC were removed from the patellar grooves of bovine animals, and cut into cylindrical specimens of radius 12mm using a thin-walled cylindrical punch (Figure 4.3). The specimen was inserted

into the base of the consolidometer cell and the one-dimensional constraining flange secured in place. It should be noted that the environment in which the disc was clamped contained de-aired saline solution of 0.15 M to avoid air bubbles influencing the result of the experiments by blocking fluid pressure signals from the transducer.

A normal intact cartilage sample was first tested in three load-unload-recovery cycles to determine the consistency of the results. This confirmed that the consolidation results were repeatable with the hydrostatic excess pore pressure and consolidation strain data in consistent agreement for the three tests. Further consolidation tests were carried out on the same specimens after lacerations of 50μm (about 2.5% of thickness), 100μm (5%), 200μm (10%), and up to 780μm (40%) depth each time to their superficial layers using a specially built precision lacerator that could be preset to an incision depth. The depth of laceration was preset using a dial gauge to measure the height of a stainless steel blade relative to the flat surfaces of the two rectangular stainless steel blocks between which it was sandwiched and held in place by two screws. This custom-built surface lacerator can produce an accuracy of approximately ± 2 μm of the required depth of laceration.

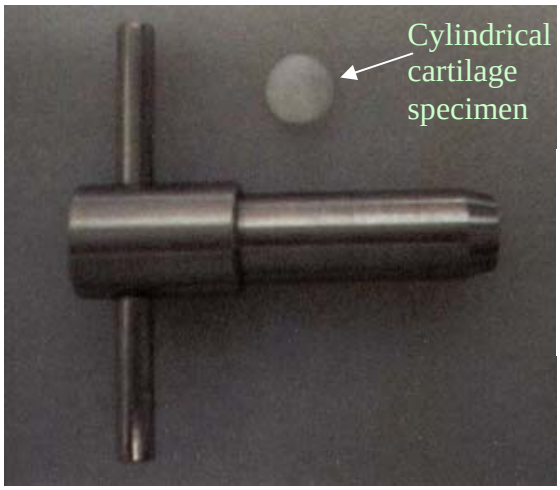

Figure 4.3: The thin-walled cylindrical punch for cutting the cartilage specimens used in experiments and cartilage specimen of 12 mm diameter

4.2.3 Consolidation tests

According to the depth-dependent structure of cartilage as discussed in Chapter 2, a cartilage matrix is assumed to be a heterogeneous material whose properties vary with depth from the surface but is homogeneous on the planes parallel to the surface in this study. Thus, cartilage specimens are cut from a selected flat matrix and laceration

directions are ignored in these experiments.

Each full-thickness cartilage disc was consolidated under static compression of 1.06MPa (8.5 kg of load) until the end of consolidation i.e, when the excess pore pressure had decayed to zero. The specimen was then unloaded and allowed to recover to its original thickness. After a recovery period of 2 hours, the superficial layer of the specimen was lacerated to either a depth of 50, 100, 150 or 200 μm as required such that the laceration remained wholly within the approximately 200 μm deep articular surface layer (Weightman, 1975; Schinagl et al., 1997), using the above mentioned custom-built surface lacerator. After this, the specimen was left to continue recovery for another thirty minutes before reloading.

The consolidometer was again reassembled with the lacerated specimen in-situ and the consolidation process was repeated until full consolidation. Each of the 50 specimens with lacerated superficial surfaces also produced repeatable consolidation results under the applied load of 1.06 MPa.

4.3 Results and discussions

Figures 4.4 – 4.10 reveal that the hydrostatic excess pore pressures at the bottom of the matrices and the total matrix strains have similar patterns for both normal and surface-lacerated matrices. The hydrostatic excess pore pressure increases up to a maximum level, which is less than the applied load, and then decays to zero; and the matrix strain increases at a fast rate in the initial stages of deformation and then much more slowly towards an asymptotic value. The maximum pressures were about 75-90% of the applied load (1.06 MPa in these tests) and varied with different specimens and the matrices were compressed up to 40-50% strain in these experiments.

For the normal cartilage matrix, the maximum excess pore pressure and the total matrix strain in the medial (Figure 4.4, 4.7 and 4.8) and lateral (Figure 4.5, 4.6, 4.9 and 4.10) samples were of the same value in magnitude and rate of decay. This suggests that both medial and lateral cartilage might have the same principal material properties, namely stiffness and permeability.

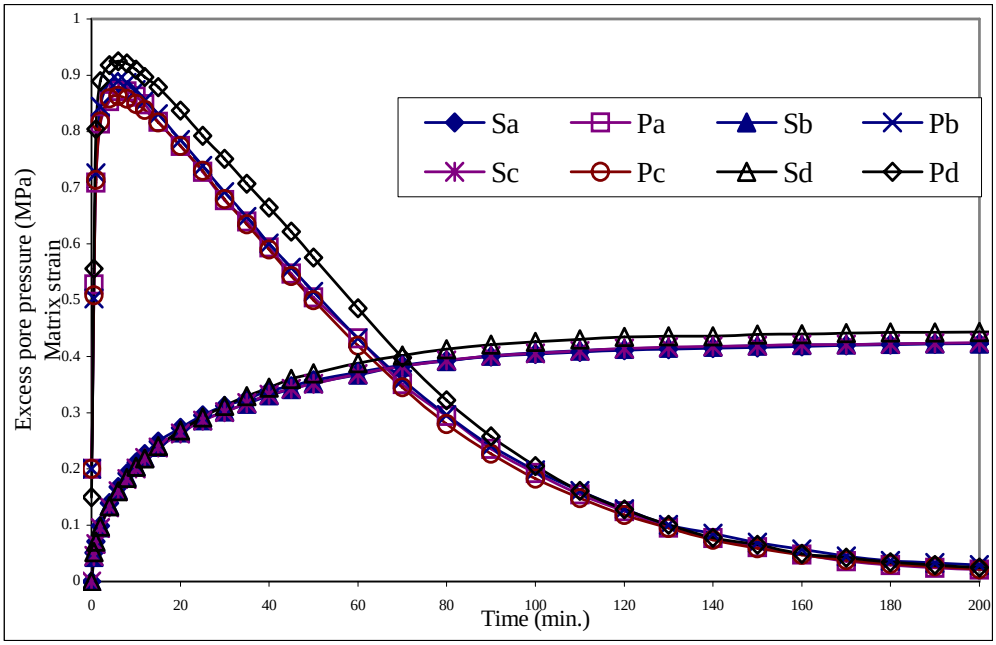

Figure 4.4: The responses of normal and artificially lacerated cartilage (Medial bovine cartilage, thickness 1.71mm). Sa= experimental values of the total matrix strain and Pa= hydrostatic excess pore pressure for normal cartilage with intact superficial layer; Sb and Pb are the data for normal cartilage with lacerated surface to 50µm; Sc and Pc are the data for normal cartilage with lacerated surface to 100µm; Sd and Pd are the data for normal cartilage with lacerated surface to 200µm.

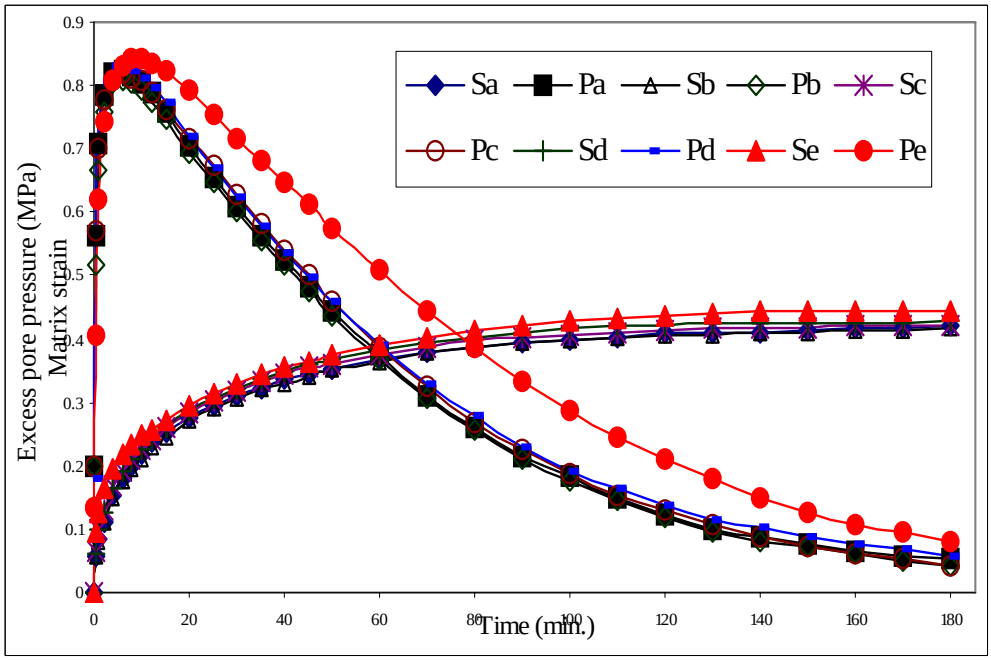

Figure 4.5: The responses of normal and artificially lacerated cartilage (lateral bovine cartilage, thickness 1.55mm). Sa= experimental values of the total matrix strain and Pa= hydrostatic excess pore pressure for normal cartilage with intact superficial layer; Sb and Pb are the data for normal cartilage with lacerated surface to 50µm; Sc and Pc are the data for normal cartilage with lacerated surface to 100µm; Sd and Pd are the data for normal cartilage with lacerated surface to 200µm; Se and Pe are the data for normal cartilage with lacerated surface to 250µm.

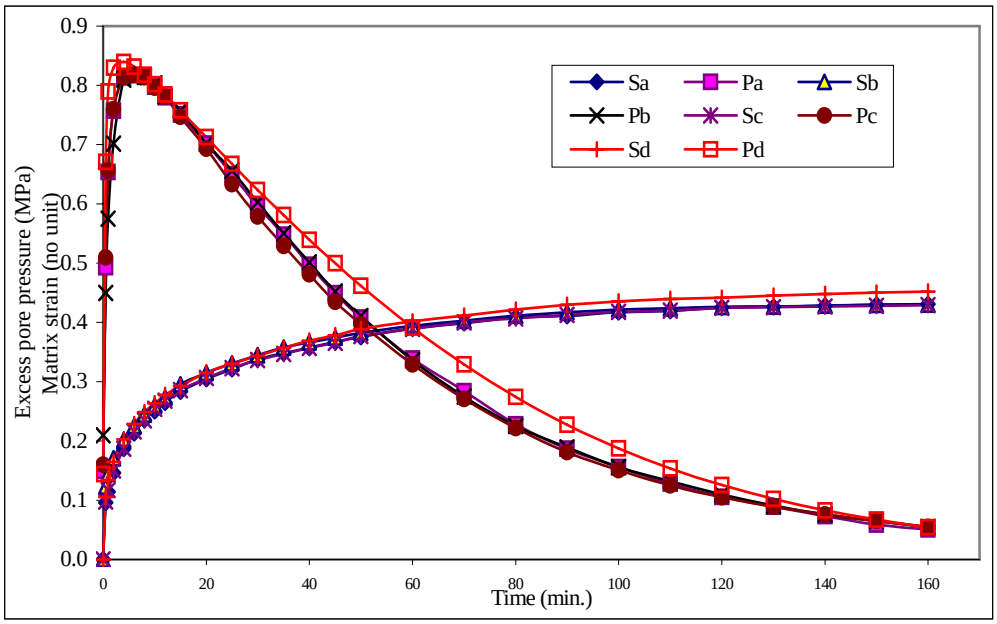

Figure 4.6: The responses of normal and artificially lacerated cartilage (lateral bovine cartilage, thickness 1.57mm). Sa= experimental values of the total matrix strain and Pa= hydrostatic excess pore pressure for normal cartilage with intact superficial layer; Sb and Pb are the data for normal cartilage with lacerated surface to 50μm; Sc and Pc are the data for normal cartilage with lacerated surface to 100μm; Sd and Pd are the data for normal cartilage with lacerated surface to 200μm.

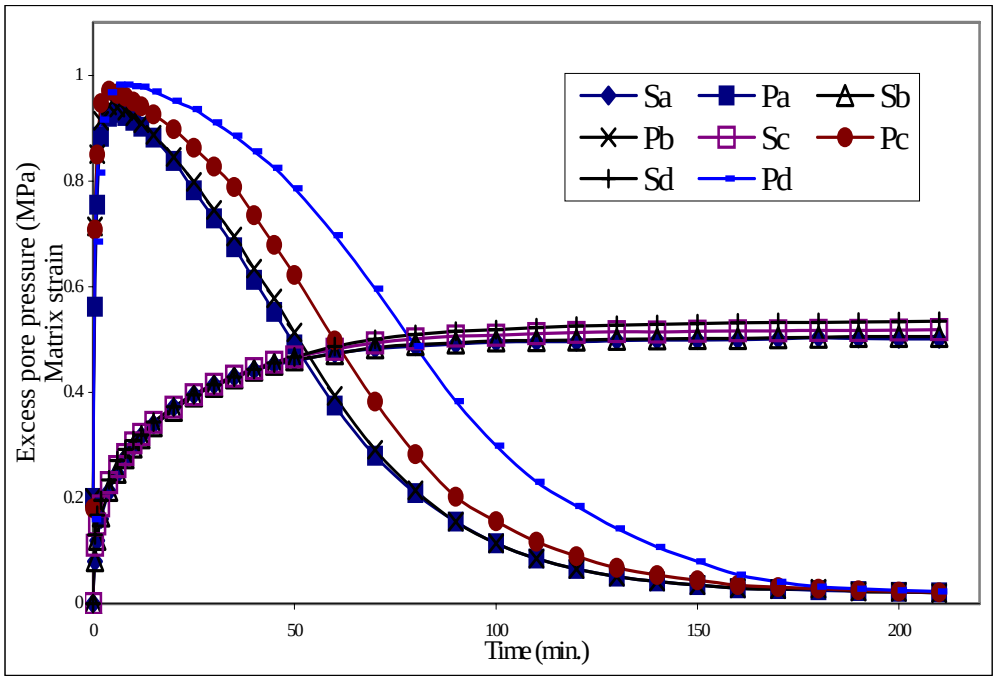

Figure 4.7: The responses of normal and artificially lacerated cartilage (medial bovine cartilage, thickness 1.59mm). Sa= experimental values of the total matrix strain and Pa= hydrostatic excess pore pressure for normal cartilage with intact superficial layer; Sb and Pb are the data for normal cartilage with lacerated surface to 110μm; Sc and Pc are the data for normal cartilage with lacerated surface to 430μm; Sd and Pd are the data for normal cartilage with lacerated surface to 780μm.

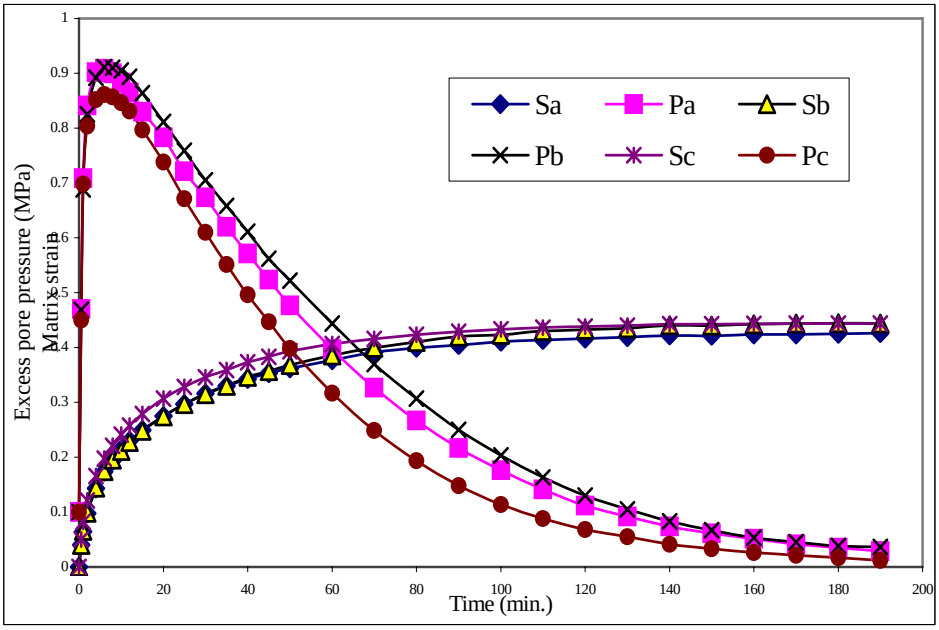

Figure 4.8: The responses of normal and artificially lacerated cartilage (medial bovine cartilage, thickness 1.53mm). Sa= experimental values of the total matrix strain and Pa= hydrostatic excess pore pressure for normal cartilage with intact superficial layer; Sb and Pb are the data for normal cartilage with lacerated surface to 430μm; Sc and Pc are the data for normal cartilage with lacerated surface to 780μm.

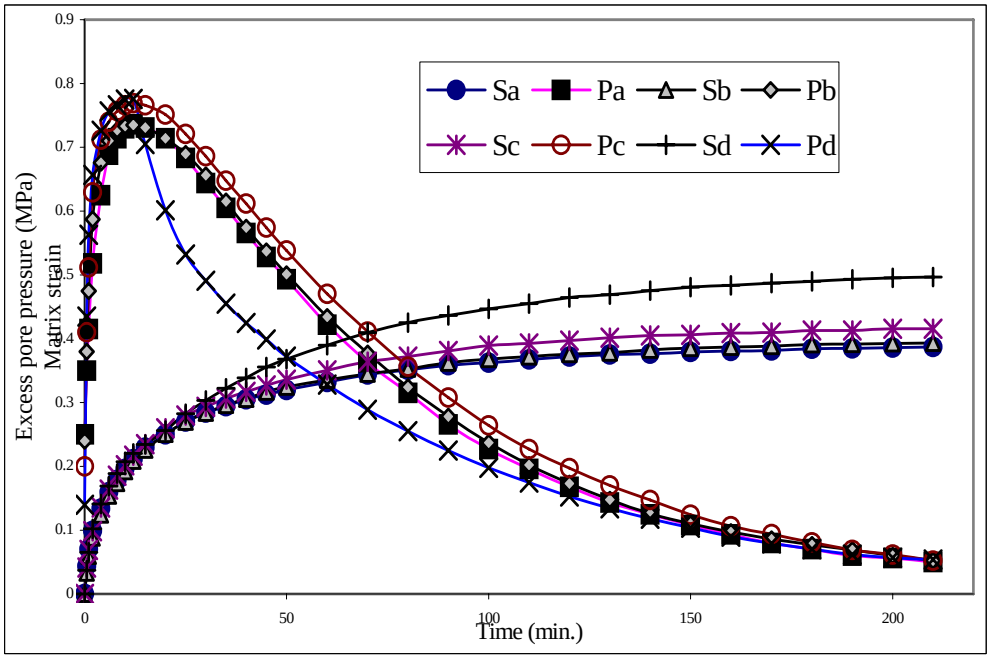

Figure 4.9: The responses of normal and artificially lacerated cartilage (lateral bovine cartilage, thickness 1.92mm). Sa= experimental values of the total matrix strain and Pa= hydrostatic excess pore pressure for normal cartilage with intact superficial layer; Sb and Pb are the data for normal cartilage with lacerated surface to 110μm; Sc and Pc are the data for normal cartilage with lacerated surface to 430μm; Sd and Pd are the data for normal cartilage with lacerated surface to 780μm.

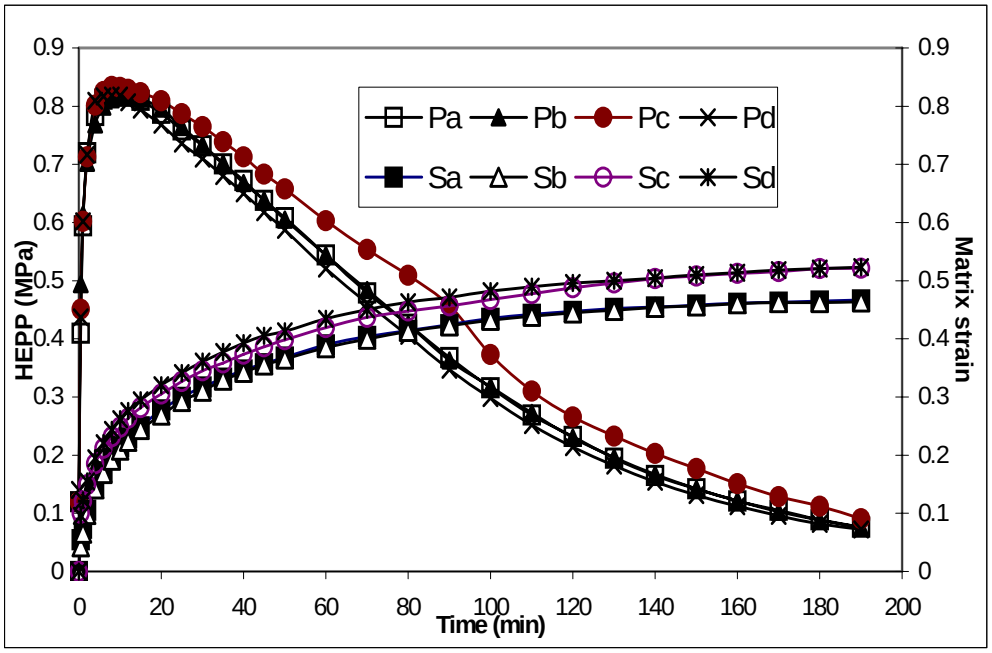

Figure 4.10: The responses of normal and artificially lacerated cartilage (lateral bovine cartilage, thickness 1.70mm). Sa= experimental values of the total matrix strain and Pa= hydrostatic excess pore pressure for normal cartilage with intact superficial layer; Sb and Pb are the data for normal cartilage with lacerated surface to 110μm; Sc and Pc are the data for normal cartilage with lacerated surface to 430μm; Sd and Pd are the data for normal cartilage with lacerated surface to 780μm.

The figures also illustrate that the excess pore pressure and the matrix strain for the surface-lacerated or damaged matrices with depths of laceration less than 200 μm are similar to those of the normal intact samples. The figures, however, show that both the excess pore pressure and strain increase in magnitude when the depth of laceration exceeds the 200 μm thickness of the superficial layer (Figure 4.4 –4.7). This may be due to the fact that the cohesivity of the collagen-proteoglycan architecture was deleteriously affected with consequence for the stiffness and permeability of the matrix.

Specifically, Figure 4.9 and 4.10 show that the excess pore pressures with a 430μm deep laceration (Figure 4.9) and the 780μm laceration (Figure 4.10) suddenly reduced either to, or lower than, the curve of that in the normal matrix while deformation was still high. When the cut was deeper, the excess pore pressure was lower than that compared to the normal. This event can be explained by noting that after a certain depth of cut into the surface layer, the stiffness of the matrix is compromised, i.e the collagen meshwork would have been so untangled/disrupted that it would be unable to entrap the

proteoglycans. This would result in a noticeable amount of change in the stiffness and permeability, as is borne out by the experimental results. In this situation, the permeability would become higher than that of the normal intact matrix, and will result in a quicker outflow of the fluid from the matrix with the consequence that the maximum hydrostatic excess pore pressure is lowered while the transient decay of this parameter is faster (see Figure 4.8 and 4.10).

4.4 Conclusion

The experiments showed that shallow lacerations did not provide any evidence of change in the responses of the hydrostatic excess pore pressures, total matrix strains and related parameters of load-carriage. It can be hypothesised that shallow lacerations mainly result in surface roughening, which may affect lubrication conditions in the joint where two cartilage surfaces make contact. On the other hand, the deep lacerations would reduce the matrix's stiffness and characteristic permeability, leading to a concomitant remodelling of the fluid response under load. The exact nature of this relationship between permeability, hydrostatic excess pore pressure and the overall deformation ("creep" strain) of the tissue after surface modification is revealed by these results presented in figures 4.4-4.10, and a viable model for predicting this type of response is presented in the following chapters. The results would provide insight into how the commonly observed degenerative symptom of superficial surface lacerations and their effects (Radin and Paul, 1971; Broom, 1982) influence the biomechanical responses of loaded articular cartilage.

Chapter 5: Theoretical prediction of normal and surface damaged cartilage using the rheological analogue model for numerical analysis.

5.1 Introduction

This chapter predicts the insight responses of the loaded matrix and investigates systematically the consequence of the impairment of the superficial layer of articular cartilage on its depth-dependent consolidation behaviour based on rheological modelling. In particular, the patterns of variation in the hydrostatic excess pore pressure, effective solid skeleton stress and strain at different positions within the matrix are determined by a combination of experimental and finite element analysis of a rheological model of the tissue.

5.2 Rheological analogues of articular cartilage

In this chapter, we hypothesize that cartilage is a planar homogeneity and any degeneration in the superficial layer would modify the magnitude and distribution of both the permeability coefficient and the modulus of compressibility of the matrix, with significant consequences for the pattern of the growth and decay of the hydrostatic excess pore pressure. In order to achieve the aim of this study a modification of the models in chapter three for one-dimensional deformation to incorporate a more rigorous consideration of the permeability and distribution of the compressive coefficient of the tissue is attempted. Extensions to the works of Lai et al (1981) and Higginson et al. (1976) to cover the depth-dependence of the permeability parameter are carried out and the results of Schinagl et al. (1997) on the variation of stiffness with position is also implemented.

The earlier rheological analogue for articular cartilage consolidation in Chapter 3 is extended to that each layer is modelled as a parallel analogue of depth-dependent parameters thereby the system of the analogues represents a matrix of the planar homogeneous cartilage. The dependence of permeability on depth and deformation is also modelled in the following section. The model assumes that the permeability is strain and position-dependent and is a solution of a second order differential equation

which, although has the same appearance as a diffusion equation, does not model diffusion, but instead describes the spatial distribution of the deformation-dependent permeability of the tissue. The rheological analogue representing a layer of the matrix is presented in Figure 5.1. The ability to model layer-by-layer responses using this modified analogue presents the opportunity for prescribing unique layer properties, especially those of the surface.

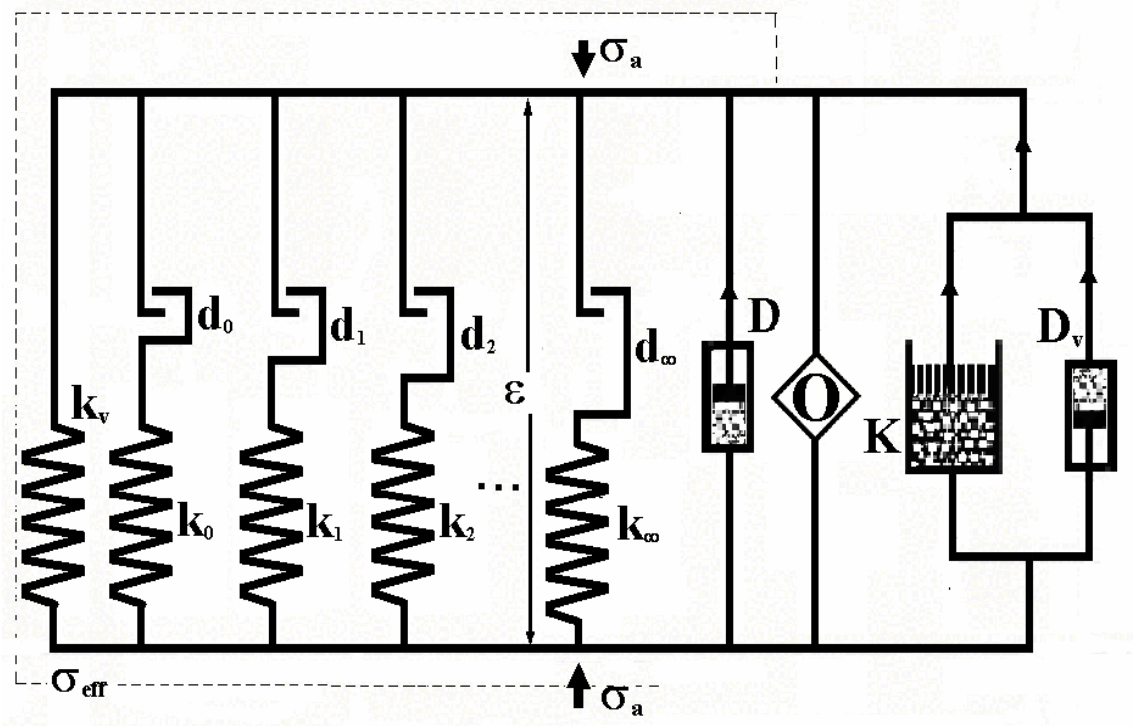

Figure 5.1: The 'parallel' rheological analogue for the articular cartilage layer featuring an improved "instantaneous" reaction element and an additional swelling element.
σ_a is the applied stress, k_v is the stiffness of the instantaneous spring, d_i(i=1, 2,…) is the length of the gap of the i^{th} dent, k_i (i=1,2,…) is the stiffness of the i^{th} spring, D is the drag coefficient due to interaction between fluid and solid, D_v is the damping coefficient of unbounded fluid, σ_{eff} is the solid's effective stress, K is the permeability of the matrix fluid. "O" is the active osmotic component (Chapter 3). This model is reconfigured in Figure 5.2 for the present analysis.

In addition, the distribution of the proteoglycans with depth (Jones et al., 1982; Khalsa et al., 1997; Maroudas, 1979; Urban et al., 1979) is incorporated into the mathematical model, so that the swelling characteristics of the dissimilar layers can be accounted for. The physical characteristics of the macroscopic layers of the matrix are described elsewhere (Gore et al., 1983; Lipshitz et al., 1976; McCutchen, 1975; Schinagl et al.,

1997) but of importance presently is the ability to study the functional characteristics of the separate layers of the tissue within a continuum analysis, and more importantly the consequence of damaging a layer of the matrix to the global deformation of the tissue.

The rheological analogue on which the predictions are based comprises a hyperelastic solid, an inviscid fluid and an osmotically active component arranged as shown in Figure 5.1, so that layer properties can be represented. Constitutive relationships are written for these components and used with the continuity equation of fluid percolation to predict the tissue's response in each of its hypothetical layers to static load applied at the surface of the matrix with and without superficial surface laceration. The resulting equations were discretized and solved numerically using a MATLAB discrete element solver. The numerical predictions were then compared to experimental data.

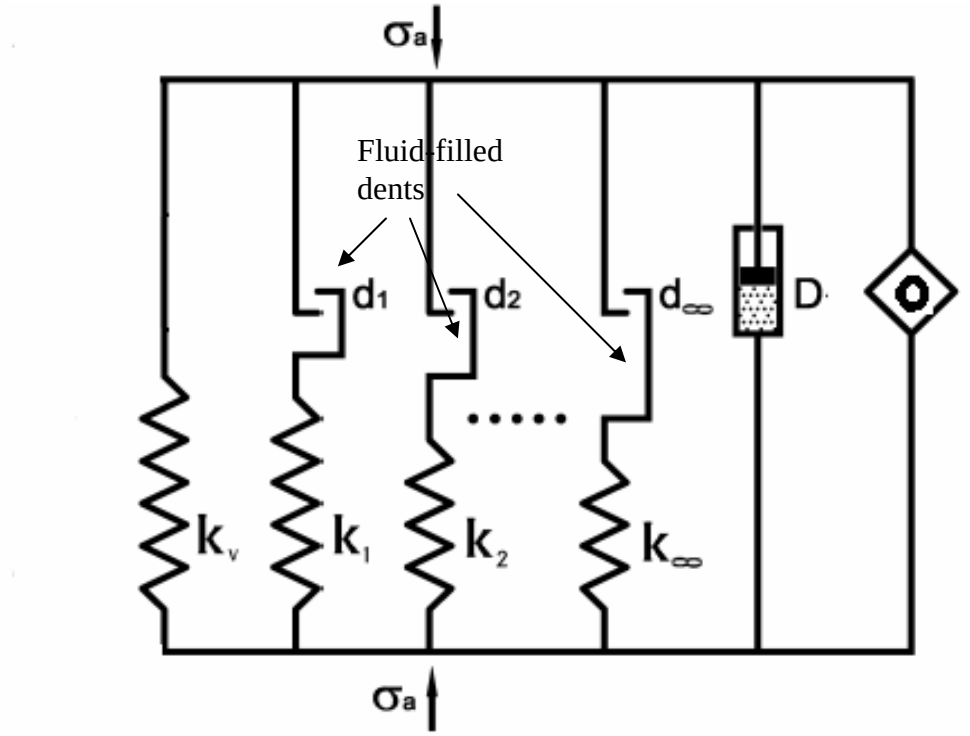

Figure 5.2: The modified 'parallel' rheological analogue for a cartilage layer in which the Q and D_v representing fluid flow are now inter-twined with the response of the dents d_i such that the dents are now modeled as fluid-filled dents.
σ_a is the applied stress; k_v is the stiffness of the instantaneous spring (instantaneous reaction element), d_i (i=1, 2, …) is the length of the gap of the i^{th} dent containing bounded fluid; k_i (i= 1, 2, …) is the stiffness of the i^{th} spring containing the unbounded fluid; D is the damping coefficient of the dashpot representing the drag force of the solid; and σ_{eff} is the solid's effective stress.

5.3 Development of constitutive relationships for the layer analogue

5.3.1 Stress-strain relationship

Figure 5.2 presents the analogue adopted for this study. This has been fully described in Chapter 3. Essentially the system of the spring-dent elements represents the solid components of the matrix and bound water and unbound fluid. The dashpot models the drag between the solid and fluid as fluid exits the loaded matrix. This system is a proven rheological representation of structural hyperelasticity which works for the consolidation response of articular cartilage (Nguyen and Oloyede, 2001; Oloyede et al., 1992). The osmotic component represents a combination of factors, which account for all types of swelling (electrostatic and Donnan), the contribution of swelling to the deformation of the solid and drag forces as the fluid is exuded.

Let the initial thickness of the layer be *h*; and assume that a given layer undergoes a total displacement *x* of the given layer at time *t* (the difference between the initial and instantaneous thicknesses of the layer) due to loading. If the gap size of any two microscopically close dents is assumed to be small, then

$$d_1 = d_2 - d_1 = d_3 - d_2 = ... = d_n - d_{n-1} = \Delta x \text{ or, } d_i = i\Delta x = x \tag{5.1}$$

where d_i is the distance between the two ends or gap of a given dent, i = 1, 2, …, n; Δx and x are the small deformation change and the instantaneous deformation in length of the layer.

The total resulting tensile force F (equivalent to the distension in the collagen-proteoglycan architecture of articular cartilage) generated by this deformation for all active springs is

$$F(x) = -k_v x - k_1(x - \Delta x) - ... - k_{i-1}(x - (i-1)\Delta x) \tag{5.2}$$

and $$F(x + \Delta x) = -k_v(x + \Delta x) - k_1(x) - ... - k_{i-1}(x + \Delta x - (i-1)\Delta x) - k_i \Delta x \tag{5.3}$$

where, k_i is the i^{th} spring stiffness and Δx is defined as in equation (5.1).
Combining equations (5.2) and (5.3) yields

$$\frac{\Delta F}{\Delta x} = \frac{F(x + \Delta x) - F(x)}{\Delta x} = -k_v - k_1 - ... - k_{i-1} - k_i \tag{5.4}$$

In order to simplify equation (5.4), we define

$$k_i = \frac{k_v h^2 \Delta x}{\left(h-(i-1)\Delta x\right)^3}$$

where $k_v = k_v(z)$ for depth-dependent stiffness and z is the displacement from the surface, so that equation (5.4) can be rewritten as

$$\frac{\Delta F}{\Delta x} = -k_v - \sum_{j=1}^{j=i} \frac{k_v h^2 \Delta x}{\left(h-(i-1)\Delta x\right)^3} \tag{5.5}$$

Using Riemann summation, equation (5.5) can be derived form for continuous deformation as

$$\frac{dF}{dx} = \lim_{\Delta x \to 0} \frac{\Delta F}{\Delta x} = -k_v - \lim_{\Delta x \to 0} \sum_{j=1}^{j=i} \frac{k_v h^2 \Delta x}{\left(h-(i-1)\Delta x\right)^3} = -k_v - \int_0^x \frac{k_v h^2 dy}{\left(h-y\right)^3} = -\frac{k_v}{2}\left(1+\frac{h^2}{(h-x)^2}\right)$$

or
$$F(x) = \int_0^{F(x)} dF = \int_0^x -\frac{k_v}{2}\left(1+\frac{h^2}{(h-x)^2}\right)dx = \frac{k_v h}{2}\left(1-\frac{x}{h}-\frac{h}{(h-x)}\right) \tag{5.6}$$

It is noted that the strain in each layer is described for the incompressible solid as

$$\varepsilon = \frac{\Delta V}{V_0} = \frac{V-V_0}{V_0} = \frac{x}{h} \approx \frac{\Delta V_f}{V_0} \tag{5.7}$$

where, ΔV and ΔV_f are respectively the changes in total layer volume and fluid content in the layer; V and V_0 are the instantaneous and initial volumes respectively; x and h are defined as above. Thereby, the total stress σ_s generated by the solid component can be formed from equation (6),

$$\sigma_s = \frac{F}{A} = \frac{k_v h}{2A}\left(1+\varepsilon-\frac{1}{1+\varepsilon}\right) = \Phi\left(1+\varepsilon-\frac{1}{1+\varepsilon}\right), \tag{5.8}$$

where $\Phi = \Phi(z) = \dfrac{h k_v(z)}{2A}$ is a depth-dependent modulus of compressibility or stiffness, A is area of the matrix and z is the displacement from the surface.

Equation (5.8) is the asymptotic approximation for the constitutive stress-strain relationship for the wet solid component in a given layer of articular cartilage undergoing incremental strain ε. This relationship is more accurate than that in the previous published paper (Nguyen and Oloyede, 2001). Equation (5.8) implicitly demonstrates that a large compressive strain of $\varepsilon = -1$ is impossible, or there can be so layer collapse in the deformation of the tissue.

Taking the derivative of equation (5.8) with respect to the strain, the depth- and strain-dependent stiffness S (slope of stress-strain curve) becomes,

$$S = \frac{\partial \sigma_s}{\partial \varepsilon} = \Phi\left(1 + \frac{1}{(1+\varepsilon)^2}\right) \tag{5.9}$$

At the initial time ($t = 0$), $\varepsilon = 0$, equation (9) will be

$$S(0, z) = \frac{\partial \sigma_s(0)}{\partial \varepsilon} = 2\Phi(z).$$

Therefore in the unloaded osmotically changed articular cartilage matrix at time $t = 0$ or $\varepsilon = 0$, the compression coefficient is half the slope of the stress-strain curve for any layer.

5.3.2 Continuity equation

Because fluid outflow from the cartilage layer is sufficiently low for Darcy's law to apply (Klausner, 1991), the low one-dimensional velocities of flow due to static loading can be described

$$v_d = -\frac{k_p}{\gamma}\frac{\partial u}{\partial z} = -K\frac{\partial u}{\partial z}, \tag{5.10}$$

where v_d is Darcy's velocity of fluid flow through the pore of the layer at a given depth, u is the hydrostatic excess pore pressure, z is the depth position from the surface of the matrix, γ (N/m^3) is the gravitational density of fluid in an element, k_p (m/s) is the permeability of the element (layer) and $K(z,\varepsilon)$ is the coefficient of permeability which is a function of position z and strain ε, which is modelled in section 5.3.6.

It should be noted that for articular cartilage, the total fluid excess pore pressure is dependent on the intrinsic osmotic pressure and transient changes in the fixed charge density (ECD)-water ratio in any layer. The relationship between the progressive decrease in fluid volume and its one-dimensional velocity, which will be derived in Section 6.3.5, is

$$\frac{1}{V}\frac{\partial V}{\partial t} = -div(\bar{v}_d) = -\frac{\partial v_d}{\partial z}. \tag{5.11a}$$

Combining equations (5.10) and (5.11a) yields

$$\frac{V_0}{V}\frac{\partial}{\partial t}\left(\frac{V}{V_0}\right)=\frac{\partial K}{\partial z}\frac{\partial u}{\partial z}+K\frac{\partial^2 u}{\partial z^2}\ \text{ or }\ \frac{1}{1+\varepsilon}\frac{\partial(1+\varepsilon)}{\partial t}=\frac{\partial K}{\partial z}\frac{\partial u}{\partial z}+K\frac{\partial^2 u}{\partial z^2}$$

so that,

$$\frac{1}{1+\varepsilon}\frac{\partial \varepsilon}{\partial t}=\frac{\partial K}{\partial z}\frac{\partial u}{\partial z}+K\frac{\partial^2 u}{\partial z^2} \tag{5.11}$$

5.3.3 Physico-chemical effect

The stiff biological gel-like response of loaded articular cartilage is partly due to its physico-chemical swelling which is in turn dependent on its proteoglycan content. Oloyede and Broom (1993 (b); 1994 (a)) have shown that the tissue's maximum hydrostatic excess pore pressure, u_{max}, and its subsequent decay over time is a function of its degree of swelling. Using Donnan equilibrium conditions, the osmotic pressure can be expressed approximately for a given layer as (Tombs and Peacocke, 1974; Broom and Oloyede, 1998)

$$u_o = RT\left(\frac{C_2}{M_2}+\beta C_2^2\right), \tag{5.12}$$

where C_2 is the instantaneous weight concentration of the proteoglycan component, M_2 is its molar mass, R is the universal gas constant, T is the temperature of the layer element and β is the second virial coefficient for a three-component biological gel under Donnan equilibrium.

A change in the concentration of the fixed charge component per fluid volume normally accompanies the outflow of fluid from the matrix. Therefore, considering the conservation of the mass of the fixed charges in an element within a layer, we can write the following relationship,

$$C_2V = C_{20}V_0 \quad or \quad C_2 = C_{20}\frac{V_o}{V}=\frac{C_{20}}{1+\varepsilon}, \tag{5.13}$$

where C_{20} is the initial weight concentration of proteoglycans and the other terms are as defined previously.

Substituting equation (5.13) into equation (5.12) yields,

$$u_o = RT\left(\frac{C_{20}}{M_2}\frac{1}{1+\varepsilon}+\beta C_{20}^2\frac{1}{(1+\varepsilon)^2}\right)=\frac{u_{o1}}{1+\varepsilon}+\frac{u_{o2}}{(1+\varepsilon)^2} \tag{5.14}$$

where, $u_{o1} = \frac{RTC_{20}}{M_2}$ *and* $u_{o2} = RT\beta C_{20}^2$

According to Tombs and Peacocke (1974), it should be noted that the first term of the right hand side of equation (5.14) is the swelling effect of the proteoglycan chains which is intertwined with the response of the solid skeleton, while the second is the Donnan effect of the fixed charges which would contribute directly to changes in the hydrostatic excess pore pressure. Therefore, only second term is described for osmotic pressure due to Donnan effect but the first is not. Furthermore, the concentration of proteoglycans and fixed charges increase from the surface to the bottom layers of the matrix (Maroudas, 1979) and this variation is hereby assumed to have the following form,

$$\Delta\pi(z,\varepsilon) = \pi(z,\varepsilon) - \pi(z,0) = u_{o2}\left(\frac{1}{(1+\varepsilon)^2} - 1\right) \tag{5.15}$$

where $\Delta\pi$ is the change in pressure π due to Donnan effect and u_{o2} is the depth-dependent initial osmotic pressure in a layer due to the difference in the proteogycan distribution which increases from zero at the superficial layer up to about 0.22 MPa at the bottom (Lipshitz, 1976; Urban et al., 1979). Base on its published values and pattern (Lipshitz, 1976; Maroudas, 1979; Urban et al., 1979), we assume the initial osmotic pressure can be expressed as,

$$u_{o2}(z) = 1 - e^{-0.22\frac{Z}{H}} \tag{5.16}$$

where H is the thickness of the cartilage matrix and z is the displacement from the surface.

5.3.4 Effective stress relationship for matrix equilibrium

For slow motion the stress equilibrium equation for the layer in one-dimension is,

$$\frac{\partial\sigma_z}{\partial z} = 0 \Rightarrow \sigma_z = \sigma_a, \tag{5.17}$$

where σ_z is the stress developed in a representative matrix layer and σ_a is the applied static stress imposed on the matrix at its surface.

With reference to Figure 5.2, the applied or total stress in each layer can be

approximated as the algebraic sum of all solid stress and fluid pressure in that layer in accordance with the effective stress principle of Terzaghi (1943), ie.

$$\sigma_z = \sigma_a = \sigma_s + D\frac{\partial \varepsilon}{\partial t} - u - \Delta\pi \tag{5.18}$$

where, D is the drag coefficient accounting for the solid-fluid interaction during consolidation. This parameter is assumed constant in the present analysis.

5.3.5 Model of permeability

Assuming that the direction of fluid outflow is perpendicular to the surface, then the change of the permeability through the surface area in the z-direction perpendicular to the articular surface can be expressed in terms of strain by

$$\frac{\partial K}{\partial \varepsilon} = -\mu\frac{\partial^2 K}{\partial z^2}, \tag{5.19}$$

where μ is a constant coefficient and $K(z,\varepsilon)$ is the coefficient of permeability which is a function of position z and strain ε.

The full derivation of equation (5.19) is presented in the next chapter. This equation represents spatial distributions of the permeability parameter depending on strain and is similar to the diffusion process. If the boundary and initial conditions for the permeability are

$$K(0,\varepsilon) = K_0, \qquad K(H,\varepsilon) = 0, \text{ and } \quad K(z,0) = f(z)$$

where K_0 is a constant permeability at the surface, which depends on the concentration of the collagen at the surface and does not consist of proteoglycans (the component is assumed to significantly effects the change in the permeability), and $f(z)$ which is assumed the linearly depth-dependent relationship in this thesis for the heterogeneous analysis is the initial distribution function for this parameter , then

$$K(z,\varepsilon) = K_0\left(1-\frac{z}{H}\right) + \sum_{r=1}^{\infty} A_r e^{\frac{\mu\pi^2 r^2}{H^2}\varepsilon}\sin\left(\frac{\pi r z}{H}\right) \tag{5.20}$$

where $$A_r = \int_0^H \left(f(z) - K_0\left(1-\frac{z}{H}\right)\right)\sin\left(\frac{\pi r z}{H}\right)dz\,.$$

We observe that this new model of permeability can describe heterogeneous materials

like articular cartilage while the previously published Mow's model which is a strain-dependent function (Lai et al., 1981) can only be applied to homogeneous materials. The comparison of these two models is presented in Figure 5.3.

5.3.6 Idealization of articular cartilage with the superficial layer impaired

As presented earlier, the modulus of compressibility of the matrix is also considered depth-dependent in this study. Consequently it is assumed to take the form previously published by Schinagl et al. (1997), i.e

$$\Phi = \Phi_0 e^{\alpha(L)\frac{z}{H}} \tag{5.21}$$

where Φ_0 is the constant representing this parameter at the surface; Φ is a distribution of the modulus of compressibility of the layers; $\alpha(L)$ is the parameter which describes the effect of any artificial damage of depth L from the surface and investigated using a curve fitting method at the level of this study.

Combining equations (5.9), (5.20) and (5.21), a relationship between stiffness and permeability can be established for the normal intact matrix (when L=0). Based on this relationship, the pattern of the permeability distribution upon laceration of the superficial layer can be established using known values of stiffness for iteration. This approach therefore provides a new model for the relationship between the compressive modulus and permeability of a given matrix with lacerated surface.

5.4 Discretized equations

The numerical solution of our model was done using the MATLAB software. Using this software, the hydrostatic excess pore pressure, solid skeleton stress and the chemical swelling stresses in each layer were determined for cartilage models with intact and lacerated superficial layers. In order to solve the equations of our model, the following discretization was carried out.

Substituting equation (5.18) into (5.11), yields,

$$\frac{1}{D(1+\varepsilon)}\left(\sigma_a-\sigma_s-u+\Delta\pi\right)=\frac{\partial K}{\partial z}\frac{\partial u}{\partial z}+K\frac{\partial^2 u}{\partial z^2}. \tag{5.22}$$

The discretized forms of equations (5.22) and (5.20) are then given in equation (5.23) and (5.24) respectively

$$\frac{1}{D(1+\varepsilon_n^m)}\left(\sigma_a-\sigma_{sn}^m-u_n^m+\Delta\pi_n^m\right)=\frac{K_{n+1}^m-K_n^m}{\Delta z}\frac{u_{n+1}^m-u_n^m}{\Delta z}+K_n^m\frac{u_{n+1}^m-2u_n^m+u_{n-1}^m}{\Delta z^2} \tag{5.23}$$

$$K_n^m=K_0\left(1-\frac{n-0.5}{N}\right)+\sum_{r=1}^{20}A_r e^{\frac{\mu\pi^2r^2}{H^2}\varepsilon_n^m}\sin\left(\frac{\pi r(n-0.5)}{N}\right) \tag{5.24}$$

where n is the iteration order per matrix layer, m is the number of time steps for each iteration, and N is the number of matrix layers consider.

Equation (5.23) can be further expressed as,

$$K_n^m u_{n-1}^m-\left(K_n^m+K_{n+1}^m+a_n^m\right)u_n^m+K_{n+1}^m u_{n+1}^m=b_n^m \tag{5.25}$$

where, $a_n^m=\frac{\Delta z^2}{D(1+\varepsilon_n^m)}$; $b_n^m=a_n^m\left(\sigma_a-\sigma_{sn}^m+\Delta\pi_n^m\right)$.

Combining equation (5.25) with the following boundary and initial conditions:

$$\frac{\partial u(h,t)}{\partial t}=0\Rightarrow u_{N+1}^m=u_N^m,\ u(0,t)=u_0^m=0 \text{ and } \varepsilon(z,0)=\varepsilon_n^1=0,$$

yields algebraic equation (5.26)

$$A^m\vec{u}=\vec{b}^m \tag{5.26}$$

where,

$$A^m=\begin{bmatrix}
-(K_1^m+K_2^m+a_1^m) & K_2^m & 0 & & & 0\\
K_2^m & -(K_2^m+K_3^m+a_2^m) & K_3^m & & & \\
0 & \ddots & \ddots & \ddots & & \\
 & & \ddots & \ddots & \ddots & \\
 & & & K_{N-1}^m & -(K_{N-1}^m+K_N^m+a_{N-1}^m) & K_N^m\\
0 & & & 0 & K_N^m & -(K_N^m+a_N^m)
\end{bmatrix}$$

The discretized forms of equations (5.21), (5.9), (5.15) and (5.16) are respectively

$$\Phi_n=\Phi_0 e^{\alpha\frac{n-0.5}{N}},\ \sigma_{Sn}^m=\Phi^m\left(1+\varepsilon_n^m-\frac{1}{1+\varepsilon_n^m}\right) \tag{5.27}$$

$$\Delta\pi_n^m = u_{o2n}\left(\frac{1}{\left(1+\varepsilon_n^m\right)^2}-1\right) \tag{5.28}$$

and

$$u_{o2n} = \left(1-e^{-0.22\frac{n+0.5}{N}}\right) \tag{5.29}$$

Combing equations (5.28) and (5.29) yields

$$\Delta\pi_n^m = \left(1-e^{-0.22\frac{n+0.5}{N}}\right)\left(\frac{1}{\left(1+\varepsilon_n^m\right)^2}-1\right) \tag{5.30}$$

The new time-step strain developed per layer is computed from the discretized form of equation (5.18):

$$\varepsilon_n^{m+1} = \varepsilon_n^m + \frac{\Delta t}{D}\left(\sigma_a - \sigma_{s\,n}^{\ m} - u_n^m + \Delta\pi_n^m\right) \tag{5.31}$$

The discretized equations (5.26-31) represent our layer analogue for articular cartilage and were subsequently solved using a discrete element analysis protocol of MATLAB to obtain the hydrostatic excess pore pressure, solid skeleton stress, chemical swelling stress and strain in the hypothetical layers of the intact and lacerated cartilage matrix.

Stimulation

An algorithm in MATLAB (see Appendix A3) was used to solve equation (5.26) yields the hydrostatic excess pore pressure in different layers at time t. The result obtained at each step when solving equation (5.26) is used in equation (5.31) to compute the level of compression ε_n^{m+1} in each layer in the subsequent time step. Each new layer strain is substituted into equation (5.30) and (5.24) to compute the new osmotic pressure change,$\Delta\pi$, and permeability, respectively for that layer in the subsequent time step. This is repeated until the deformation reaches equilibrium. The solid stress is also computed for the layer in each time step using equation (5.23).

5.5 Result and discussions

The previous experimental data in Chapter 4 presented in Figure 5.3 demonstrate that the fluid's excess pore pressures for both normal and lacerated specimens of the chosen near-flat cartilage increased in the initial stage to a maximum value and then decayed

over time. It also reveals that the excess pore pressure and total matrix strain for the normal intact and lacerated matrices, with 100μm (5% of the depth and less than the thickness of the superficial layer) cut into the superficial layer were similar, with both a marginal increase of approximately 10% over the normal intact maximum hydrostatic excess pore pressure and total strain was observed for the matrix lacerated to 200 μm (10% of the depth and just thicker than the superficial layer) into the surface. Furthermore, these experimental results revealed that the rate of transient decay of the excess pore pressure was quicker for the matrix with the 200 μm laceration to its superficial layer.

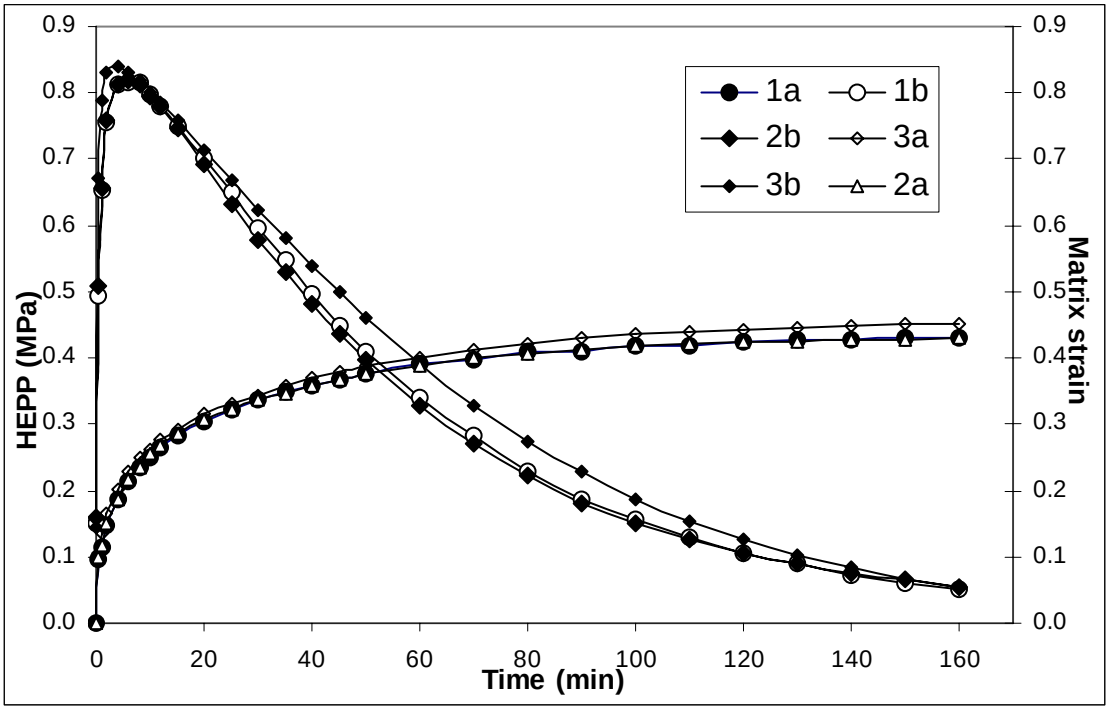

Figure 5.3: Experimental values of the total matrix strain (MS) (1a) and hydrostatic excess pore pressure (HEPP) (1b) for normal cartilage with intact superficial layer; 2a and 2b are MS and HEPP data after surface laceration of 100μm respectively; and 3a and 3b are MS and HEPP transient values after 200μm superficial surface laceration.

Figure 5.4 presents the pattern of variation with depth (z-direction) and strain of the permeability coefficients for an intact matrix

$$K = 7\times10^{-17}\left(1-\frac{z}{H}\right)+\sum_{r=1}^{\infty}A_r e^{\frac{3\pi^2 r^2}{H^2}\varepsilon}\sin\left(\frac{\pi r z}{H}\right)\ \frac{m^4}{NS}$$

where $$A_r = \frac{2}{H}\int_0^H\left(f(z)-K_0\left(1-\frac{z}{H}\right)\right)\sin\left(\frac{r\pi z}{H}\right)dz \approx -\frac{3.2\times10^{-7}}{\pi r}(-1)^r (r=1,2,...)$$

It also shows the comparison of the model to the function published previously by Lai

et al. (1981) namely ($K = K_0 \exp(M\varepsilon)$, where M = 4.3 and 30 respectively). There is good agreement between Lai's model (M2) and our model with respect to the variation with strain in a position of 0.775mm in depth approximately, thereby demonstrating the viability of our new conceptual approach to permeability variation in articular cartilage. This result also demonstrates that there is a significant difference in the permeabilities of the different layers of the matrix and that the pattern of change with deformation is consistently a likely diffusion partial differential equation for the intact articular cartilage.

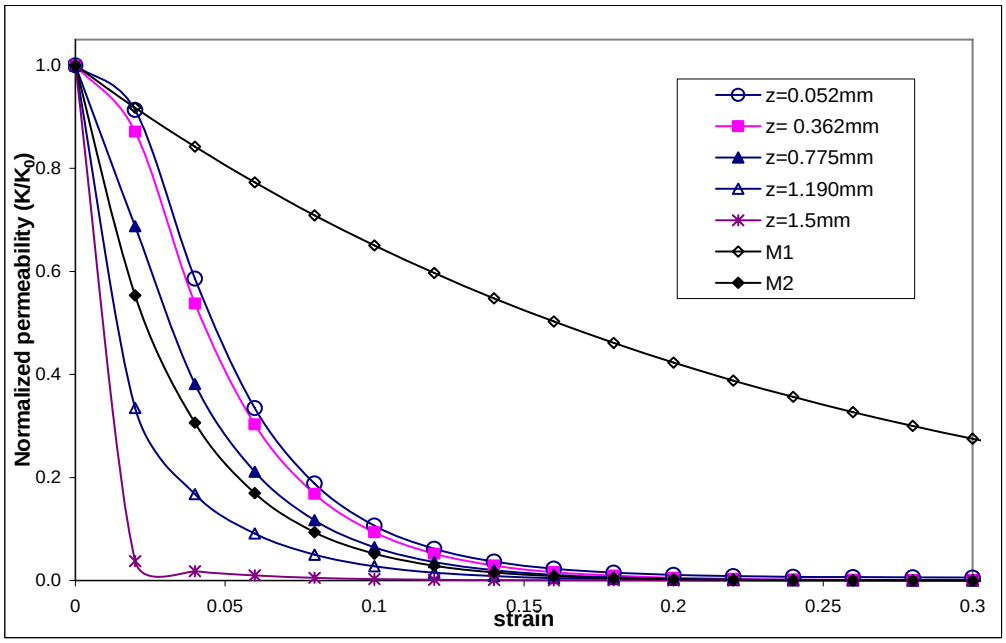

Figure 5.4: Patterns of the variation of permeability with strain and position within the matrix of articular cartilage (The legend presents the value of depths). It can be seen that the exponential variation of permeability with strain is exhibited per layer in accordance with Lai et al. as illustrated by M1 and M2.

Figure 5.5 shows the variation of the modulus of compressibility with depth $\Phi = 0.09Exp(4.1z/H)$ from the model developed and its comparison with the experimental data of Schinagl et al. (1997). This result demonstrates good agreement between predicted and experimental values, thereby supporting the adequacy of our new model in predicting the dependence of cartilage compression modulus on position.

Figure 5.6 presents an approximate distribution of the intrinsic Donnan osmotic pressure for the articular cartilage which is similar to the linear pattern of proteogycan

distribution for the tissue experimentally determined by Maroudas (1979). Therefore, the assumption model can be validate.

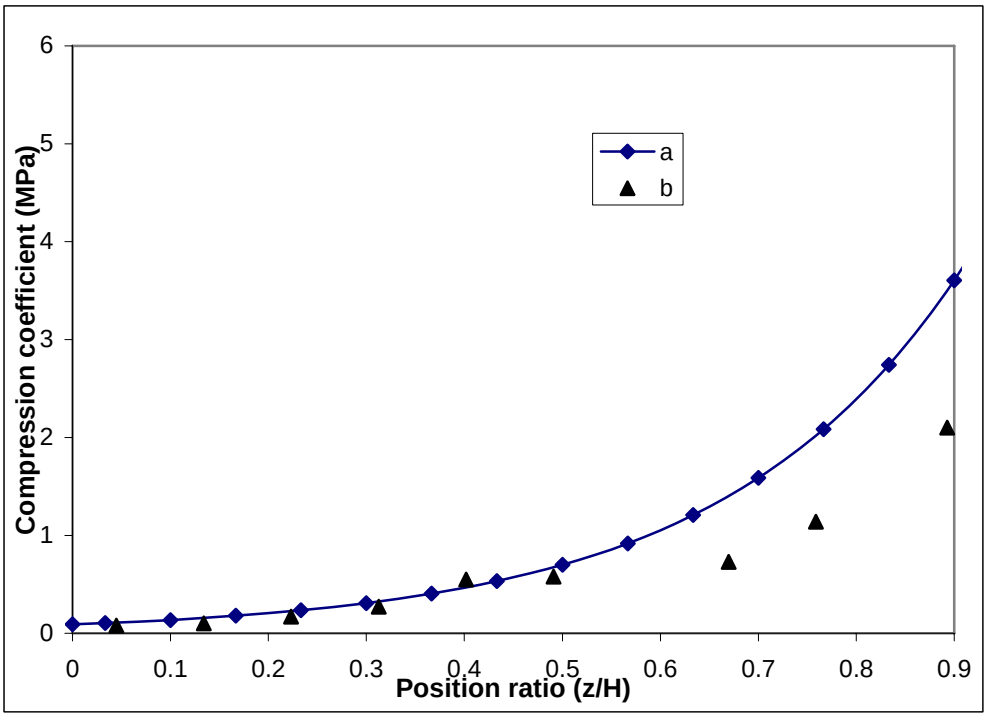

Figure 5.5: Predicted depth-dependent compression coefficients i.e. $\Phi = 0.09Exp(4.1z/H)$. (a) is the variation of the present model for the normal intact cartilage matrix, while (b) is experimental data of Schinagl et al (1997)

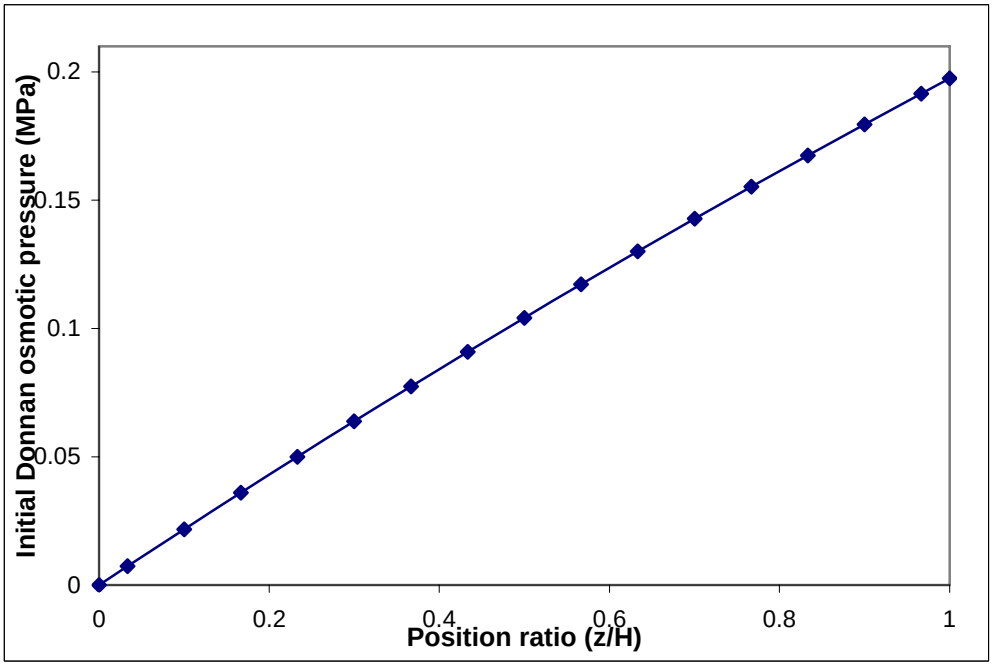

Figure 5.6: Predicted depth-dependent initial Donnan osmotic pressure for the normal intact cartilage matrix, which was assumed for numerical analysis.

Figure 5.7 adequately predicts values of the transient patterns of the fluid component's hydrostatic excess pore pressure and the effective stress of the solid constituent in each layer, for the normal intact matrix. It also compares experimental values (ExP) of the hydrostatic excess pore pressure at the bottom layer to those obtained from numerical analysis (4b) at the same position. The results reveal good agreement between the experimental and predicted patterns of variation. The drag coefficient ($D = 170\ \ MPas$) was carried out in this numerical analysis to obtain the results. It should be noted that this drag coefficient only refers to the relationship between the deforming solid and moving fluid.

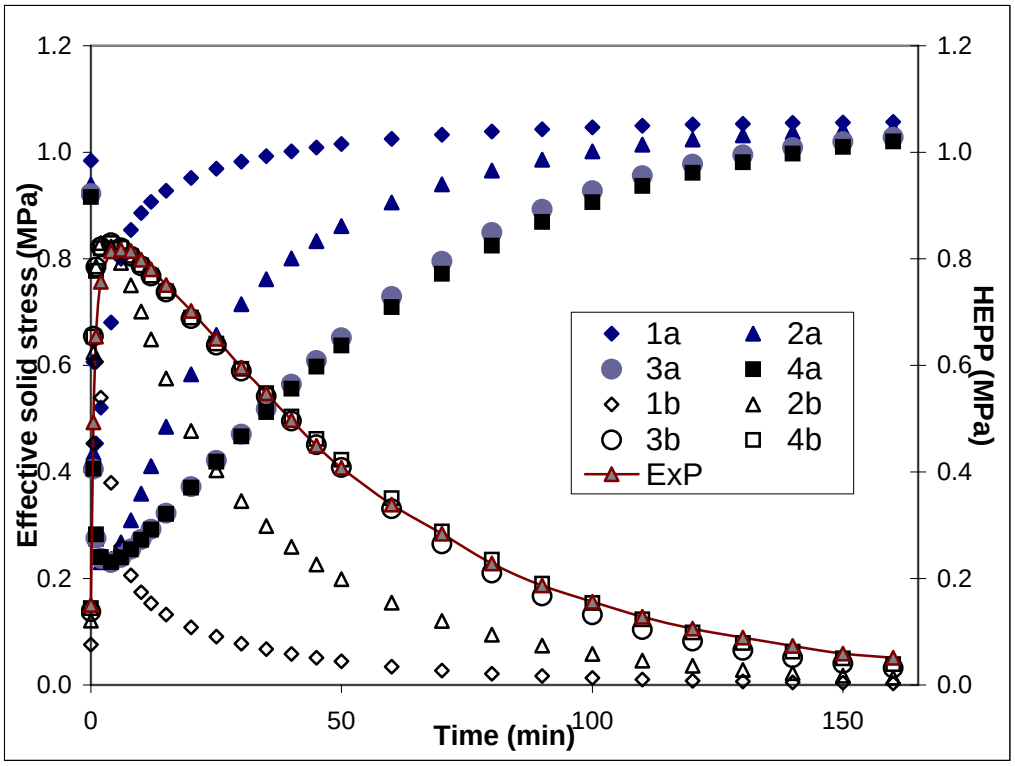

Figure 5.7: Predicted values of the effective solid stress at the depths of 0.052mm (1a), 0.362mm (2a), 0.775mm (3a) and 1.5mm (4a); and their corresponding hydrostatic excess pore pressures using the data in figures 5.4, 5.5 and 5.6. ExP= experimental hydrostatic excess pore pressure.

Figure 5.8 demonstrates the agreement between the patterns of the strains for the bulk matrix and the individual layers of the tissue. The trend is a expected especially for the superficial and midzone layers, i.e (a) and (c) respectively which can be inferred from analytical methods.

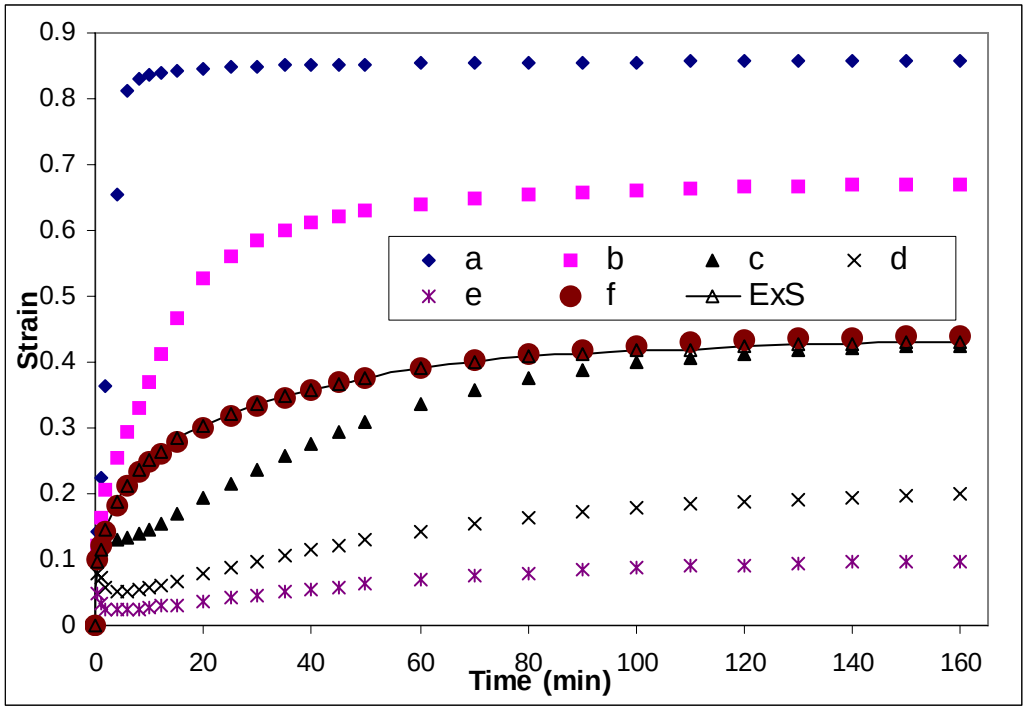

Figure 5.8: Comparison of the experimental total matrix strain (g) with the predicted values of the time-dependent strain at the depths of 0.052mm (a), 0.362mm (b), 0.775mm (c), 1.19mm (d) and 1.5mm (e), and total matrix strain (f). The predicted values were obtained using the predicted data in figures 5.4, 5.5, and 5.6. ExS= experimental creep strain.

Figure 5.9 presents the distribution up to the maximum value and over transient decay of the hydrostatic excess pore pressure with respect to the depth of the matrix at specific times for the normal intact cartilage matrix. These data demonstrates the capability of the new model presented and provides a tool of analysis, which can assist in determining material properties in the making of artificial cartilage and the assessment of cultured cartilage.

Figure 5.10 establishes the relationship between the stiffness and permeability of each layer. These curves were obtained numerically and the curve-fitting exercise produced the equations plotted in figures 5.4 and 5.5. These data in turn, were used to arrive at the finite element values of cartilage load-carriage parameters in figures 5.7 and 5.8. The iterations for permeability and stiffness were stopped when the experimental and numerical analysis values agreed. Figure 5.10 reveals that the permeability remains unchanged relative to reduction in the compressive stiffness for small lacerations into the superficial layer.

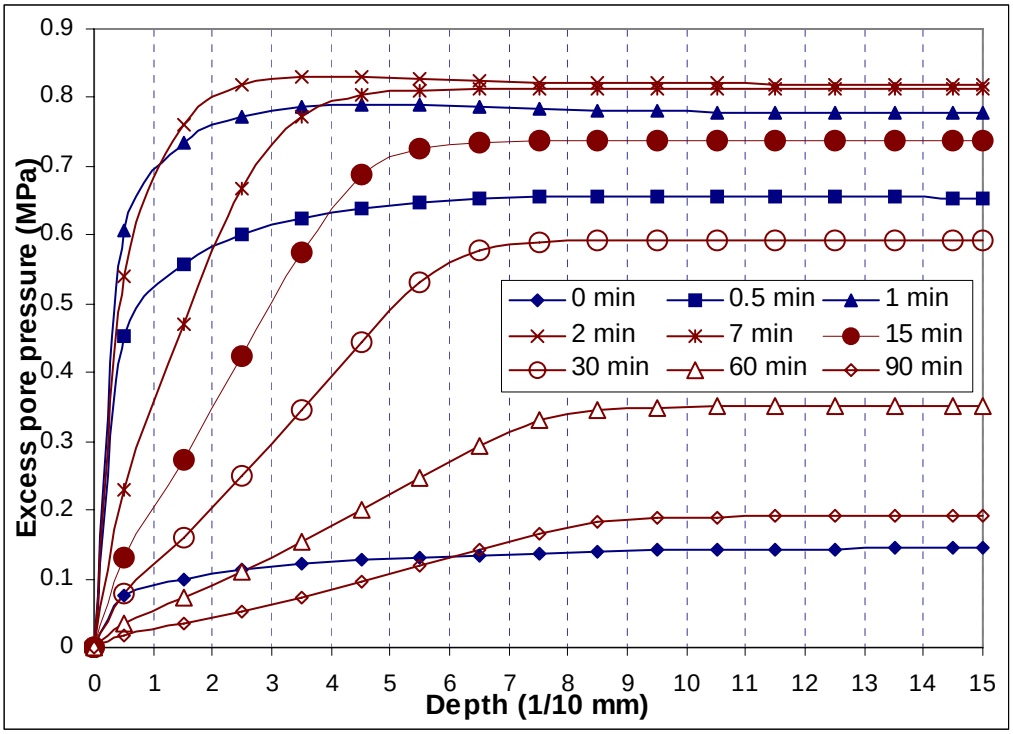

Figure 5.9: Predicted distribution of the hydrostatic excess pore pressure in the normal matrix at time 0, 0.5 min., 1 min,…, 90 min. The predicted values were obtained using the predicted data in figures 5.4, 5.5, and 5.6. These curves capture the developmental stages of the hydrostatic excess pore pressure in the incipient period of loading

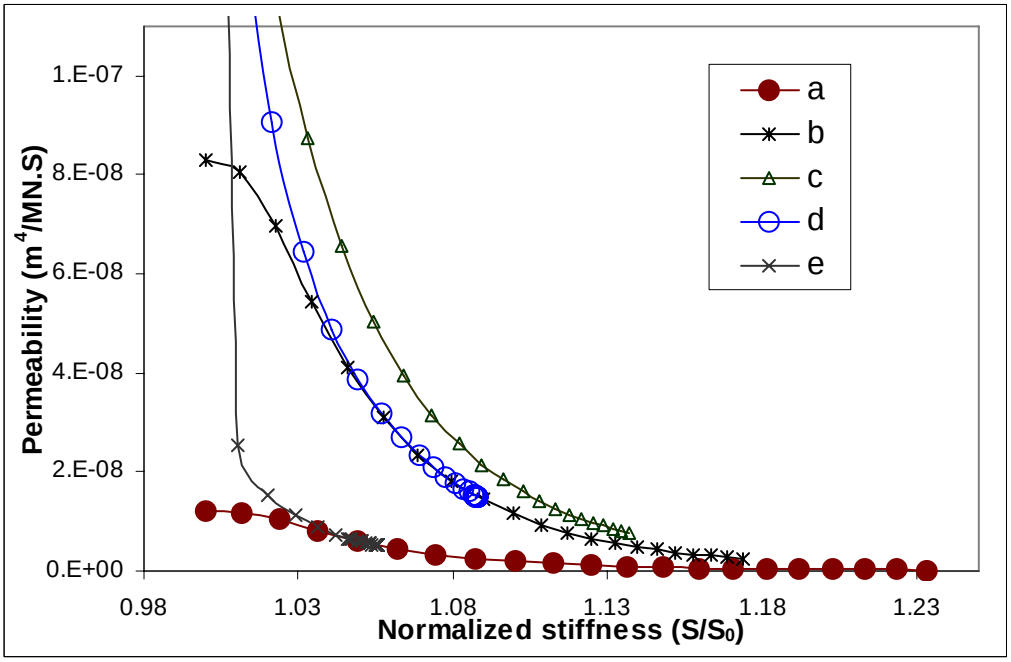

Figure 5.10: Predicted values of the permeability versus the normalized stiffness at the depths of the 0.052mm (a), 0.362mm (b), 0.775mm (c), 1.3mm (d) and 1.5mm (e) for the normal matrix. The predicted values were obtained using the data in figures 5.4, 5.5, and 5.6.

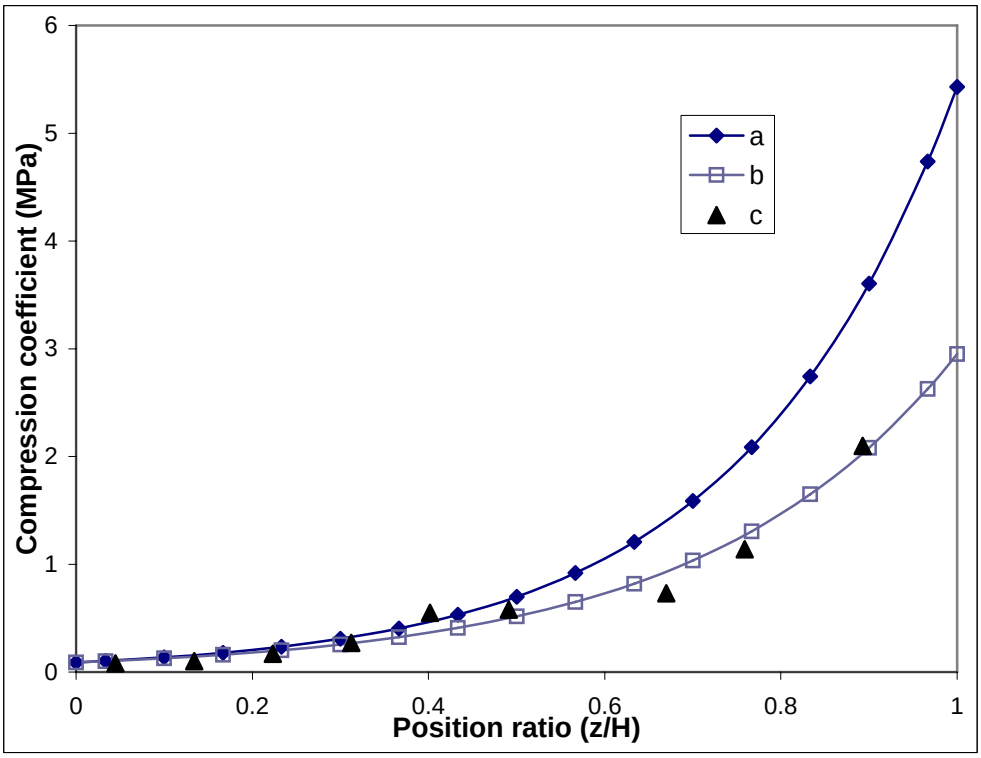

Figure 5.11: Comparison of the predicted depth-dependent compression coefficients of the present model $\Phi = 0.09Exp(4.1z/H)$ ($L(\alpha)$=4.1) for the normal intact cartilage matrix (a) to those of the model $\Phi = 0.09Exp(3.49z/H)$ ($L(\alpha)$=3.9) for the normal lacerated cartilage matrix (b). These values are compared to the experimental data (c) obtained by Schinagl et al (1997).

Based on these data, we kept the permeability function the same for lacerations within the superficial layer and varied the distribution of the compression modulus in our finite element analysis. Figure 5.11 is the comparison between the prediction of the modulus of compressibility by the present model for the normal cartilage matrix with intact superficial layer ($\Phi = 0.09Exp(4.1z/H)$) and that for one carrying laceration in its superficial layer of 200 μm ($\Phi = 0.09Exp(3.49z/H)$), and the experimental data of Schinagl et al. (1997). This figure demonstrates that the predicted and experimental (Schinnagl et al, 1997) distributions of stiffness coefficient with respect to depth differ progressively with depth. This difference ranges from about 5% to 46% from the surface layer to the bottom layer respectively. The predicted distribution of stiffness coefficient for the lacerated tissue differs from that of the normal intact matrix by 0% to 43% from the surface to the bottom layer but still remains in the ballpack values for the predicted and experimental values for the normal intact matrix. This demonstrates that laceration alone might not account for severe lowering of cartilage stiffness coefficient.

It should however be noted that the comparison made here is adventurously subject to the effect of tissue variation. Regardless of this result, using the data of figures 5.4, 5.6 and 5.11, the hydrostatic excess pore pressure and the total matrix strain for the normal intact cartilage matrix (figures 5.7 and 5.8) and the one lacerated to 200 μm at its superficial layer (Figure 5.12) were obtained and fitted to the experimental values. The data demonstrate good agreement between these.

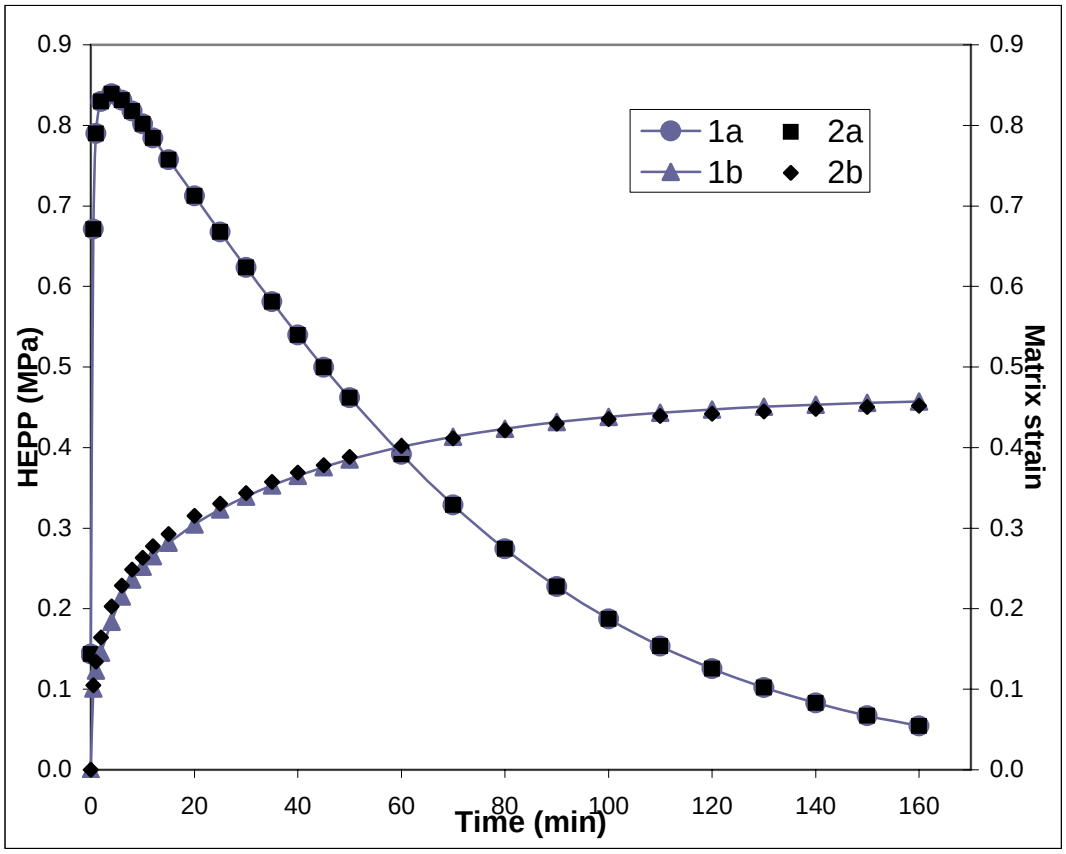

Figure 5.12: Comparison of the predicted values of the hydrostatic excess pore pressure at the bottom (1a) and the total matrix strain (1b) of the normal matrix with the same parameter for the lacerated matrix where the depth of laceration is 200 μm using the data in figures 5.4, 5.6 and 5.11. These show no noticeable variation from the experimental data (2a, 2b).

Figure 5.13 presents the characteristic effective stress-strain curves for different layers for the intact and lacerated matrices using the data in figures 5.4, 5.6 and 5.11. The slopes of these stress-strain curves are smallest at the superficial layer and highest at the bottom. It should be noted that these result demonstrate that there is no change in the stress-strain characteristics of the superficial layer even after laceration, while there is significant change in this parameter in the deeper zone. This is to be expected under a

static compressive loading regime and therefore credence to the representative capacity of our model for predicting the responses of the lacerated and cartilage with intact superficial layer, thereby providing a biomechanic insight into the factors.

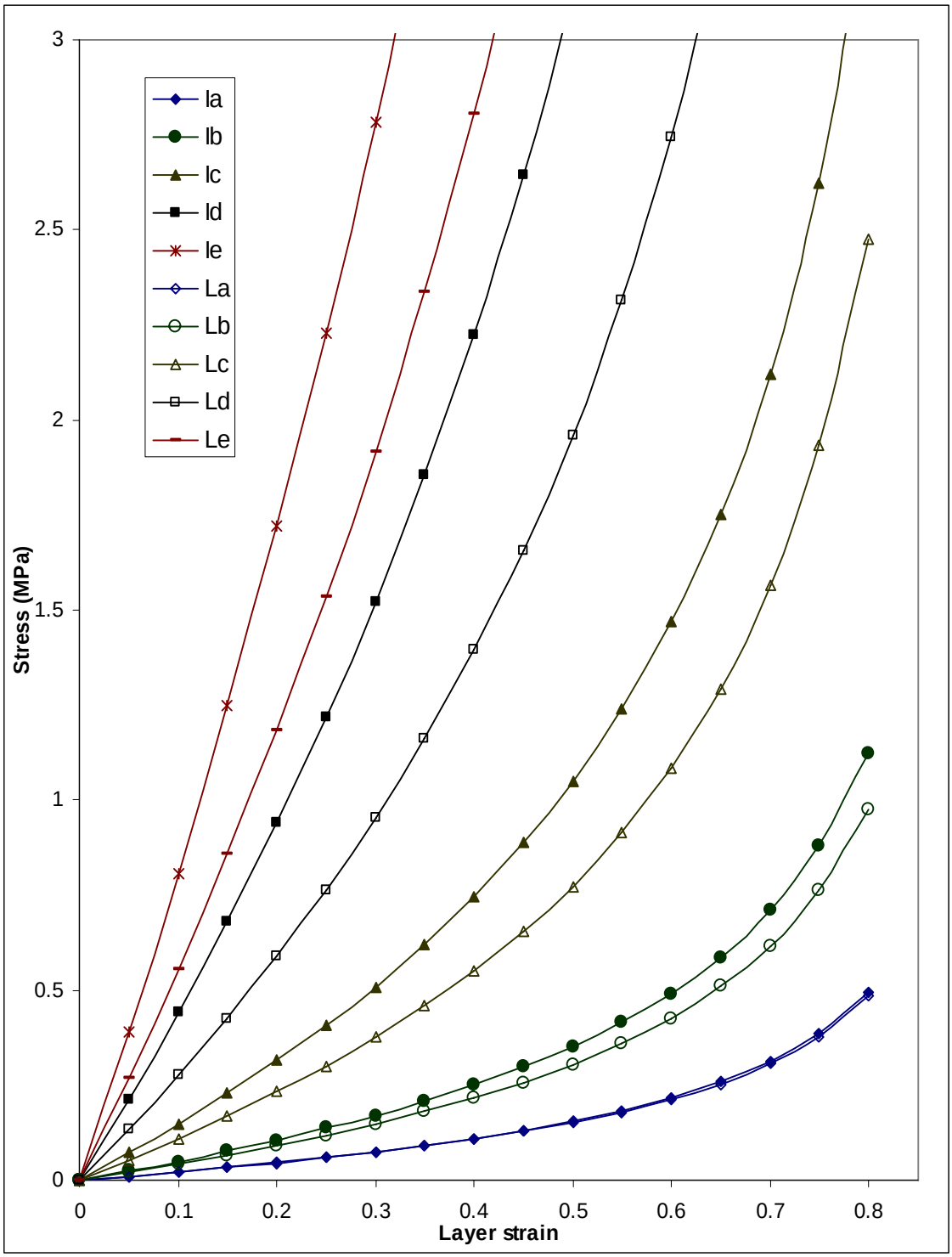

Figure 5.13: Comparison of the predicted stress-strain responses of articular cartilage for the normal intact and normal lacerated matrices up to 200 μm at the depths of 0.052mm (Ia, La), 0.362mm (Ib, Lb), 0.775mm (Ic, Lc), 1.190mm (Id, Ld) and 1.50mm (Ie, Le).

5.6 Conclusion

This chapter has investigated systematically the consequence of the impairment of the superficial layer of articular cartilage on its consolidation behaviour based on rheological modelling for the numerical analysis. The patterns of variation in the hydrostatic excess pore pressure including the layer effective solid skeleton stress at different positions within the matrix agreed well with the experimental data. This chapter shows promise for the analysis and prediction of the load-induced responses of articular cartilage at static load and speeds well below impact. The various parameters of the deformation can be explicitly calculated while the new layer-based models of the permeability and compression modulus provide a powerful tool for studying and comparing the characteristics of loaded intact and degenerate articular cartilage especially where degeneration is restricted to the superficial layer, as often seen in the early stages of osteoarthritis degeneration.

Chapter 6: Generalized continuum theory for articular cartilage consolidation.

6.1 Introduction

The proposed model is based on the phenomenological model of soil and clay consolidation (Biot,and Willis, 1957; Terzaghi, 1943) and the experimental studies of Oloyede and Broom (1991), Higginson et al. (1976) and Soltza and Ateshian (1998). Some of the pertinent arguments have also been proposed by other investigators (Maroudas et al., 1987; McCutchen, 1982; 1998). A scouting of the literature reveals the following agreement between authors, namely,

(i) Articular cartilage is a heterogeneous fluid saturated tissue which is capable of large hyperelastic deformation. This hyperelastic property is due to the deformation of its proteoglycan chains and collagen fibrils that form a dense meshwork with radial alignment in its midzone region and parallel orientation in the superficial layer. This meshwork when combined with the fluid-swollen proteoglycans produces the deformation of gels which have characteristics as similar as most rubbers and other polymeric materials.

(ii) The tissue's permeability varies with position and time.

(iii) Osmotic swelling due to its fixed charges and ion transport is an important factor contributing to the development of its functional stiffness under load-bearing conditions. component in determining its response to load and is related to the distribution of proteoglycans or fixed charge density of the matrix.

While it will be extremely difficult or even unrealistic to develop a model that captures every aspect of articular cartilage structure and biomechanics, in this paper attempts will be made to develop a generalized mathematical hybrid model of the tissue. This model will borrow from both phenomenological and fundamental approaches incorporating essentially the following important relationships:

1. The constitutive hyperelastic stress-strain relationship for the collagen fibrillar meshwork combining with proteoglycan chains and its distention following the finite elasticity principles used in the analysis of rubber-like materials including the consideration of the entropy of the structural order of this skeletal architecture. Strain energy density balance in the deformed and undeformed conditions will be written for the meshwork and any distention in either of these states will be considered as an integral component of the extension/stretch ratio of the fibrous structure;

2. A phenomenological submodel of the variation of its permeability with respect to position within a given matrix and deformation.

3. Equivalent relationships for the overall or bulk deformation of the tissue's solid skeleton in the depth-dependent non-linear elastic stiffness;

4. Depth-dependent swelling as a function of the fixed-charge density and its distribution, and a function of the large deformation of the tissue. However, because of its hydrostatic nature, this relationship has been represented in terms of volumetric deformation.

The intention is to achieve the aims stated above within the framework of the principle of consolidation or poroelastic deformation of a fluid-saturated swollen gel-like material.

6.2 Simplifying assumptions

The following assumptions on the behaviour of the cartilage sample are adopted in the present study:

* The cartilage matrix is loaded in the z- (axial) direction.

* The cartilage matrix is heterogeneous in the z-direction (depth-dependence) and exhibits planar isotropy in the xy-plane (the same properties in the xy-plane).

* Both the solid and fluid components of the matrix are incompressible.

* Both the stiffness and permeability of the matrix are deformation and position-dependent.

* The collagen-proteoglycan entrapment constitutes the solid skeleton and can be modelled as a hyperelastic component.

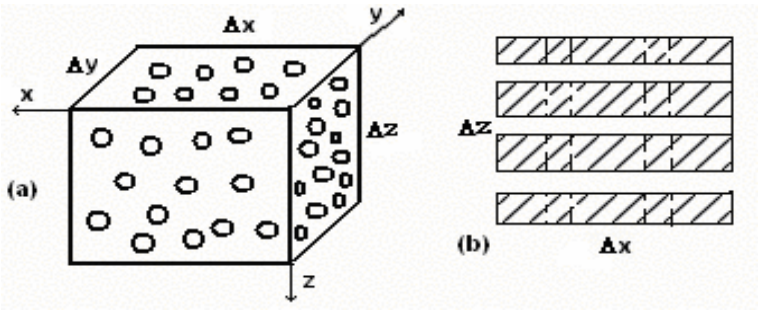

Figure 6.1: Schematic diagram of the idealized porous structure used for developing the new permeability function. All pores are assumed to run through the cubical element so that they cross one another along the principal planes of deformation and are cylindrical in shape.
(a) Schematic diagram; (b) Its cross-sections A_y.
Circles in (a) are cross-section areas of pores on the elemental surfaces.

* Darcy's law of percolation can be applied to the movement of fluid through the matrix.
* The principal directions of the fluid flow are in the x,y and z-directions, which are the principal directions of deformation in an element of the tissue as shown in Figure 6.1.

6.3 Mathematical description in Cartesian coordinate

6.3.1 Volumetric deformation

The instantaneous large deformation of a control volume within an element in a given specimen can be defined in three-dimensions as,

$$\lambda_1 = \frac{w_x}{w_{x0}},\ \ \lambda_2 = \frac{w_y}{w_{y0}},\ \ \lambda_3 = \frac{w_z}{w_{z0}} \ \text{ and } \quad \lambda = \frac{V}{V_0} = \lambda_1\lambda_2\lambda_3$$

where w_x, w_y, and w_z are the instantaneous lengths of the element in the x, y and z directions at time t; w_{x0}, w_{y0}, and w_{z0} are the initial lengths of the element in the x, y and z-directions, respectively; V_0 and V are initial and instantaneous volumes of the element respectively; and λ is the volumetric stretch ratio of the deformation of the element; λ_1, λ_2 and λ_3 are the normal stretch ratios (diagonal elements of the stretch ratio tensor) in the axial directions (the x, y and z-directions) of the deformation. It should be noted that these directions are assumed to be be coincident with the principal axes of the fluid-filled or wet element deforming under an axial static loading, hence shear stresses and ratios of stretch are not considered presently.

Given the above relationships, the rate of change of the bulk stretch ratio with respect to time can be written for the principal directions as

$$\frac{1}{\lambda}\frac{\partial\lambda}{\partial t} = \frac{1}{V}\frac{\partial V}{\partial t} = \frac{1}{\lambda_1}\frac{\partial\lambda_1}{\partial t} + \frac{1}{\lambda_2}\frac{\partial\lambda_2}{\partial t} + \frac{1}{\lambda_3}\frac{\partial\lambda_3}{\partial t}. \qquad (6.1)$$

6.3.2 Hyperelastic formulation for collagen fibril meshwork deformation.

The solid skeleton of a cartilage matrix consists of fibrous collagen meshwork entrapping fluid swollen proteoglycan macromolecules. It is assumed here that the deformation of this entrapment architecture is manifested in the distension of the

collagen meshwork and proteoglycan chains, which can be treated as polymeric chains for the purpose of modeling. Therefore, using the statistical theory of rubber elasticity the hyperelastic deformation can be developed as follows.

Hyperelastic Deformation Relationship

Let us assume that the entropy per unit volume of structural polymeric chains within a rubber-like element is described by the statistical theory of rubber elasticity (Ward and Hadley, 1993) as,

$$\Delta S_1 = -kb^2\left\{\left(\lambda_1^2-1\right)\sum_{i=1}^{N} l_{x_i}^2 + \left(\lambda_2^2-1\right)\sum_{i=1}^{N} l_{y_i}^2 + \left(\lambda_3^2-1\right)\sum_{i=1}^{N} l_{z_i}^2\right\}, \tag{6.2}$$

where l_{x_i}, l_{y_i} and l_{z_i} are the lengths of the i[th] molecular chain in the x-,y- and z-directions of the undeformed network respectively when this is applied to an element of articular cartilage matrix, *N* is the number of fibrous and proteoglycan chains in the network of the element, *k* is Boltzmann's constant, *b* is a constant that is determined using the following relationship (Ward and Hadley, 1993),

$$\sum_{i=1}^{N} r_i^2 = \sum_{i=1}^{N} l_{x_i}^2 + \sum_{i=1}^{N} l_{y_i}^2 + \sum_{i=1}^{N} l_{z_i}^2 = N\left(\frac{3}{2b^2}\right), \tag{6.3a}$$

where r_i is the distance between two ends of the i[th] chain.

To simplify equation (6.2), it is assumed that the element dimensions of the anisotropic material are selected to satisfy the relationship below,

$$\sum_{i=1}^{N} l_{x_i}^2 = \sum_{i=1}^{N} l_{y_i}^2 = \sum_{i=1}^{N} l_{z_i}^2 . \tag{6.3b}$$

It is noted that this assumption of total length of the chains in the given element is applicable to both the isotropic and anisotropic cases depending on the selected dimensions of a given element.

Combining equations (6.2), (6.3a) and (6.3b) yields

$$\Delta S_1 = -\frac{1}{2}kN\left(\lambda_1^2+\lambda_2^2+\lambda_3^2-3\right). \tag{6.3}$$

Furthermore, when a chemical component exists, a change in the average concentration of the solute in the matrix due to fluid loss will contribute to the entropy of the fibrous chains and the ground substance (Tombs and Peacocke, 1974; Broom and Oloyede, 1998). This component of entropy can be written as,

$$\Delta S_2 = -Nk \ln\left(\frac{C}{C_0}\right) \tag{6.4a}$$

where, C_0 and C are the initial and instantaneous mass concentrations of all molecules, respectively.

The conservation of mass due to the outflow of fluid from the element within the assuming no loss of solute under the deformation is therefore,

$$m_s = CV = C_0 V_0 \tag{6.4b}$$

where, m_s is the total mass of all molecules; V_0 and V are the initial and instantaneous volumes of the element respectively.

Combining equations (6.4a) and (6.4b) yields,

$$\Delta S_2 = -Nk \ln\left(\frac{V_0}{V}\right) = Nk \ln(\lambda) = Nk \ln(\lambda_1 \lambda_2 \lambda_3). \tag{6.4}$$

Therefore, the total change in the entropy per unit volume is,

$$\Delta S = \Delta S_1 + \Delta S_2 = -\frac{1}{2} kN\left(\lambda_1^2 + \lambda_2^2 + \lambda_3^2 - 3\right) + Nk \ln(\lambda_1 \lambda_2 \lambda_3). \tag{6.5}$$

Assuming that the strain energy function per unit volume required for load carriage, U, is zero in the undeformed state then

$$U = -T\Delta S = kNT\left(\frac{1}{2}\left(\lambda_1^2 + \lambda_2^2 + \lambda_3^2 - 3\right) - \ln(\lambda_1 \lambda_2 \lambda_3)\right) \tag{6.6}$$

where, T is the absolute temperature of the element measured in Kelvin. The product NkT is recognized as the shear modulus of the deforming element.

Stress-Deformation Relationship

The change in the normal stress components in each independent direction can be shown to be,

$$\sigma_1 = \alpha_{11}\frac{\partial U}{\partial \lambda_1} + \alpha_{12}\frac{\partial U}{\partial \lambda_2} + \alpha_{13}\frac{\partial U}{\partial \lambda_3} = \alpha_{11} kNT\left(\lambda_1 - \frac{1}{\lambda_1}\right) + \alpha_{12} kNT\left(\lambda_2 - \frac{1}{\lambda_2}\right) + \alpha_{13} kNT\left(\lambda_3 - \frac{1}{\lambda_3}\right)$$

or,
$$\sigma_1 = \Phi_{11} e_1 + \Phi_{12} e_2 + \Phi_{13} e_3 \tag{6.7a}$$

where, σ_1 is the axial stress in the x-direction; α_{11}, α_{12} and α_{13} are the material constants of the element in the x, y and z-directions, respectively; $\Phi_{11} = \alpha_{11} kNT$; $\Phi_{12} = \alpha_{12} kNT$ and $\Phi_{13} = \alpha_{13} kNT$; and e_1, e_2 and e_3 are defined as

$$e_1 = \lambda_1 - \frac{1}{\lambda_1}; \qquad e_2 = \lambda_2 - \frac{1}{\lambda_2}; \qquad e_3 = \lambda_3 - \frac{1}{\lambda_3}.$$

Similarly, $$\sigma_2 = \Phi_{21} e_1 + \Phi_{22} e_2 + \Phi_{23} e_3 \tag{6.7b}$$

and $$\sigma_3 = \Phi_{31} e_1 + \Phi_{32} e_2 + \Phi_{33} e_3 \tag{6.7c}$$

where, σ_2 and σ_3 are the axial stresses in the y and z-directions, respectively.

Combining equations (6.7a-c) yields the stress-strain equations for a heterogeneous anisotropic material, i.e.,

$$\sigma_i = \sum_{j=1}^{3} \Phi_{ij} e_j \text{ (i=1,2,3)}$$

or,
$$\begin{bmatrix} \sigma_1 \\ \sigma_2 \\ \sigma_3 \end{bmatrix} = \begin{bmatrix} \Phi_{11} & \Phi_{12} & \Phi_{13} \\ \Phi_{21} & \Phi_{22} & \Phi_{23} \\ \Phi_{31} & \Phi_{32} & \Phi_{33} \end{bmatrix} \begin{bmatrix} e_1 \\ e_2 \\ e_3 \end{bmatrix}. \tag{6.7d}$$

Furthermore, the parameter $\Phi_{ij} = \alpha_{ij} kNT$ is synonymous with the shear modulus of the material, which is a function of both the Poisson's ratio and its modulus of elasticity. Beacause both the collagen-proteoglycan distribution vary within a matrix, the meshwork properties and more important the number of chains N can be assumed to vary accordingly with position. Such variation is characterized in different direction by the values of α_{ij} (i, j=1,2,3).

It should be noted that the maximum shear and principal stresses developed in the solid skeleton can be evaluated from known stresses in accordance with fundamental stress analysis in the x, y and z-directions (non-principal directions).

The principal stresses σ_p (p=1,2,3) are calculated from the following equation,

$$\det \begin{vmatrix} \sigma_x - \sigma_p & \tau_{xy} & \tau_{xz} \\ \tau_{xy} & \sigma_y - \sigma_p & \tau_{yz} \\ \tau_{xz} & \tau_{yz} & \sigma_z - \sigma_p \end{vmatrix} = 0,$$

and the maximum shear stress is computed using $\tau_{\max} = \dfrac{\sigma_{\max} - \sigma_{\min}}{2}$

where, σ_x, σ_y and σ_z are the axial stresses in the x, y and z-directions respectively; τ_{xy}, τ_{xz} and τ_{yz} are three shear stresses of the stress tensor.

6.3.3 Determination of the material parameters

Background of the classical consolidation theory

In order to completely identify the material properties of the solid skeleton of consolidating articular cartilage under an axial load, we have to resolve to the fundamental principles of stress analysis and more specifically aspects of the deformation laws for composite materials. Unlike many treatments of the tissue in the literature, we propose here that it is the collagen fibrous meshwork-proteoglycan entrapment, rather than the whole matrix of cartilage that is a composite material.

In the classical consolidation theory, the mechanical properties of an isotropic linear elastic solid are defined by the generalized Hooke's law, which can be written as,

$$\underline{\sigma} = \underline{\underline{C}}\,\underline{\varepsilon} \tag{6.8}$$

$$\underline{\sigma} = \begin{bmatrix} \sigma_{11} \\ \sigma_{22} \\ \sigma_{33} \\ \sigma_{32} \\ \sigma_{31} \\ \sigma_{12} \end{bmatrix}, \quad \underline{\underline{C}} = \begin{bmatrix} c_{11} & c_{12} & c_{13} & c_{14} & c_{15} & c_{16} \\ c_{12} & c_{22} & c_{23} & c_{24} & c_{15} & c_{26} \\ c_{13} & c_{23} & c_{33} & c_{34} & c_{35} & c_{36} \\ c_{14} & c_{24} & c_{34} & c_{44} & c_{45} & c_{46} \\ c_{15} & c_{25} & c_{35} & c_{45} & c_{55} & c_{56} \\ c_{16} & c_{26} & c_{36} & c_{46} & c_{56} & c_{66} \end{bmatrix}, \quad \underline{\varepsilon} = \begin{bmatrix} \varepsilon_{11} \\ \varepsilon_{22} \\ \varepsilon_{33} \\ \varepsilon_{32} \\ \varepsilon_{31} \\ \varepsilon_{12} \end{bmatrix}$$

where, σ_{ij} are the elements of a symmetric stress tensor; c_{ij} are the constant coefficients of the symmetric stiffness matrix $\underline{\underline{C}}$; and ε_{ij} are the elements of a symmetric elastic strain tensor.

Assuming both loading and geometrical symmetry in the z-direction, the stiffness matrix reduces to

$$\underline{\underline{C}} = \begin{bmatrix} c_{11} & c_{12} & c_{13} & 0 & 0 & 0 \\ c_{12} & c_{22} & c_{23} & 0 & 0 & 0 \\ c_{13} & c_{23} & c_{33} & 0 & 0 & 0 \\ 0 & 0 & 0 & c_{44} & 0 & 0 \\ 0 & 0 & 0 & 0 & c_{44} & 0 \\ 0 & 0 & 0 & 0 & 0 & 2(c_{11} - c_{12}) \end{bmatrix}.$$

It can be assumed that under consolidation-type deformation where fluid exudation is the principal driver of the deformation process, the shear stress is small relative to the

direct stress components and can therefore be ignored. Therefore equation (6.8) can be rewritten as,

$$\begin{bmatrix}\sigma_{11}\\ \sigma_{22}\\ \sigma_{33}\end{bmatrix}=\begin{bmatrix}c_{11} & c_{12} & c_{13}\\ c_{12} & c_{22} & c_{23}\\ c_{13} & c_{23} & c_{33}\end{bmatrix}\begin{bmatrix}\varepsilon_{11}\\ \varepsilon_{22}\\ \varepsilon_{33}\end{bmatrix}. \tag{6.9}$$

This equation presents the stress-strain relationship for the tissue element under small strain conditions when the shear stress is negligible in the linear classical consolidation theory for an anisotropic material (for an isotropic material if $c_{11}=c_{22}=c_{33}$ and $c_{12}=c_{13}=c_{23}$, and for a planar isotropic material if $c_{11}=c_{22}\neq c_{33}$ and $c_{13}=c_{23}\neq c_{12}$)

In order to determine the constants in equation 6.9, the generalized Hooke's law for a composite material is considered. We assume that the matrix is heterogeneous throughout its depth (z-direction), but isotropic in the xy-plane. Following this assumption, the following relationship can be written (Ward and Hadley, 1993)

$$\varepsilon_{11}=\frac{\sigma_{11}}{E_1}-\nu_{12}\frac{\sigma_{22}}{E_2}-\nu_{13}\frac{\sigma_{33}}{E_3} \tag{6.10a}$$

$$\varepsilon_{22}=-\nu_{12}\frac{\sigma_{11}}{E_1}+\frac{\sigma_{22}}{E_2}-\nu_{23}\frac{\sigma_{33}}{E_3} \tag{6.10b}$$

$$\varepsilon_{33}=-\nu_{13}\frac{\sigma_{11}}{E_1}-\nu_{23}\frac{\sigma_{22}}{E_2}+\frac{\sigma_{33}}{E_3} \tag{6.10c}$$

where, E_1, E_2 and E_3 are the Young's moduli in the x, y and z-directions respectively and ν_{12}, ν_{13} and ν_{23} are the Poison's ratios of the anisotropic material.

Equations (6.10a-c) can be written for the plane-isotropic material of the skeleton (ie. $E_1=E_2$, $\nu_{12}=\nu_1$ and $\nu_{13}=\nu_{23}=\nu_2$) as,

$$\begin{bmatrix}\varepsilon_{11}\\ \varepsilon_{22}\\ \varepsilon_{33}\end{bmatrix}=\begin{bmatrix}1 & -\nu_1 & -\nu_2\\ -\nu_1 & 1 & -\nu_2\\ -\nu_2 & -\nu_2 & 1\end{bmatrix}\begin{bmatrix}E_1 & 0 & 0\\ 0 & E_1 & 0\\ 0 & 0 & E_3\end{bmatrix}^{-1}\begin{bmatrix}\sigma_{11}\\ \sigma_{22}\\ \sigma_{33}\end{bmatrix}$$

or,

$$\begin{bmatrix}\sigma_{11}\\ \sigma_{22}\\ \sigma_{33}\end{bmatrix}=\begin{bmatrix}\frac{(\nu_2^2-1)E_1}{2\nu_2^2\nu_1+2\nu_2^2+\nu_1^2-1} & -\frac{(\nu_1+\nu_2^2)E_1}{2\nu_2^2\nu_1+2\nu_2^2+\nu_1^2-1} & -\frac{\nu_2E_1}{2\nu_2^2+\nu_1-1}\\ -\frac{(\nu_1+\nu_2^2)E_1}{2\nu_2^2\nu_1+2\nu_2^2+\nu_1^2-1} & \frac{(\nu_2^2-1)E_1}{2\nu_2^2\nu_1+2\nu_2^2+\nu_1^2-1} & -\frac{\nu_2E_1}{2\nu_2^2+\nu_1-1}\\ -\frac{\nu_2E_2}{2\nu_2^2+\nu_1-1} & -\frac{\nu_2E_2}{2\nu_2^2+\nu_1-1} & \frac{(\nu_1-1)E_2}{2\nu_2^2+\nu_1-1}\end{bmatrix}\begin{bmatrix}\varepsilon_{11}\\ \varepsilon_{22}\\ \varepsilon_{33}\end{bmatrix}. \tag{6.11}$$

Equation (6.11) ia a symmetric stiffness matrix similar to equation (6.9), and hence

yields

$$E_1 = E_2 = E\,,$$

so that equation (6.11) then becomes

$$\begin{bmatrix}\sigma_{11}\\ \sigma_{22}\\ \sigma_{33}\end{bmatrix} = E\begin{bmatrix} \dfrac{(\nu_2^2-1)}{2\nu_2^2\nu_1+2\nu_2^2+\nu_1^2-1} & -\dfrac{(\nu_1+\nu_2^2)}{2\nu_2^2\nu_1+2\nu_2^2+\nu_1^2-1} & -\dfrac{\nu_2}{2\nu_2^2+\nu_1-1} \\ -\dfrac{(\nu_1+\nu_2^2)}{2\nu_2^2\nu_1+2\nu_2^2+\nu_1^2-1} & \dfrac{(\nu_2^2-1)}{2\nu_2^2\nu_1+2\nu_2^2+\nu_1^2-1} & -\dfrac{\nu_2}{2\nu_2^2+\nu_1-1} \\ -\dfrac{\nu_2}{2\nu_2^2+\nu_1-1} & -\dfrac{\nu_2}{2\nu_2^2+\nu_1-1} & \dfrac{(\nu_1-1)}{2\nu_2^2+\nu_1-1} \end{bmatrix}\begin{bmatrix}\varepsilon_{11}\\ \varepsilon_{22}\\ \varepsilon_{33}\end{bmatrix}. \quad (6.12)$$

Definition of parameters in the developed consolidation theory

Noting that equations (6.9) and (6.7d) are similar in form, it can be established that equation (6.9) represents the stress-strain relationship for non-linear large strain consolidation deformation where the parameters e_i (i=1, 2, 3) are non-linear functions of the stretch ratios. Therefore, e_i (i=1,2,3) are namely the normal effective strains for large deformation, Φ_{ij} (i, j=1,2,3) (N/m^2) are thus defined as the depth-dependent stiffness of the matrix for a heterogeneous and planar isotropic material and σ_i (i=1,2,3) (N/m^2) are the normal stresses of the solid skeleton (the collagen and proteoglycan chains).

Differentiating equations (6.7a), (6.7b) and (6.7c) yields the stiffness elements, S_{ij} of the stiffness matrix $\underline{\underline{S}}$, i.e.

$$S_{ij} = \frac{\partial\sigma_i}{\partial\lambda_j} = \Phi_{ij}\left(1+\frac{1}{\lambda_j^2}\right)\ (i,\,j=1,3,3)\ \text{ or }\ S_{ij} = \frac{\partial\sigma_i}{\partial\lambda_j} = \Phi_{ij}\dot{e}_j \qquad (6.13)$$

where, $\dot{e}_1 = 1+\dfrac{1}{\lambda_1^2}$, $\dot{e}_2 = 1+\dfrac{1}{\lambda_2^2}$ and $\dot{e}_3 = 1+\dfrac{1}{\lambda_3^2}$. Thereby, Φ_{ij} are called the stiffness coefficients of the non-linear stress-strain relationship since the stiffness elements S_{ij} are the non-linear functions of the stretch ratios.

Determination of the stiffness coefficients Φ_{ij}

It must be noted that the condition of planar isotropy in the xy-plane assumed here is a gross simplification of the real property of the tissue's skeletal material. However, this

assumption is not expected to compromise the prediction of the resulting equations significantly. Most importantly, the anisotropic nature of the material is still preserved.

If the Young's modulus (E) and the Poison's ratios (ν_1, ν_2) in equation (6.12) are depth-dependent functions and the strains in the equations are the effective large strains e_i, equation (6.12) would be considered as the equivalent non-linear large deformation form of equations (6.7d). Therefore, the constants in the stress-strain relationship for the solid skeleton of the heterogeneous, plane-isotropic articular cartilage material with non-linear and large strain deformation can be written as

$$\begin{bmatrix} \sigma_1 \\ \sigma_2 \\ \sigma_3 \end{bmatrix} = \begin{bmatrix} \Phi_{11} & \Phi_{12} & \Phi_{13} \\ \Phi_{12} & \Phi_{11} & \Phi_{13} \\ \Phi_{13} & \Phi_{13} & \Phi_{33} \end{bmatrix} \begin{bmatrix} e_1 \\ e_2 \\ e_3 \end{bmatrix} \tag{6.14}$$

where, the elements Φ_{ij} of the depth-dependent stiffness coefficient matrix are related to the depth-dependent elastic moduli $E(z)$ and Poison's ratios $\nu_1(z)$ and $\nu_2(z)$ are similar to the definitions in the classical consolidation theory, ie.

$$\Phi_{33} = \frac{(\nu_1 - 1)E}{2\nu_2^2 + \nu_1 - 1};\ \Phi_{11} = \Phi_{22} = \frac{(\nu_2^2 - 1)E}{2\nu_2^2\nu_1 + 2\nu_2^2 + \nu_1^2 - 1} = \frac{(\nu_2^2 - 1)}{(\nu_1^2 - 1)}\Phi_{33};$$

$$\Phi_{12} = \frac{-(\nu_2^2 + \nu_1)E}{2\nu_2^2\nu_1 + 2\nu_2^2 + \nu_1^2 - 1} = \frac{-(\nu_2^2 + \nu_1)}{(\nu_1^2 - 1)}\Phi_{33};$$

and $\Phi_{13} = -\frac{\nu_2 E}{2\nu_2^2 + \nu_1 - 1} = -\frac{\nu_2}{\nu_1 - 1}\Phi_{33}$.

6.3.4 Large strain poroelasticity theory for articular cartilage consolidation

It is well established that swelling mediates in the stress sharing mechanism between the solid and fluid components of articular cartilage. In this respect, the classical consolidation theory is further modified to include the effects of chemical components and their concomitant swelling stress contribution to the development of cartilage stiffness. Based on the work of Oloyede and Broom (1994), the effective stress principle (Tezaghi, 1943) and poroelasticity theory (Disilvestro and Suh, 2001; Li et al, 1999), the constitutive effective stress relationship (equation 6.14) for the heterogeneous and anisotropic solid is reconstituted for an element of articular cartilage matrix to include physico-chemical properties, i.e.,

$$\sigma_i = \Phi_{ij} e_j + D_i \frac{\partial \lambda_i}{\partial t} - \Delta\pi - u \qquad (i, j = 1,2,3) \tag{6.15}$$

where u is the hydrostatic excess pore pressure arising from external loading, excluding the component of the osmotic pressure generated from the concentration of exchangeable ions; $D_i\,(Pa.s)(i = 1,2,3)$ are constant drag coefficients in the x, y and z-directions; $\Delta\pi$ is the change in Donnan osmotic pressure which can be expressed using equations (5.28) and (5.29),

$$\Delta\pi = u_{o2}\left(\frac{1}{\lambda^2} - 1\right),$$

where, u_{o2} is the depth-dependent initial osmotic pressure of the element.

The component $D_i \frac{\partial \lambda_i}{\partial t}$ in equation (6.15)) is the portion of stress contributed by the combination of drag and electrical effects as the fluid finds it increasingly more difficult to exude due to matrix deformation and related discrease in permeability, and increasing fixed charge density to water ratio. The fixed charges are those associated with the proteoglycans and all other charged components, which are intimately associated with them. It should be noted that drag will vary with time as the matrix pores decrease in size with increasing compression; however, it has been assumed constant for simplicity in the present work.

6.3.5 Continuity equation

The rate of fluid exudation from cartilage under static and moderate rates of loading is known to be slow with the consequence that Darcy's law of percolation is applicable. This law can be generalized to include both multi-dimensional fluid flow and the influence of electro-chemical activities including variations in pressure due to temperature gradients. Therefore, using the generalized Darcy's law (Kezdi, 1979; Klausner, 1991) and making plausible assumption on the deformation of cartilage, and adopting the principle of effective stress (Tezaghi, 1943) it can be shown that for low velocities of flow due to static loading,

$$\vec{\upsilon}_d = -\underline{\underline{K}}\, grad(u), \tag{6.16}$$

where $\underline{\underline{K}}$ is a symmetrical coefficient tensor of six different components, which is modelled in next section; $\vec{\upsilon}_d$ is Darcy's velocity of fluid outflow (flow rates per unit

area).

If the fluid and solid are incompressible with constant densities, the conservation of mass of solid and fluid under a fluid outflow regime can be respectively described by,

$$\frac{\partial}{\partial t}\int_V (1-\phi)\rho_s dV + \oint_s (1-\phi)\rho_s \vec{v}_s .\hat{n}ds = 0 \text{ and } \frac{\partial}{\partial t}\int_V \phi\rho_f dV + \oint_s \phi\rho_f \vec{v}_f .\hat{n}ds = 0, \quad (6.17)$$

where ρ_s and ρ_f are the densities of the solid and fluid respectively, $\phi = \frac{V_f}{V} = 1 - \frac{V_s}{V}$ is the space occupied by water in a given element, V_f is the instant volume of the fluid in the given element, $\vec{\upsilon}_s$ is the velocity of the solid component and $\vec{\upsilon}_f$ is the velocity of the fluid.

Applying convergence theory on the second term of equations (6.17) becomes

$$\frac{\partial}{\partial t}\int_V (1-\phi)dV + \int_V div[(1-\phi)\vec{v}_s] = 0 \text{ or } -\frac{\partial \phi}{\partial t} + div[(1-\phi)\vec{v}_s] = 0 \quad (6.18)$$

and

$$\frac{\partial}{\partial t}\int_V \phi dV + \int_V div(\phi\vec{v}_s) = 0 \text{ or } \frac{\partial}{\partial t}\phi + div(\phi\vec{v}_f) = 0. \quad (6.19)$$

Combining equations (6.18) and (6.19) yields

$$div(\phi\vec{v}_f) + div[(1-\phi)\vec{v}_s] = 0 \text{ or } div[\phi(\vec{v}_f - \vec{v}_s)] + div(\vec{v}_s) = 0. \quad (6.20)$$

Darcy velocity through the porous medium is defined by

$$\vec{v}_d = \phi(\vec{v}_f - \vec{v}_s) \text{ or } div(\vec{v}_d) = div[\phi(\vec{v}_f - \vec{v}_s)]. \quad (6.21)$$

Equation (6.18) can be written as

$$-\frac{\partial \phi}{\partial t} + (1-\phi)div(\vec{v}_s) - \vec{v}_s .grad\phi = 0. \quad (6.22)$$

Substituting equations (6.21) and (6.20) into (6.22) yields

$$-\frac{\partial \phi}{\partial t} - (1-\phi)div(\vec{v}_d) - \vec{v}_s .grad\phi = 0 \text{ or } div(\vec{v}_d) = -\frac{1}{1-\phi}\left(\frac{\partial \phi}{\partial t} + \vec{v}_s .grad\phi\right) \quad (6.23)$$

It is known that cartilage can be argued as a plane-isotropic material, thus $grad(\phi)$ is a vector in the z-(depth) direction only. Also, it does not deform when there is no fluid loss from its matrix, then can be discussed that equation (26) only depends on the change in the fluid space (porosity). Therefore, the second term in the equation can be negligible (i.e. $\vec{v}_s .grad\phi = 0$) to result the solid spreads over the plane when the matrix is compressed or the velocity of solid in the z-direction is very small compared to that

in the x and y-directions under the deformation. So that, the Darcy velocity only depends on the rate of change of the porosity inside the matrix and equation (6.23) can be reconstituted as

$$div(\vec{v}_d) \approx -\frac{1}{1-\phi}\frac{\partial \phi}{\partial t} \tag{6.24}$$

It is noted that $\phi = 1 - \frac{V_s}{V}$ (where V_s does not change as only fluid is lost under cartilage compression) which can be substituted into equation (6.24) to yield

$$\frac{\partial \phi}{\partial t} = -\frac{\partial}{\partial t}\left(\frac{V_s}{V}\right) \text{ or } \frac{1}{(1-\phi)}\frac{\partial \phi}{\partial t} = \frac{1}{V}\frac{\partial V}{\partial t} = \frac{1}{\lambda}\frac{\partial \lambda}{\partial t} \tag{6.25}$$

Combining equations (6.24), (6.25) and (6.16) yields

$$\frac{1}{\lambda}\frac{\partial \lambda}{\partial t} = div\left(\underline{\underline{K}} grad(u)\right). \tag{6.26}$$

Equation (6.26), which is the full continuity equation for fluid flow out of the loaded porous matrix, describes the relationship between the hydrostatic excess pore pressure, permeability coefficients and volumetric stretch ratio.

6.3.6 Model for permeability variation

An external load producing stresses that change the structure and texture of the porous matrix causes a change in permeability; the permeability of articular cartilage is a function of time and position. The time variation is due to deformation, while the positional variation is a cosequence of the heterogeneous property, and specially, the distribution/ concentration of the proteoglycan contents.

The studies on artificially degenerated and normal cartilage matrices have revealed that the creep and hydrostatic excess pore pressure variation patterns with time vary significantly, where degeneration involves either the enzymatic depletion of proteoglycan. We propose that these differences are major contribution from the attention of the permeability of the degenerate tissue.

The permeability of cartilage depends on the volume occupied by fluif and the activities of its proteoglycan macromolecules. With respect to Figure 1, the permeability of the articular cartilage matrix can be modelled for the plane-isotropic medium so that it varies with position and deformation. Let us assume that the solid skeleton of the element is made up of microscopic elements which are spaced such that there is

allowance for fluid percolation along the x, y and z directions as shown in Figure 1. Then the permeability in these direction can be expressed as,

$$\underline{\underline{K}} = \underline{\underline{K}}(t,x,y,z) = \begin{bmatrix} K_{xx} & K_{xy} & K_{xz} \\ K_{yx} & K_{yy} & K_{yz} \\ K_{zx} & K_{zy} & K_{zz} \end{bmatrix} \text{ or } \underline{\underline{P}}^T \underline{\underline{K}} \underline{\underline{P}} = \begin{bmatrix} K_1 & 0 & 0 \\ 0 & K_2 & 0 \\ 0 & 0 & K_3 \end{bmatrix}, \qquad (6.27)$$

where $\underline{\underline{K}}$ is a symmetrical tensor of six different components; K_1, K_2 and K_3 are permeability coefficients in the principal directions; and $\underline{\underline{P}}$ is a matrix to transform from the matrix $\underline{\underline{K}}$ in the x, y and z- directions to the principal ones.

Assuming that the principal directions of fluid are in x, y and z-directions, then equation (6.27) can be written as

$$\underline{\underline{K}} = \begin{bmatrix} K_1 & 0 & 0 \\ 0 & K_2 & 0 \\ 0 & 0 & K_3 \end{bmatrix}, \qquad (6.28)$$

and the permeability $\underline{\underline{K}}$ can be conceptualized as a parameter that is influenced by both collagen and proteoglycan (and probably lipid) content and mechanical deformation, thereby varies with respect to the total volume occupied by pore fluid (or porosity), which will change with deformation (strain) due to the fluid outflow and will depend on the position of the element within a given tissue. Following these assumptions, the change in permeability in a given direction can be approximated as:

$$\Delta K_i \approx \frac{\partial K_i}{\partial V} \Delta V \qquad (i = 1,2,3) \qquad (6.29)$$

Furthermore, both fluid and solid components are assumed incompressible, thus the change in volumetric deformation due to fluid exudation from a loaded cartilage matrix results in the change in the shape and size distribution of the pores or in the total cross-sectional area of the pores where the fluid flows. Therefore, the change in permeability can be written as

$$\Delta K_i \approx \frac{\partial K_i}{\partial A_{fx}} \Delta y \Delta z + \frac{\partial K_i}{\partial A_{fy}} \Delta x \Delta z + \frac{\partial K_i}{\partial A_{fz}} \Delta x \Delta y \qquad (i = 1,2,3), \qquad (6.30)$$

where A_{fx}, A_{fy} and A_{fz} are the total cross-sectional areas of pores whose normal vectors coincide with the x, y and z-directions respectively.

Substituting equation (6.29) into (6.30) yields,

$$\frac{\partial K_i}{\partial V}\Delta V \approx \frac{\partial K_i}{\partial A_{fx}}\Delta y\Delta z + \frac{\partial K_i}{\partial A_{fy}}\Delta x\Delta z + \frac{\partial K_i}{\partial A_{fz}}\Delta x\Delta y \qquad (i = 1,2,3)\,. \tag{6.31}$$

Assuming that the average distribution of pores in any given direction is equivalent to the total cross-sectional area of pores in that direction, then

$$\frac{\partial A_{fx}}{\partial x} = n_x,\ \frac{\partial A_{fy}}{\partial y} = n_y \text{ and } \frac{\partial A_{fz}}{\partial z} = n_z \tag{6.32}$$

where n_x, n_y and n_z are constants for a simple pore distribution.

Substituting equation (6.32) into (6.31) yields

$$\frac{\partial K_i}{\partial V}\Delta V \approx \frac{\partial K_i}{n_x\partial x}\Delta y\Delta z + \frac{\partial K_i}{n_y\partial y}\Delta x\Delta z + \frac{\partial K_i}{n_z\partial z}\Delta x\Delta y \qquad (i = 1,2,3)$$

or in integral form,

$$\int_V \frac{\partial K_i}{\partial V}dV = \oint_S \vec{F}.\hat{n}ds \qquad (i = 1,2,3)\,, \tag{6.33}$$

where $\hat{n}ds = (dydz, dxdz, dxdy)$; s is the enclosed surface area of the matrix; and $\vec{F} = \left(\frac{1}{n_x}\frac{\partial K_i}{\partial x}, \frac{1}{n_y}\frac{\partial K_i}{\partial y}, \frac{1}{n_z}\frac{\partial K_i}{\partial z}\right)$.

Applying the Gauss Divergence law to the right hand side of equation (6.33), results in,

$$\int_V \frac{\partial K_i}{\partial V}dV = \int_V div\vec{F}dV$$

or,
$$\frac{\partial K_i}{\partial V} = div\vec{F} = \frac{1}{n_x}\frac{\partial^2 K_i}{\partial x^2} + \frac{1}{n_y}\frac{\partial^2 K_i}{\partial y^2} + \frac{1}{n_z}\frac{\partial^2 K_i}{\partial z^2}\,. \tag{6.34}$$

Also, equation (6.34) can be written in term of the stretch ratio or large strain as,

$$\frac{\partial K_i}{\partial \lambda} = -\left(\mu_x\frac{\partial^2 K_i}{\partial x^2} + \mu_y\frac{\partial^2 K_i}{\partial y^2} + \mu_z\frac{\partial^2 K_i}{\partial z^2}\right),\ (i=1,2,3) \tag{6.35}$$

where,
$$\lambda = \frac{V}{V_0},\ \mu_x = -\frac{V_0}{n_x},\ \mu_y = -\frac{V_0}{n_y}, \text{ and } \mu_z = -\frac{V_0}{n_z}\,.$$

Equation (6.35) is the partial differential equation which expresses the spartial distribution of the deformation-dependent permeability of articular cartilage. It is noted that when equation (6.35) applied to one-dimensional deformation, it results in equation (5.32), where $\lambda = 1+\varepsilon$ is defined as the bulk stretch ratio.

6.4 Mathematical description in cylindrical coordinates

A typical articular cartilage specimen, which is loaded in the consolidometer, is cylindrical in shape. Consequently in order to be able to represent more accurately the test geometry and also write a general mathematical solution for the deformation process an axially symmetric model of the cylindrical specimen is presented below.

6.4.1 Description of large strain

An element of an articular cartilage matrix is shown in Figure 6.2 with the stretch ratios λ_r, λ_θ, λ_z in cylindrical coordinates, where

$$\lambda_r = \frac{w_r}{w_{r_0}} \quad (6.36a), \qquad \lambda_\theta = \frac{r}{r_0} \quad (6.36b), \quad \text{and } \lambda_z = \frac{w_z}{w_{z_0}} \quad (6.36c)$$

where, w_r, r and w_z are the lengths of the element in the radial direction, radial displacement and the length of the element in the axial direction at time t respectively; If w_{r_0}, r_0 and w_{z_0} are the initial values of these parameters before loading, then the total elemental volumetric stretch ratio, λ is

$$\lambda = \frac{V}{V_0} = \lambda_r \lambda_\theta \lambda_z \qquad (6.36d)$$

and

$$\frac{1}{\lambda}\frac{\partial \lambda}{\partial t} = \frac{1}{V}\frac{\partial V}{\partial t} = \frac{1}{\lambda_r}\frac{\partial \lambda_r}{\partial t} + \frac{1}{\lambda_\theta}\frac{\partial \lambda_\theta}{\partial t} + \frac{1}{\lambda_z}\frac{\partial \lambda_z}{\partial t} \qquad (6.37)$$

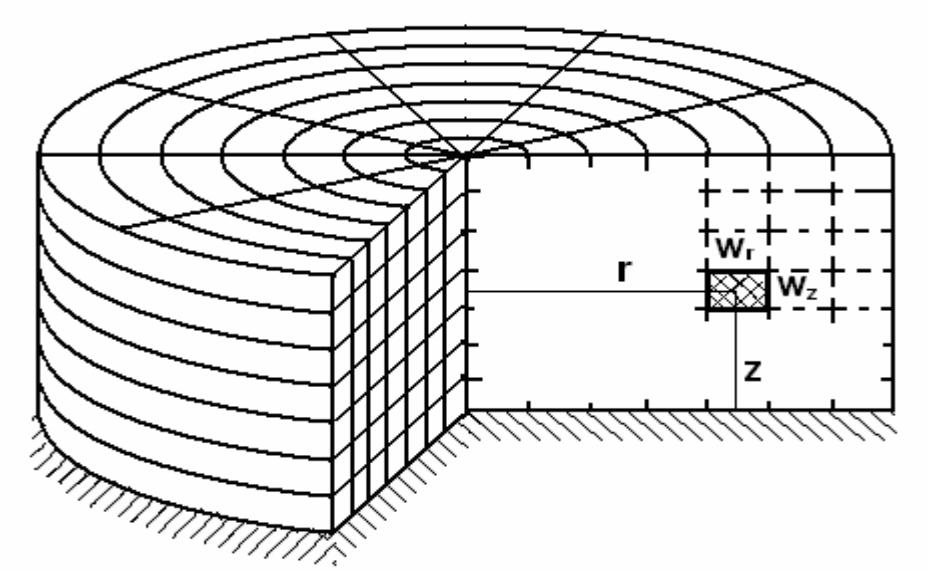

Figure 6.2: Mesh for the 3-dimensional axi-symmetric disc representing an articular cartilage sample and a selected element with its lengths and position.

6.4.2 Constitutive equation for a cylindrical matrix

Since articular cartilage is assumed to be a heterogeneous, planar-isotropic, hyperelastic and porous material, the constitutive relationship of motion for an element from its solid skeleton and fluid, which exhibit these properties can be written, using equation (6.15), in cylindrical coordinates as

$$\sigma_i = \Phi_{ij} e_i + D_i \frac{\partial \lambda_i}{\partial t} - \Delta\pi - u \qquad (i, j = r, \theta, z) \tag{6.38}$$

where, σ_r, σ_θ and σ_z are the principal stresses in the r, θ and z-directions in a given element respectively; u is the hydrostatic excess pore pressure associated with the fluid content excluding the osmotic pressure arising from the concentration of exchangeable ions; λ_r, λ_θ and λ_z are the principal stretch ratios in the r, θ and z directions respectively; D_r, D_θ and D_z are the drag coefficients representing the forces emanating from the resistance to fluid flow as the matrix is increasingly deformed in the r, θ and z directions respectively; $\Delta\pi$ is the change in Donnan osmotic pressure, and is defined in section 6.3 and Φ_{ij} are the stiffness values, which are also defined under stress-deformation relationship.

Then, equation (6.38) can be rewritten as,

$$\sigma_i = \Delta_i + D_i \frac{\partial \lambda_i}{\partial t} - u \qquad (i = r, \theta, z) \tag{6.39}$$

where, $\Delta_i = \sum_{j=r,\theta,z} \Phi_{ij} e_j - \Delta\pi$ and $e_j = \lambda_j - \frac{1}{\lambda_j}$.

6.4.3 Continuity equation

Since Darcy's law of fluid percolation applies as argued in section 6.3.5, we can write the continuity relationship in cylindrical coordinates as follows,

$$\vec{v} = \left(-K_r \frac{\partial u}{\partial r}, \frac{K_\theta}{r} \frac{\partial u}{\partial \theta}, K_z \frac{\partial u}{\partial z} \right), \tag{6.40}$$

where, $\vec{v}$ is the velocity of the outflowing fluid. Then,

$$-\frac{1}{V}\frac{\partial V_f}{\partial t} = div(\vec{v}) = -\left(\frac{1}{r}\frac{\partial}{\partial r}\left(rK_r \frac{\partial u}{\partial r} \right) + \frac{1}{r}\frac{\partial}{\partial \theta}\left(\frac{K_\theta}{r}\frac{\partial u}{\partial \theta} \right) + \frac{\partial}{\partial z}\left(K_z \frac{\partial u}{\partial z} \right) \right) \tag{6.41}$$

V_f is the total instantaneous volume of fluid in the element.

As the matrix is assumed to be axially symmetrical, u is independent of θ, so that equations (6.41) and (6.19) can be written as

$$\frac{1}{V}\frac{\partial V_f}{\partial t} = \frac{1}{\lambda}\frac{\partial \lambda}{\partial t} = \frac{1}{r}\frac{\partial}{\partial r}\left(rK_r\frac{\partial u}{\partial r}\right) + \frac{\partial}{\partial z}\left(K_z\frac{\partial u}{\partial z}\right) \tag{6.42}$$

where $\lambda = \lambda_r\lambda_\theta\lambda_z$ is the volumetric stretch ratio due to fluid loss from the element at time t. In addition, the relationship for permeability variation can also be expressed in cylindrical coordinates with axial symmetry as

$$\frac{\partial K_i}{\partial \lambda} = -\mu_r\left(\frac{\partial^2 K_i}{\partial r^2} + \frac{1}{r}\frac{\partial K_i}{\partial r}\right) - \mu_z\frac{\partial^2 K_i}{\partial z^2} \tag{6.43}$$

where μ_r and μ_z are constant coefficients in the r and z directions respectively.

6.5 Conclusion

The model of articular cartilage has been developed in accordance with the principle of mechanical consolidation, where its matrix is characterized as a heterogeneous (depth-dependent), anisotropic and porous material. The constitutive relationships have been developed to account for the interactions between the tissue's structure, large-strain deformation and physico-chemistry. The equations relating both the stress-strain behaviour of the tissue's solid skeleton and its permeability, to structure and physico-chemistry will be solved numerically and used to predict the responses of the tissue under static loading conditions. The constitutive equation of the model presents the hyperelastic behaviour of the solid component with the effect of the osmotic pressure and the drag of the interaction for the heterogeneous and anisotropic material under the large deformation. Darcy's law has been applied to describe the slow fluid exudation normally associated with this tissue and the new permeability submodel will help in the differentiation of tissue condition and allow the modeling of the degeneration and its effect on the biomechanics of loaded articular cartilage.

Chapter 7: Prediction of the consolidation responses of normal intact and lacerated articular cartilage matrices- a case study.

7.1 Introduction

This case study applies the new generalized model of articular cartilage discussed in chapter six to the prediction of the responses of statically loaded normal and lacerated cartilage. In order to ascertain the predictive capacity of the continuum model, both radially constrained and unconstrained matrices were analysed under static loading. The resulting system of equations is discretized and numerically solved using MATLAB and consolidation parameters, namely the hydrostatic excess pore pressure of the fluid component, effective stress of the solid skeleton (collagen meshwork and entrapped proteoglycans) and the creep strain were obtained, subject to a given swollen state of the tissue for the hypothetical layers of the tissue.

7.2 Assumption of the model for case study

The following three assumptions have been used to define the axial compression modulus, initial osmotic pressure, permeability and Poison's ratios applied in the numerical analysis.

i) The matrix exhibits plane-isotropic behaviour in the xy-plane.

ii) The axial stiffness parameter Φ_{33} and the initial osmotic pressure u_{o2} are depth-dependent exponential functions as establish in Chapter 5, i.e.

$$\Phi_{33} = \Phi_0 e^{\alpha_s \frac{z}{H}} \text{ and } u_{o2} = 1 - e^{-\alpha_o \frac{Z}{H}}$$

where Φ_0 is the stiffness in the z-direction at the superficial layer, α_s is a constant relating to the initial stiffness distribution and α_o is a constant relating to the distribution of the proteoglycan content of the unloaded matrix.

iii) Because of the assumption of planar isotropy in the xy-plane, the permeability coefficients are assumed to be only strain and depth-dependent functions i.e., with

variation in the z-direction or thickness direction. Under a one-dimensional constraint, the initial and boundary conditions for the coefficient of permeability K_z in the z-direction can be expressed as

$$K_z(0,\lambda) = K_0, \qquad \lambda \geq 0,$$
$$K_z(H,\lambda) = 0, \qquad \lambda \geq 0,$$
$$K_z(z,1) = f(z) = az + b, \quad 0 \leq z \leq H$$

where, K_0 is the permeability at the surface, a and b are constants in the linear variation assumed for the simplest depth-dependence permeability before loading and H is the initial thickness of the matrix, z is the location of a point within the matrix in the thickness direction.

iv) The Poison's ratios also reflect planar isotropy and heterogeneity, with $\nu_{xy} = 0.5$ due to the same properties in xy-plane and $\nu_{xz} = \nu_{yz} = 0.1 + 0.35z/H$ is a depth-dependent linear function assumed for analysis according with the previous published range and pattern of its values (Li et al, 1999 (a); 2000).

7.3 Analysis of the intact cartilage model

A one-dimensional numerical model of a cylindrical specimen of articular cartilage consisting of M layers was loaded statically with axial load P as shown in Figure 7.1. The constraint and loading simulate the one-dimensional consolidation experiment of Oloyede and Broom (1991) and restricts fluid exudation from the tissue to a single exit through the articular surface.

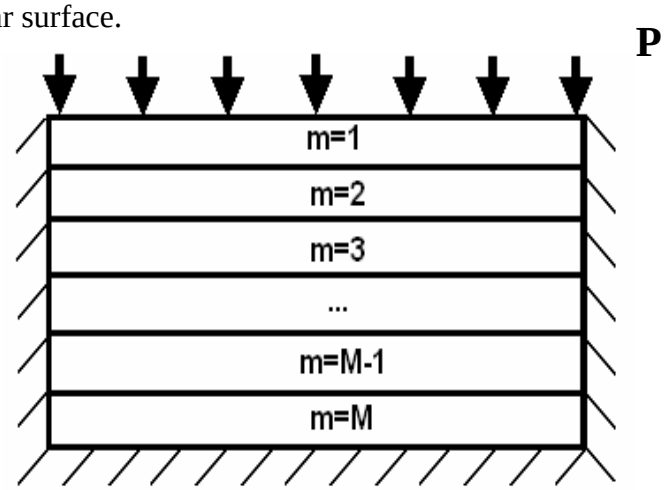

Figure 7.1: Schematic numerical analysis mesh of the articular cartilage matrix under one-dimensional constraints and axial static loading (1.06 MPa).

7.3.1 Theoretical formulation

Equation of equilibrium

The equilibrium equation for the total axial stress in a given layer is,

$$\frac{\partial \sigma_3}{\partial z} = 0 \Rightarrow \sigma_3 = \sigma_a \tag{7.1}$$

where σ_a is the axial static pressure or stress applied at the surface of the matrix .

Constitutive equations

When the model is subjected to radial constraints as shown in Figure 7.1, we have $\lambda_1 = \lambda_2 = 1 \Rightarrow \lambda = \lambda_3$, and consequently equation (6.15) becomes

$$\sigma_3 = \Phi_{33}\left(\lambda - \lambda^{-1}\right) + D_3 \frac{\partial \lambda}{\partial t} - \Delta\pi - u\,. \tag{7.2}$$

Substituting equation (7.1) into (7.2) yields

$$\sigma_a = \Phi_{33}\left(\lambda - \lambda^{-1}\right) + D_3 \frac{\partial \lambda}{\partial t} - \Delta\pi - u \tag{7.3}$$

where the parameters $\Phi_{33}, D_3, \Delta\pi$ and u are defined as in chapter 6.

Continuity equation

The generalized continuity relationship equation (6.20) can be written in one-dimensional form as

$$\frac{1}{\lambda}\frac{\partial \lambda}{\partial t} = \frac{\partial}{\partial z}\left(K \frac{\partial u}{\partial z}\right) \tag{7.4}$$

where K is the strain and depth-dependent permeability.

Combining equations (7.3) and (7.4) yields

$$\sigma_a - \Phi_{33}\left(\lambda - \lambda^{-1}\right) + \Delta\pi + u = D_3 \lambda \frac{\partial}{\partial z}\left(K \frac{\partial u}{\partial z}\right). \tag{7.5}$$

Strain and depth-dependent Permeability

The distribution with respect to position and variation with deformation of the

permeability coefficient is described by equation (6.35). Under the assumptions of one-dimensional constraints, the permeability K will not vary in the x and y-directions, so that

$$\frac{\partial K}{\partial \lambda} = -\mu_z \frac{\partial^2 K}{\partial z^2} \tag{7.6}$$

where the boundary and initial conditions are

$$\begin{aligned} &K(0,\lambda) = K_0, && \lambda \geq 0, \\ &K(H,\lambda) = 0, && \lambda \geq 0, \\ &K(z,1) = f(z), && 0 \leq z \leq H \end{aligned}$$

where $f(z) = az + b$ is the initial distribution of the permeability assumed in the previous section (7.2). Using these boundary and initial conditions together with equation (7.6) it can be shown, according to the method of separation of variables, that the permeability varies in both space and time (i.e., with deformation or volumetric stretch ratio) according to the similar expression in Appendix A1:

$$K(z,\lambda) = \frac{-K_0}{H} z + K_0 + \sum_{n=1}^{\infty} b_n e^{\frac{\mu_z n^2 \pi^2}{H^2}(\lambda - 1)} \sin\left(\frac{n\pi z}{H}\right) \tag{7.7}$$

where, $$b_n = \frac{2}{H}\int_0^H \left(f(z) - K_0 + \frac{K_0}{H} z \right) \sin\left(\frac{n\pi z}{H}\right) dz .$$

When dependence on position within the matrix is not considered, equation (7.7) will assume a similar function to that presented earlier by Lai et al. (1981). The importance is that this new model includes the depth dependence of the permeability, which is an important factor for heterogeneous (depth-dependent) materials as articular cartilage, which is not included in Lai et al's formulation. This strain and depth-dependent permeability is used to obtain the results presented in this chapter.

7.3.2 Discretized equations for numerical analysis

If the matrix consists of M layers, with the first layer being the superficial layer as shown in Figure 7.1, then the non-linear equations (7.3) and (7.5) can be written in discrete forms for the mth layer at the nth iteration of a known time step as,

$$\lambda_{n+1}^m = \lambda_n^m + \frac{\Delta t}{D_3}\left(\sigma_a - \Phi_{33}^m \left(\lambda_n^m - \frac{1}{\lambda_n^m} \right) + \Delta \pi_n^m + u_n^m \right) \tag{7.8}$$

and, $$\frac{\lambda_{n+1}^m - \lambda_n^m}{\lambda_n^m \Delta t} = \frac{1}{\Delta z^2}\left(K_n^{m+1}\left(u_n^{m+1} - u_n^m\right) - K_n^m\left(u_n^m - u_n^{m-1}\right)\right). \quad (7.9)$$

Combining equation (7.8) and (7.9) yields

$$\sigma_a - \Phi_{33}^m\left(\lambda_n^m - \frac{1}{\lambda_n^m}\right) + \Delta\pi_n^m + u_n^m = \frac{D_3\lambda_n^m}{\Delta z^2}\left(K_n^{m+1}\left(u_n^{m+1} - u_n^m\right) - K_n^m\left(u_n^m - u_n^{m-1}\right)\right) \quad (7.10)$$

or, $$K_n^m u_n^{m-1} + \left(-\frac{\Delta z^2}{D_3\lambda_n^m} - K_n^m - K_n^{m+1}\right)u_n^m + K_n^{m+1}u_n^{m+1} = A_n^m \quad (7.11)$$

where, $$A_n^m = \frac{\Delta z^2}{D_3\lambda_n^m}\left(\sigma_a - \Phi_{33}^m\left(\lambda_n^m - \frac{1}{\lambda_n^m}\right) + \Delta\pi_n^m\right).$$

The boundary conditions for fluid movement is given as,

$$\frac{\partial u(h,t)}{\partial z} = 0 \Rightarrow u_n^{M+1} = u_n^{M1}, \text{ and } u(0,t) = 0 \Rightarrow u_n^0 = 0.$$

Combining the boundary conditions with equation (7.11) yields a system of linear equations for a fixed time in the algebraic form

$$\underline{\underline{B}}\,\underrightarrow{u} = \underrightarrow{a} \quad (7.12)$$

where, $\underrightarrow{a}$, $\underrightarrow{u}$ and $\underline{\underline{B}}$ are the vectors and the tri-diagonal square matrix, which are defined respectively as

$$\underrightarrow{a} = \left(A_n^1, A_n^2, ..., A_n^M\right)'; \quad \underrightarrow{u} = \left(u_n^1, u_n^2, ..., u_n^M\right)';$$

and,
$$\underline{\underline{B}} = \begin{bmatrix} B_1 & K_n^2 & 0 & 0 & \cdots & 0 \\ K_n^2 & B_2 & K_n^3 & 0 & \ddots & \vdots \\ 0 & \ddots & \ddots & \ddots & \ddots & 0 \\ 0 & \ddots & K_n^m & B_m & \ddots & 0 \\ \vdots & \ddots & \ddots & \ddots & \ddots & K_n^M \\ 0 & \cdots & 0 & 0 & K_n^M & B_M \end{bmatrix}$$

where m is the order of iteration for a given layer, n is the number of iterations in a given time step and the diagonal elements of the matrix are defined as

$$B_{11} = -\frac{\Delta z^2}{D_3\lambda_n^1} - K_n^1 - K_n^2; \; B_{mm} = -\frac{\Delta z^2}{D_3\lambda_n^m} - K_n^m - K_n^{m+1}; \text{ and } B_{MM} = -\frac{\Delta z^2}{D_3\lambda_n^M} - K_n^M.$$

Furthermore, the permeability and osmotic pressure in each element are respectively computed using the discrete forms of equation (7.7) and discrete equations (5.28 and 5.29) as,

$$K_n^m = K_0\left(1-\frac{m-1/2}{M}\right)+\sum_{i=1}^{10} b_i e^{\frac{\mu_z i^2\pi^2}{H^2}\left(\lambda_n^m-1\right)}\sin\left(\frac{i\pi(m-1/2)}{M}\right) \qquad (7.13)$$

and $$\Delta\pi_n^m = u_{o2}^m\left(\frac{1}{(\lambda_n^m)^2}-1\right), \text{ where } u_{o2}^m = 1-e^{-0.22\frac{m-1/2}{M}}. \qquad (7.14)$$

The system of discrete equations was solved using the algorithm in MATLAB code as similar as that in Chapter 5 for the simulation but replaced by the stretch ratio in equation (7.9) instead of the strain. The solution yields the hydrostatic excess pore pressure and stretch ratios in different positions at time t until the deformation reaches equilibrium.

7.3.3 Results and discussions

Figures 7.2 and 7.3 demonstrate the agreement between experimental (curves Sa and Pa, Figure 4.6) and computed patterns of the strains for the whole specimen and the hydrostatic excess pore pressure at the bottom of the matrix results the parameters of the model as shown in Table 7.1. Using these parameters the depth-dependent strains and hydrostatic excess pore pressures, which are not obtained with the recent technology of the experiment, are predicted in the figures. The effective solid stress at the different depths of the specimen can also be estimated in Figure 7.4.

Table 7.1: Parameters for the analysis resulting in Figure 7.2-7.4

Parameters	Symbols	value
Thickness (mm)	H	1.70
Axial stiffness modulus (MPa)	Φ_{33}	$0.08e^{3.8\frac{z}{H}}$
Poison's ratios	ν_1, ν_2	0.5, 0.1+0.25z/H
Elastic modulus (MPa)	E	$\left(1-4\nu_2^2\right)\Phi_{33}$
Permeability (m^4/Ns)	K_0	7×10^{-17}
	$f(z)$	$1.75\times10^{-13}z/H+K_0$
	μ_z	$3H^2$
Drag constant (MPa.s)	D	500
Initial osmotic pressure (MPa)	u_{o2}	$1-e^{-0.22\frac{z}{H}}$

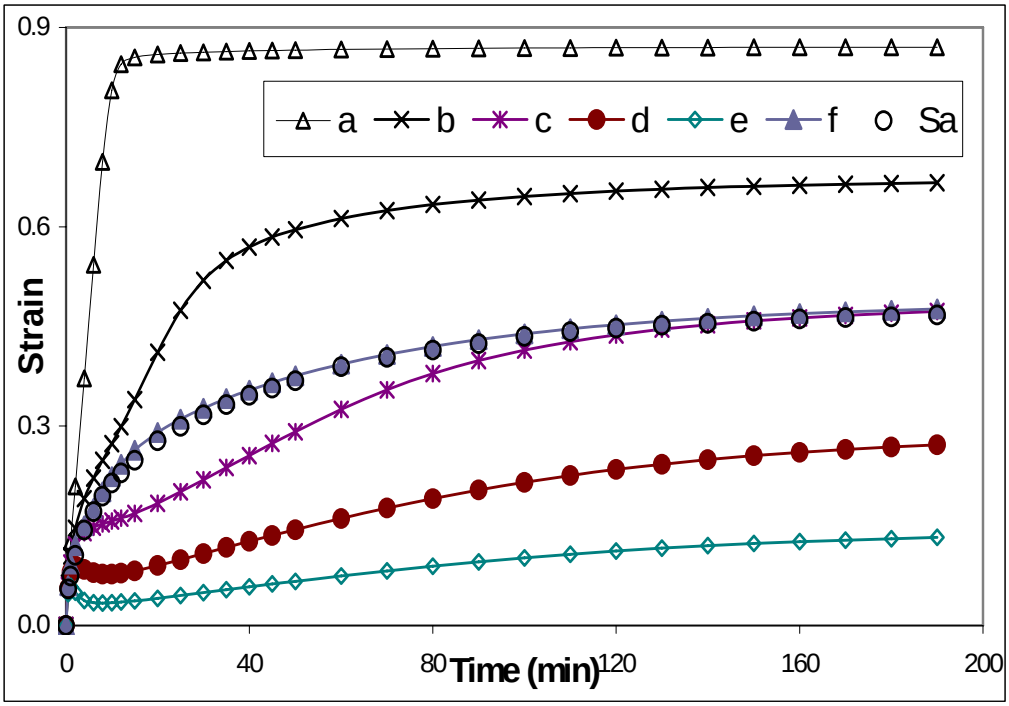

Figure 7.2: Comparison of the total matrix strain from the experimental data, Sa (Appendix Table A7) to the computed value (f) as well as the predicted values of the time-dependent strain at the depths of 0.05mm (a), 0.45mm (b), 0.85 mm (c), 1.25mm (d) and 1.7mm (e), and total matrix strain (f). The predicted values were obtained using the coefficients in Table 7.1.

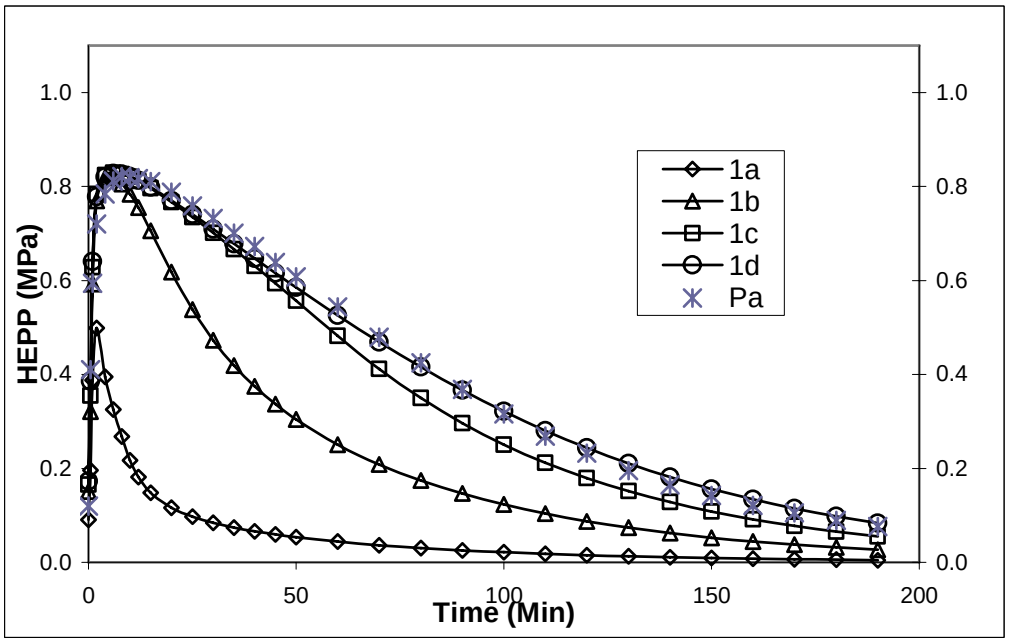

Figure 7.3: Comparison of the hydrostatic excess pore pressure at the bottom of the matrix from the experimental data, Pa (Appendix Table A7) to the computed value (1d) as well as the predicted values of the time-dependent hydrostatic pressure at the depths of 0.05mm (1a), 0.45mm (1b), 0.85 mm (1c) and 1.7mm (1d). The predicted values were obtained using the coefficients in Table 7.1.

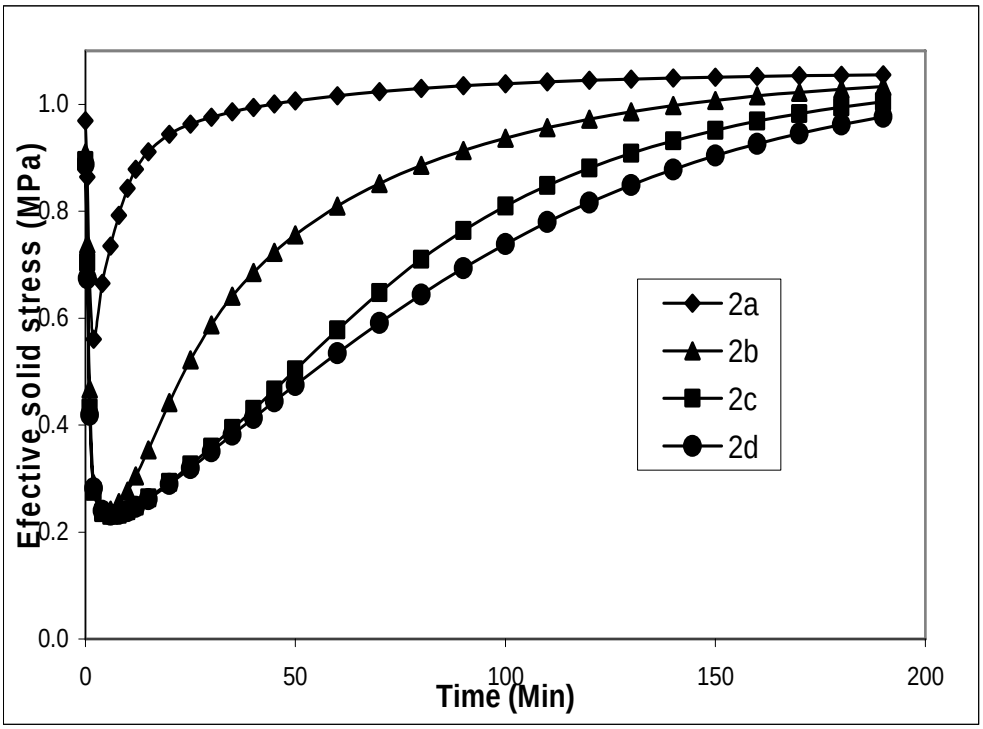

Figure 7.4: Predicted values of the effective solid stress at the depths of 0.05mm (2a), 0.45mm (2b), 0.85mm (2c) and 1.7mm (2d) of the normal intact cartilage matrix. The coefficients were used to obtain the predicted data are in Table 7.1.

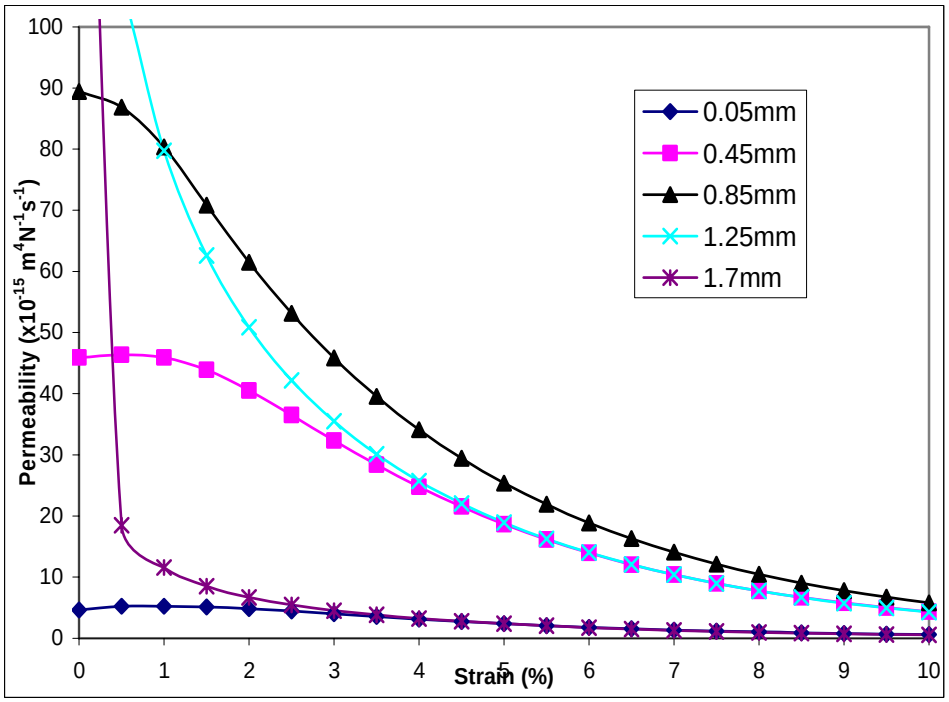

Figure 7.5: Predicted values of the permeability versus strain at the different depths (0.05, 0.45, 0.85, 1.25 and 1.7mm).

The predicted responses were obtained using the coefficients tabulated in Table 7.1 and the iteration reputed in the following permeability function as shown in Figure 7.5

$$K = 7\times10^{-17}\left(1-\frac{z}{H}\right)+\sum_{i=1}^{\infty}A_i e^{\frac{3\pi^2 i^2}{H^2}(\lambda-1)}\sin\left(\frac{\pi i z}{H}\right),$$

where $A_i \approx -\dfrac{3.5\times10^{-13}(-1)^i}{\pi i}$ and $i = 1,2,...$

Figure 7.5 shows that the permeability with respect to strain in each layer varies from the superficial layer to the bottom layer. Its pattern is approximately constant at the surface because there is no proteoglycans in the superficial layer, but decays as the compressive strain increases in the other layers and the decay rate of change of the permeability with respect to the strain is greater as the increasing depth.

It can be inferred that the parallel alignment of the collagen fibrils at the surface would affect the variation of the permeability in this region while the different concentration of the proteoglycans in each underlying layer would be expected to determine the permeability variation across the matrix. Both of this surface permeability and its distribution into the depth of the matrix considerably influence the response of the articular cartilage matrix when loaded. Consequently, surface laceration, proteoglycan depletion or change in the collagen architecture would be expected to play significant roles in determining the response of the tissue to load as a consequence of remodeling the structural equilibrium distribution of the unaltered sample.

Figure 7.6 illustrates the effect of the permeability function (effect of permeability variation) on the total matrix strain and hydrostatic excess pore pressure in the bottom layer for the normal intact cartilage matrix to simulate the effect of surface laceration(s). While the level of total matrix strain at equilibrium was unchanged, considerable increase in the hydrostatic excess pore pressure and reduction in strain relative to the experimental curve were observed when the superficial layer's permeability was changed from $K_0 = 7\times10^{-17}$ to $K_0 = 3\times10^{-17}\,(m^4/Ns)$. Also, a significant decrease in the hydrostatic excess pore pressure against an increase in the strain was obtained when the surface permeability was changed from $K_0 = 7\times10^{-17}$ up to $K_0 = 14\times10^{-17}\,(m^4/Ns)$.

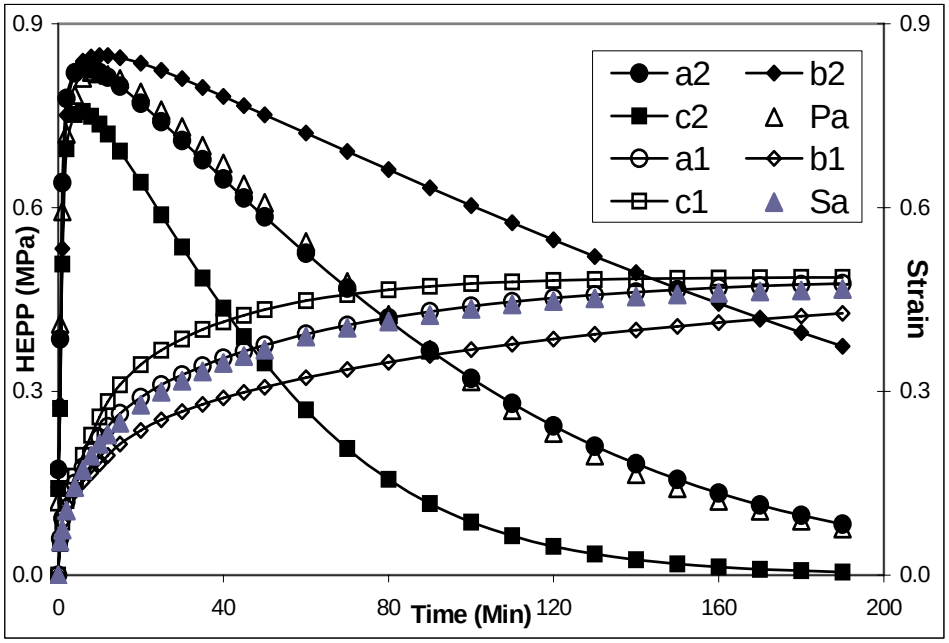

Figure 7.6: The influence of permeability on the total matrix strain (a1, b1, c1) and the hydrostatic excess pore pressure (a2, b2, c2) at the bottom of the normal intact cartilage matrix. Experimental values of the total matrix strain (Sa, appendix Table A3) and hydrostatic excess pore pressure (Pa appendix Table A3). The predicted data were obtained by using the permeability at the surface in Table 7.2 and the parameters in Table 7.1.

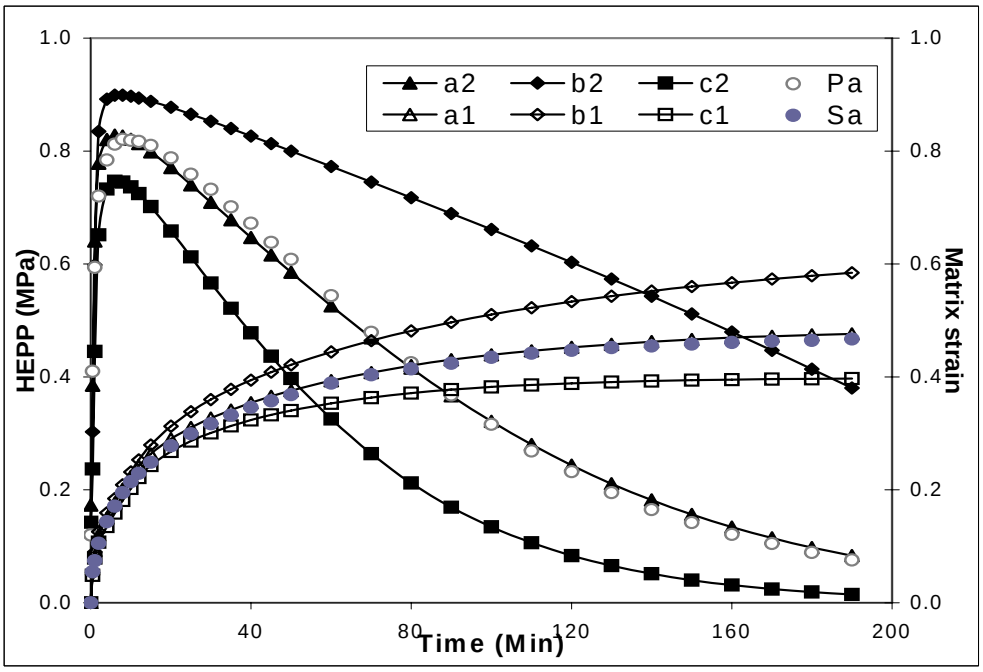

Figure 7.7: The influence of the axial stiffness modulus on the total matrix strain (a1, b1, c1) and the hydrostatic excess pore pressure (a2, b2, c2) at the bottom of the normal intact cartilage matrix. Experimental values of the total matrix strain (Sa, appendix Table A7) and hydrostatic excess pore pressure (Pa, appendix Table A3). The predicted data were obtained by using the stiffness coefficients in Table 7.2 and the parameters in Table 7.1

Table 7.2: Parameters for analysis resulting in figures 7.7 and 7.8

Symbols	Legend (Fig. 7.7)	Legend (Fig. 7.8)	value
Φ_{33} (MPa)	a1, a2	a1 (λ =1), a2 (λ =0.9)	$0.08e^{2\frac{z}{H}}$
	b1, b2	b1 (λ =1), b2 (λ =0.9)	$0.08e^{3.8\frac{z}{H}}$
	c1, c2	c1 (λ =1), c2 (λ =0.9)	$0.08e^{5\frac{z}{H}}$

Figure 7.7 reveals the influence of the distribution of axial stiffness modulus on the hydrostatic excess pore pressure and total matrix strain. It shows that the softening and stiffening of the matrix influence its condition responses in different but interesting ways. The hydrostatic excess pore pressure and the equilibrium level of the matrix strain increased significantly when the distribution of the axial stiffness coefficient was changed from $\Phi_{33} = 0.08e^{3.8\frac{z}{H}}$ to $\Phi_{33} = 0.08e^{2\frac{z}{H}}$ (MPa), and decreased when changed from $\Phi_{33} = 0.08e^{3.8\frac{z}{H}}$ to $\Phi_{33} = 0.08e^{5\frac{z}{H}}$ (MPa). The distributions of stiffness were also predicted in Figure 7.8 with respect to these stiffness coefficients.

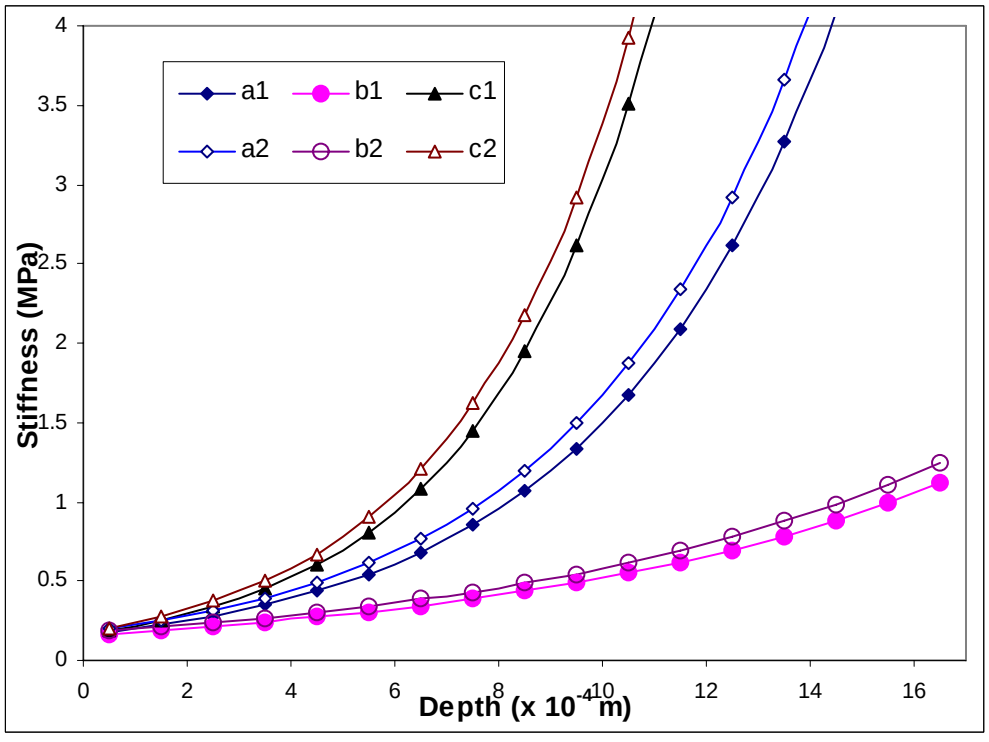

Figure 7.8: Predicted distribution of stiffness with respect to the stiffness coefficients and the stretch ratios as shown on Table 7.2. The values were used to analyse the influence of the stiffness on the responses of the loaded cartilage matrix

The time lag in the development of the fluid's hydrostatic excess pore pressure is governed by the level of drag forces and electrical repulsive and attractive forces as the fluid flows out of the matrix over time. Consequently, the effect of these two parameters on both the hydrostatic excess pore pressure and creep strain are investigated and predicted in Figure 7.9. It can be seen that the maximum level of hydrostatic excess pore pressure decreased as the drag coefficient was increased from 50 MPa.s to 500 and 2000 MPa.s, respectively. On the other hand, the rate of decay of the hydrostatic excess pore pressure from its maximum to equilibrium condition did not change significantly. These observations demonstrate that this present model is capable of predicting the experimentally observed phenomenon in which the time lag in the development of the hydrostatic excess pore pressure varied between an intact and proteoglycan depleted matrix of articular cartilage (Oloyede and Broom, 1994 (a)). In addition, the modelling of this drag in equation (7.3) can also explain the strain-rate dependence of the effective stress of solid skeleton (Oloyede and Broom, 1993 (b); 1994 (a)). These have not been possible with any of the existing models in the literature.

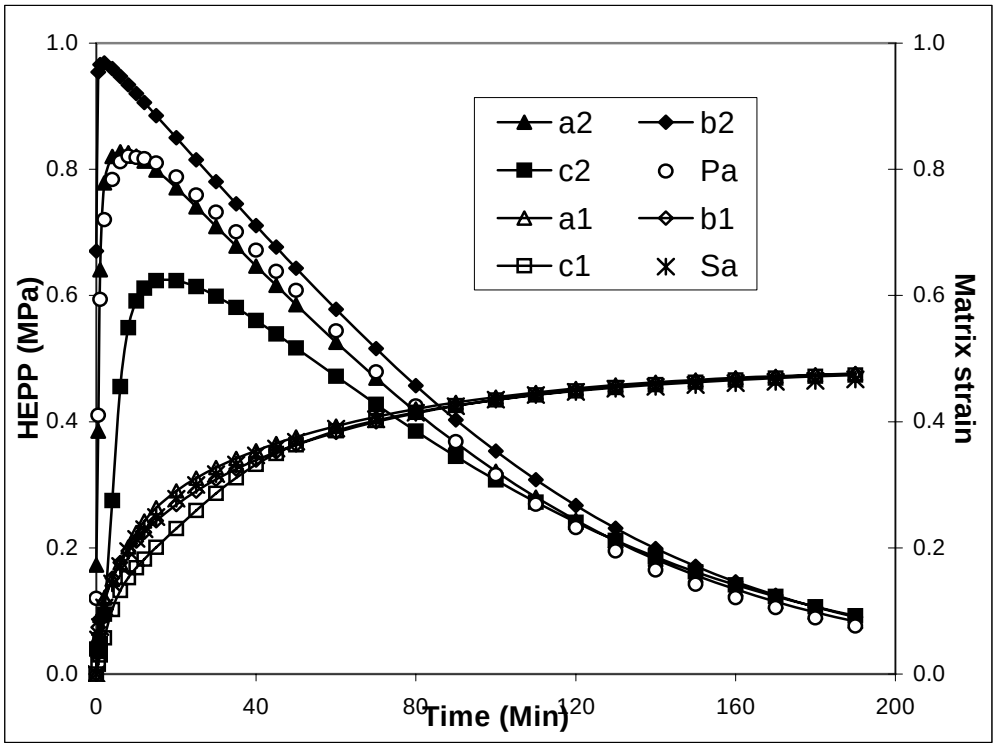

Figure 7.9: The influence of changing the drag coefficient D_z on the load carriage parameters of articular cartilage. The legends (a1, b1, c1) represent matrix strain and (a2, b2, c2) represent the hydrostatic excess pore pressure. Experimental values of the total matrix strain (Sa) and hydrostatic excess pore pressure (Pa) from appendix Table A7. The predicted data were obtained by using the drag coefficients in Table 7.3.

Table 7.3: Parameters for analysis resulting in Figure 7.9

Symbols	legend	value
D_z (MPa.s)	a1, a2	50
	b1, b2	500
	c1, c2	2000

7.4 Modelling and analysis of the effects of surface lacerations in articular cartilage

Surface fibrillation is commonly associated with osteoarthritic symptoms in mammalian joints (Broom, 1982; Vasan, 1983). In this section, the mathematical equations discretized earlier in chapter 5 and the last section are applied to the understanding of this clinically relevant condition. The situation described is that of a small damage to the articular cartilage and how it responds to load when it contains surface cracks or lacerations of particular depths into its top layers immediately underlying the load.

7.4.1 Mathematical description

The constitutive equations for one-dimensional constrained deformation, continuity equation and permeability variation for the cartilage matrix under axial compressive loading have been described in section 7.3 for the normal intact cartilage. It is hypothesized in this section that surface lacerations will modify both the compression modulus and permeability of the matrix. This argument is now tested below.

7.4.2 Idealization of surface laceration in articular cartilage

For depth-dependent compressive stiffness, the data published by Schinagl et al. (1997), can be used to obtain

$$\Phi_{33} = \Phi_0 e^{\alpha \frac{z}{H}} \tag{7.15}$$

where Φ_0 is the constant representing the stiffness coefficient of the superficial layer in the unloaded and unlacerated condition and α is a constant parameter. Φ_{33} accounts for how the stiffness is distributed across the layers of the unloaded tissue i.e. the initial condition.

This relationship is modified to represent a matrix with surface laceration by introducing the parameter $\alpha = \alpha(L)$, where L is the depth of the deepest laceration in the superficial layer of a given matrix. In chapters 4 and 5, models of articular cartilage bearing surface lacerations of depths less than 200 μm were studied. As mentioned earlier the thickness of the superficial layer of the tissue is between 150 to 200 μm. Hence such lacerations are confined within the superficial layer. In this case study matrices with lacerations confined within the superficial layer and those deeper than 200 μm are studied.

7.4.3 Results and discussions

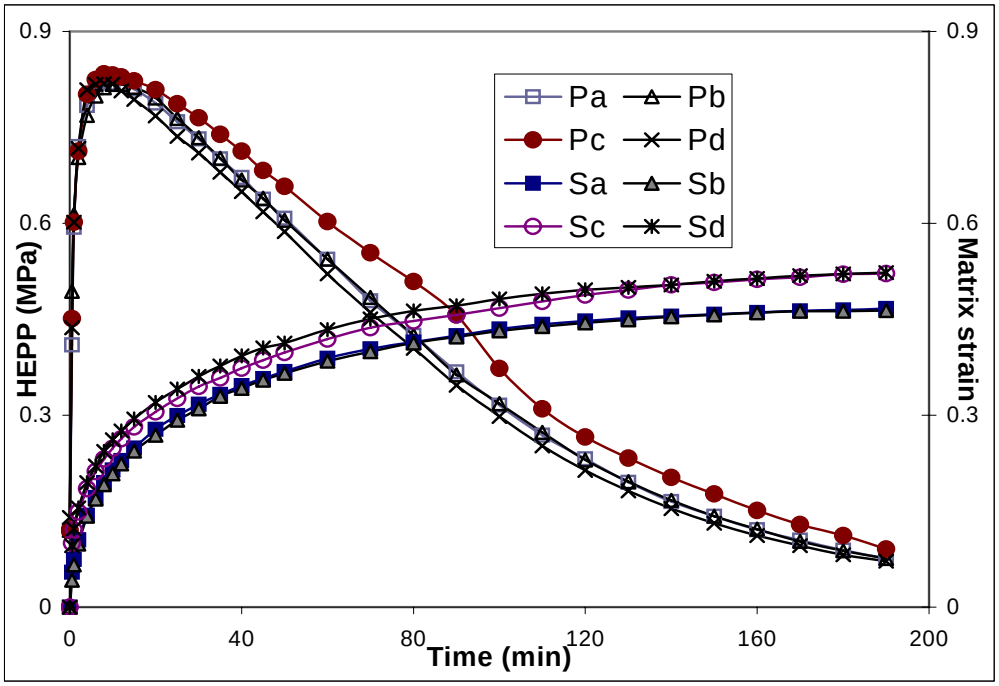

Figure 7.10: Experimental values of the total matrix strain (S) and hydrostatic excess pore pressure (P) for normal cartilage with intact superficial layer (Sa and Pa); normal cartilage with lacerated surface to 110μm (Sb and Pb); lacerated surface to 430μm (Sc and Pc); and lacerated surface to 780 μm (Sd and Pd). The data are tabulated in appendix Table A7.

The experimental results from Chapter 4 as shown in Figure 7.10 demonstrate the influence of surface lacerations of various depths on the consolidation (or load carriage) parameters of the cartilage matrix. It can be seen from these curves that only marginal increases of less than 10% in hydrostatic excess pore pressure and less than 12% in

creep strain occurred as the depth of laceration was increased up to 430 μm. However, there existed an abnormal behaviour in the decay position of the hydrostatic excess pore pressure curve. When the depth of laceration increased to 780 μm deep, about 3% decrease in the hydrostatic excess pore pressure and 15% increase in the total matrix strain for the lacerated matrix relative to the normal intact matrix were obtained.

Predicted results

Figure 7.11 presents the predicted results using the system of equations developed in section 7.3 with the appropriate modifications to accommodate lacerations; e.g. equation 7.12. This graph demonstrates that the predicted values of the hydrostatic excess pore pressure (S1) and creep strains (P1) agreed with the experimental data in the first third of consolidation (first 72 minutes) when the value of the initial distribution of the axial stiffness coefficient varied between $\Phi_{33} = 0.08e^{3.28\frac{z}{H}}$ and $\Phi_{33} = 0.08e^{3.8\frac{z}{H}}$ for the normal intact matrix, where this was accompanied by no changes in any of the other parameters used in analysis presented in Table 7.1. However, these predicted values did not accord well with the experimental data in the latter stages of consolidation (i.e. after 72 minutes) if the permeability remains unchanged throughout the consolidation. Table 7.4 presents the values of the depth-dependent stiffness and the permeability of the superficial layer of the lacerated articular cartilage matrix before and after 72 minutes in this analysis. When juxtaposed with the results presented in Figure 7.11, it can be seen that only the values of the stiffness were affected while the permeability remained at its value for the normal intact cartilage matrix in the first 72 minutes of deformation. However, good agreement was obtained between predicted (S2, P2) and experimental consolidation parameters for the whole consolidation when the permeability was increased by 32% for the latter stages relative to the value for the analysis in the first 72 minutes stages.

Figure 7.12 shows that the combination of the change in the stiffness (i.e. $\Phi_{33} = 0.08e^{3.28\frac{z}{H}}$ relative to $\Phi_{33} = 0.08e^{3.8\frac{z}{H}}$ of the normal intact tissue) and the surface permeability ($9.27\times10^{-17}\,\mathrm{m^4N^{-1}s^{-1}}$ against 7×10^{-17} for normal one) also yielded good

agreement between predicted and experimental data for the artificially damaged matrix up to a cut of 0.78 mm in depth. The average error and standard deviation of these fitted curves are 5.5% and 3.5% for the total matrix strain; 3.7 % and 6.4% for the hydrostatic excess pore pressure respectively.

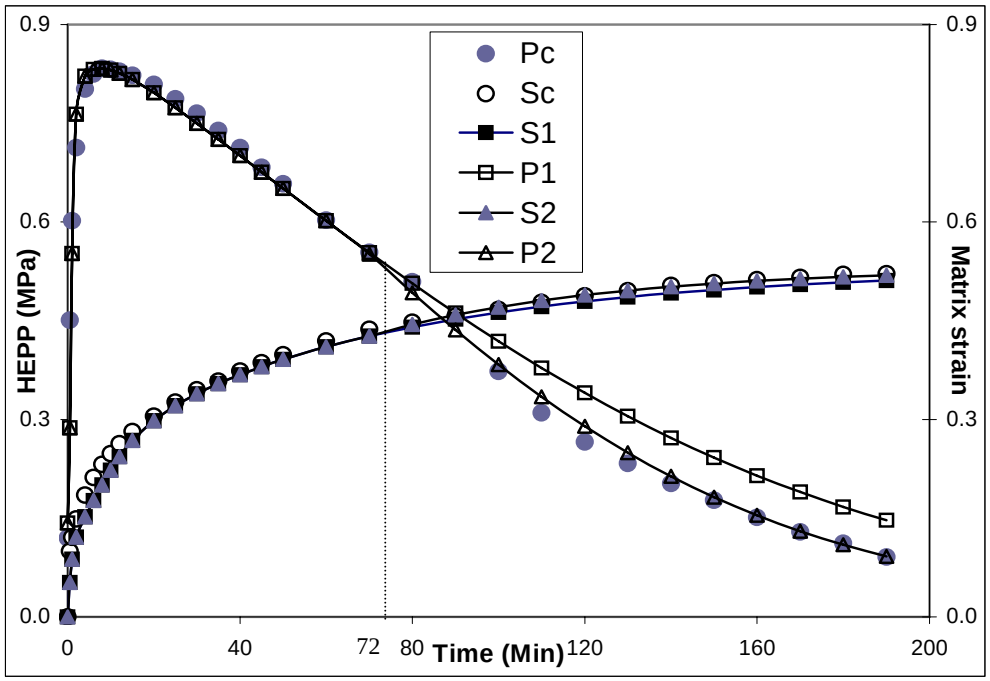

Figure 7.11: Comparison of the experimental and predicted values of the total matrix strain (S1, S2) and the hydrostatic excess pore pressure (P1, P2) for the matrix with laceration of 430 μm in depth. (i) Predicted values (S1, P1) using only the decrease in the stiffness; (ii) Predicted values (S2, P2) using both the decrease in the stiffness and the increase in the permeability; (iii) Experimental data (Sc, Pc) of appendix Table A7. The predicted data were obtained by using the coefficients in Table 7.4 and the others in Table 7.1.

Table 7.4: Parameters used for the analysis of results in Figure 7.11

Legends	Φ_{33} (MPa)	K_0 x 10^{-17} (m^4/Ns)	
		Before 72 minutes	After 72 minutes
S1, P1	$0.08e^{3.28\frac{z}{H}}$	7	7
S2, P2	$0.08e^{3.28\frac{z}{H}}$	7	9.27

The analysis presented above revealed that for the deep lacerations with depths spanning beyond the superficial layer, but not reaching the midzone region, the tissue's behaviour was more dominated by the stiffness where changes in this parameter resulted in matrix response to loading without any changes in permeability values

required. On the other hands, the depth of lacerations inflicted was increased into the midzone and beyond, a change in permeability values in combination with stiffness value variation was necessary before any agreement between experimental and predicted patterns of the consolidation parameters was possible.

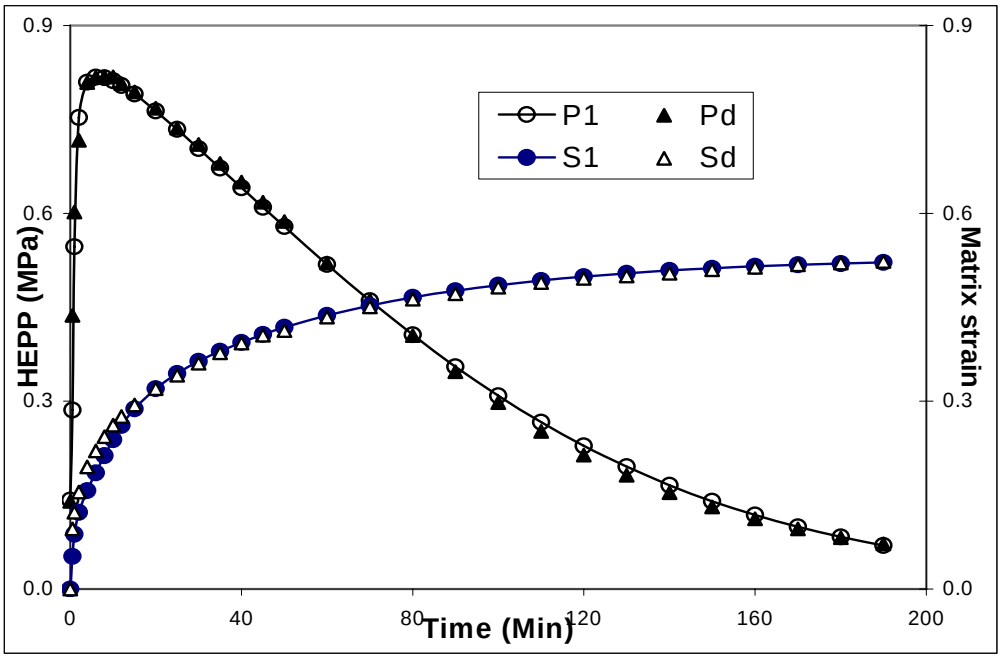

Figure 7.12: Predicted values of the total matrix strain (S1) and the hydrostatic excess pore pressure at the bottom (P1) and the comparison of those to the experimental data (Sd and Pd, appendix Table A7) for the normal matrix lacerated to the depth cut of 780 μm. The predicted data were obtained by using the coefficients in Table 7.5 and the others in Table 7.1

Table 7.5: Parameters used for analysing the results depicted in Figure 7.12

Legends	Φ_{33} (MPa)	K_0 x 10^{-17} (m^4/Ns)
S1, P1	$0.08e^{3.28\frac{z}{H}}$	9.27

7.5 Static axial loading of unconfined cartilage matrix – A case study

7.5.1 Model relationships and parameters

The numerical mesh for an unconstrained disc of articular cartilage matrix which will be subjected to axial loading is shown in Figure 7.13. Under this condition, equation (6.39) would be rewritten as

$$\frac{\partial \sigma_z}{\partial z} = 0 \Rightarrow \sigma_z = \sigma_a = \Delta_z + D_z \frac{\partial \lambda_z}{\partial t} - u\,, \tag{7.16}$$

with the initial and boundary conditions for the stretch ratio and the hydrostatic excess pore pressure as,

$$\lambda_r(r,z,0) = \lambda_\theta(r,z,0) = \lambda_z(r,z,0) = 1\,, \tag{7.16a}$$

$$u(r,0,t) = 0\,,\ \left.\frac{\partial u}{\partial z}\right|_{z=H} = 0\,,\ \left.\frac{\partial u}{\partial r}\right|_{r=0} = 0\,,\ u(R,z,t) = 0\,. \tag{7.16b}$$

Because the unconfined disc deforms without radial constraint and it has an axi-symmetric property then,

$$\sigma_x = \sigma_y \Rightarrow \begin{pmatrix} \sigma_r & \tau_{r\theta} \\ \tau_{r\theta} & \sigma_\theta \end{pmatrix} = \begin{pmatrix} \cos\theta & \sin\theta \\ -\sin\theta & \cos\theta \end{pmatrix} \begin{pmatrix} \sigma_x & 0 \\ 0 & \sigma_y \end{pmatrix} \begin{pmatrix} \cos\theta & -\sin\theta \\ \sin\theta & \cos\theta \end{pmatrix} = \begin{pmatrix} \sigma_x & 0 \\ 0 & \sigma_y \end{pmatrix}$$

Therefore,

$$\sigma_r = \sigma_\theta \text{ and } \tau_{r\theta} = 0\,. \tag{7.17}$$

The stresses also satisfy the following equilibrium relationship in the radial direction:

$$\frac{\partial \sigma_r}{\partial r} + \frac{\sigma_r - \sigma_\theta}{r} = 0\,. \tag{7.18}$$

Combining equations (7.17) and (7.18), yields

$$\sigma_r = \sigma_\theta = \sigma_r(r = R) = 0 \text{ and } \lambda_r = \lambda_\theta\,. \tag{7.19}$$

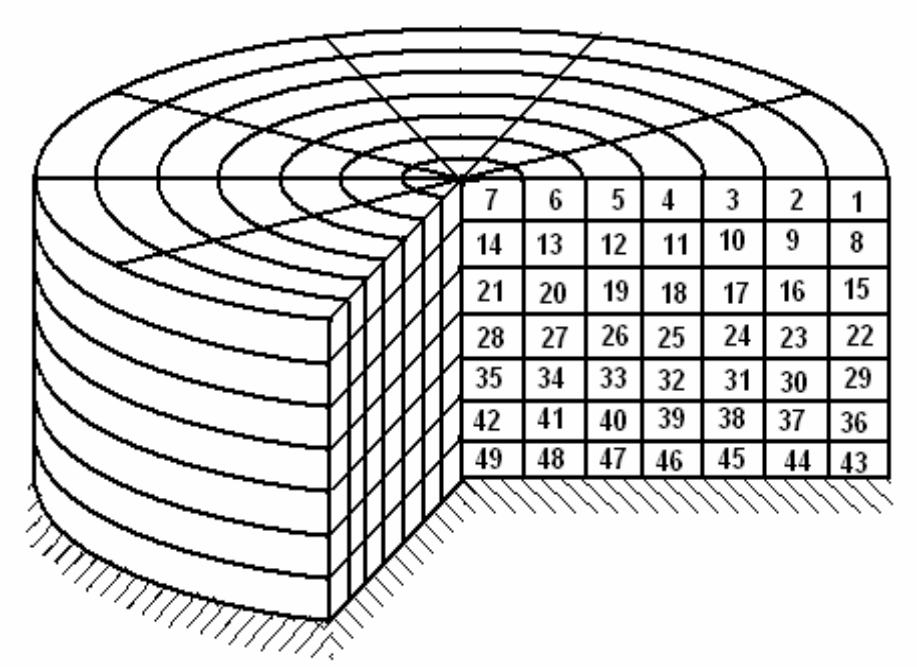

Figure 7.13: Element mesh of a three-dimensional axi-symmetric disc. The fluid can flow out at the top and in the radial direction under the axial applied load at the top.

Therefore, equations (7.16) and (6.39) can be rewritten as

$$\begin{aligned} \sigma_a &= \Delta_z + D_z\dot{\lambda}_z - u \\ 0 &= \Delta_r + D_r\dot{\lambda}_r - u \end{aligned} \tag{7.20}$$

where, $\Delta_z = \Phi_{33}\left(\lambda_z - \lambda_z^{-1}\right) + 2\Phi_{13}\left(\lambda_r - \lambda_r^{-1}\right) - \Delta\pi$,

and $\Delta_z = \left(\Phi_{11} + \Phi_{12}\right)\left(\lambda_r - \lambda_r^{-1}\right) + \Phi_{13}\left(\lambda_z - \lambda_z^{-1}\right) - \Delta\pi$.

In addition, the relationship between the stiffness coefficients in equation (6.12) yields,

$$\Phi_{11} = \frac{\nu_2^2 - 1}{\nu_1^2 - 1}\Phi_{33},\ \Phi_{12} = -\frac{\nu_2^2 + \nu_1}{\nu_1^2 - 1}\Phi_{33} \text{ and } \Phi_{11} = -\frac{\nu_2}{\nu_1 - 1}\Phi_{33}. \tag{7.21}$$

Substituting equation (7.19) into (6.37d), yields

$$\lambda = \lambda_z\lambda_r^2, \tag{7.22a}$$

or,

$$\frac{\dot{\lambda}}{\lambda} = \frac{\dot{\lambda}_z}{\lambda_z} + 2\frac{\dot{\lambda}_r}{\lambda_r}. \tag{7.22b}$$

Furthermore, within each layer,

$$\frac{\partial\lambda_z}{\partial r} = 0. \tag{7.23}$$

7.5.2 Permeability distribution

Under constant axial load with radial matrix deformation (unconfined) and assuming axial symmetry and planar isotropy, equation (6.43) can be written as

$$\frac{\partial K_r}{\partial\lambda} = -\mu_z\frac{\partial^2 K_r}{\partial z^2} \text{ and } \frac{\partial K_z}{\partial\lambda} = -\mu_z\frac{\partial^2 K_z}{\partial z^2}. \tag{7.24}$$

Because the articular cartilage is the planar isotropic material as its structure discussed in Chapter 2, it is assumed that the permeability is independent on the radial displacement and that the initial and boundary conditions for the permeability variation for a given cartilage specimen are approximately in the simplest form at this study level, ie.

$$K_z(r,z,1) = \omega K_r(r,z,1) = a.z + b, \tag{7.25a}$$

$$K_z(r,0,\lambda) = \omega K_r(r,0,\lambda) = K_0 \text{ and } K_z(r,H,\lambda) = K_r(0,z,\lambda) = 0, \tag{7.25b}$$

where, a, b and ω are constants. It is noted that ω presents the ratio between the axial and radial coefficients of the permeability, which represents the anisotropic property of the outflow.

Equation (7.24) with the assumption of the conditions in (7.25a) and (7.25b) has the solution using the same method in Appendix A1

$$K_z(r,z,\lambda) = \omega K_r(r,z,\lambda) = K_0\left(1-\frac{z}{H}\right) + \sum_{n=1}^{\infty} A_n e^{\mu_z \frac{n^2\pi^2}{H^2}(\lambda-1)} \sin\left(\frac{n\pi}{H} z\right) \qquad (7.26)$$

where $A_n = \frac{2}{H}\int_0^H \left(az + b - K_0\left(1-\frac{z}{H}\right)\right)\sin\left(\frac{n\pi}{H} z\right)dz = \frac{-2}{n\pi}\left(K_0 - b + (aH+b)(-1)^n\right).$

This relationship for direction-dependent permeability is also a function of depth and deformation of the articular cartilage matrix. The equation is similar to the exponential function proposed previously (Mow et al, 1998) with respect to the dependence on deformation but differentiates itself by accounting for anisotropy and heterogeneity through depth and planar variation.

For axial symmetry, the permeability function in equation (7.26) is independent of the lateral or θ direction, so that the continuity equation (6.42) can now be written as,

$$\frac{1}{\lambda}\frac{\partial \lambda}{\partial t} = K_r\left(\frac{\partial^2 u}{\partial r^2} + \frac{1}{r}\frac{\partial u}{\partial r}\right) + \frac{\partial}{\partial z}\left(K_z \frac{\partial u}{\partial z}\right) \qquad (7.27)$$

The system of equations (7.15-7.27) and (5.15, 5.16) describes the model of the unconfined matrix when the fluid flows out from its surface and along the radial direction. This system of equation is numerically solved to predict the response of an axially symmetric cylindrical cartilage specimen.

In order to solve the developed equations, a numerical investigation was conducted using MATLAB to evaluate the stretch ratios, hydrostatic excess pore pressure, solid skeleton effective stress and swelling pressure. These analyses were carried out on a model of a cartilage matrix loaded via a porous metallic disc, so that there is fluid exudation through its surface, but non through the bottom of the matrix as shown in figures 7.13 and 7.14.

The model was discretized into discrete elements of M layers and N radial intervals (*N*=*M*=7) as shown on figures 7.13 and 7.14. The system of equations (7.15-7.27) was discretized to form an algebraic equation (see Appendix A4), ie.

$$\underrightarrow{u} = \underline{\underline{C}}^{-1}\underrightarrow{W} \qquad (7.28)$$

where, $\underrightarrow{u} = \left(u^1, u^2, ..., u^l, ..., u^{MN}\right)^T$ is a column vector that consists of unknown hydrostatic excess pore pressure parameters of all elements; $\underrightarrow{W}$ and $\underline{\underline{C}}$ are a column

vector and a square matrix of (M.NxM.N) dimensions respectively, which are defined in the appendix.

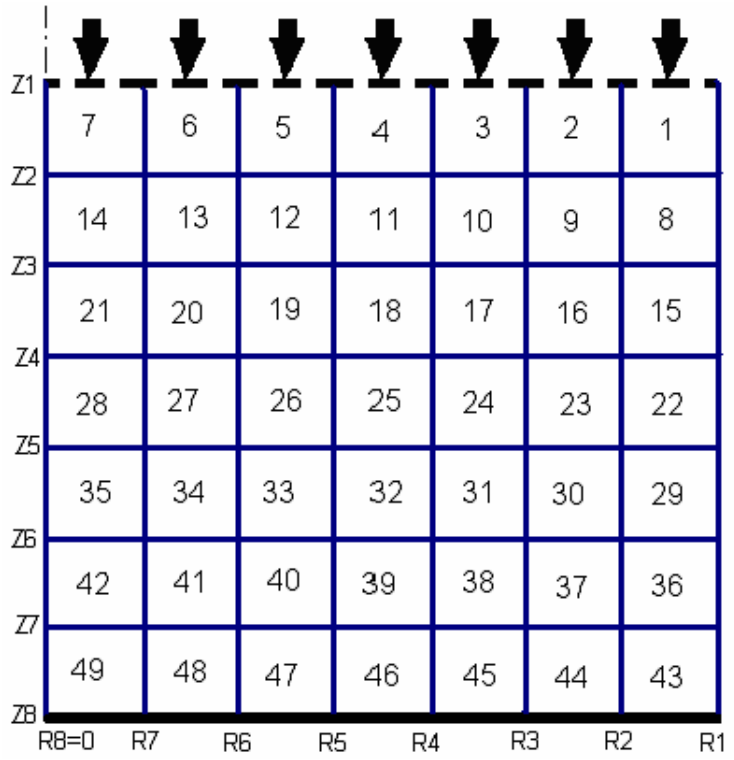

Figure 7.14: Mesh for the discrete elements of an axial symmetric disc. The central axis is at the left side. The right side is unconstrained. The porous plate is at the top. The bottom is bonded with a polish plate so that the fluid can flow out at the top and the right side under the axial applied load at the top.

The value of these hydrostatic excess pore pressures can be computed using equation (7.28) and used to evaluate the new stretch ratios, the new change in osmotic pressure and the new permeability parameters of the elements using the discretized forms of equations (7.27), (7.22a, b), (5.28) and (7.26) for the new time iteration. The system of discretized equations is solved using MATLAB (Appendix A5) to obtain the best fit responses and to predict the parameters.

7.5.3 Results and discussion

The equations of the generalized continuum model expressing the relationships between the stress-strain behaviour of the collagenous solid skeleton, strain, and hence, swelling-dependent permeability, and proteoglycan physico-chemistry have been developed in cylindrical coordinates for a three-dimensional unconfined disc of bovine cartilage. The

resulting system of equations in axially symmetric cylindrical coordinates has been solved using trial coefficients for fitting curves as shown in Figure 7.15 and 7.16. The coefficients as predicted in Table 7.6 were obtained from the fitting then used for the numerical analysis in this section to predict the consolidation responses (hydrostatic excess pore pressure and strain).

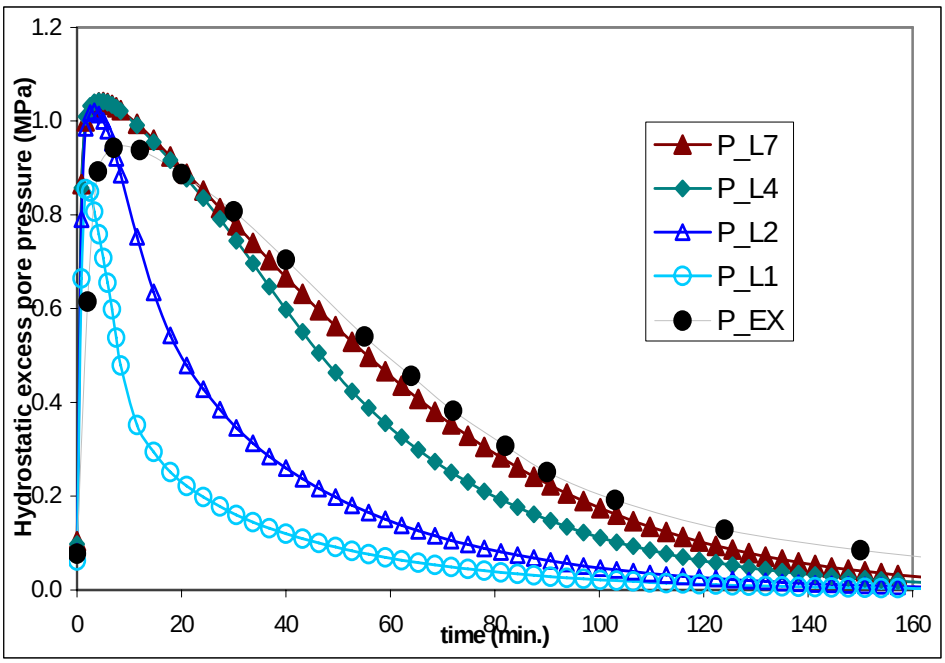

Figure 7.15: The prediction of the hydrostatic excess pore pressure at the depths of 0.1mm (P_L1), 0.3mm (P_L2), 0.7mm (P_L4) and 1.5mm (P_L7). These are compared to the experimental data (P_Ex) published by Oloyede et al. (1996).

Table 7.6: Parameters used for the analysis presented in figures 7.15 to 7.17

Applied load P=1.15 MPa; thickness H=1.2 mm; Radius R=10mm; time step dt=1 s		
	Axial coefficients	Radial coefficients
Comp. coefficients	$\Phi_{33} = 0.09e^{3.8\frac{z}{H}}$ MPa	
Poisson's ratios	$\nu_z = 0.1 + 0.25\dfrac{z}{H}$	$\nu_r = 0.5$
Drag coeff.	$D_z = 450$ MPaS	$D_r = D_\theta = 50$ MPaS
Permeability	$\mu_z = 3H^2$ $K_z(0,\lambda) = K_0 = 5\times10^{-17}$; $K_z(z,1) = f(z)$ $f(z) = 6.4\times10^{-13}z + K_0$ (m^4/NS)	$K_r(r,\lambda) = \dfrac{1}{10}K_z(z,\lambda)$ (m^4/NS)

The results from the computations using these coefficients in Table 7.7 are shown in Figures 7.15-7.17. Figure 7.15 shows the patterns of the time-dependent hydrostatic excess pore pressures at the different positions on the axis of the loaded cylindrical cartilage matrix. The curves show the same treads in that they rise to a maximum level then decay to zero after 3 hours, but are much different in magnitude. The maximum level of the excess pore pressure at the bottom layer (curve P_L7) approaches 80% of the applied load. This level is approximately 5% higher than that previously obtained for the one-dimensional case. These hydrostatic excess pore pressures at the bottom layer agree well with the published generalized three-dimensional experimental data of Oloyede and Broom (1996) for the whole consolidation process.

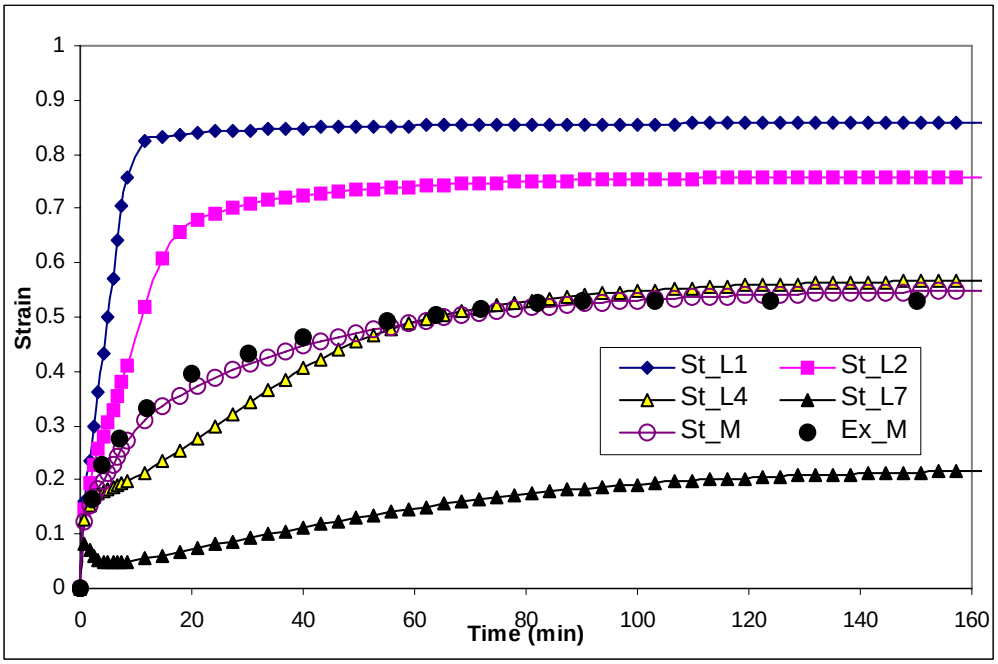

Figure 7.16: The prediction of the strain at the depths of 0.1mm (St_L1), 0.3mm (St_L2), 0.7mm (St_L4) and 1.5mm (St_L7) and total matrix strain (St_M). This total matrix strain is compared to the published experimental data (Ex_M) (Oloyede et al., 1996).

Figure 7.16 presents the results of total axial matrix strain and the strains of the layers. This figure shows that the deformations of the layers are different to each other and the patterns of strains of the layers that are close to the surface have the greatest gradient and its equilibrium level is up to 90% of the surface thickness. These patterns can be explained by possible softening at the superficial layer resulting in fast fluid outflow from the layer. It also shows that the layers close to the bottom are the first to deform compression under load, followed by swelling and then continuous compressive

deformation right up to the equilibrium level. This can be explained as a possible consequence of internal fluid diffusion within the layers. Overall the predicted total matrix strain agrees well with the published experimental data of Oloyede and Broom (1996).

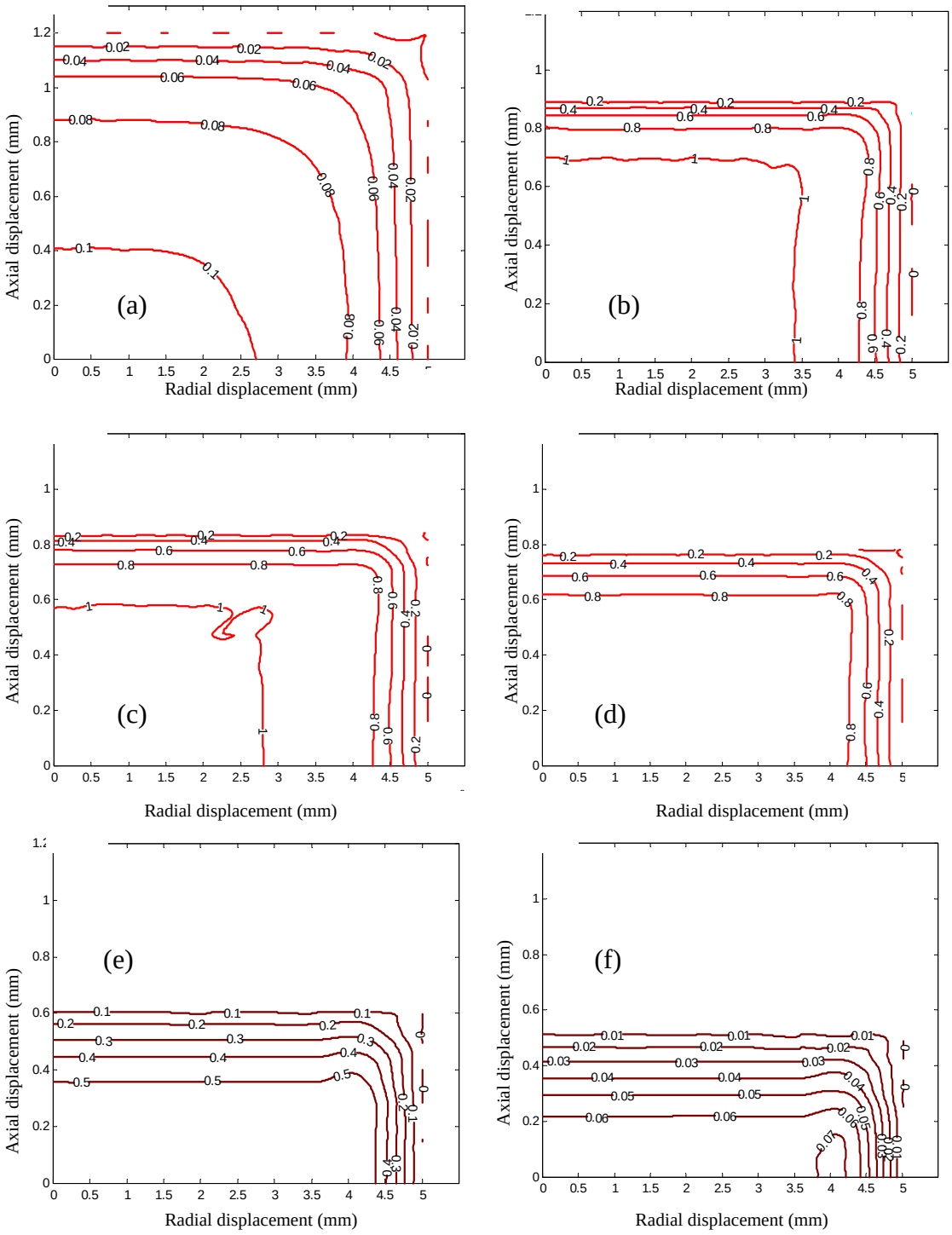

Figure 7.17: The contour plots of the predicted hydrostatic excess pore pressures (MPa) at time t=0 (a), t=400s (b), t=600s (c), t=1000s (d), t=3000s (e) and t=8000s (f) against the predicted radial and axial positions from the numerical solution.

The transient pattern of the hydrostatic excess pore pressure (Figure 7.17) and the time to the end of consolidation when the applied load is transferred fully to the solid skeleton and the hydrostatic excess pore pressure is zero provides a picture of how the matrix of articular cartilage responds to load.

The figure shows that there is negligible deformation in the radial direction compared to that observed in the axial direction of the model, thereby demonstrating that the unconfined cartilage matrix behaves similarly to the confined matrix with respect to the patterns of their hydrostatic excess pore pressure. It also revealed that swelling is negligible in the radial direction under the axial static load. In addition, the value of the hydrostatic excess pore pressure changes with time with its maximum occurring at the centre of the bottom layer. It is also noted that the distributions of hydrostatic excess pore pressures in figures 7.17c and 7.17f have different patterns when compared to the others (figures a, b, d and e). In general, the predictions present rigorous biomechanical insight into what occurs transiently within the loaded cartilage matrix. Although the patterns and trends of the important parameters such as the hydrostatic excess pore pressure, strain and osmotic pressure have been predicted in this study, experimental investigation to determine the confident level of the parameters at the different positions and the accurate values of the coefficients used for iterations of the solution to the equations developed for the cartilage as the anisotropic and heterogeneous material will be required. As this is out of the scope of this thesis, it has been left for future studies.

7.6 Conclusion

Both one-dimensional and two or three-dimensional continuum models of articular cartilage accounting for the behaviours of its fluid, solid, and swelling components and their interaction have been applied to predict the biomechanical responses of the tissue. Numerical analysis was used extensively to solve the resulting system of equations to predict various aspects of cartilage load-carriage mechanism in three separate case studies. The models were used to determine the parameters of deformation, such as permeability, stiffness and osmotic pressure for both normal intact and degenerate/damaged cartilage. Most importantly representative models that can account for the most observable load-carriage characteristics of articular cartilage, including its

swelling, have been developed and shown to produce results that accord well with experimental data. In consequence, the results from analysis in this chapter demonstrate that the new model presented in Chapter 6 is capable of analyzing the biomechanical properties of normal intact cartilage matrix and the effects of the laceration on these responses.

Chapter 8: Conclusion and future research.

8.1 Conclusion

This thesis has presented models of articular cartilage including one-dimensional analogues and fundamental mathematical versions within the framework of the principle of mechanical consolidation. The approach has been mostly phenomenological since it is believed by the author that this methodology provides the best means of capturing the structural and deformational characteristics of this three-component biological gel. The model is mostly restricted to the prediction of the matrices' behaviour to loads at sub-impact velocities. Both experimental and predicted results, including comparisons between them, have been presented leading to insightful information relating to the applicability of the consolidation theory to the analysis/modelling of the normal and altered articular cartilage.

The models that have been presented include parameters, which vary according to position, deformation, time and tissue condition, thereby making them close to realistic and reliable. They improve on the earlier works of the authors by extending the mathematical modelling of cartilage to include:

1. Dependence of the deformation-dependent coefficient of permeability on position with consequence for representing degenerate articular cartilage.

2. Dependence of the osmotic pressure on the deformation of the matrix at any instance of deformation.

3. Hyperelastic formulation for the solid skeletal structure including both anisotropy and heterogeneity of this component.

4. An explicit parameter for the drag or time lag encounter in the development of the hydrostatic excess pore pressure, thereby ensuring the capability to capture more accurately the early behaviour of the tissue in the incipient stages of loading.

5. The capability to analyse hypothetical layers of the tissue and explicitly determine how each layer from the superficial to the calcified zone influence the response of the tissue to loading at sub-impact velocities.

6. Because of the ability to distinguish between layers there is now a possibility to model explicitly surface laceration or fibrillation as demonstrated by a case study in chapters 5 and 7.

In summary, this thesis has presented the application of the consolidation theory approach to the understanding of the load-induced behaviour of articular cartilage. It has also provided more insight into the position-dependent internal load-carriage mechanisms through the heterogeneous layers and the anisotropic characteristic of either confined or unconfined matrix, thereby leads to further understanding of the osteoarthritic condition which adversely affects cartilage structure and function in the future.

8.2 Future research

The solutions to the systems of equations developed have been carried out numerically to demonstrate their ability to capture articular cartilage behaviour under load. This demonstration presents the opportunity for finite element analysis discretization of these equations and it is suggested that a portion of any future work should be denoted to this.

Detailed experimental work is required to obtain data at different depths, which will improve the parameters of analysis and which will reconcile any disparity between the iterated data for these parameter numerical analysis and measured values.

Application of the models both in the one-dimensional and generalized forms to other situations of articular cartilage degeneration is required in order to ascertain their universal applicability or otherwise to the prediction of impaired articular cartilage’s response to load.

REFERENCES

1. www.rheumatology.org/press/am2002/pr10.asp

2. www.niams.nih.gov/hi/topics/arthritis/artrheu.htm

3. www.arthritis.ca/toolbox/headline%20news/news%20releases/canada%20in%20motion/default.asp?s=1

4. www.statistics.gov.uk/lib

5. www.arc.org.uk/about_arth/bigpic.htm#4

6. www.arthritis.org.au/found3.html

7. www.uoguelph.ca/zoology

[Afoke et al., 1987] Afoke N.Y.P., Byers P.D. and Hutton W.C., 1987. Contact pressures in the human hip joint. Journal of Bone and Joint Surgery, B69: 536-541.

[Akizuki et al., 1986] Akizuki S., Mow V.C., Muller F., Pita J.C., Howell D.S. and Manicourt D.H., 1986. Tensile properties of human knee joint cartilage: I. Influence of ionic conditions, weight bearing, and fibrillation on the tensile modulus. Journal of Orthopaedics Research, 4:379-392.

[Anderson et al., 1990] Anderson D.D., Brown T.D., Yang K.H. and Radin E.L., 1990. A dynamic finite element analysis of impulsive loading of the extension-splinted rabbit knee. Journal of Biomechanical Engineering, 112:119-128.

[Anderson et al., 1993] Anderson D.D., Brown T.D. and Radin E.L., 1993. The influence of basal cartilage calcification on dynamic juxta articular stress transmission. Clinical Orthopaedics, 286:298-307.

[Armstrong and Mow, 1982] Armstrong C.G. and Mow V.C., 1982. Variations in the intrinsic mechanical properties of human articular cartilage with age, degeneration, and water content. Journal of Bone and Joint Surgery, vol. 64-A, 88-94.

[Armstrong et al., 1985] Armstrong C., Mow V. and Wirth C., 1985. Biomechanics of

impact-induced microdamage to articular cartilage — A possible genesis for chondromalacia patella. In: Finerman G. (Eds.) AAOS Symposium on Sports Medicine: The Knee. (pp. 70-84) St. Louis: C.V. Mosby Co.

[Ateshian, 1997] Ateshian G.A., 1997. A theoretical formulation for boundary friction in articular cartilage. Journal of Biomechanical Engineering ASME, 119:81-86.

[Ateshian and Wang, 1995] Ateshian G.A. and Wang H., 1995. A theoretical solution for the frictionless rolling contact of cylindrical biphasic articular cartilage layers. Journal of Biomechanics, 28:1341-1355.

[Ateshian et al., 1994] Ateshian G.A., Lai W.M., Zhu W.B. and Mow V.C., 1994. An asymptotic solution for the contact of two biphasic cartilage layers. Journal of Biomechanics, vol. 27:11:1347-1360.

[Ateshian et al., 1997] Ateshian, G.A., Warden, W.H., Kim, J.J., Grelsamer, R.P., Mow, V.C., 1997. Finite deformation biphasic material properties of bovine articular cartilage from confined compression experiments. Journal of Biomechanics 30, 1157–64.

[Atkinson and Haut, 1995] Atkinson P.J. and Haut R.C., 1995. Subfracture insult to the human cadaver patellofemoral joint produces occult injury. Journal of Orthopaedic Research, 13:936-944.

[Bachrach et al., 1998] Bachrach N.M., Mow V.C. and Guilak F., 1998. Incompressibility of the solid matrix of articular cartilage under high hydrostatic pressures. Journal of Biomechanics, 31:445-451.

[Barocas and Tranquillo, 1997] Barocas V.H. and Tranquillo R.T., 1997. An anisotropic biphasic theory of tissue-equivalent mechanics: the interplay among cell traction, fibrillar network deformation, fibril alignment, and cell contact guidance. Journal of Biomechanical Engineering, 119:2:137-145.

[Basser et al., 1998] Basser, P.J., Schneiderman, R., Bank, R.A., Wachtel, E., and Maroudas, A., 1998. Mechanical properties of the collagen network in human articular cartilage as measured by osmotic stress technique. Archieves of Biochemistry and Biophysics. Vol. 351, 2, pp. 207-219.

[Bentley and Minas, 2000] Bentley G. and Minas T., 2000. Science, medicine, and the future: Treating joint damage in young people. BMJ, 320: 1585-1588.

[Berkenblit et al., 1994] Berkenblit S.I., Frank E.H., Salant E.P. and Grodzinsky A.J., 1994. Non destructive detection of cartilage degeneration using electromechanical surface spectroscopy. Journal of Biomechanical Engineering, vol. 116, 384-392.

[Biot, 1941] Biot, M.A., 1941. General theory of three-dimensional consolidation. Journal of Applied Physics, vol. 12, pp 155-164.

[Biot and Willis, 1957] Biot, M.A. and Willis, D.G., 1957. The elastic coefficients of the theory of consolidation, Journal of Applied Physics, vol. 12, p. 155-164.

[Bonassar et al., 1996] Bonassar L.J., Stinn J.L., Paguio C.G., Frank E.H., Poole A.R., Sandy J.D. and Grodzinsky A.J., 1996. Activation and inhibition of endogenous matrix metalloproteinases in articular cartilage-effects on composition and biophysical properties. Archives of Biochemistry and Biophysics, vol. 333, 359-367.

[Broom, 1982] Broom N. D., 1982. Abnormal softening in articular cartilage. Arthritis and Rheumatism, 25:1209-1216.

[Broom, 1984] Broom N.D., 1984. The altered biomechanical state of human femoral head osteoarthritic articular cartilage. Arthritis and Rheumatism, 27:1028-1039.

[Broom, 1986] Broom, N.D., 1986. Structural consequences of traumatising articular cartilage Annals of the Rheumatic Diseases 45, 225–234.

[Broom et al., 2001] Broom, N.D, Chen, M.H and Hardy, A., 2001. The degeneration-

based hypothesis for interpreting fibrillar changes in the osteoarthritic cartilage matrix. Journal of Anatomy, vol. 199, pp. 683-698

[Broom and Marra, 1985] Broom, N.D. and Marra, D.L., 1985. New structure concepts of articular cartilage demonstrated with a physical model**.** Connective Tissue Research, vol. 14, 1-8.

[Broom and Marra, 1986] Broom, N.D. and Marra, D.L., 1986. Ultrastructural evidence for fibril-to-fibril associations in articular cartilage and their functional implication, Journal of Anatomy, vol. 146, pp. 185-200.

[Broom and Oloyede, 1992] Broom, N. D. and Oloyede, A., 1992. Experimental determination of the subchondral stress-reducing role of articular cartilage under static and dynamic compression, Clin. Biomech., vol.8, pp.102-108.

[Broom and Oloyede, 1998] Broom N. D. and Oloyede A., 1998. The importance of physico-chemical swelling in cartilage illustrated with a model hydrogel system. Biomaterials, vol.19, pp.1179-1188.

[Broom and Silyn – Roberts, 1989] Broom, N.D. and Silyn - roberts, H., 1989. The three -dimensional 'knit' of collagen fibrils in articular cartilage. Connective Tissue Research, vol. 23, 261 -277.

[Broom and Silyn – Roberts, 1990] Broom, N.D. and Silyn - roberts, H., 1990. Cohesive strength of cartilage is determined largely by collagen - collagen and not collagen - protoeglycan interactions. Arthritis and Rheumatism, vol. 33, 1512 - 1517.

[Brown and Singermann, 1986] Brown, T.D. and Singermann, R.J., 1986. Experimental determination of the linear biphasic constituent of human fetal proximal femoral chondroepiphysis. Journal of Biomechanics, vol. 19, 597-605.

[Buckwalter and Mankin, 1997] Buckwalter J.A. and Mankin H.J., 1997. Articular cartilage Part II: degeneration and osteoarthrosis, repair, regeneration, and

transplantation. Journal of Bone and Joint Surgery, 79-A: 612-632.

[Burton-Wurster et al., 1993] Burton-Wurster, N., Vernier-Singer, M., Farquhar, T., Lust, G., 1993. Effect of compressive loading and unloading on the synthesis of total protein proteoglycan, and bronectin by canine cartilage explants. Journal of Orthopaedic Research, vol. 11, 717-29.

[Buschmann and Grodzinsky, 1995] Buschmann M.D. and Grodzinsky A.J., 1995. A molecular model of proteoglycan-associated electrostatic forces in cartilage mechanics. Journal of Biomechanical Engineering, 117:179-192.

[Chen and Broom, 1999] Chen, MH. And Broom, N.D., 1999. Concerning ultrastructural origin of large-scale swelling in articular cartilage. Journal of Anatomy, vol. 194, pp. 445-461.

[Chen et al., 2001] Chen A.C., Bae W.C., Schinagl R.M. and Sah, R.L., 2001. Depth- and strain-dependent mechanical and electromechanical properties of full-thickness bovine articular cartilage in confined compression. Journal of Biomechanics, vol. 34, pp.1-12.

[Cohen et al., 1993] Cohen, B., Gardner, T.R., Ateshian, G.A., 1993. The influence of transverse isotropy on cartilage indentation behavior — A study of the human humeral head. In: Transactions Orthopaedic Research Society. Orthopaedic Research Society, Chicago, IL, pp. 185.

[Disilvestro and Suh, 2001] Disilvestro M.R. and Suh J.-K.F., 2001. A cross-validation of the biphasic poroviscoelastic model of articular cartilage in unconfined compression, indentation, and confined compression. Journal of Biomechanics, vol. 34, 519-525.

[Donzelli and Spilker, 1998] Donzelli P.S. and Spilker R.L., 1998. A contact finite element formulation for biological soft hydrated tissues. Comp Methods in Appllied Mechanical Engineering, 153:63-79.

[Dumont et al., 1999] Dumont, J., Ionescu, M., Reiner, A., Poole, A.R., Tran-Khanh, N., Hoemann, C.D., McKee, M.D., Buschmann, M.D., 1999. Mature full-thickness articular cartilage explants attached to bone are physiologically stable over long-term culture in serum-free media. Connective Tissue Research 40, 259–72.

[Edwards, 1976] Edwards, S., 1976. The theory of rubber elasticity. Proc. R. Soc. Lond. A. 351, pp.397-406.

[Eggli et al., 1988] Eggli P.S., Hunziker E.B. and Schenk R.K., 1988. Quantitation of structural features characterizing weight- and less-weight-bearing regions in articular cartilage: a stereological analysis of medical femoral condyles in young adult rabbits. Anatomical Record, vol. 222, 217-227.

[Eisenberg and Grodzinsky, 1985] Eisenberg S.R. and Grodzinsky A.J, 1985. Swelling of articular cartilage and other connective tissues: Electromechanochemical forces. J. Orthopaedic Research, vol. 3, pp. 148-159.

[Elmore et al., 1963] Elmore, S.M., Sokoloff,L., Norris,G. & Carmeci,P., 1963. Nature of 'imperfect' elasticity of articular cartilage, Journal of Applied Physics, vol. 18, 393-396.

[Fortin et al., 2000] Fortin M., Soulhat J., Shirazi-Adl A., Hunziker E.B. and Buschmann M.D., 2000. Unconfined compression of articular cartilage: nonlinear behavior and comparison with a fibril-reinforced biphasic model. J. Biomechanical Engineering. V.122, pp.189-195.

[Frank et al., 1987] Frank E.H., Grodzinsky A.J., Koob T.J. and Eyre D.R., 1987. Streaming potentials: a sensitive index of enzymatic degradation in articular cartilage. Journal of Orthopaedic Research, vol. 5, 497-508.

[Fosang and Hardingham, 1996] Fosang, A.J. and Hardingham, T.E., 1996. Matrix proteoglycans. In: Comper, W.D. (Ed.), Extracellular Matrix, Vol. 2. Harwood Academic Publishers, Australia, pp. 200-229.

[Garcia et al., 1996] Garcia A.M., Frank E.H., Grimsaw P.E., and Grodzinsky A.J, 1996. Contributions of fluid fonvection and electrical migration to transport in cartilage: Relevance to Loading, 1996. Archives of Biochemistry and Biophysics, vol. 333, no. 2, pp. 317-325.

[Glenister, 1976] Glenister, T.W., 1976. An embryological view of cartilage, Journal of Anatomy, vol. 122, 323-332.

[Gore et al., 1983] Gore D.M., Higginson G.R. and Minns R.J., 1983. Compliance of articular cartilage and its variation through the thickness. Physics in Medicine and Biology, 28:233-247.

[Grodzinsky, 1983] Grodzinsky A.J., 1983. Electromechanical and physicochemical properties of connective tissue. CRC Critical Reviews in Bioengineering 1983, vol. 9, 133-199.

[Guilak et al., 1995] Guilak F., Ratcliffe A. and Mow V.C., 1995. Chondrocyte deformation and local tissue strain in articular cartilage: a confocal microscopy study. Journal of Orthopaedic Research 1995, 13:410-421.

[Harrigan, 1987] Harrigan, T.P., 1987. Cartilage is poroelastic but not bi-phasic. Journal of Biomechanics, vol. 20, 827-829.

[Harrigan and Mann, 1987] Harrigan, T.P. and Mann, R.W., 1987. State variables for modelling physical aspects of articular cartilage. Int. Journal of Solids and Structures, vol. 23. 9, 1205-1218.

[Hayes and Bodine, 1978] Hayes W.C. and Bodine A.J., 1978. Flow-independent viscoelastic properties of articular cartilage matrix. J. Biomechanics. Vol. 11, pp. 407-419.

[Hayes et al., 1972] Hayes W.C., Keer L.M., Herrmann G. and Mockros L.F., 1972. A mathematical analysis for indentation tests of articular cartilage. Journal of

Biomechanics, vol. 5, 541-551.

[Haut et al., 1995] Haut R.C., Ide T.M. and Decamp C.E., 1995. Mechanical responses of the rabbit patello-femoral joint to blunt impact. Journal of Biomechanical Engineering, vol. 117, 402-408.

[Higginson et al., 1976] Higginson G.R., Litchfield M.R., and Snaith J., 1976. Load-displacement- time characteristics of articular cartilage. Int. Journal of Mechanical Science, vol. 18, 481-486.

[Higginson and Snaith, 1979] Higginson G.R. and Snaith J.E., 1979. The mechanical stiffness of articular cartilage in confined oscillating compression. Journal of Mechanical Engineering., vol. 8, no. 1, pp. 11-14.

[Hunziker, 1992] Hunziker E.B., 1992. Articular cartilage structure in humans and experimental animals. In: Kuettner K.E., Schleyerbach R., Peyron J.G. and Hascall V.C. (Eds.) Articular Cartilage and Osteoarthritis. pp.183-199. New York: Raven Press

[Jacob, 1967] Jacob B., 1967. Dynamics of fluid in porous media. American Elsevier Publishing Company, New York.

[Johnson and Wilson, 1967] Johnson J.A. and Wilson T.A., 1967. Osmotic volume changes induced by a permeable solute. Journal of Theoretical Biology, vol. 17, pp. 304-311.

[Jones et al., 1982] Jones, I.L., Klamfeldt, A., Sanstrom, T., 1982. The effect of continuous mechanical pressure upon the turnover of articular cartilage proteoglycans in vitro. Clinical Orthopaedics, vol. 165, 283-289.

[Jurvelin et al., 1995] Jurvelin J.S., Räsänen T., Kolmonen P. and Lyyra T., 1995. Comparison of optical, needle probe and ultrasonic techniques for the measurement of articular cartilage thickness. Journal of Biomechanics, 28:231-235.

[Jurvelin et al., 1997] Jurvelin J.S., Buschmann M.D. and Hunziker E.B., 1997.

Optical and mechanical determination of Poisson's ratio of adult bovine humeral articular cartilage. Journal of Biomechanics 1997, 30:235-241.

[Kelly and O'Connor, 1996] Kelly P.A. and O'Connor J.J., 1996. Transmission of rapidly applied loads through articular cartilage. Part 1: Uncracked Cartilage. Int. Journal of Mechanical Engineering, vol. 210, pp. 27-37.

[Kempson, 1979] Kempson, G.E., 1979. Mechaical properties of articular cartilage. In: Adult Articular Cartilage, edited by M.A.R. Freeman: Pitman Medical, London, 333-414.

[Kempson et al., 1976] Kempson, G.E., Tuke M.A., Dingle J.T., Barrett A.J. and Horsefield P.H., 1976. The effects of proteolytic enzymes on the mechanical properties of adult human articular cartilage. Biochimica Biophysica Acta, vol. 428, 741.

[Kezdi,, 1979] Kezdi, A., 1979. Soil Physics: Selected Topics. Elsevier Scientific Publishing company, New York, Chap. 4.

[Khalsa and Eisenberg, 1997] Khalsa P. and Eisenberg S.R., 1997. Compressive behavior of articular cartilage is not completely explained by proteoglycan osmotic pressure. Journal of Biomechanics, 30:6:589-594.

[Klausner, 1991] Klausner, Y., 1991. Fundamentals of Continuum Mechanics of Soils. Springer-Verlag. London.

[Lai and Mow, 1980] Lai W.M. and Mow V.C., 1980. Drag induced compression of articular cartilage during a permeation experiment. Biorheology, vol. 17, 111-123.[Medline]

[Lai et al., 1981] Lai W.M., Mow V.C. and Roth V., 1981. Effects of nonlinear strain-dependent permeability and rate of compression on the stress behavior of articular cartilage. Journal of Biomechanical Engineering, vol. 103, 61-66.

[Lai et al., 1991] Lai W.M., Hou J.S., Mow V.C., 1991. A triphasic theory for the swelling and deformation behaviors of articular cartilage. Journal of Biomechanical. Engineering, Vol. 113, pp. 245-258.

[Lanir, 1987 (a)] Lanir, Y., 1987. Biorheology and fluid flux in swelling tissues I. Bicomponent theory for small deformations, including concentration effects. Biorheology, vol. 23, 173-188.

[Lanir, 1987 (b)] Lanir, Y., 1987. Biorheology and fluid flux in swelling tissues. II Analysis of unconfined compressive response of transversely isotropic cartilage disc, Biorheology, vol. 24, pp.189-205.

[Li et al., 1999 (a)] Li L.P., Buschmann M.D. and Shirazi-Adl A., 1999. A fibril reinforced poroelastic model of articular cartilage including depth dependent material properties. Transactions of the ASME BED, vol. 43, 213-214.

[Li et al., 1999 (b)] Li L.P., Cederbaum G. and Schulgasser K., 1999. A finite element model for poroelastic beams with axial diffusion. Computers and Structures, vol. 73, 595-608.

[Li et al., 1999 (c)] Li L.P., Soulhat J., Buschmann M.D. and Shirazi-Adl A., 1999. Nonlinear analysis of cartilage in unconfined ramp compression using a fibril reinforced poroelastic model. Clinical Biomechanics, vol. 14, 673-682.

[Li et al., 2000] Li L.P., Buschmann M.D. and Shirazi-Adl A., 2000. A fibril reinforced nonhomogeneous poroelastic model for articular cartilage: Inhomogeneous Response in Unconfined Compression. J. Biomechanics, vol. 33, pp. 1533-1541.

[Lipshitz et al., 1975] Lipshitz H., Etheridge R. and Glimcher M.J., 1975. In vitro wear of articular cartilage. Journal of Bone and Joint Surgery, vol. 57A, 527-537.

[Lipshitz et al., 1976] Lipshitz H., Etheridge R. and Glimcher M.J., 1976. Changes in hexosamine content and swelling ratio of articular cartilage as a function of depth from

the surface. Journal of Bone and Joint Surgery 1976, vol. 58A, 1149-1153.

[MacConnail, 1951] MacConnail M.A., 1951. The movement of bones and joints 4: the mechanical structure of articulating cartilage. Journal of Bone and Joint Surgery, B33:251-257.

[McCormick et al., 1995] McCormick A, Fleming D, Charlton J, 1995. Morbidity statistics from general practice. 4th national study 1991-1992. London, HMSO (1995)

[Macirowski et al., 1994] Macirowski T, Tepic S, Mann RW, 1994. Cartilage stresses in the human hip joint. Journal of Biomechanical Engineering, vol. 116, 10-8.

[Mak, 1986] Mak A. F., 1986. The apparent viscoelastic behavior of articular cartilage-the contributions from the intrinsic matrix viscoelasticity and interstitial fluid flows. Journal of Biomechanical Engineering, vol. 108, pp. 123-129.

[Maroudas, 1975] Maroudas A., 1975. Biophysical chemistry of cartilaginous tissues with special reference to solute and fluid transport. Biorheology 1975, 12:233-248.[Medline]

[Malvern, 1969] Malvern L.E., 1969. Introduction to the Mechanics of a Continuous Medium. (1969) Englewood Cliffs, NJ: Prentice-Hall

[Mansour and Mow,1976] Mansour, J.M. and Mow, V.C. ,1976. The permeability of Articular Cartilage under compressive strain and at high pressures. Journal of Bone and Joint Surgery, vol. 58-A4, pp.509-516.

[Maroudas and Bullough, 1968] Maroudas A. and Bullough P., 1968. Permeability of articular cartilage. Nature, 219:1260-1261.[Medline]

[Maroudas et al., 1987] Maroudas A., Mizrahi J., BenHaim E. and Ziv I., 1987. Swelling pressure in cartilage. Advances in Microcirculation, vol.13, 203-212.

[Maroudas, 1968] Maroudas A., 1968. Physicochemical properties of cartilage in the

light of ion exchange theory. Biophysics Journal, vol.8, 575-595.

[Maroudas, 1979] Maroudas A., 1979. Physico-chemical properties of articular cartilage. In: Freeman M.A.R.(Eds.) Adult Articular Cartilage. pp. 215-290. Tunbridge Wells, England: Pitman Medical.

[Maroudas, 1985] Maroudas, A., 1985. The function of articular cartilage in terms of its structure in a healthy joint. How is it altered in the degenerative joint? In: Verbruggen, G., Veys, E.M. (Eds.), Degenerative Joints, Vol. 2. Elsevier Science Publishers B.V. (Biomedical Division), Amsterdam, pp. 99-115.

[Maroudas and Bannon, 1981] Maroudas A. and Bannon C., 1981 Measurement of swelling pressure in cartilage and comparison with the osmotic pressure of constituent proteoglycans. Biorheology, vol. 18, 619-632.[Medline]

[Maroudas et al., 1969] Maroudas A., Muir H. and Wingham J., 1969. The correlation of fixed negative charge with glycosaminoglycan content of human articular cartilage. Biochimica et Biophysica Acta, vol. 177, 492-500.

[McCutchen C.W., 1962] McCutchen C.W., 1962. The frictional properties of animal joints. Wear 1962, 5:1-17.

[McCutchen, 1975] McCutchen C.W., 1975. An approximate equation for weeping lubrication, solved with an electrical analogue. Annals Rheumatic Diseases. Vol. 34 (supplement), pp. 85-90.

[McCutchen, 1980] McCutchen C.W., 1980. The joint and synovial fluid. Academic Press, New York), pp. 438-477.

[McCutchen, 1982] McCutchen C.W., 1982. Cartilage is poroelastic, not viscoelastic (including an exact theorem about strain energy & viscous loss, and an order of magnitude relation for equilibrium time). J. Biomechanics. Vol. 15 (4), pp. 325-327.

[McCutchen, 1998] McCutchen C.W., 1998. Consolidation theory derived without invoking porosity. Int. Journal of Solids Structures, vol. 35, nos. 1-2, pp. 69-81.

[Mizrahi et al., 1986] Mizrahi J., Maroudas A., Lanir Y., Ziv I. and Webber T.J., 1986. The "instantaneous" deformation of cartilage: effects of collagen fiber orientation and osmotic stress. Biorheology, vol. 23, 311-330.[Medline]

[Mow and Ratcliffe,1997] Mow V.C. and Ratcliffe A.,1997. Structure and function of articular cartilage and meniscus. In: Mow V.C. and Hayes W.C. (Eds.) Basic Orthopaedic Biomechanics. (pp. 113-178) New York: Raven Press

[Mow and Ateshian, 1997] Mow, V.C. and Ateshian, G.A., 1997. Lubrication and wear of diarthrodial joints. In: Mow, V.C., Hayes, W.C. (Eds.), Basic Orthopaedic Biomechanics, Ch.8. LippincottRaven Publication, Philadelphia.

[Mow et al., 1980] Mow, V.C., Kuei, S.C., Lai, W.M., and Armstrong, C.G., 1980. Biphasic creep and stress relaxation of articular cartilage in compression: theory and experiments. J. Biomechanics, vol. 102, 73-84.

[Mow et al., 1987] Mow, V.C., Kwan, M.K., Lai, W.M., and Holmes, M.H., 1987. A finite deformation theory for nonlinearly permeable soft hydrated biological tissues. In: Frontiers in Biomechanics, edited by G.W. Schmid - Schoenbien, S.L.Y. Woo and B. W.Zweifach, Springer Verlag, New York, 153-179.

[Mow et al., 1989] Mow V.C., Gibbs M.C., Lai W.M., Zhu W.B. and Athanasiou K.A., 1989. Biphasic indentation of articular cartilage: II A numerical algorithm and an experimental study. Journal of Biomechanics, 22:853-861.

[Mow et al., 1990] Mow V.C., Hou J.S., Owens J.M. and Ratcliffe A., 1990. Biphasic and quasilinear viscoelastic theories for hydrated soft tissue. In: Mow V.C., Ratcliffe A. and Woo S.L-Y. (Eds.) Biomechanics of Diarthrodial Joints. (pp. 215-260) New York: Springer-Verlag.

[Mow et al., 1993] Mow,VC, Ateshian, GA and Spilker, RL., 1993. Biomechanics of Diarthrodial Joints: A review of twenty years of progress. J. Biomechanical Engineering, vol. 115, pp460-467.

[Mukherjee and Wayne, 1998] Mukherjee N. and Wayne J.S., 1998. Load sharing between solid and fluid phases in articular cartilage: I- experimental determination of in situ mechanical conditions in a porcine knee. Transactions of the ASME, vol. 120, pp.614-619.

[Myers and Mow, 1983] Myers E.R. and Mow, V.C., 1983. Biomechanics of cartilage and its response to biomechanical stimuli. In: Cartilage vol.1 Structure, Function, and Biochemistry, edited by B.R.Hall, 318-322. New York: Academic Press.

[Myers et al., 1995] Myers S.L., Dines K., Brandt D.A., Brandt K.D. and Albrecht M.E., 1995. Experimental assessment by high frequency ultrasound of articular cartilage thickness and osteoarthritic changes. Journal of Rheumatology, vol. 22, 109-116.

[Newberry et al., 1997] Newberry W.N., Zukosky D.K. and Haut R.C., 1997. Subfracture insult to a knee joint causes alterations in the bone and in the functional stiffness of overlying cartilage. Journal of Orthopedic Research, 15:450-455.

[Nguyen and Oloyede, 2001] Nguyen, T. and Oloyede, A., 2001. Predictive rheological models for the consolidation behaviour of articular cartilage under static loading. Proc Instn Mechanical Engineering, vol. 215 Part H, pp 565-577.

[Nguyen and Oloyede, 2002] Nguyen, T. and Oloyede, A., 2002. Continuum modelling of the large strain behaviour of the constrained articular cartilage. Proceedings of 5th Biennial Engineering Mathematics and Applications Conference, pp 151-156.

[Ogston, 1970] Ogston A.G., 1970. The biological functions of the glycosamino-glycans. In: Biological function of the matrix, edited by E.A. Balazs, Academic Press

Inc., London, 1231-1240.

[Oloyede and Broom, 1991] Oloyede, A. and Broom, N. D., 1991. Is classical consolidation theory applicable to articular cartilage deformation. Clinical Biomechanics, vol. 6, pp 206-212.

[Oloyede and Broom, 1993 (a)] Oloyede A and Broom N.D., 1993 (a). A physical model for the time-dependent deformation of articular cartilage. Connective Tissue Research, vol. 29, pp. 256-261.

[Oloyede and Broom, 1993 (b)] Oloyede A. and Broom N.D., 1993 (b). Stress-sharing between the fluid and solid components of articular cartilage under varying rates of compression. Connect Tissue Research, vol.30, pp127-141.

[Oloyede and Broom, 1994 (a)] Oloyede A, and Broom N.D., 1994 (a). Complex nature of stress inside loaded articular cartilage. Clinical Biomechanics, vol.9, pp 149-156.

[Oloyede and Broom, 1994 (b)] Oloyede, A. and Broom, N.D., 1994 (b). The generalized consolidation of articular cartilage: an investigation of its near-physiological response to static load. Connective Tissue Research, vol. 31, 1:75-86.

[Oloyede and Broom, 1996] Oloyede, A. and Broom, N. D., 1996. The biomechanics of cartilage load carriage. Connective Tissue Research, Vol. No. 2, pp. 119-143.

[Oloyede et al., 1992] Oloyede, A., Flachsmann, R., and Broom, N.D., 1992. The dramatic influence of loading velocity on the compression response of articular cartilage. Connective Tissue Research, vol. 27, 1-15.

[Oloyede et al., 2003] Oloyede, A., Gudimetla P., Crawford R. and Hills B.A., 2003. Consolidation responses of delipidized articular cartilage. Clinical Biomechanics, in press.

[Pickard et al., 1998] Pickard, J., Ingham, E., Egan, J. and Fisher, J; 1998. Investigation into the effect of proteoglycan molecules on the tribological properties of cartilage joint tissues, Proc Instn. Mech. Eng. Vol. 212, part H, pp 177-182.

[Preston et al., 1972] Preston B.N., Snowden J.M. and Houghton K.T., 1972. Model connective tissue systems: the effect of proteoglycans on the distribution of small non-electrolytes and micro-ions. Biopolymers, 11:1645-1659.[Medline]

[Quinn et al., 1998] Quinn T.M., Grodzinsky A.J., Buschmann M.D., Kim Y.J. and Hunziker E.B., 1998. Mechanical compression alters proteoglycan deposition and matrix deformation around individual cells in cartilage explants. Journal of Cell Science, 111:573-583.

[Radin and Paul, 1971] Radin E.L. and Paul I.L., 1971. The response of joints to impact loading. I – In Vitro Wear. Arthritis and Rheumatism 1971, vol. 14, p.356.

[Radin et al., 1970] Radin, E. L., Paul, I. L. and Lowy, M., 1970. A comparison of the dynamic force transmitting properties of subchondral bone and articular cartilage, Journal of Bone Joint Surgery, V.52-A(3), pp. 444-455.

[Rendulic,1936] Rendulic L., 1936. Porenziffer and porenwasserdruck in tonen. Die Baueringenieur, vol. 17 (51/52), pp.559-564.

[Rybicki et al. 1977] Rybicki E.F., Glaeser W.A., Strenkowski J.S. and Tamm M.A., 1977. Effects of cartilage stiffness and viscosity on a nonporous compliant bearing lubrication model for living joints. Journal of Biomechanics, vol. 12, pp. 403-409.

[Sah et al., 1996] Sah R.L., Trippel S.B. and Grodzinsky A.J., 1996. Differential effects of serum, IGF-I, and FGF-2 on the maintenance of cartilage physical properties during long-term culture. Journal of Orthopaedic Research, vol. 14, 44-52.

[Sah et al., 1997] Sah R.L., Yang A.S., Chen A.C., Hant J.J., Halili R.B., Yoshioka M., Amiel D. and Coutts R.D., 1997. Physical properties of rabbit femoral articular cartilage

after transection of the anterior cruciate ligament. Journal of Orthopaedic Research, vol. 15, 197-203.

[Sah et al., 2002] Sah R.L., Wong, B.L., Li, K.W., Bae, W.C., Price, J.H. and Schumacher, B.L., 2002. Three dimensional histomorphometric analysis of normal adult human articular cartilage. The 48th Annual Meeting of the Orthopaedic Research Society, 2002, Poster No. 0363.

[Schenk et al., 1986] Schenk R.K., Eggli P.S. and Hunziker E.B., 1986. Articular cartilage morphology. In: Kuettner K.E., Schleyerbach R. and Hascall V.C. (Eds.) Articular Cartilage Biochemistry, pp. 3-22. New York: Raven Press.

[Schmidt et al., 1990] Schmidt M.B., Mow V.C., Chun L.E. and Eyre D.R., 1990. Effects of proteoglycan extraction on the tensile behavior of articular cartilage. Journal of Orthopedic Research, 8:353-363.

[Schneiderman et al., 1986] Schneiderman R., Keret D. and Maroudas A., 1986. Effects of mechanical and osmotic pressure on the rate of glycosaminoglycan synthesis in the human adult femoral head cartilage: an in vitro study. Journal of Orthopaedic Research, 4:393-408.

[Schinagl et al., 1996] Schinagl R.M., Ting M.K., Price J.H. and Sah R.L., 1996. Video microscopy to quantitate the inhomogeneous equilibrium strain within articular cartilage during confined compression. Annals of Biomedical Engineering 1996, v. 24, 500-512.

[Schinagl et al., 1997] Schinagl R.M., Gurskis D. and Sah R.L., 1997. Depth-dependent confined compression modulus of full-thickness bovine articular cartilage. Journal of Orthopedic Research, vol. 15, 499-506.

[Setton et al., 1997] Setton, L.A., Mow, V.C., Muller, F.J., Pita, J.C., Howell, D.S., 1997. Altered material properties of articular cartilage after periods of joint disuse and joint disuse followed by remobilization. Osteoarthritis and Cartilage 5, 1-16.

[Silman and Hochberg, 2001] Silman A.J. and Hochberg M.C., 2001. Epidemiology of the Rheumatic Diseases. 2nd Ed. Oxford Medical Publications, 2001.

[Simon, 1990] Simon, B.R., 1990. Poroelastic finite element methods for soft tissue structures. In connective tissue matrix. Part 2, edited by D.W.L. Hukins, Macmillan Press Scientific and Medical. UK., 66-90.

[Soltza and Ateshian, 1998] Soltza M.A. and Ateshian G. A., 1998. Experimental verification and theoretical prediction of cartilage interstitial fluid pressurization at an impermeable contact interface in confined compression. Jour. of Biomechanics, vol. 32.

[Spilker, 1992] Spilker R.L., Suh J.-K. and Mow V.C., 1992. A finite element analysis of the indentation stress-relaxation response of linear biphasic articular cartilage. Journal of Biomechanical Engineering, vol. 114, 191-201.

[Suh, and Bai, 1997] Suh, J.K., Bai, S., 1997. Biphasic poroviscoelastic behavior of articular cartilage in creep indentation test. In: Sandell, L.J. (Ed.), Transactions of the Ortho. Research Society, Orthopaedic Research Society, San Francisco, CA, pp. 823.

[Taylor, 1948] Taylor, D.W., 1948. Fundamentals of Soil Mechanics. John Wiley and Sons, Inc. New York, 238-242.

[Terzaghi, 1943] Terzaghi, K., 1943. Theoretical Soil Mechanics. John Wiley, New York.

[Thompson et al., 1991] Thompson R., Oegema T., Lewis J. and Wallace L., 1991. Osteoarthritic changes after acute transarticular load. Journal of Bone and Joint Surgery, vol. 73A, 990-1001.

[Tombs and Peacocke, 1974] Tombs, M.P. and Peacocke, A.R., 1974. The Osmotic Pressure of Biological Macromolecules. Clarendon Press, Oxford, UK.

[Torzilli, 1990] Torzilli P.A., 1990. Measurement of the compressive properties of thin cartilage slices: evaluating tissue inhomogeneity. In: Maroudas A. and Kuettner K. (Eds.) Methods in Cartilage Research. (pp. 304-308) London: Academic Press

[Torzilli et al., 1983] Torzilli P.A., Dethmers D.A. and Rose D.E., 1983. Movement of interstitial water through loaded articular cartilage. Journal of Biomechanics, vol. 16, 169-179.

[Torzilli et al., 1990] Torzilli P.A., Askari E. and Jenkins J.T., 1990. Water content and solute diffusion properties in articular cartilage. In: Mow V.C., Ratcliffe A. and Woo S.L-Y. (Eds.) Biomechanics of Diarthrodial Joints. (pp. 363-390) New York: Springer

[Urban et al., 1979] Urban, J.P.G., Maroudas, A., Bayliss, M.T., Dillon, J., 1979. Swelling pressures of proteoglycans at the concentrations found in cartilaginous tissues. Biorheology, vol. 16, 447-464.

[Valhmu et al., 1998] Valhmu, W.B., Stazone, E.J., Bachrach, N.M., Said-Nejad, F. Fischer, S. G., Mow, V.C. and Ratcliffe, A., 1998. Load-controlled compression of articular cartilage induces a transient stimulation of aggrecan gene expression. Archives of Biochemistry and Biophysics, vol. 535, 1, pp. 29-36.

[Vasan, 1983] Vasan N., 1983. Effects of physical stress on the synthesis and degradation of cartilage matrix. Connective Tissue Research, vol. 12, 49-58.

[Vener et al., 1992] Vener J., RC T., Lewis J. and Oegema T., 1992. Subchondral damage after acute transarticular loading: An in vitro model of joint injury. Journal of Orthopedic Research, 10:759-765.

[Ward and Hadley, 1993] Ward, I.M and Hadley, D.W., 1993. An introduction to the mechanical properties of solid polymers. Edited by John Wiley & Sons, England.

[Weightman, 1975] Weightman B., 1975. In vitro fatigue testing of articular cartilage.

Annals of the Rheumatic Diseases, 34:108.

[Weightman and Kempson, 1979] Weightman, B. and Kempson, G.E , 1979. Load carriage. In: Adult Articular Cartilage. Edited by M.A.R.Freeman, 291-331. London: Pitman Medical.

[Weightman et al., 1973] Weightman B., Freeman M.A.R. and Swanson S.A.V. Fatigue of articular cartilage. Nature (London) 1973, 224:303.

[Wong et al., 1995] Wong M., Wuethrich P., Eggli P. and Hunziker E., 1995. Zone-specific cell biosynthetic activity in mature bonvine articular cartilage: a new method using confocal microscopic stereology and quantitative autoradiography. Journal of Orthopaedic Research, vol.14, pp.424-432.

[Wong et al., 1997] Wong M., Wuethrich P., Buschmann M.D., Eggli P. and Hunziker E., 1997. Chondrocyte biosynthesis correlates with local tissue strain in statically compressed adult articular cartilage. Journal of Orthopaedics Research, vol. 15, 189-196.

[Woo et al., 1976] Woo, S.L - Y., Akeson, W.H., Jemmot, G.F., 1976. Measurement of the nonhomogeneous directional properties of articular cartilage in tension. Journal of Biomechanics, vol. 9, 785 - 791.

[Woo et al., 1979] Woo S.L.Y., Lubock P., Gomez M.A., Jemmott G.F., Kuei S.C. and Akeson W.H., 1979. Large deformation nonhomogeneous and directional properties of articular cartilage in uniaxial tension. Journal of Biomechanics, vol. 12, 437-446.

[Wu et al., 1998] Wu J.Z, Herzog W., Epstein, M. 1998. Evaluation of the finite element software ABAQUS for biomechanical modelling of biphasic tissue. Journal of Biomechanics, v.31, pp. 165-169.

APPENDICES

Appendix A1: Separation method to solve the partial different equation

The partial different equation:

$$\frac{\partial K}{\partial t} = \alpha \frac{\partial^2 K}{\partial z^2} \tag{A1.1}$$

with the boundary and initial conditions

$$K(0,t) = K_0, \qquad t > 0,$$
$$K(H,t) = K_H, \qquad t > 0,$$
$$K(z,0) = f(z) = (K_H - K_0)\frac{z}{H} + K_0, \qquad 0 < x < H$$

We define a new variable ξ(z,t) by,

$$K(z,t) = \xi(z,t) + \psi(z)$$

where $\frac{d^2\psi}{dz^2} = 0 \Rightarrow \psi(z) = Az + B$, then

$$\frac{\partial \xi}{\partial t} = \alpha\left(\frac{\partial^2 \xi}{\partial z^2} + \frac{d^2\psi}{dz^2}\right) \tag{A1.2}$$

and,

$$K(0,t) = \xi(0,t) + \psi(0) = K_0,$$
$$K(H,t) = \xi(H,t) + \psi(H) = K_H,$$

Let $\xi(0,t) = 0$ and $\xi(H,t) = 0$, so $\psi(0) = K_0$ and $\psi(H) = K_H$

We can thus find ψ(z)

$$\psi(z) = Az + B,$$
$$\psi(0) = B = K_0,$$
$$\psi(H) = AH + K_0 = K_H$$

Hence,

$$\psi(z) = \frac{K_H - K_0}{H} z + K_0$$

Equation (A1.2) becomes,

$$\frac{\partial \xi}{\partial t} = \alpha \frac{\partial^2 \xi}{\partial z^2} \tag{A1.3}$$

with the boundary and initial conditions as,

$$\xi(0,t) = 0, \qquad t > 0,$$
$$\xi(H,t) = 0, \qquad t > 0,$$
$$\xi(z,0) = f(z) - \frac{K_H - K_0}{H} z - K_0, \qquad 0 < x < H$$

Using separation method to solve equation (A1.3) as the following,

Let $\xi(z,t) = Z(z).T(t)$, equation (A1.3) becomes,

$$\frac{1}{\alpha T}\frac{dT}{dt} = \frac{1}{Z}\frac{\partial Z}{\partial z} = -\omega^2 = cons\tan t$$

also, $Z(0)=0$ and $Z(H)=0$, then

$$\frac{1}{\alpha T}\frac{dT}{dt} = -\omega^2 \Rightarrow T = Ae^{-\alpha\omega^2 t}$$

and,

$$\frac{1}{Z}\frac{\partial Z}{\partial z} = -\omega^2 \Rightarrow Z = B\sin\omega z + C\cos\omega z$$
$$Z(0) = 0 \Rightarrow C = 0$$
$$Z(H) = 0 \Rightarrow \sin\omega z = 0 \Rightarrow \omega = \frac{n\pi}{H}$$

Therefore,

$$\xi(z,t) = \sum_{n=1}^{\infty} A_n e^{-\frac{\alpha n^2\pi^2}{H^2}t} \sin\left(\frac{n\pi z}{H}\right)$$

where, A_n is computed by,

$$\xi(z,0) = f(z) - \frac{K_H - K_0}{H} z - K_0 = \sum_{n=1}^{\infty} A_n \sin\left(\frac{n\pi z}{H}\right)$$

then,

$$A_n = \frac{2}{H}\int_0^H \left(f(z) - K_0 - \frac{K_H - K_0}{H} z \right) \sin\left(\frac{n\pi z}{H}\right) dz$$

Finally we have,

$$K(z,t) = \frac{K_H - K_0}{H} z + K_0 + \sum_{n=1}^{\infty} A_n e^{-\frac{\alpha n^2\pi^2}{H^2}t} \sin\left(\frac{n\pi z}{H}\right)$$

Appendix A2: MAPLE algorithm to obtain results of rheological analogues.

A2.1 Series rheological analogue (chapter 3)

```
with(linalg):

(functions for calculation)
u:=-(c*exp((2-a)*x))*x1:
po:=(p1*exp(-x)+p2*exp(-2*x))*(1-vs*exp(-x))-(p1+p2)*(1-vs):
uc:=(p1*exp(-x)+p2*exp(-2*x))*(1-vs*exp(-x))-(p1+p2)*(1-vs)-m2*x21:

(Input constant coefficients)
m := 6000.0:    (m=0 for 'OB'analogue)
c := 6500.0:
a := 2.49:
k:= 30.0:
p2 := .16:
p1:= .20e-1:
B:=1.14:
pa:=1.13:
vs:=0.255:
vc:=0.0:
m1:=0.0:
m2:=950.0:

(Input initial strains and time step)
x:=0.0:      (total strain)
x10:=0.0:   (strain of instantaneous element)
x20:=0.0:   (strain of deformed elements)
dt:=0.1:     (time step)

(Define arrays of parameters)
Upor:=array(1..100):   (pore pressure)
Usw:=array(1..100):    (Osmotic swelling pressure)
permea:= array(1..100):  (permeability)
Usol:=(1..100):          (Effective solid stress)
disp:=(1..100):          (instantaneous thickness of matrix)
tEps:=array(1..100):     (instantaneous strain of matrix)
suc:=array(1..100):      (hyperelastic solid stress)

(Compute rate of the  initial strains)
x1:=(-pa+B*x20^2-m2/(m1+m2)*(B*x20^2+k*x10)+po)/(m1*m2/(m1+m2)-
m+c*exp((2-a)*x)):
x21:=(B*x^2+k*x10+m1*x1)/(m1+m2):
x11:=x1-x21:
```

```
(Compute initial values of the parameters)
Upor[1]:=(u+m*x1)/(1-vs*exp(-x)):
Usw[1]:=(p1*exp(-x)+p2*exp(-2*x))*(1-vs*exp(-x)):
permea[1]:= (1.5e-3)^2*exp(a*x)/c:
suc[1]:=uc;
Usol[1]:=B*x20^2:
disp[1]:=1-exp(x):
tEps[1]:=x:
suc[1] := 0

(Compute  values of the parameters for each time step)
for i from 2 to 100 do
      for j from 1 to 1000 do
          x:=x+x1*dt:
          x10:=x10+x11*dt:
          x20:=x20+x21*dt:
           x1:=(-pa+B*x20^2-m2/(m1+m2)*(B*x20^2+k*x10)+po)/(m1*m2/(m1+m2)-
m+c*exp((2-a)*x)):
           x21:=(B*x^2+k*x10+m1*x1)/(m1+m2):
           x11:=x1-x21:
      od:   (end do)
       Upor[i]:=(u+m*x1)/(1-vs*exp(-x)): Usw1[i]:=(p1*exp(-x)+p2*exp(-2*x)):
        permea[i]:= (1.5e-3)^2*exp(a*x)/c:
        suc[i]:=uc:
        Usol[i]:=B*x20^2:
        disp[i]:=1-exp(x):
         tEps[i]:=x:
od:   (end do)

(Represent data as curve results)
ddis:=plot([seq([100*(i-1),disp[i]],i=1..100)],color=violet,thickness=3):
dUpor:=plot([seq([100*(i-1),Upor[i]],i=1..100)],color=red,thickness=3):
dUsw:=plot([seq([100*(i-1),Usw1[i]],i=1..100)],style=point,color=blue,symbol=circle):
dUsol:=plot([seq([100*(i-1),Usol[i]],i=1..100)],color=red,thickness=3):
dsuc:=plot([seq([100*(i-1),suc[i]],i=1..100)], color=red,thickness=3):
dpa:=plot([seq([100*(i-1),pa],i=1..100)], color=red,thickness=3):

(Input and plot the published data)
ph1:=[0,.45],[400,.85],[800,.9],[1600,.805],[2400,.69],[3200,.59],[4000,.44],[4800,.32],
[5600,.22],[6400,.155],[7200,.11],[8000,.07],[8800,.05],[9600,.04]:
fh1:=PLOT(POINTS(ph1,SYMBOL(DIAMOND))): (HEPP)
eps:=[0,0],[12.5*60,0.31],[25*60,0.41],[37.5*60,0.47],[50*60,0.51],[100*60,.575],[150
*60,.592]:
feps:=PLOT(POINTS(eps,SYMBOL(DIAMOND))): (strain)

(Display all curves on a graph)
with(plots):
display({ddis,fh1,feps,dUsol,dUpor,dUsw,dpa});
```

A2.2 Parallel rheological analogue (chapter 3)

```
with(linalg):

(functions for calculation)
u:=-(c*exp((2-a)*x))*x1:
po:=(p1*exp(-x)+p2*exp(-2*x))*(1-vs*exp(-x))-(p1+p2)*(1-vs):
uc:=(p1*exp(-x)+p2*exp(-2*x))*(1-vs*exp(-x))-(p1+p2)*(1-vs)-m2*x1:

(Input constant coefficients)
m := 6000.0:
c := 6500.0:
a := 2.49:
p2 := .16:
p1:= .20e-1:
B:=1.14:
pa:=1.13:
vs:=0.265:
vc:=0.0:
m2:=950.0:

(Input initial strain and time step)
 x:=0.0:
dt:=0.1:

(Define arrays of parameters)
Upor:=array(1..100):
Usw:=array(1..100):
permea:= array(1..100):
Usol:=(1..100): disp:=(1..100):
tEps:=array(1..100):suc:=array(1..100):

(Compute initial parameters)
x1:=(-pa+B*x^2+po)/(m2-m+c*exp((2-a)*x)): (strain rate)
Upor[1]:=(u+m*x1)/(1-vs*exp(-x)):
Usw[1]:=(p1*exp(-x)+p2*exp(-2*x))*(1-vs*exp(-x)):
permea[1]:= (1.5e-3)^2*exp(a*x)/c:
suc[1]:=uc:
Usol[1]:=B*x^2:
disp[1]:=1-exp(x):
tEps[1]:=x:
(Compute the values of parameters at each time step)
for i from 2 to 100 do
      for j from 1 to 1000 do
      x:=x+x1*dt:
      x1:=(-pa+B*x^2+po)/(m2-m+c*exp((2-a)*x)):
      od:    (end do)
 Upor[i]:=(u+m*x1)/(1-vs*exp(-x)): Usw1[i]:=(p1*exp(-x)+p2*exp(-2*x)):
```

```
permea[i]:= (1.5e-3)^2*exp(a*x)/c: suc[i]:=uc:
Usol[i]:=B*x^2: disp[i]:=1-exp(x): tEps[i]:=x:
od:   (end do)

(Represent data as curve results)
ddis:=plot([seq([100*(i-1),disp[i]],i=1..100)],color=violet,thickness=3):
dUpor:=plot([seq([100*(i-1),Upor[i]],i=1..100)],color=red,thickness=3):
dUsw:=plot([seq([100*(i-1),Usw1[i]],i=1..100)],style=point,color=blue,symbol=circle):
dUsol:=plot([seq([100*(i-1),Usol[i]],i=1..100)],color=red,thickness=3):
dsuc:=plot([seq([100*(i-1),suc[i]],i=1..100)], color=red,thickness=3):
dpa:=plot([seq([100*(i-1),pa],i=1..100)], color=red,thickness=3):

(Input and plot the published data)
ph1:=[0,.45],[400,.85],[800,.9],[1600,.805],[2400,.69],[3200,.59],[4000,.44],[4800,.32],
[5600,.22],[6400,.155],[7200,.11],[8000,.07],[8800,.05],[9600,.04]:
fh1:=PLOT(POINTS(ph1,SYMBOL(DIAMOND))):
eps:=[0,0],[12.5*60,0.31],[25*60,0.41],[37.5*60,0.47],[50*60,0.51],[100*60,.575],[150
*60,.592]:
feps:=PLOT(POINTS(eps,SYMBOL(DIAMOND))):

(Display all curves on a graph)
with(plots): display({ddis,fh1,feps,dUsol,dUpor,dUsw,dsuc,dpa});
```

Appendix A3: **MATLAB algorithm for 1-D numerical analysis (chapters 5 and 7).**

```
% main Program feaRhe.m
format short e
%N is number of layers, M is number of time step
N=17;
M=12000;
pa=-1.06;
dt=1; %time step
H=1.7*10^(-3); %thickness of the matrix
%call function to input constant coefficients
[S,mu,osp0,dz0,al]=para(N,H);
for i=1 : N
   x(i)=0; %initial strain of each layer
end
dz=dz0;
for j=1:M % time step
   osP= osmp(osp0,x); %call function to compute osmotic
pressure
   K=permea(H,x);  %call function to compute permeability
of each layer
   [a,b]=vectAB(mu,dz,x,pa,S,osP,al); %call function to set
up algebraic matrices
   u=hydP(K,a,b); %call function to compute HEPP of each
layer
   tim(j)=(j-1)*dt; %compute time
%compute thickness of each layer
   for l=1:N
      if l==1
         w(N+1-l)=dz0(N+1-l)*(1+x(N+1-l));
      else
         w(N+1-l)=dz0(N+1-l)*(1+x(N+1-l))+w(N+2-l);
      end;
   end;
   x1(j)=(H-w(1))/H;%data of total matrix strain
   y1(j)=u(17);%data of the HEPP at the bottom layer
   for l=1:N %set up new parameter for next step
      x(l)=x(l)+(b(l)/a(l)+u(l))*dt/mu(l);
      dz(l)=dz0(l)*(1+x(l));
   end;
 end;
```

```
% Function to input constant coefficients (para.m)
function [S,mu,osp0,dz0,alfa]=para(N,H)
for i=1 : N
   mu1(i)=500; dz01(i)=H/N;
   S1(i)=0.08*exp(3.8*(i-0.5)/N);
   osp01(i)=1-exp(-0.22*(i-0.5)/N);
end
```

```
S=S1';mu=mu1';osp0=osp01';dz0=dz01';

%Function to compute osmotic pressure (osmp.m)
function yos= osmp(osmP0,x)
N=length(x);
for ii = 1:N
   y31(ii)=osmP0(ii)*(1/(1+x(ii))^2-1);
end
yos=y31';

% Function to compute permeability (permea.m)
function yK=permea(H,x)
Dz=3.0*H^2; K0=7.0*10^(-11);
bk=K0; ak=1.6*10^(-7)/H; N=length(x);
for l=1:N
         sum(l)=K0*(1-(l-0.5)/N);
   for i=1:30
      aln=3.1416*i;
      ai=2*(-(ak*H+bk)*(-1)^i+bk-K0)/aln;
sum(l)=sum(l)+ai*exp(Dz*aln^2*x(l)/H^2)*sin(aln*(l-
0.5)/N);
   end
   Kb(l)=sum(l);
end
yK=Kb';
% Function to set up algebraic vectors (vectAB.m)
function [vA,vB] =vectAB(mu,dz,x,pa,S,os,al)
N=length(x);
for i=1 : N
   yA(i)=dz(i)^2/mu(i)/(1+x(i)-al(i));
   yB(i)=yA(i)*(pa-S(i)*(1+x(i)-1/(1+x(i)))+os(i));
end;
vA=yA';vB=yB';

%Function to compute hydrostatic excess pore pressure (hydp.m)
function yp=hydp(K,a,b)
N=length(K);
for i=1 : N
   for j=1 : N
      MA(i,j)=0;
   end
end
MA(1,1)= -(K(1)+K(2)+a(1));MA(1,2)=K(2);
MA(N,N)=-(K(N)+a(N));MA(N,N-1)=K(N);
for i=2 : N-1
   MA(i,i)=-(K(i)+K(i+1)+a(i));
   MA(i,i-1)=K(i);
   MA(i,i+1)=K(i+1);
end;   yp=MA\b;
```

Appendix A4: Discretization of the equations describing the response of the unconfined cartilage matrix

The instantaneous value of the axial stretch ratio of an element located in the m^{th} layer and n^{th} column as shown in Figure 7.12 is discretized from equations (7.20) and (7.22b) to obtain,

$$\dot{\lambda}_z^{m,n} = \frac{1}{D_z}\left(\sigma_a - \Delta_z^{m,n} + u^{m,n}\right) \text{ and } \dot{\lambda}_r^{m,n} = \frac{1}{D_r}\left(-\Delta_r^{m,n} + u^{m,n}\right) \tag{A4.1}$$

and

$$\frac{\dot{\lambda}^{m,n}}{\lambda^{m,n}} = \frac{\dot{\lambda}_z^{m,n}}{\lambda_z^{m,n}} + 2\frac{\dot{\lambda}_r^{m,n}}{\lambda_r^{m,n}} = \frac{\sigma_a - \Delta_z^{m,n} + u^{m,n}}{D_z\lambda_z^{m,n}} + 2\frac{-\Delta_r^{m,n} + u^{m,n}}{D_r\lambda_r^{m,n}}. \tag{A4.2}$$

We also have the following finite difference approximations,

$$\frac{\partial u}{\partial r} \approx \frac{1}{\left(\Delta r^{m,n}\right)}\left(u^{m,n+1} - u^{m,n}\right),$$

$$\frac{\partial^2 u}{\partial r^2} \approx \frac{1}{\left(\Delta r^{m,n}\right)^2}\left(u^{m,n+1} - 2u^{m,n} + u^{m,n-1}\right),$$

$$\frac{\partial u}{\partial z} \approx \frac{1}{\Delta z^{m,n}}\left(u^{m+1,n} - u^{m,n}\right),\ K_z\frac{\partial u}{\partial z} \approx \frac{K_z^{m,n}}{\Delta z^{m,n}}\left(u^{m+1,n} - u^{m,n}\right),$$

and,

$$\begin{aligned}\frac{\partial}{\partial z}\left(K_z\frac{\partial u}{\partial z}\right) &\approx \frac{1}{\Delta z^{m,n}}\left(\left(K_z\frac{\partial u}{\partial z}\right)^{m+1,n} - \left(K_z\frac{\partial u}{\partial z}\right)^{m,n}\right)\\ &\approx \frac{1}{\left(\Delta z^{m,n}\right)^2}\left(K_z^{m+1,n}\left(u^{m+1,n} - u^{m,n}\right) - K_z^{m,n}\left(u^{m,n} - u^{m-1,n}\right)\right)\\ &\approx \frac{1}{\left(\Delta z^{m,n}\right)^2}\left(K_z^{m+1,n}u^{m+1,n} - \left(K^{m+1,n} + K^{m,n}\right)u^{m,n} + K_z^{m,n}u^{m-1,n}\right)\end{aligned}$$

Substituting these approximations into equation (7.27) yields

$$\frac{1}{\lambda^{m,n}}\dot{\lambda}^{m,n} = C_1^{m-1,n}u^{m,n-1} + C_2^{m,n}u^{m,n-1} + C_{3T}^{m,n}u^{m,n} + C_4^{m,n}u^{m,n+1} + C_5^{m,n}u^{m+1,n} \tag{A4.3}$$

where,

$$C_1^{m,n} = \frac{K_z^{m,n}}{\left(\Delta z^{m,n}\right)^2},\ C_2^{m,n} = \frac{K_r^{m,n}}{\left(\Delta r^{m,n}\right)^2},\ C_4^{m,n} = \frac{K_r^{m,n}}{r^{m,n}\Delta r^{m,n}} + C_2^{m,n},\ C_5^{m,n} = \frac{K_z^{m+1,n}}{\left(\Delta z^{n}\right)^2},$$

and

$$C_{3T}^{m,n} = -C_2^{m,n} - C_1^{m,n} - C_4^{m,n} - C_5^{m,n}$$

Combining equations (A4.2), (A4.3) and the boundary conditions in equation (7.16a,b), gives

$$\frac{\sigma_a - \Delta_z^{m,n}}{D_z \lambda_z^{m,n}} + \frac{-2\Delta_r^{m,n}}{D_r \lambda_r^{m,n}} = C_1^{m,n} u^{m-1,n} + C_2^{m,n} u^{m,n-1} + C_3^{m,n} u^{m,n} + C_4^{m,n} u^{m,n+1} + C_5^{m,n} u^{m+1,n}$$

where, $C_3^{m,n} = -\left(C_1^{m,n} + C_2^{m,n} + C_{3b}^{m,n} + C_4^{m,n} + C_5^{m,n}\right)$ and $C_{3b}^{m,n} = \left(\frac{1}{D_z \lambda_z^{m,n}} + \frac{2}{D_r \lambda_r^{m,n}}\right)$

or, $$\underline{\underline{C}}\,\underline{\vec{u}} = \underline{\vec{W}} \qquad \text{(A4.4)}$$

where, $\underline{\vec{u}} = \left(u^1, u^2, ..., u^l, ..., u^{MN}\right)^T$ is a column vector that consists of unknown hydrostatic excess pore pressure parameters of all elements; $\underline{\vec{W}}$ and $\underline{\underline{C}}$ are a column vector and a square matrix of (M.NxM.N) dimensions respectively, which are evaluated as follows with the note that *l* is the order of the element during iteration as shown in Figure 7.12:

For transpose vector $\vec{W} = \left(W^1, W^2, ..., W^l, ..., W^{MN}\right)^T$, where

$$W^l = \frac{\sigma_a - \Delta_z^{m,n}}{D_z \lambda_z^{m,n}} + \frac{-2\Delta_r^{m,n}}{D_r \lambda_r^{m,n}} \qquad \text{(A4.5)}$$

For matrix $\overline{C}$,

i) Case *l* =1 (m=1, n=1), i.e $u^{1,0} = u^{0,1} = 0$

$$C_{1,1} = -\left(C_1^{1,1} + C_2^{1,1} + C_{3b}^{1,1} + C_4^{1,1} + C_5^{1,1}\right),\ C_{1,2} = C_4^{1,1},\ C_{1,1+N} = C_5^{1,1}$$

ii) Case 1<*l*<*N* (m=1,1<*n*<*N*), i.e $u^{0,n} = 0$

$$C_{l,l} = -\left(C_1^{1,n} + C_2^{1,n} + C_{3b}^{1,n} + C_4^{1,n} + C_5^{1,n}\right), C_{l,l-1} = C_2^{1,n},\ C_{l,l+1} = C_4^{1,n},\ C_{l,l+N} = C_5^{1,n}$$

iii) Case *l* = N (m=1, n=N), i.e $u^{0,N} = 0; u^{1,N+1} = u^{1,N}$

$$C_{l,l} = -\left(C_1^{1,N} + C_2^{1,N} + C_{3b}^{1,N} + C_5^{1,N}\right), C_{l,l-1} = C_2^{1,N},\ C_{l,l+N} = C_5^{1,N}$$

iv) Case *l* = mN+1 (1<m<M, n=1), i.e $u^{m,0} = 0$

$$C_{l,l} = -\left(C_1^{m,1} + C_2^{m,1} + C_{3b}^{m,1} + C_4^{m,1} + C_5^{m,1}\right),\ C_{l,l+1} = C_4^{m,1},\ C_{l,l-N} = C_1^{m,1}, C_{1,1+N} = C_5^{m,1}$$

v) Case *l* = mN (1<m<M, n=N), i.e $u^{m,N+1} = u^{m,N}$

$$C_{l,l} = -\left(C_1^{m,N} + C_2^{m,N} + C_{3b}^{m,N} + C_5^{m,N}\right), C_{l,l-1} = C_2^{m,N},\ C_{l,l-N} = C_1^{m,N},\ C_{l,l+N} = C_5^{m,N}$$

vi) Case *l* = NM-N+1 (m=M, n=1), i.e $u^{M+1,1} = u^{M,1}$ and $u^{M,0} = 0$

$$C_{l,l} = -\left(C_1^{M,n} + C_2^{M,n} + C_{3b}^{M,n} + C_4^{M,n}\right),\ C_{l,l+1} = C_4^{M,n},\ C_{l,l-N} = C_1^{M,n}$$

vii) Case NM-N+1 <*l*<NM (m=M, 1<n<N), i.e $u^{M+1,n} = u^{M,n}$

$$C_{l,l} = -\left(C_1^{M,n} + C_2^{M,n} + C_{3b}^{M,n} + C_4^{M,n}\right), C_{l,l-1} = C_2^{m,N},\ C_{l,l+1} = C_4^{m,N},\ C_{l,l-N} = C_1^{m,N}$$

viii) Case l = NM (m=M, n=N), i.e $u^{M+1,N} = u^{M,N+1} = u^{M,N}$

$$C_{l,l} = -\left(C_1^{M,N} + C_2^{M,N} + C_{3b}^{M,N}\right), C_{l,l-1} = C_2^{M,N},\ C_{l,l-N} = C_1^{M,N}$$

ix) Case of the others (1<m<M, 1<n<N)

$$C_{l,l} = C_3^{m,n}, C_{l,l-1} = C_2^{m,n},\ C_{l,l+1} = C_4^{m,n}, C_{l,l-M} = C_1^{m,n},\ C_{l,l+M} = C_5^{m,n}$$

where, $C_i^{m,n}$ (i =1, 2, 3, 3b, 4, 5) are evaluated using the previous definition in equations (A4.3) and (A4.4); The other elements of the matrix are zero.

The algebraic equation (A4.4) can be solved using MATLAB protocol (Appendix A5) to obtain the hydrostatic excess pore pressure in each element of the cartilage disc for the fixed time iteration, ie.

$$\underrightarrow{u} = \underline{\underline{C}}^{-1}\underrightarrow{W}. \qquad \text{(A4.6)}$$

Appendix A5: MATLAB algorithm for 3-D numerical analysis (chapter 7).

A5.1 Algorithm to solve the model

An algorithm was written in MATLAB to solve the system of equations. This is presented in the next section. The follows is its solution steps:

Input the parameters, D_z, D_r, Φ_{33}, ν_x, ν_z, u_{o2}

Compute Φ_{11}, Φ_{12} and Φ_{13}

Input stretch ratios $\lambda^{m,n} = \lambda_r^{m,n} = \lambda_z^{m,n} = 1$

For loop j

$t(j) = (j-1)\Delta t$

Record stretch ratios $Lam(j) = \lambda$, $LamZ(j) = \lambda_z$ and $LamR(j) = \lambda_r$

Compute the positions and the change in the positions $z^{m,n}$, $r^{m,n}$, $\Delta z^{m,n}$ and $\Delta r^{m,n}$

Compute osmotic pressures $\Delta\pi^{m,n} = u_{o2}^{m,n}\left(\left(\lambda^{m,n}\right)^{-2} - 1\right)$

Compute $\Delta_r^{m,n} = \left(\Phi_{11}^{m,n} + \Phi_{12}^{m,n}\right)\left(\lambda_r^{m,n} - \left(\lambda_r^{m,n}\right)^{-1}\right) + \Phi_{13}^{m,n}\left(\lambda_z^{m,n} - \left(\lambda_z^{m,n}\right)^{-1}\right) - \Delta\pi^{m,n}$

and $\Delta_z^{m,n} = 2\Phi_{13}^{m,n}\left(\lambda_r^{m,n} - \left(\lambda_r^{m,n}\right)^{-1}\right) + \Phi_{33}^{m,n}\left(\lambda_z^{m,n} - \left(\lambda_z^{m,n}\right)^{-1}\right) - \Delta\pi^{m,n}$

Compute the permeability, $K_r^{m,n}$ and $K_z^{m,n}$

Set up matrix $\overline{C}$ and vector $\overline{W}$

Solve the algebraic equation (7.27) to obtain $u^{m,n}$

Record the hydrostatic to display, $udis(j) = u$

Compute the rate of stretch ratios, $\dot{\lambda}_z^{m,n}$ and $\dot{\lambda}_r^{m,n}$ then $\dot{\lambda}^{m,n}$

Compute new stretch ratios $\lambda_z^{m,n} = \lambda_z^{m,n} + \Delta t\dot{\lambda}_z^{m,n}$ and $\lambda_r^{m,n} = \lambda_r^{m,n} + \Delta t\dot{\lambda}_r^{m,n}$

Next *j*

The programming of this algorithm in Matlab is shown as in appendix A4.

A5.2 MATLAB programming

```
% Main program (main.m)
format short e;
M=7;N=7; %Number of collumns and rows
dR0=0.01/M; H=1.2*10^(-3);
dZ0=H/N;
dT= 2.0;
pa1=-1.15;
%set up the initial parameters by calling function
ini_parameter
[E1,E2,nu1,nu2,Dz,Dr,Dp,pi0]=ini_parameter(N);
% Start program
for j=1:M
   Rm0(j)=(M-j+1)*dR0; %Initial radial Displacement of the
elements.
   for jr=1:N
      Rm(jr,j)=Rm0(j); dR(jr,j)=dR0; dZ(jr,j)=dZ0;
   end;
end;
for jr=1:N
   for jc=1:M
      lam(jr,jc)=1.0; lamR(jr,jc)=1.0; lamT(jr,jc)=1.0;
lamZ(jr,jc)=1.0; %Initial ratio of compressions
      Rm(jr,jc)=(M-jc+1)*dR0; dR(jr,jc)=dR0;
dZ(jr,jc)=dZ0;
   end;
end;
%Set mtrices and vectors
for j=1:2000
   t(j)=(j-1)*dT;
   % Sketch specimen
   Rdis((N+1)*(M+1))=0; Zdis((N+1)*(M+1))=0;
   for ord=1:M
      nd=(N+1)*(M+1)-ord;
      Rdis(nd)=Rm(N,M+1-ord);Zdis(nd)=0;
   end;
   for ordZ=N:-1:1
      sum=0;
      for lr=N:-1:ordZ
         sum=sum+dZ(lr,M);
      end;
      Rdis(ordZ*(M+1))=0;
      Zdis(ordZ*(M+1))=sum;
      for ord=ordZ*(M+1)-1:-1:ordZ*(M+1)-M
         ordR=ord-ordZ*(M+1)+M+1;
         if ordZ>1
            Rdis(ord)=Rm(ordZ-1,ordR);
         else
            Rdis(ord)=Rm0(ordR);
```

```
         end;
         Zdis(ord)=sum;
      end;
   end;
      % Display value of the matrix strain
   xZ(j)=1-Zdis(M)/H;
   x(j)=1-lamZ(1,M); x1(j)=1-lamZ(2,M); x2(j)=1-lamZ(4,M);
x3(j)=1-lamZ(7,M);
   % Compute Osmotic pressure
   Osp=os_pre(lam,pi0);
  % Compute permeability
   [Kr, K]=perm3(lam,lamZ,H,Rm);
   for lr=1:N
      for lc=1:M
         eR(lr,lc)=lamR(lr,lc)-1.0/lamR(lr,lc);
       eT(lr,lc)=lamT(lr,lc)-1.0/lamT(lr,lc);
         eZ(lr,lc)=lamZ(lr,lc)-1.0/lamZ(lr,lc);
IR(lr,lc)=E1(lr)*eR(lr,lc)+nu1(lr)*eT(lr,lc)+nu2(lr)*eZ(lr
,lc)-Osp(lr,lc);
IT(lr,lc)=nu1(lr)*eR(lr,lc)+E1(lr)*eT(lr,lc)+nu2(lr)*eZ(lr
,lc)-Osp(lr,lc);
IZ(lr,lc)=nu2(lr)*eR(lr,lc)+nu2(lr)*eT(lr,lc)+E2(lr)*eZ(lr
,lc)-Osp(lr,lc);
         pa(lr,lc)=pa1;
      end; %End for loop
   end; % End for loop
   % Form matrices [FM], [FC] and vector FW2
[FM,FC,FW2]=matrixMC3(M,N,Rm,dR,Rm0,dR0,dZ,lam,lamR,lamT,l
amZ,Kr,K,Dz,pa,IZ,nu2);
   u=inv(FC)*FW2;
   % Compute the rate of Lamda
      % Compute new stretch ratio in each direction
   for l=M*N:-1:1
      if mod(l,M)==0
         lc=M; lr=l/M;
      else
         lc=mod(l,M); %column order of the element
         lr=(l-lc)/M+1; %row order of the element
      end;  % End if
      RateLamZ(l)=(pa(lr,M)-IZ(lr,M)+u(lr*M))/Dz(lr);
      lamZ(lr,lc)=lamZ(lr,lc)+RateLamZ(l)*dT;
      lam(lr,lc)=lamZ(lr,lc)*(1+nu2(lr)-
nu2(lr)*lamZ(lr,lc))^2;
      if lc==M
         Rm(lr,lc)=Rm0(lc)*(lam(lr,lc)/lamZ(lr,lc))^0.5;
         lamT(lr,lc)=Rm(lr,lc)/Rm0(lc);
         lamR(lr,lc)=Rm(lr,lc)/Rm0(lc);
      else
         Rm(lr,lc)=(((Rm0(lc)^2Rm0(lc+1)^2)*lam(lr,lc)/
lamZ(lr,lc))+Rm(lr,lc+1)^2)^0.5;
```

```
lamT(lr,lc)=(Rm(lr,lc)+Rm(lr,lc))/(Rm0(lc)+Rm0(lc+1));
lamR(lr,lc)=(Rm(lr,lc)-Rm(lr,lc+1))/dR0;
      end;
      % Compute new dimensions of each element and its
position
      dR(lr,lc)=dR0*lamR(lr,lc);
      dZ(lr,lc)=dZ0*lamZ(lr,lc);
   end; % End for loop
   % Display value of hydrostatic excess pore pressure at
the centre of the required layers
   y(j)=u(M);  y1(j)=u(M*2); y2(j)=u(M*4); y3(j)=u(M*7);
   for jj=1:(M+1)*(N+1)
      positR(jj,j)=Rdis(jj); positZ(jj,j)=Zdis(jj);
   end;
end; % End for loop of time
```

% Function to input constant coefficients (ini_parameter.m)

```
function [a,b,c,d,e,f,g,h]= ini_parameter(n)
%set up depth-dependent stiffness
%Set up depth-dependent poission ratio
%Set up the initial depth-dependent volume of proteoglycan
in each layer
% Set up the initial depth-dependent osmotic presure in
each layer
for i=1:n
  E_1(i)=0.1; % radial stiffness
  E_2(i)=0.09*exp(3.8*(i-0.5)/n); % axial stiffness
% Poission ratio
   nu_1(i)=0.5;
   nu_2(i)=0.10+0.25*(i-0.5)/n;
% drag coefficients
   Dz(i)=450-0.0*(i-0.5)/n; Dr=50; Dp=50;
% Initial Donnan osmotic pressure
   ini_op(i)=1-exp(-0.22*(i-0.5)/n);
end
a=E_1'; b=E_2'; c= nu_1'; d=nu_2'; e=Dz; f=Dr; g=Dp;
h=ini_op';
```

% Function to compute osmotic pressure (os_pre.m)

```
function ops=os_pre(lamda,pi0)
n=length(lamda(:,1));m=length(lamda(1,:));
for ir=1:n
   for ic=1:m
      op(ir,ic)=pi0(ir)*(1/lamda(ir,ic)^2-1);
   end;
end;
ops=op;
```

% Function to compute permeability (perm3.m)

```
function [Kr, Kz]=perm3(lam,lamZ,H,Rm)
```

```
m=length(lam(1,:));n=length(lamZ(:,1));
D0z=3*H^2;
Khz=3.2*10^(-11); Kor=7.0*10^(-11);
b=7.0*10^(-11)/2;
a=1.75*10^(-7)/H/2;
for ic=1:m
   for ir=1:n
      sumZ=Khz*(ir-0.5)/n;
      for lbe=1:16
         ome=3.1416*(lbe); az=ome^2*D0z/H^2;
         An=2*(-(a*H-Khz+b)*(-1)^lbe+b)/ome;
         sumZ=sumZ+An*exp(az*(lam(ir,ic)-1))*sin(ome*(ir-
0.5)/n);
            %sum=sum+Cn*exp(D0z*ome^2*(lam(ir,ic)-
1))*sin(ome*(ir-0.5)/n);
      end;
      Kz(ir,ic)=sumZ;Kr(ir,ic)=Kz(ir,ic)/10;%sumR;
   end;
end;


% Function to set up algebraic matrices and vectors
function
[matC,vecW]=matC_vecW(M,N,Rm,dR,dZ,lamT,lamZ,Kr,Kz,Dz,DT,p
a,IZ,IT)
% Set up zero matrices C
   for ll=1:M*N
         for lj=1:M*N
            C(ll,lj)=0;
         end;
   end;
   % Set up empty matrices [F] and [E]
  for l=1:M*N
      if mod(l,N)==0
         lc=N; lr=l/N;
      else
         lc=mod(l,N); %column order of the element
         lr=(l-lc)/N+1; %row order of the element
      end;  % End if
      %Compute vector W
      W2(l)=(pa(lr,lc)-IZ(lr,lc))/lamZ(lr,lc)/Dz(lr)-
2*IT(lr,lc)/lamT(lr,lc)/DT(lr);
      %Set up matrix C
      C3b=1/Dz(lr)/lamZ(lr,lc)+2/DT(lr)/lamT(lr,lc);
      C2=Kr(lr,lc)/dR(lr,lc)^2;
      C1=Kz(lr,lc)/dZ(lr,lc)^2;
      if lr==1  % m=1
         if lc==1    % Case m=1 & n=1
C4=Kr(lr,lc)/dR(lr,lc)^2+Kr(lr,lc)/dR(lr,lc)/Rm(lc);
            C5=Kz(lr+1,lc)/dZ(lr,lc)^2;
```

```
            C(l,l)=-C1-C2-C3b-C4-C5; C(l,l+1)=C4;
C(l,l+N)=C5;
         elseif lc==N    % Case m=1 & n=N
            C5=Kz(lr+1,lc)/dZ(lr,lc)^2;
            C(l,l)=-C1-C2-C3b-C5; C(l,l-1)=C2;
C(l,l+N)=C5;
         else     % Case m=1 & 1<n<N
C4=Kr(lr,lc)/dR(lr,lc)^2+Kr(lr,lc)/dR(lr,lc)/Rm(lc);
            C5=Kz(lr+1,lc)/dZ(lr,lc)^2;
            C(l,l)=-C1-C2-C3b-C4-C5; C(l,l-1)=C2;
C(l,l+1)=C4; C(l,l+N)=C5;
         end;  %End Case m=1
      elseif lr==M    % Case m=M
         if lc==1     % Case m=M & n=1
C4=Kr(lr,lc)/dR(lr,lc)^2+Kr(lr,lc)/dR(lr,lc)/Rm(lc);
            C(l,l)=-C1-C2-C3b-C4; C(l,l+1)=C4; C(l,l-
N)=C1;
         elseif lc==N   % Case m=M & n=N
            C(l,l)=-C1-C2-C3b; C(l,l-1)=C2; C(l,l-N)=C1;
         else    % Case m=M & 1<n<N
C4=Kr(lr,lc)/dR(lr,lc)^2+Kr(lr,lc)/dR(lr,lc)/Rm(lc);
            C(l,l)=-C1-C2-C3b-C4; C(l,l-1)=C2;
C(l,l+1)=C4; C(l,l-N)=C1;
         end;   %End Case m=M
      else  % Case 1<m<M
         if lc==1   % Case n=1

C4=Kr(lr,lc)/dR(lr,lc)^2+Kr(lr,lc)/dR(lr,lc)/Rm(lc);
            C5=Kz(lr+1,lc)/dZ(lr,lc)^2;
            C(l,l)=-C1-C2-C3b-C4-C5; C(l,l+1)=C4; C(l,l-
N)=C1; C(l,l+N)=C5;
         elseif lc==N   % Case 1<m<M & n=N
            C5=Kz(lr+1,lc)/dZ(lr,lc)^2;
            C(l,l)=-C1-C2-C3b-C5; C(l,l-1)=C2; C(l,l-
N)=C1; C(l,l+N)=C5;
         else    % Case 1<m<M & 1<n<N
C4=Kr(lr,lc)/dR(lr,lc)^2+Kr(lr,lc)/dR(lr,lc)/Rm(lc);
            C5=Kz(lr+1,lc)/dZ(lr,lc)^2;
            C(l,l)=-C1-C2-C3b-C4-C5; C(l,l-1)=C2;
C(l,l+1)=C4; C(l,l-N)=C1; C(l,l+N)=C5;
         end;  %End Case 1<m<M
      end; %End all Cases
   end;  %End for loop (l=MN)
   matC=C; vecW=W2';

% Program 'postdata.m'to store solved data into a file called 'data1.m'
fid=fopen('data1.m','w');
fprintf(fid,'data=[\n');
for ii=1:j
   fprintf(fid,'%6.5e %6.5e\n',[positR(:,ii)
```

```
positZ(:,ii)]');
end;
fprintf(fid,'];\n\n');
status=fclose(fid);

% Program ‘plotdata.m’to grid the deformation of the matrix
nj=[1 101 251 501 1001 2000]; %time=*2 second; some
required data is selected for grid.
for kk=1:1
   ii=nj(kk);
   da1=data((ii-1)*(M+1)*(N+1)+1:ii*(M+1)*(N+1),1);
   da2=data((ii-1)*(M+1)*(N+1)+1:ii*(M+1)*(N+1),2);
   plot(0,1.2*10^(-3),0.012,0)
   Hold on;
   for jj=1:N+1
      linX1=da1((jj-1)*(M+1)+1:(jj-1)*(M+1)+1+M)';
      linX2=da2((jj-1)*(M+1)+1:(jj-1)*(M+1)+1+M)';
      plot(linX1,linX2)
   end;
   for jj=1:M+1
      linY1=da1(jj:(M+1):(M+1)*(N+1))';
      linY2=da2(jj:(M+1):(M+1)*(N+1))';
      plot(linY1,linY2)
   end;
   Hold off; end;
```

Table A1: **Experimental data presented in Figure 4.4**

Type: Medial bovine cartilage					Thickness: 1.71 mm			
t (min.)	Sa	Pa	Sb	Pb	Sc	Pc	Sd	Pd
0	0	0.2	0	0.2	0	0.17	0	0.17
0.5	0.039	0.53	0.041	0.503	0.041	0.509	0.042	0.556
1	0.06391	0.709	0.06791	0.726	0.06883	0.714	0.07138	0.804
2	0.09094	0.814	0.0963	0.844	0.09694	0.818	0.09842	0.889
4	0.1338	0.864	0.13441	0.888	0.13391	0.859	0.13435	0.918
6	0.16261	0.872	0.16218	0.89	0.16265	0.863	0.16303	0.925
8	0.18575	0.871	0.18585	0.886	0.18613	0.858	0.18666	0.921
10	0.20497	0.859	0.20379	0.874	0.20299	0.849	0.20434	0.91
12	0.2199	0.842	0.22005	0.855	0.22173	0.838	0.21958	0.897
15	0.24259	0.812	0.2397	0.831	0.24054	0.816	0.24139	0.879
20	0.26678	0.754	0.26514	0.785	0.26491	0.774	0.26949	0.837
25	0.28907	0.698	0.28675	0.739	0.28813	0.73	0.29248	0.792
30	0.30561	0.648	0.30225	0.692	0.30274	0.68	0.31309	0.751
35	0.31781	0.6	0.31604	0.648	0.31947	0.635	0.33034	0.707
40	0.33282	0.554	0.33078	0.601	0.33423	0.59	0.34485	0.665
45	0.34088	0.507	0.34224	0.558	0.34443	0.543	0.3604	0.622
50	0.34808	0.465	0.35276	0.515	0.35342	0.5	0.37053	0.576
60	0.36533	0.382	0.36784	0.432	0.37091	0.419	0.3885	0.486
70	0.37574	0.311	0.3832	0.359	0.38429	0.345	0.40263	0.398
80	0.38683	0.254	0.39193	0.296	0.39527	0.28	0.41351	0.322
90	0.39138	0.206	0.40122	0.241	0.403	0.227	0.42184	0.258
100	0.39707	0.163	0.40687	0.198	0.40745	0.183	0.42658	0.205
110	0.40159	0.131	0.41041	0.161	0.41184	0.148	0.43097	0.161
120	0.40438	0.105	0.41389	0.129	0.41604	0.118	0.43513	0.128
130	0.40752	0.081	0.41719	0.098	0.41849	0.095	0.43657	0.101
140	0.40854	0.067	0.42036	0.075	0.41973	0.074	0.43684	0.078
150	0.40982	0.053	0.421	0.069	0.42141	0.059	0.43985	0.065
160	0.4096	0.043	0.42238	0.057	0.42279	0.047	0.44041	0.049
170	0.41311	0.035	0.42589	0.049	0.42338	0.038	0.44225	0.042
180	0.41326	0.027	0.42604	0.04	0.42439	0.031	0.44362	0.034
190	0.41338	0.02	0.42616	0.032	0.42544	0.027	0.44336	0.029
200	0.41343	0.019	0.42621	0.029	0.42679	0.022	0.44392	0.025

Table A2: Experimental data presented in Figure 4.5

Type: Lateral bovine cartilage						Thickness: 1.55 mm				
T(min.)	Sa	Pa	Sb	Pb	Sc	Pc	Sd	Pd	Se	Pe
0	0	0.2	0	0.2	0	0.2	0	0.18	0	0.134
0.5	0.0559	0.562	0.0574	0.516	0.0658	0.569	0.0622	0.623	0.0972	0.405
1	0.0828	0.707	0.0807	0.668	0.0992	0.701	0.0981	0.74	0.1281	0.622
2	0.1117	0.785	0.1104	0.759	0.1299	0.778	0.128	0.805	0.1642	0.744
4	0.1519	0.821	0.1483	0.804	0.1668	0.81	0.165	0.83	0.1963	0.808
6	0.1819	0.822	0.1758	0.81	0.1904	0.821	0.1913	0.831	0.2186	0.831
8	0.2006	0.815	0.1955	0.806	0.2117	0.812	0.2113	0.825	0.2347	0.841
10	0.2184	0.806	0.2111	0.794	0.2277	0.809	0.2275	0.811	0.2489	0.843
12	0.2358	0.788	0.2295	0.773	0.2422	0.789	0.2421	0.798	0.258	0.835
15	0.2523	0.76	0.246	0.745	0.2604	0.762	0.2592	0.772	0.2733	0.825
20	0.2772	0.706	0.2715	0.694	0.2848	0.718	0.286	0.721	0.2954	0.794
25	0.2949	0.653	0.2919	0.647	0.3039	0.675	0.3051	0.672	0.3147	0.756
30	0.3093	0.609	0.3062	0.603	0.319	0.628	0.322	0.625	0.3297	0.718
35	0.3218	0.564	0.32	0.556	0.3323	0.581	0.3354	0.579	0.3439	0.681
40	0.3354	0.523	0.33	0.516	0.3431	0.541	0.3486	0.536	0.3552	0.648
45	0.3442	0.483	0.3421	0.475	0.355	0.501	0.3586	0.499	0.3653	0.612
50	0.3532	0.446	0.3507	0.435	0.3613	0.458	0.3678	0.461	0.3749	0.576
60	0.3672	0.376	0.3646	0.367	0.377	0.385	0.3825	0.392	0.391	0.51
70	0.3796	0.312	0.3775	0.306	0.3879	0.324	0.3932	0.328	0.4038	0.446
80	0.3875	0.261	0.386	0.255	0.3981	0.27	0.4022	0.278	0.4134	0.387
90	0.3938	0.215	0.3926	0.21	0.4017	0.225	0.41	0.228	0.4215	0.335
100	0.3989	0.182	0.3983	0.178	0.4073	0.187	0.4156	0.192	0.4277	0.286
110	0.4035	0.149	0.4024	0.144	0.4115	0.154	0.4195	0.164	0.4324	0.244
120	0.4088	0.121	0.4058	0.118	0.4146	0.131	0.4226	0.138	0.4374	0.21
130	0.41	0.101	0.4061	0.097	0.4169	0.107	0.4244	0.115	0.4395	0.18
140	0.4108	0.089	0.4106	0.081	0.4182	0.089	0.4255	0.103	0.4424	0.151
150	0.4147	0.078	0.4116	0.071	0.4192	0.074	0.4262	0.09	0.4428	0.127
160	0.4171	0.064	0.4142	0.06	0.4199	0.062	0.4266	0.077	0.4438	0.109
170	0.4183	0.058	0.4152	0.05	0.4202	0.052	0.427	0.068	0.444	0.096
180	0.4202	0.052	0.4183	0.043	0.4205	0.042	0.4273	0.058	0.4445	0.081

Table A3: Experimental data presented in Figure 4.6

Type: Lateral bovine cartilage					Thickness: 1.57 mm			
T(min.)	Sa	Pa	Sb	Pb	Sc	Pc	Sd	Pd
0	0.00E+00	1.50E-01	0	0.21	0.00E+00	1.60E-01	0	1.44E-01
0.5	9.60E-02	4.93E-01	0.123	0.45	9.80E-02	5.10E-01	0.105	6.71E-01
1	1.14E-01	6.54E-01	0.14472	0.575	0.11731	6.56E-01	0.1342	7.90E-01
2	1.46E-01	7.57E-01	0.17073	0.702	0.15024	7.60E-01	0.1645	8.30E-01
4	1.87E-01	8.14E-01	0.20188	0.81	0.18662	8.14E-01	0.2029	8.39E-01
6	2.13E-01	8.17E-01	0.22536	0.814	0.21601	8.18E-01	0.2286	8.31E-01
8	2.35E-01	8.15E-01	0.24438	0.8143	0.23505	8.14E-01	0.2487	8.18E-01
10	2.51E-01	7.98E-01	0.25951	0.8037	0.25435	7.96E-01	0.2632	8.02E-01
12	2.65E-01	7.80E-01	0.27295	0.7816	0.26822	7.81E-01	0.2777	7.84E-01
15	2.84E-01	7.51E-01	0.29537	0.7579	0.28558	7.47E-01	0.2928	7.58E-01
20	3.04E-01	7.02E-01	0.31468	0.7021	0.30644	6.93E-01	0.3152	7.12E-01
25	3.21E-01	6.50E-01	0.33113	0.6562	0.32284	6.33E-01	0.3304	6.68E-01
30	3.38E-01	5.96E-01	0.34443	0.603	0.3363	5.79E-01	0.3437	6.24E-01
35	3.48E-01	5.48E-01	0.35788	0.55	0.34702	5.29E-01	0.3573	5.81E-01
40	3.57E-01	4.97E-01	0.36621	0.501	0.35727	4.81E-01	0.3691	5.40E-01
45	3.67E-01	4.49E-01	0.37436	0.452	0.36585	4.35E-01	0.3783	5.00E-01
50	3.76E-01	4.08E-01	0.38217	0.411	0.377	3.97E-01	0.3885	4.62E-01
60	3.91E-01	3.39E-01	0.39422	0.336	0.38903	3.29E-01	0.4018	3.92E-01
70	3.99E-01	2.84E-01	0.40309	0.275	0.4002	2.71E-01	0.4115	3.29E-01
80	4.08E-01	2.28E-01	0.41164	0.225	0.40699	2.22E-01	0.4216	2.74E-01
90	4.11E-01	1.87E-01	0.4171	0.189	0.41239	1.81E-01	0.4296	2.27E-01
100	4.17E-01	1.56E-01	0.42167	0.1561	0.41754	1.51E-01	0.4353	1.87E-01
110	4.20E-01	1.28E-01	0.42377	0.132	0.4202	1.25E-01	0.4394	1.54E-01
120	4.25E-01	1.06E-01	0.4262	0.11	0.42448	1.05E-01	0.442	1.26E-01
130	4.26E-01	8.90E-02	0.4271	0.091	0.42586	8.90E-02	0.445	1.02E-01
140	4.28E-01	7.30E-02	0.4284	0.076	0.42668	7.60E-02	0.448	8.29E-02
150	4.30E-01	5.90E-02	0.4296	0.065	0.428	6.50E-02	0.4505	6.72E-02
160	4.31E-01	5.10E-02	0.4301	0.055	0.429	5.50E-02	0.452	5.43E-02

Table A4: Experimental data presented in Figure 4.7

Type: Medial bovine cartilage					Thickness: 1.59 mm			
T(min.)	Sa	Pa	Sb	Pb	Sc	Pc	Sd	Pd
0	0	0.2	0	0.2	0	0.18	0	0.16
0.5	0.08	0.562	0.081	0.714	0.11	0.708	0.13	0.685
1	0.11972	0.755	0.12188	0.851	0.15024	0.85	0.16729	0.816
2	0.16015	0.883	0.16603	0.914	0.18499	0.947	0.19529	0.916
4	0.2118	0.921	0.21409	0.943	0.22905	0.971	0.2344	0.968
6	0.24561	0.929	0.24891	0.939	0.25906	0.965	0.27066	0.982
8	0.27466	0.923	0.27575	0.933	0.28232	0.959	0.29164	0.982
10	0.29714	0.914	0.29649	0.922	0.3038	0.95	0.30847	0.979
12	0.31716	0.902	0.31408	0.909	0.31981	0.941	0.3193	0.978
15	0.33906	0.882	0.33706	0.887	0.34268	0.926	0.3436	0.969
20	0.37138	0.838	0.36585	0.845	0.37202	0.898	0.37213	0.952
25	0.39562	0.782	0.39295	0.798	0.39549	0.863	0.39515	0.936
30	0.41464	0.729	0.41161	0.745	0.41484	0.827	0.41398	0.911
35	0.42898	0.674	0.42692	0.695	0.43033	0.788	0.4286	0.886
40	0.44136	0.613	0.44171	0.634	0.44467	0.735	0.4431	0.856
45	0.45201	0.552	0.45311	0.578	0.45654	0.679	0.4552	0.825
50	0.45899	0.49	0.46141	0.513	0.46691	0.622	0.46647	0.786
60	0.47358	0.375	0.47279	0.393	0.48154	0.498	0.4862	0.697
70	0.48257	0.28	0.4842	0.2911	0.49301	0.382	0.5001	0.596
80	0.48765	0.209	0.4904	0.214	0.50126	0.283	0.50916	0.487
90	0.49123	0.155	0.49359	0.155	0.50627	0.202	0.51529	0.383
100	0.49457	0.114	0.49693	0.114	0.50789	0.156	0.51863	0.299
110	0.49559	0.085	0.49795	0.085	0.51071	0.117	0.52256	0.23
120	0.49574	0.065	0.4986	0.065	0.51311	0.09	0.5252	0.185
130	0.49784	0.051	0.5002	0.051	0.51468	0.068	0.5269	0.142
140	0.49839	0.042	0.50095	0.042	0.51398	0.054	0.52841	0.107
150	0.499	0.035	0.50159	0.035	0.51535	0.044	0.5301	0.08
160	0.49948	0.029	0.50184	0.029	0.51584	0.035	0.531	0.055
170	0.50066	0.027	0.50302	0.027	0.51641	0.031	0.53201	0.041
180	0.50295	0.025	0.50431	0.028	0.51682	0.028	0.53242	0.032
190	0.50195	0.0235	0.50531	0.023	0.51702	0.025	0.53262	0.028
200	0.50103	0.022	0.50539	0.022	0.51794	0.023	0.53354	0.025
210	0.50081	0.021	0.505471	0.02	0.51866	0.021	0.53426	0.023

Table A5: Experimental data presented in Figure 4.8

Type: Medial bovine cartilage				Thickness: 1.53 mm		
T (min.)	Sa	Pa	Sb	Pb	Sc	Pc
0	0	0.47	0	0.469	0	0.45
1	0.11759	0.709	0.12732	0.688	0.15068	0.698
2	0.15071	0.841	0.15879	0.815	0.1821	0.804
4	0.1944	0.902	0.19465	0.892	0.22448	0.852
6	0.22656	0.908	0.22409	0.911	0.25632	0.861
8	0.24672	0.9	0.24545	0.91	0.2835	0.857
10	0.26728	0.883	0.26151	0.905	0.30056	0.846
12	0.28282	0.86	0.2773	0.894	0.31671	0.829
15	0.30231	0.828	0.29782	0.868	0.33786	0.802
20	0.32772	0.773	0.3243	0.811	0.36586	0.738
25	0.3497	0.716	0.34661	0.755	0.38716	0.671
30	0.36915	0.664	0.36482	0.7	0.40489	0.61
35	0.3831	0.62	0.38016	0.652	0.41794	0.551
40	0.39528	0.571	0.3961	0.611	0.43234	0.496
45	0.40628	0.524	0.40689	0.566	0.44185	0.447
50	0.41511	0.477	0.41791	0.524	0.45203	0.398
60	0.42996	0.397	0.43547	0.444	0.46261	0.317
70	0.44425	0.327	0.44936	0.37	0.47644	0.249
80	0.45249	0.263	0.46015	0.304	0.48208	0.194
90	0.4575	0.217	0.47016	0.25	0.48805	0.148
100	0.46335	0.176	0.47292	0.203	0.49216	0.114
110	0.467	0.141	0.47983	0.163	0.49531	0.088
120	0.4695	0.112	0.48227	0.13	0.49727	0.068
130	0.47179	0.092	0.48515	0.105	0.4988	0.055
140	0.47498	0.074	0.49041	0.085	0.50125	0.041
150	0.47397	0.061	0.49025	0.067	0.50173	0.033
160	0.47671	0.051	0.49228	0.053	0.50286	0.026
170	0.47687	0.041	0.494	0.045	0.50159	0.021
180	0.47819	0.035	0.49414	0.038	0.50385	0.017
190	0.47916	0.029	0.49364	0.036	0.50345	0.012

Table A6: Experimental data presented in Figure 4.9

Type: Lateral bovine cartilage					Thickness: 1.92 mm			
T(min.)	Sa	Pa	Sb	Pb	Sc	Pc	Sd	Pd
0	0	0.35	0	0.38	0	0.41	0	0.435
1	0.05856	0.415	0.07576	0.475	0.08827	0.512	0.08979	0.563
2	0.08707	0.478	0.10446	0.587	0.11761	0.629	0.11672	0.657
4	0.12199	0.625	0.14076	0.676	0.15457	0.712	0.15571	0.726
6	0.14812	0.678	0.17039	0.71	0.1825	0.74	0.18337	0.756
8	0.16707	0.704	0.18988	0.727	0.20447	0.757	0.20349	0.766
10	0.18449	0.72	0.2085	0.733	0.22068	0.766	0.22204	0.775
12	0.19961	0.724	0.22471	0.735	0.23614	0.769	0.23466	0.776
15	0.21743	0.721	0.24244	0.731	0.25395	0.766	0.24898	0.705
20	0.23864	0.704	0.26676	0.714	0.27884	0.746	0.27094	0.601
25	0.25852	0.673	0.28599	0.69	0.29883	0.714	0.29712	0.532
30	0.27251	0.634	0.29979	0.656	0.31254	0.676	0.3179	0.491
35	0.28289	0.595	0.31266	0.625	0.32532	0.638	0.33677	0.455
40	0.29346	0.556	0.32209	0.59	0.33612	0.605	0.35351	0.425
45	0.30045	0.518	0.33293	0.556	0.34613	0.568	0.37023	0.399
50	0.30819	0.483	0.34105	0.521	0.35521	0.533	0.3832	0.372
60	0.32053	0.412	0.3567	0.457	0.37002	0.472	0.40437	0.328
70	0.33215	0.353	0.36635	0.397	0.38315	0.411	0.42408	0.289
80	0.33945	0.3	0.37629	0.344	0.39095	0.356	0.43961	0.255
90	0.34661	0.256	0.38253	0.298	0.39982	0.308	0.45103	0.225
100	0.35076	0.217	0.38933	0.259	0.40833	0.264	0.46111	0.198
110	0.35571	0.186	0.39351	0.222	0.41209	0.227	0.46854	0.175
120	0.36027	0.158	0.39691	0.191	0.41664	0.197	0.47899	0.155
130	0.36338	0.133	0.39996	0.163	0.42109	0.17	0.48377	0.134
140	0.3647	0.115	0.40416	0.14	0.42417	0.147	0.48792	0.118
150	0.36761	0.098	0.40687	0.119	0.42546	0.124	0.49548	0.104
160	0.36917	0.083	0.40849	0.103	0.42793	0.106	0.49824	0.09
170	0.36999	0.07	0.40925	0.088	0.42897	0.094	0.5013	0.079
180	0.37256	0.06	0.41128	0.077	0.43191	0.081	0.50426	0.07
190	0.37331	0.05	0.41106	0.069	0.43201	0.069	0.50781	0.062
200	0.3744	0.046	0.4142	0.06	0.43506	0.062	0.51009	0.057
210	0.37549	0.037	0.41437	0.052	0.43505	0.052	0.51121	0.054

Table A7: Experimental data presented in Figure 4.10

Type: Lateral bovine cartilage					Thickness: 1.70 mm			
T (min.)	Sa	Pa	Sb	Pb	Sc	Pc	Sd	Pd
0	0	0.12	0	0.12	0	0.12	0.00E+00	0.14
0.5	0.05472	0.41	0.04224	0.494	0.09995	0.451	9.60E-02	0.437
1	0.0745	0.594	0.06592	0.614	0.1208	0.602	1.22E-01	0.602
2	0.10542	0.72	0.09856	0.703	0.14884	0.713	1.55E-01	0.717
4	0.14347	0.784	0.14204	0.769	0.18493	0.802	1.95E-01	0.809
6	0.17135	0.812	0.16876	0.799	0.21174	0.825	2.20E-01	0.817
8	0.19484	0.821	0.19152	0.812	0.23179	0.834	2.44E-01	0.818
10	0.2144	0.819	0.20869	0.817	0.24822	0.832	2.62E-01	0.8179
12	0.22942	0.817	0.22389	0.817	0.26294	0.829	2.76E-01	0.807
15	0.24872	0.81	0.24419	0.813	0.28162	0.823	2.94E-01	0.794
20	0.27803	0.788	0.26881	0.796	0.30505	0.809	3.20E-01	0.768
25	0.2995	0.759	0.29231	0.764	0.32638	0.787	3.41E-01	0.736
30	0.31705	0.732	0.31008	0.734	0.34505	0.765	3.61E-01	0.71
35	0.33236	0.701	0.32945	0.702	0.35836	0.739	3.77E-01	0.68
40	0.34628	0.672	0.34222	0.668	0.3735	0.713	3.93E-01	0.65
45	0.35731	0.638	0.35503	0.639	0.38629	0.683	4.05E-01	0.618
50	0.36835	0.608	0.36535	0.605	0.39802	0.658	4.13E-01	0.587
60	0.38914	0.544	0.38487	0.544	0.41914	0.603	4.34E-01	0.521
70	0.40373	0.479	0.39959	0.484	0.43705	0.554	4.51E-01	0.461
80	0.4142	0.425	0.41299	0.425	0.44754	0.509	4.63E-01	0.405
90	0.42436	0.368	0.42245	0.363	0.45694	0.457	4.72E-01	0.347
100	0.4349	0.316	0.43208	0.318	0.4674	0.373	4.82E-01	0.298
110	0.44207	0.269	0.43881	0.273	0.4779	0.31	4.90E-01	0.252
120	0.4473	0.232	0.44462	0.23	0.48798	0.266	4.96E-01	0.214
130	0.45197	0.195	0.44924	0.196	0.49567	0.233	5.00E-01	0.182
140	0.45489	0.165	0.45396	0.167	0.50374	0.203	5.04E-01	0.154
150	0.45791	0.142	0.45697	0.142	0.50777	0.177	5.10E-01	0.131
160	0.46099	0.121	0.46022	0.122	0.51234	0.151	5.14E-01	0.112
170	0.46311	0.105	0.46259	0.103	0.51578	0.129	5.18E-01	0.096
180	0.46464	0.089	0.46251	0.088	0.52041	0.112	5.21E-01	0.082
190	0.46711	0.076	0.46387	0.076	0.52155	0.091	5.23E-01	0.072